Omdurman Islamic University – Faculty of Engineering Sciences

A Dissertation Presented for the Degree of D. Eng.

Research Title

Evaluation of Regenerative Chatter Stability of High-Speed Turning of Nickel-based Super Alloy GH4169 using PCBN Cutting Tool

تقييم إستقرار الإصطكاك المتجدد للخراطة عالية السرعة للسبيكة الفائقة القائمة على النيكل GH4169 بإستخدام أداة القطع PCBN

Candidate: MSc Eng. Mubarak Ahmed Mohammed Fadulalmula

Supervisor: Associate Professor Osama Mohammed Elmardi Suleiman Khayal

March 2023

Acknowledgements

The author would like to acknowledge with deep thanks and profound gratitude Mr. Osama Mahmoud Mohammed Ali of Dania Center for Computer and Printing Services, Atbara, and Awad Ali Bakri of faculty of engineering and technology, Atbara who they spent many hours in editing, re – editing of the manuscript in compliance with the standard format of most theses publishing. In addition, my appreciation is extended to Associate Professor Dr. Osama Mohammed Elmardi Suleiman Khayal and Associate Professor Hassan Abdelwahab Abdelkariem for close supervision, revising and correcting the manuscript several times.

Abstract

Nickel-based super alloy was widely used in many industrial applications due to their good structural, physical and chemical properties, such as the aerospace industry, which is one of the strategic industries. Poor cutting performance is troublesome problem for machine operators due to low accuracy and poor surface finish. In the cutting process of the nickel-base super alloy, the cutting chatter is somewhat highly unstable due to complicated mechanical vibration phenomenon, which can reduce the production efficiency and machining precision. When using cutting tools with high hardness and high brittleness such as PCBN, the blade chatter easily leads to crack. So, the principles of metal cutting, cutting chatter theory, cutting experiment and MATLAB software are adopted. These principles are used to explore the rule of the influence of cutting parameters on chatter, stability and surface quality in the process of high-speed cutting nickel-based super alloy with PCBN cutting tools. Specific studies are as follows:

1) The study of chatter vibration mechanics of model in cylindrical turning. The two degrees of freedom dynamic model was established in the feeding and radial direction. It was based on the cylindrical turning processing mechanism of vibration and chatter, the criteria of the stability of cutting system were determined, and the limit cutting width of the cutting system were given in this

research, and the influences of cutting vibration also were analyzed by computer simulation.

2) The dynamic parameters of the machine tool cutting system were given in this research. The mechanical parameters (intrinsic frequency ω_n, stiffness k, damping ratio ζ) and dynamic parameters (proportional cutting force coefficient k_{cu}, k_{cv}) of machine tool cutting system were determined by using impulse technique modal test and orthogonal cutting tests method. The limit cutting b_{lim} in the nickel-based super alloy were predicted; the main components of machine tool also was used for the modal test, which provides the basic for determining the main vibrating system.

3) The simulation study is regeneration cutting chatter model based on MATLAB/Simulink platform. This platform was used to build two degrees of freedom (2DOF), three degrees of freedom (3DOF) regenerative model of the cylindrical turning chatter, and established a method for determining the effective cutting state based on cutting parameter. The simulation model was used to predict the stability limit cutting depth of nickel-based super alloy to determine the main chatter vibration direction of cutting process. According to the results of numerical simulations, explored the process parameters such as cutting speed, feed rate and cutting depth for regenerative effect under the action of the influence law of cylindrical turning vibration characteristics.

4) Experimental study on the stability and quality of the nickel-based superalloy cutting. By the test of cutting time-varying cutting depth, to test the predicted limiting cutting width of nickel-based superalloy and determine the validity of the main vibration system choice; using a single factor of cylindrical turning test and combining with the results of numerical simulation to study the cutting parameters such as spindle speed, feed rate and depth of cut to the PCBN cutting tool's vibration characteristics of high-speed turning of nickel-base superalloy; under the condition of machining vibration, analyze the influence law of process parameters on surface roughness.

In conclusion, the researches in this topic provide a theoretical reference to improve the nickel-base superalloy processing performance and improve workpiece quality.

Keywords: Nickel-based superalloy; regenerative chatter; cutting depth limit of stability; PCBN cutting tools; high-speed cutting.

مستخلص

Arabic Abstract

تم إستخدام السبائك الفائقة ذات قاعدة النيكل على نطاق واسع في العديد من التطبيقات الصناعية نظرًا لخصائصها الهيكلية والفيزيائية والكيميائية الجيدة، مثل صناعة الطيران التي تعد من الصناعات الإستراتيجية. يعد أداء القطع الضعيف مشكلة مزعجة لمشغلي الآلات بسبب الدقة المنخفضة وسوء تشطيب السطح. في عملية القطع للسبيكة الفائقة ذات قاعدة النيكل، يكون إصطكاك القطع غير مستقر إلى حد ما بسبب ظاهرة الإهتزاز الميكانيكية المعقدة، والتي يمكن أن تقلل من كفاءة الإنتاج ودقة التصنيع. عند إستخدام أدوات القطع ذات الصلادة العالية والهشاشة العالية مثل PCBN، فإن إصطكاك الشفرة يؤدي بسهولة إلى التشقق. لذلك، تم إعتماد مبادئ قطع المعادن، نظرية قطع الإصطكاك، تجربة القطع وبرنامج MATLAB. تُستخدم هذه المبادئ لإستكشاف قاعدة تأثير متغيرات القطع على الإصطكاك، والإستقرار وجودة السطح في عملية قطع السبائك الفائقة القائمة على النيكل عالية السرعة بإستخدام أدوات القطع PCBN. هنالك دراسات محددة يمكن إدراجها فيما يلي:

1) دراسة ميكانيكية إهتزاز الإصطكاك النموذجي في الدوران الأسطواني. تم إنشاء النموذج الديناميكي لدرجتي الحرية في إتجاه التغذية والإتجاه الشعاعي أو الإتجاه نصف القطري. وقد إعتمد على آلية معالجة الدوران الأسطوانية من الإهتزاز والإصطكاك، وتم تحديد معايير إستقرار نظام القطع، وتم تقديم الحد الأقصى لعرض القطع لنظام القطع في هذا البحث، كما تم تحليل تأثيرات إهتزاز القطع بواسطة محاكاة الكمبيوتر.

2) تم تقديم المتغيرات الديناميكية لنظام قطع الأدوات الآلية في هذا البحث. تم تحديد المتغيرات الميكانيكية (التردد الداخلي ω_n، والصلابة k، ونسبة التخميدζ) والمتغيرات الديناميكية (معامل قوة القطع المتناسبة k_{cu}، k_{cv}) لنظام قطع الأدوات الآلية بإستخدام إختبار مشروط لتقنية الدفع وطريقة إختبارات القطع المتعامدة. تم التنبؤ بحدود القطع القصوى في السبائك الفائقة القائمة على النيكل. تم أيضًا إستخدام

المكونات الرئيسية للأداة الآلية في إختبار الوسائط، والذي يوفر الأساس لتحديد نظام الإهتزاز الرئيسي.

3) دراسة المحاكاة هي نموذج تجديد قطع الإصطكاك على أساس منصة MATLAB/Simulink. تم إستخدام هذه المنصة لبناء نموذج متجدد لدرجتين من الحرية (2DOF)، وثلاث درجات من الحرية (3 DOF) لإصطكاك الدوران الأسطوانية، وإنشاء طريقة لتحديد حالة القطع الفعالة بناءً على مغير القطع. تم إستخدام نموذج المحاكاة للتنبؤ بعمق القطع الحدي للثبات للسبيكة الفائقة القائمة على النيكل لتحديد إتجاه إهتزاز الإصطكاك الرئيسي لعملية القطع. وفقا لنتائج المحاكاة العددية، تم إستكشاف متغيرات العملية مثل سرعة القطع ومعدل التغذية وعمق القطع للتأثير التجديدي تحت تأثير قانون تأثير خصائص إهتزاز الدوران الأسطواني.

4) دراسة تجريبية على ثبات وجودة قطع السبائك الفائقة القائمة على النيكل. من خلال إختبار عمق القطع المتغير بمرور الوقت، لإختبار عرض القطع المحدد المتوقع للسبائك الفائقة القائمة على النيكل وتحديد صلاحية إختيار نظام الإهتزاز الرئيسي؛ إستخدام عامل واحد لإختبار الدوران الأسطواني والدمج مع نتائج المحاكاة الرقمية لدراسة متغيرات القطع مثل سرعة عمود الدوران ومعدل التغذية وعمق القطع لخصائص إهتزاز أداة القطع PCBN للتحول عالي السرعة للسبائك الفائقة ذات قاعدة النيكل؛ في حالة إهتزاز الآلة، قم بتحليل قانون تأثير متغيرات العملية على خشونة السطح.

في الختام، توفر الأبحاث في هذا الموضوع يعد مرجعًا نظريًا لتحسين أداء معالجة السبائك الفائقة القائمة على النيكل وتحسين جودة قطعة الشغل.

Table of Contents

Description		Page
Acknowledgements		ii
Abstract		iii
Arabic Language Abstract (مستخلص)		vi
Table of Contents		viii
Chapter 1	Introduction	
	1.1 Research Background and Significance	1
	1.2 Research Methods Compared with Previous Research Studies	3
	1.2.1 Research Status and Mechanism of Cutting Chatter	3
	1.2.2 Control and Prevention Methods for Cutting Chatter	6
	1.2.2.1 Passive Chatter Control	7
	1.2.2.2 Active Control of Chatter	8
	1.2.2.3 Active Control of	9

	Chatter Online Monitoring Chatter Control	
	1.2.2.4 Predictive Chatter Control	10
	1.2.3 Research Status of High-Speed Machining of Nickel-Based Superalloys	12
	1.2.4 The Major Problems Currently in Existence	16
	1.3 Research Objectives	17
Chapter 2	Literature Review	
	2.1 Introduction	20
	2.2 Analytical Techniques for Chatter Stability Prediction	21
	2.2.1 Stability Lobes Diagram (SLD)	21
	2.2.1.1 Analytical Models Based on the Number of DOF	23
	2.3 Turning Operation	26
	2.4 Vibration in Machining	30
	2.5 Chatter Noise in Turning Operation	32

2.5.1 Mode Coupling	36
2.5.2 Regenerative Chatter	36
2.6 Regenerative Chatter Mechanism in Turning Operation	39
2.6.1 Chatter Modelling Theory	42
2.7 Nickel Based Superalloys	46
2.7.1 Nickel-Base Super Alloy Classification	47
2.7.2 Properties of Nickel - Base Alloys	49
2.7.3 Industrial applications	49
2.8 Polycrystalline Cubic Boron Nitride	50
2.8.1 Brief History of PCBN Development	51
2.8.2 The Properties of PCBN	52
2.8.3 Application of PCBN Tool	54

	2.8.4 Performance of PCBN Tool	55
Chapter 3	Mechanism Analysis and Study of Regenerative Chatter Stability	
	3.1 Introduction	60
	3.2 The Mechanism of Regenerative Chatter	61
	3.2.1 Chatter Overview	61
	3.2.2 Machine Cutting System	63
	3.3 Dynamic Model of Turning Regenerative Chatter	65
	3.3.1 Turning Process	65
	3.3.2 Dynamic Model of Turning Regenerative chatter	66
	3.4 Study of Stability Limit for Machine Tool Cutting System	73
	3.4.1 Calculation of Stability Limit	73
	3.4.2 The Stability Lobe	76

Diagram
3.5 Analysis of Factors Affecting the Stability of the Machine Tool Cutting System 78
3.5.1 Influence of Natural Frequency on the Limit Cutting Width 78
3.5.2 The Effect of Stiffness on the Limit Cutting Width 79
3.5.3 Influence of unit cutting force coefficient on ultimate cutting width 80
3.5.4 Influence of Damping Ratio on the Limit Cutting Width 81
3.5.5 Effect of Coincidence Degree on the Limit Cutting Width 82
3.6 Three Degrees of Freedom Dynamic Model 83
3.7 Results and Discussion 84
3.7.1 Formulation of the 84

	Dynamic Model	
	3.8 Mathematical Model	87
	3.8.1 The Natural Frequency of Vibrated System	89
	3.8.2 The Main Modes of the Vibrated System	90
	3.9 Transient Response of the Cutter	91
	3.10 MATLAB / SIMULINK Simulation	94
	3.11 Chapter Summary	96
Chapter 4	Determination the Dynamic Parameters of the Machine Tool Cutting System	
	4.1 Introduction	99
	4.2 Experimental Techniques	99
	4.2.1 Introduction to Modal Analysis	100
	4.2.2 Determination of Transfer Function	101
	4.2.3 Identification of	102

Modal Parameters
4.3 The Measurement of the Modal Parameters of the Tool System 107
4.3.1 The Test Equipment 107
4.3.2 Test Process Experimental Procedure 110
4.3.3 Test Result 115
4.4 The Natural Frequency of the Main Components of the Machine Tool 118
4.4.1 Purpose of the Experiment 118
4.4.2 Experiment Results 118
4.5 Calculation of the Cutting Force Coefficient Unit in X and Y Directions 120
4.5.1 Calculation Principle 120
4.5.2 Test Method and Test Conditions 122
4.5.3 Test Results 123
4.6 Prediction of Stable Limit Cutting Width 125
4.7 Chapter Summary 128

Chapter 5	The Simulation Study of Cutting Stability on Nickel-Based Super Alloy	
	5.1 Introduction	131
	5.2 MATLAB / Simulink Simulation Software	131
	5.3 Simulation Study of Regenerative Chatter Model	133
	5.3.1 Simulation Block Diagram	133
	5.3.2 Simulation Parameters Setting	137
	5.4 Numerical Simulation and Analysis	138
	5.4.1 Simulation Verification of Stability Limit	138
	5.4.2 The Effect of Cutting Speed on Chatter Characteristics	147
	5.4.3 Influence of Feed Rate on Chatter Characteristics	152

	5.4.4 Influence of Cutting Depth on Chatter Characteristics	153
	5.5 Chapter Summary	154
Chapter 6	Experimental Study of the Cutting Stability and Machined Surface Quality on Nickel-Base Super-Alloy	
	6.1 Introduction	157
	6.2 Experimental Design	157
	6.2.1 The Experimental Setup	157
	6.2.2 The Test Equipment	158
	6.2.3 Experimental Material	163
	6.2.4 Experiment Method	164
	6.3 Identification of Chatter and Verification of Stability Limits	166
	6.3.1 Identification of Chatter	166
	6.3.2 Testing Method	167
	6.3.3 Experiment Results	168

	6.4 Effect of Cutting Parameters on Vibration Characteristics	174
	6.4.1 Effect of Cutting Speed	174
	6.4.2 Effect of Feed Rate	178
	6.4.3 Effect of Cutting Depth	181
	6.5 Effect of Cutting Parameters on Workpiece Surface Roughness	185
	6.5.1 Effect of Cutting Speed	185
	6.5.2 Effect of Feed Rate	187
	6.5.3 Effect of Cutting Depth	189
	6.6 Chapter Summary	190
Chapter 7	Results and Discussion	
	7.1 Simulation	193
	7.2 Turning Test	195
	7.3 Chapter Summary	202
Chapter 8	Conclusions and Recommendations for Future Works	

	8.1 Conclusions	205
	8.2 Recommendations for Future Works	207
References		209
Student Autobiography		232
Supervisor Autobiography		236

Chapter 1

Introduction

1.1 Research Background and Significance

The rapid development of science and technology in the twentieth century has led the development of aerospace industry from the initial exploration stage into strategic stage of industries in the today's world. In this field, due to the harshness and complexity of the working environment, the mechanical properties of engineering materials are required to be very high quality [1] – [5]. Nickel-based superalloys are one of these materials which are widely used in many industrial applications due to their good structural, physical, chemical, and mechanical properties. In addition, they have strong work hardening tendency, low-thermal conductivity and severe tool wear under high temperature and corrosion conditions [6] and [7]. Therefore, nickel-based superalloy has become one of the most superiorly used material in this field, especially it is used to process the core components in the aerospace field, such as axles in rocket, aircraft and other spacecraft engines [8] and [9].

However, nickel-based superalloys have special physical properties that make them difficult to prepare for the final uses, but these difficulties of preparing can be handled with special technics. Because the main causes of the poor cutting performance of superalloy is that the cutting force is relatively high and the cutting temperature is extremely high during the processing. In this regard many experts and scholars paid special attention to these issues of how to process the preparation of these materials. This was achieved through high efficiency and precision during the process of cutting. The machining of metals is often accompanied by a violent relative motion between tool and workpiece which is called chatter vibration. Chatter is a wide range of self-excited vibration caused by dynamic cutting forces existing in tool and workpiece systems; also, chatter is considered from the most obscure and delicate of all problems facing the machinist [10]. In the machining process, chatter is a highly unstable and complex mechanical vibration phenomenon generated, which significantly affect the production efficiency as well as reduces machining accuracy, and produces noise. When high-hardness tools such as ceramics and PCBN are used, they are highly brittle and can be easily chipped after being affected by chatter vibration, and as a result the process cannot be completed [11] – [13]. Therefore, analyzing the mechanism of chattering and studying the influence of cutting parameters stability has important practical significance for processing properties of nickel-based superalloys and the surface quality of workpieces [14].

In the recent time, researchers' attention on nickel-based superalloys mainly includes a cutting mechanism, processing performance, tool wearing, and so on. However, there is less attention on the problems of chatter stability that generated during the cutting process, therefore, in this work, we will investigate the chatter stability prediction, and chatter control techniques during the cylindrical turning of nickel-based superalloy

GH4169. firstly, the status of the previous search results was summarized. Then the following procedures were carried out: a theoretical analysis for the cutting chatter mechanism and the cutting stability, the vibration mechanics model and a simulation model of turning regenerative vibration which established in some studies. Through the modal hammering and cutting test, the kinetic parameters required for the simulation of the system are obtained, and the limit cut width is predicted. The turning test of the nickel-based superalloy GH4169 is analyzed, the influence of cutting parameters on stability and surface quality of workpiece is obtained. The obtained results provide a reference for improving process efficiency and improving the actual process quality.

1.2 Research Methods Compared with Previous Research Studies

The difficulties faced in the materials cutting and the wide range of its application has brought the researchers attention to study the influences of the chatter on the efficiency of the materials cutting quality, many experts and scholars across the world have been conducting active researches in this field. However, there are still sub-problems and deficiencies. According to the reviewed and summarization of reported previous research studies in the field and therefore the current research we aimed to provide a comparable study with the previous researches in three aspects: a model of cutting chatter mechanism, chatter control and prevention, and cutting process of nickel base superalloy.

1.2.1 Research Status and Mechanism of Cutting Chatter

In the cutting process for the machine tool, the cutting vibration is generated by the interaction between the tool and workpiece. That is, which divided into four categories according to vibration characteristics differences: free vibration, self-excited vibration, forced vibration, and random vibration. The self-excited vibration is the strongest, and this vibration refers to the vibration generated by the change of the dynamic force of the cutting system. This leads to the cutting chatter despite the absence of external influences regarding the cutting process.

Research on the problem of cutting chatter can be traced back to the early part of the last century. Taylor E. W. proposed in 1907 that the main cause of chatter is that the generation period of discontinuous chips is the same as the vibration period of a certain part of the machine tool [11]. Although the cause of chatter cannot be simply attributed to this reason, the theory for the studying of cutting chatter has laid a good groundwork. In the past century, according to the physical causes of chatter, cutting chatter has been classified into three main mechanisms: mode coupling effect, friction effect, and regeneration effect. Regeneration effect is considered to be ubiquitous in the machining process, and its theoretical application is the most extensive [15].

The chatter theory based on mode coupling effect was proposed by J. Tlusty in 1981, its mechanism constitutes two actuators of the system that vibrate at two degrees of freedom perpendicular to each other. In this theory, the modal coupling will cause chatter [16]. Gasparetto [17], studied the stability and instability of model trajectories of the tool and obtained the conditions for stable cutting. Kong Fansen [18], and others studied the influence of uncertainties in coupled modes by fuzzy mathematical analysis and obtained distribution law based on the chatter mode coupling effect.

Friction-type chatter, firstly was proposed by R. N. Arnold in 1946 and provided an experimental result in wide range of speed. Thus, with increase of the cutting speed and decrease of the main cutting force in the direction of cutting speed, the negative friction of the main cutting force will decrease the cutting speed and cause self-excited vibration between the tool and the workpiece [19]. Based on that, many scholars have achieved results in the study of friction chatter [20]. Chen Hualing et al. established a model based on the nonlinear theory and determined the equivalent limit stability of the model by using the equivalent linearization method [21]. In addition, the chatter model created by N. Stelter, which simplifies the tool into a cantilever beam simulated the change of cutting force and cutting speed, and the first two models of the system have been introduced to the diffusion and were verified by experiment [22].

Regenerative chatter which is a troublesome problem nowadays for machine operators to obtain high accuracy and acceptable surface finish, was proposed by R. S. Hahn in 1954. One of the reasons for the occurrence of regenerative chatter was the self-excited vibration caused by the phase difference between the previous cutting and the current cutting in one workpiece [23]. Continuous development of in this field was due to the efforts of many scholars such as Tobias, Tlusty, Merrit. In 1958, Tobias [24] studied the regenerative chatter of the drilling process, and mapped the chatter stability lobe diagram. This extended the research method for milling and turning machines, and laid a theoretical foundation for the research in this field. Tlusty [16], proposed the theory of cutting chatter generated by the regeneration effect and pointed out that the cutting width is one of the factors affecting the regenerative chatter. According to the principles of control theory, Merrit [25] introduced the feedback effect model of machining process. In addition to the linear model of regenerative chatter effect, Hanna [26] studied the nonlinear factors of the cutting process and machine tool structure. Tlusty et al. [16] considered that the increase in vibration causes the workpiece to separate from the tool and causes nonlinear factors. Shi Hanmin et al. [27] studied nonlinear systems by using time-delay differential-difference equations. Wu Ya [28] introduced the theory of forced vibration into regenerative chatter and proposed the theory of forced regenerative chatter by the frequency characteristics of vibration.

1.2.2 Control and Prevention Methods for Cutting Chatter

Based on the in-depth study of cutting chatter mechanism, the effective control, and prevention against the occurrence of cut, the chatter has become an important topic. In recent years, scholars across the world have carried out much research on this topic, which includes the following four aspects:

1.2.2.1 Passive Chatter Control

In early studies on chatter prediction, it has been observed that machining stability can be enhanced by increasing damping of the whole system. Therefore, passive vibration control techniques generally aim to increase damping [29] and [30]. Several kinds of dampers are used, such as Lanchester dampers [31], impact dampers [32] and [33], tuned mass dampers [34] – [36], or vibration absorbers [37] – [41]. As an example, in reference [37] a passive vibration control system using a dynamic vibration absorber mounted on a cutting tool has been developed to suppress vibrations in turning operations. The dynamic vibration absorber has to satisfy two conditions: 1) the natural frequency of the dynamic vibration absorber should be close to the natural frequency of the tool and 2) the dynamic vibration absorber should have a larger damping ratio than the tool. Whereas in most cases a single damper is used. Yang et al. [36] presents an optimization strategy for multiple tuned mass dampers to maximize the minimum value of the real part of the tooltip frequency response function, which is beneficial for stability, see references [42] and [43]. In [44] and [45], the development of a so-called multi-fingered centrifugal damper, which is inserted inside a hollow tool, is discussed. As a result of centrifugal forces, the flexible fingers press against the inner surface of the hollow tool which constrains the bending of the tool.

Passive dampers are relatively cheap and easy to implement and do not require external energy. More importantly, passive control methods never destabilize the system. However, drawbacks regarding the use of passive damping techniques are the fact that the amount of damping which is practically achievable is rather limited. Furthermore, vibration absorbers needed to be accurate. Consequently, lack robustness with respect to changing machining conditions and some other deficiencies with machine tools lead to less promotion and popularization of the method.

1.2.2.2 Active Control of Chatter

Chatter mitigation by active controller design is a growing research field. Active control of chatter in machining processes has been proposed in different ways.

Firstly, different control laws are used. Examples are model-based control procedures based on linear quadratic Gaussian (LQG) and/or optimal control [46] – [51], H_∞-norm based control [52] – [54], and μ-synthesis [55] – [58], and non-modal based active damping procedures, see reference [59], based on positive position feedback [60], acceleration feedback [61] and [62], and velocity feedback [63] and [64].

Secondly, several kinds of actuators are applied, such as active vibration absorbers [49], [53], and [65], active magnetic bearings [55], [56], and [66], piezo-electric actuators [48], [60], [67] and [68], Tefenol-D actuators [61], [62], [69] and [70] and electro-rheological fluids [71] – [73]. An extensive overview of the use of active materials in machining processes can be found in the literature of reference [74].

However, compared with the passive chatter control methods, the active control method is more effective. However, the structure of the machine cutting system is relatively complicated. Due to the need to introduce an external device, and the accurate identification of the control signal the difficulty of control increases. In addition, the additional device vibrates before the control signal, this will increase the instability of the system [50], [75], and [76]. Therefore, the application of the active control method has been very scarce.

1.2.2.3 Active Control of Chatter Online Monitoring Chatter Control

This method refers to the direct measurement and collects vibration signals during the cutting process by using computer technology, sensor technology, and artificial intelligence system. After analyzing the characteristic parameters, the cutting chatter can be controlled early by adjusting cutting parameters online. Variable cutting parameters method can be classified as a semi-active control method, which can suppress the chatter vibration by changing the cutting parameters cutting speed [77], feed rate [78], depth of cut, and the tool angles [79]. Theoretically, the main purpose of the method is to increase the area of the stable cutting area or change its shape by changing the cutting parameters, which can quickly and directly supplement the deficiencies of theoretical analysis. In this regard, a lot of research on the mechanism of chatter and the strategy of changing cutting parameters have been conducted [80]. However, this method has high requirements for the machine feed drive system and the motor servo system, and the versatility of the key equipment is poor, and many related technologies have not been solved. Hence, the promotion of this method has been very limited.

1.2.2.4 Predictive Chatter Control

This method initially predicts the limit of stability of the system by using the chatter theory and then determines the working state at the stable cutting area of the system by adjusting the cutting parameters. Thus, it achieves the suppression of the chattering effect. This method is different from the variable parameter method, in which the range of the stable cutting is changed by changing the cutting parameters, while in this method it remains unchanged, it only works in the stable area. Since this method only needs to adjust the cutting parameters, it has the widest applicability and reflects the important application value. In this respect, Weck M [81], obtained an adaptive control method for face milling by automatically adjusting and setting the cutting parameters. In another research Sata T. [82], obtained a method for predicting and controlling chatter based on the analysis of the influence of dynamic characteristics on cutting stability, the control strategies of cutting speed, feed rate and tool working angle. Bason [83], established a cutting dynamics model based on three-dimensional cutting force in turning process and carried out experimental verification. The results showed that the chatter of the system was the weakest in the direction of cutting speed. Davies [84], implemented computer simulation, which proved that, the analysis of prediction results of intermittent cutting stability is better than continuous cutting. However, their results lack experimental verification. Fofana et al. [85], found that the wear of the tool occurs at the limit or marginal stability of the turning system, and concluded that the stability decreases as the wear amount increases. Zhao Hongwei [86], used the theoretical formula for calculating the change of spindle speed of the lathe with the limit cutting width of the system of regenerative chatter at a single-degree-of-freedom turning and proposed a method for predicting the limit stability of lathe cutting system. On this basis, Li Jinhua [87], developed a special software package for chatter analysis of turning by using numerical simulation technology, and carried out the simulation analysis with relevant test data, and obtained the influence of spindle speed, direction coefficient, coincidence degree, and cutting stiffness on the ultimate cutting width. Zhang Yong, et al. [88], used MATLAB/Simulink software to simulate the regenerative chatter turning model of two-degree-of-freedom, and analyzed the limit cutting width of the system from the point of view of energy supplement. However, the influence of cutting parameters on the regenerative chatter was not considered comprehensively in the model, and no experimental verification was carried out. Based on the regenerative chatter model, Huang Qiang et al. [12], conducted a variable a depth-cut test on 45 steel and found that the chatter occurred at the natural frequency of the tool and workpiece.

1.2.3 Research Status of High-Speed Machining of Nickel-Based Superalloys

A nickel-based superalloy is one of the four high-temperature alloys (iron-based, iron-nickel-based, nickel-based, and cobalt-based), it is ranked first among the four superalloys. The GH4169 alloy (American brand Inconel718) is one of the most widely used nickel-based superalloys [44]. According to the material properties, they are characterized by great cutting force, large deformation, high cutting temperature, serious hardening phenomenon and easy wear of cutting tools, which results in poor processing performance and low machining accuracy. In the thirties of the twentieth century, Salomon [89], proposed the theory of high-speed turning, pointing out that when the cutting speed is increased to a certain extent, the cutting force, and cutting temperature, etc. are decreased. At present experimental research on the cutting performance of nickel-base superalloy and cutting tools is still an area of interest for many researchers. For nickel-based superalloy cutting tools, it is usually required to have high strength, high hardness, good chemical stability and wear resistance. Common tools are carbide tools, high-speed steel tools, coated tools, ceramic tools and polycrystalline cubic boron nitride tools. Because they have different mechanical properties of materials, and they show different characteristics in processing.

High-speed steel tools were first used to process nickel-based superalloys, and their strength and toughness were good, however they have some disadvantages such as poor workability and low efficiency [90]. Ceramic tools and carbide tools come in the second stage. Ceramic tools are characterized by strong wear resistance, high hardness, good chemical stability, and are not easily bonded at high temperatures. Altin [91] used different types of ceramic tools to carry out cutting experiments on GH4169, pointing out that circular blades can withstand higher cutting speed than square blades in cutting. Kitagawa T. [92], compared the cutting performance of two different tools Al_2O_3-Ti_3C and Si_3N_4 and found that when the cutting speed reached 250 m/min, the cutting performance of the former tool was much better than the latter tool. Generally, In the ceramic tools study, their high fragility restricted their widespread application. Although cemented carbide tools are widely used, they can produce large cutting force and high heat during cutting nickel-base superalloy and are prone to plastic deformation and severe collapse. Deng Jianxin et al. [93] compared the cutting performance, and tool wear of Al_2O_3/TiB_2/SiCW ceramic tools and YG8 cemented carbide tools on nickel-base superalloys, they concluded that there was little difference in the wear resistance of the two tools at low cutting speed; while at the high speeds, the latter was less than the previous one. In an experimental investigation carried out Luca Stetner [94], revealed that, the cemented carbide cutters are suitable for low-speed cutting and found that when the cutting speed exceeds 50 m/min, the wear increased by the sharp increase of temperature. They concluded that the coated tools can relieve the wear of carbide tools. Ducros C. [95], compared between uncoated and coated tools, their results showed that the TiN/AlTiN coatings relieved the wear of tools effectively. Arunachalam et al. [96] compared the cutting performance of PVD and CVD coated tools for cutting nickel-based superalloys, they concluded that the hardness of PVD coated tools was higher than that of CVD coated tools and are more suitable for finishing and semi-finishing. Polycrystalline cubic boron nitride (PCBN) is an advanced ceramic tool material which appeared in the mid-1970s principally for the machining of hardened steels (turning, milling etc.). It can also be employed as an advantage for the finishing turning of some nickel-based alloys. PCBN is the second super-hard tool material, and its crystal structure is similar to diamonds, and it is appropriate for cutting, and its characteristics include, high hardness and abrasive resistance, high heat stability, excellent chemical stability, large coefficient of heat conductivity and low friction coefficient etc., [79].

Over the last 15 years, the range and variety of PCBN products increased dramatically. Significant benefits in terms of tool life and surface roughness have been seen with PCBN inserts in the machining of hardened steels and cast iron [97] – [102]. The key advantage and/or benefit associated with PCBN tooling is the possibility of enhancing productivity by employing higher cutting speeds, i.e., within the range of 300-600 m/min, also has a good physical and chemical stability when cutting temperatures reaches 1500 °C [103]. Even at this temperature, it maintains good mechanical property for a long time. It has considerable plasticity, mechanical fatigue and thermal fatigue resistance and corrosion resistance etc., [104]. Compared with the Turning Nickel-based Superalloy GH4169 Using PCBN Cutting Tool, most research on cutting nickel-base superalloy with PCBN tools are mainly focused on cutting force, tool wear, tool life, and cutting temperature etc. This suggests that there are considerable scope and potential for a wider evaluation of cutting nickel-base superalloy with PCBN tools. RS Pawade, et al. [105], used a PCBN tool to test-cut a nickel-base superalloy GH4169. They found that when the cutting force is $v = 125\sim475 m/min$, feed rate $f = 0.05\sim0.15 mm/r$, cutting depth $ap = 0.15\sim1.0 mm$, the radial force and the feed force were approximately equal, and tangential force was $1/3\sim1/2$. Peng Ruitao, et al. [106], proposed a method for active control of cutting force, chip shape and surface quality by using different prestressing conditions through the development of the axial prestressing device. Barry and Tiffe [101] and [107], studied the chips generated during machining and indicated that when the cutting speed increases within a certain range, the chip shape changes to serrated, and the chips become more serrated with the increasing feed rate and cutting depth. Costes et al. [101], studied the wear process of PCBN cutting tools in detail through energy spectrum analysis, they found that the elements of the tool and the workpiece were overlapping with each other, and the tool wear was mainly diffusion and bonding.

In summary, the studies on Nickel-based Superalloy mainly includes cutting mechanism, machining performance, tool wear and other aspects, however the studies on the influences of the chatter on the efficiency of the materials cutting quality and the problems of chatter stability that is generated during the high-speed cutting process are scarce. Therefore, it is very important to analyze the mechanism of chatter, study the influence of cutting parameters on the chatter stability, improve the machining performance and improve the machining quality and surface finish.

1.2.4 The Major Problems Currently in Existence

Although experts and researchers across the world have achieved satisfactory results in the research of cutting chatter and nickel-based superalloy processing, there still exists the following problems and deficiencies:

(1) At present, the research on cutting nickel-base superalloy mainly focuses on the cutting mechanism, tool wear and surface quality, however there is lack of relevant research experiment on the chattering problem when cutting nickel-base superalloy at high-speed using high-hardness cutting tools such as PCBN tools, and also there are no clear conclusions on the influence of cutting parameters on cutting vibration.

(2) In the current regenerative turning chatter model, most of the researches were based on a single-degree-of-freedom system that only considers the radial feed direction. However, in actual machining, the vibration of the tool system in the axial feed direction will also have a

significant effect on the machining quality of the workpiece surface, and there is still a large possibility for the occurrence of cutting chatter. However, the determination of the direction of the main vibration of the cutting tool system has not been thoroughly studied.

(3) In the prediction of the turning chatter stability limit, a fast and effective simulation prediction method has not been established, which would help to obtain the stability characteristics of the cutting system quickly and intuitively according to the cutting parameters, and thus the optimization of the cutting parameters can be realized.

In view of the aforementioned problems, this research focused on the numerical and experimental analysis of evaluation of regenerative chatter stability of high-speed turning of nickel-based superalloy GH4169 using PCBN cutting tool.

1.3 Research Objectives

With the wide application of nickel-based superalloys, problems related with the cutting chatter processing have become a serious problem affecting the processing efficiency and the machining accuracy. Therefore, the study on the influence of cutting parameters on chatter to improve the processing properties of nickel-based superalloys and the surface quality of workpieces by analyzing the machinability of chatter generation is very crucial. This research focuses on the principles and methods of metal cutting, cutting chatter theory and cutting test using MATLAB/Simulink software. In this regard, the influence of cutting parameters on cutting chatter stability and surface quality during high-speed turning of nickel-base superalloys with PCBN tools were studied and the following are the major objectives of this work:

(1) Based on the generating mechanism of vibration and chatter in cylindrical turning, a two-degree-of-freedom dynamic model of turning regenerative chatter in the axial feed direction and radial feed direction was established, and the stability criterion of machine tool cutting system was determined. Moreover, the limit cutting width of the machine tool cutting system was calculated, and the factors that influence vibration characteristics of the machine tool cutting system were analyzed using computer simulation.

(2) Based on the accurate vibration mechanics model of turning regenerative chatter developed , the dynamic parameters of cutting system such as (natural frequency ω_n, stiffness k, damping ratio ζ) and the kinetic parameters (unit cutting force coefficients k_{cu}, k_{cv}) for a cutting process of nickel-base superalloy were determined using the hammering modal test and orthogonal cutting test, the limit stability cutting width (b_{lim}) of nickel-base superalloy was also calculated, and the hammering test of other main parts of the machine tool was also carried out to provide a basic system for determination of the main vibration of the system.

(3) MATLAB/Simulink platform was used to design a two-degree-of-freedom turning regenerative vibration model, and a method to effectively determine the cutting state according to cutting parameters was also

developed. The simulation model was used to predict the stable limit cutting depth of the nickel-base superalloy and determine the main vibration direction of the chatter during the cutting process. Based on the numerical simulation results, the influence of cutting parameters (cutting speed, feed rate, and cutting depth) on the vibration characteristics of cylindrical turning under the effect of regeneration chatter was investigated.

(4) The influence of cutting parameters (spindle speed, feed rate, and cutting depth) on the vibration characteristics of nickel-base superalloy with PCBN tools for high-speed turning were studied using cylindrical turning test along with numerical simulation. Moreover, the accuracy of the main vibration system and the predicted limit cutting width of the nickel-based superalloy were verified by the cutting depth test.

The analysis results showed the surface roughness varies with the cutting parameters under the effect of machining vibration.

Chapter 2

Literature Review

2.1 Introduction

With the development of science and technology, scientists begin to focus on the machinery's precision and efficiency. This means, meeting the criteria for the high-performance process and acquiring high quality manufactured materials in manufacturing processes. The vibration would undoubtedly occur during the turning and would impact the precision and efficiency of the operation [108] and [109]. This is usually triggered by the extreme self-exciting vibrations between the cutter and the work piece, which is often called chatter. This indicates that, chatter has been the biggest challenge to improve the capacity of a lathe machine to produce high-quality products. Therefore, it is very important to study and evaluate chatter during turning process [110] and [111]. Chatter reduces the tool's life and impacts productivity by impairing the ordinary working of the machining process. The issue has been affecting the production sector for a long time and has been a popular subject for research in academia and the industry. Since then, many researchers have studied the tool chatter for turning operation to detect, characterize and suppress it. This chapter discusses some of the important contributions in the area of tool chatter analysis with an emphasis on turning operations. Generally, the complete review is classified in two methods of chatter stability prediction: Analytical and Experimental Techniques.

2.2 Analytical Techniques for Chatter Stability Prediction

Different methods for analytical chatter stability prediction are available in the literature. The most commonly used techniques in the literature such as construction of stability lobes diagram (SLD), Nyquist plots and finite element method are reviewed critically here. Because of their simple and clear definition of stable and unstable cutting states, SLD construction is the most popular technique among researchers. The SLD can be produced for mathematical models containing any number of DOF (Degrees of Freedom) cutting processes.

2.2.1 Stability Lobes Diagram (SLD)

The most critical cutting parameter that defines chatter production in the process of turning is the cutting depth (i.e., chip width) b. When the chip width is smaller, the cutting process is more stable. By increasing the width of the chip, chatter begins to appear at a certain chip width b_{lim} (i.e., limiting depth of cut). It also becomes more powerful for all $b > b_{lim}$ values. b_{lim} is therefore the most critical parameter for cutting stability. The value of b_{lim} depends on the structure's dynamic characteristics, the workpiece material, cutting speed, feed rate, and the geometry of the tool [112]. In turning process, SLD can be used to predict chatter stability. Figure 2.1 depicts a typical plot of the limiting depth of cut b_{lim} versus spindle speed (N) on the SLD. Vibration between the tool and work-piece appears as various lobes $(n = 1, 2, 3 \ldots)$ and any depth of cut and spindle speed combination which falls below these lobes results in a stable (i.e., chatter-free) operation and above these an unstable (i.e., chatter) operation. The ideal spindle speed and depth of cutting combinations for maximum metal removal rate (MRR) can be chosen in a turning process with the help of SLDs.

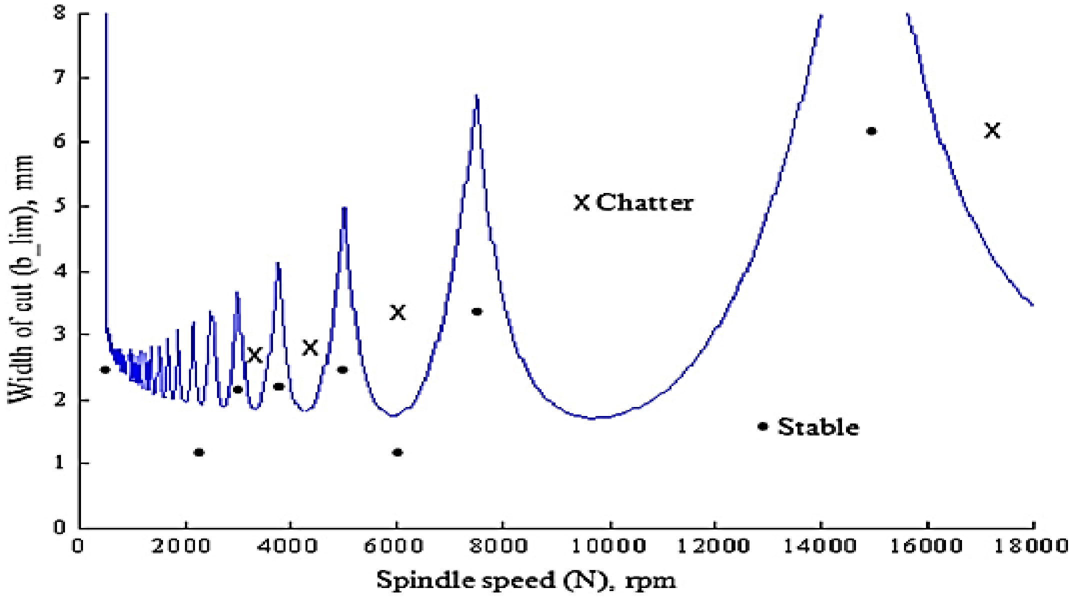

Figure 2.1: Stability Lobe Diagram

Meritt [25], evaluated the stability conditions via stability charts in which chatter can be predicted in terms of system parameters, such as cutting depth and spindle speed. This was a significant contribution as it allowed the material removal level to be improved without chatter by choosing suitable process parameters. The linear stability models of chatter presented by Das and Tobias [43] and Tlusty [113] have taken into account the impact on dynamic forces of instantaneous regenerative chip thickness. Their proposed stability models did not include the entire chip formation process.

Nevertheless, the CIRP team, which was led by Tlusty, found that in turning and other operations, chatter does not result from negative damping of the chip formation process, but from self-excited vibrations due to force-displacement interaction between the machine tool and the cutting process. Analytical modelling can be done to generate SLDs through the consideration of various parameters of the model which are reviewed in the following subsections.

2.2.1.1 Analytical Models Based on the Number of DOF

The SDOF orthogonal process [43] and [114], 2DOF, or 3DOF systems can be used to model a turning process. Analytical prediction of the chatter stability limit for orthogonal cutting is required to achieve critical chatter-free cutting parameters, as well documented by Tobias and Fishwick [115], Merritt [25], Tobias [116], Tlusty, Altintas, and Weck [117]. In most of these studies, the turning tool is portrayed by an SDOF spring-mass system which is cutting a rigid work-piece where the cutting force is linear with the process parameters. The Research undertaken under those assumptions is known as linear stability analysis and/or theory. To understand its effects on chatter stability, cutting tool parameters such as tool angles and wear have been considered in the models. An SDOF time delay-differential equations with square and cubic polynomial terms was reported by Hanna and Tobias [26], the non-linear terms refer to structural rigidity and cutting force. The model has predicted chatter stability, which is impacted in 3 ranges of cutting width such as an unconditionally stable range, a conditionally stable range, and an unstable range. But the work shows quite clearly that, although the cutting process is regarded as stable, there exists unstable periodic movements, that restrict the application of the linear stability theory for manufacturing industries.

Chandiramani and Pothala [118], demonstrated the chatter dynamics with a 2DOF model of the cutting tool, which is too simplified. A change in the cutting width was found to create repeated tool-leaving-cut incidents and increased chatter amplitudes. The frequency of the tool disengagement was increased with cutting speed, although cutting force in the shank direction remained constant over a certain velocity range. The chatter amplitude increases and then decreases as cutting velocity or uncut chip thickness increases. Since chatter vibration is between the tool and the work-piece, models are generally taken into account for both. The shooting method used to compute periodic solutions is inadequate, and certain structural nonlinearities should also have been included in the model in order to make it more accurate. Budak and Ozlu [119] and [120], used several simulations and chatter experiments to compare an SDOF and multi-dimensional stability models. In the cutting system 3DOF models, the effects of the three cutting angles, the insert nose radius and the dynamics of the components were taken into account in all direction. Since these parameters cannot be included in an SDOF model, incorrect results can be obtained. It was also demonstrated that a multi-dimensional solution is necessary when inclination angle or nose radius exists on the tool, since the SDOF stability formulation does not accurately represent the dynamics of the process. Dassanayake [121] used a 3DOF model to investigate tool chatter with turning dynamics and compared it with an SDOF model. The work-piece is modelled in a 3DOF model as a system consisting of three rotors namely, machined, being machined, and unmachined regions linked a flexible shaft. In the simulation of a fine-turning process, it was found that neglecting workpiece vibrations would misinterpret machining dynamics and eventually affect the surface finish and geometric tolerance of the final product. This ensures the vibrations of the workpiece must also be taken into consideration with tool vibration in order to model the turning process more accurately.

Suzuki et al. [122] investigated an SDOF and a 2DOF analytical model by specifying the corresponding transfer function to study the effects of the cross-transfer function and the cutting force ratio on chatter stability. The critical cutting widths in the clockwise (CW) and the counter-clockwise (CCW) rotation processes were found to be significantly different even under the same conditions. Both analytical models based on SDOF and 2DOF systems give the same solutions. SDOF System analysis easily provides the solutions and clarifies the impacts of cross-transfer function and the cutting force ratio on chatter stability. Stability limits were estimated from the corresponding transfer function vector diagram. The

2DOF model was also found to be redundant and not relevant in understanding the process of plunge cutting.

In order to analyse large-amplitude movements, Dombovari et al. [123] investigated a SDOF orthogonal cutting model. The model was developed as a delay differential-algebraic equation (DDAE) and comprises the regenerative effect of the turning process and the non-smoothness when contact between the cutting tool and the work-piece is lost. A simple SDOF model has been used to determine a smooth version with no algebraic effects of the orthogonal cutting system, and shows complex dynamics including disordered oscillation in the process. After analysing these analytical models based on the number of DOFs, the authors find that the development of a two- or higher degree model with no much greater prediction is not worthwhile than the SDOF model. Even a basic SDOF model predicts the chatter stability of the turning process very accurately. Nevertheless, to construct a more practical, multi-dimensional system chatter model would be difficult if all the geometric and dynamic parameters were integrated together with the nonlinear relations between these parameters.

2.3 Turning Operation

There are three principals of machining process that are turning, milling, and drilling. The other operations divided into miscellaneous categories such as planning, shaping, boring, broaching and sawing. This thesis concentrates on turning operation. Turning means that the work piece is rotating during its being machined. Turning operation is one of the oldest and most versatile traditional ways of manufacturing parts that are basically in round shape. The starting material is generally a work piece that made by other methods, such as forging, casting or extrusion. Figure 2.2 below shows the HTM-TC40 CNC turning center which was produced in Haitian Precision Machinery Company Ltd. On the same angled surface, a headstock and carriage are positioned, and the main spindle is supported at 2 points, the front end is equipped with a double row cylindric roller bearing and high-speed circular ball bearing, and the rear end is supported by a super-precise double row cylindrical roller bearing. The high rigid 45-degree inclined bed easy access to workplace for operator and allows fine chip flow. For ground assuring long-life high accuracy and heavy duty cutting, wide bed and sideways was 1.080 mm. The chip conveyor is detached type from machine body to prevent thermal influence of hot chips and coolant. A diameter of tailstock spindle is 160 mm, and the built-in rotating center has ability to support heavy work piece. The travel for hydraulic tailstock spindles is 150 mm. Quil and tailstock body advance/retract and clamping/unclamping were carried out through program commands which save setup time.

Figure 2.2 below shows the basic components of an HTM-TC40 CNC Turning Center.

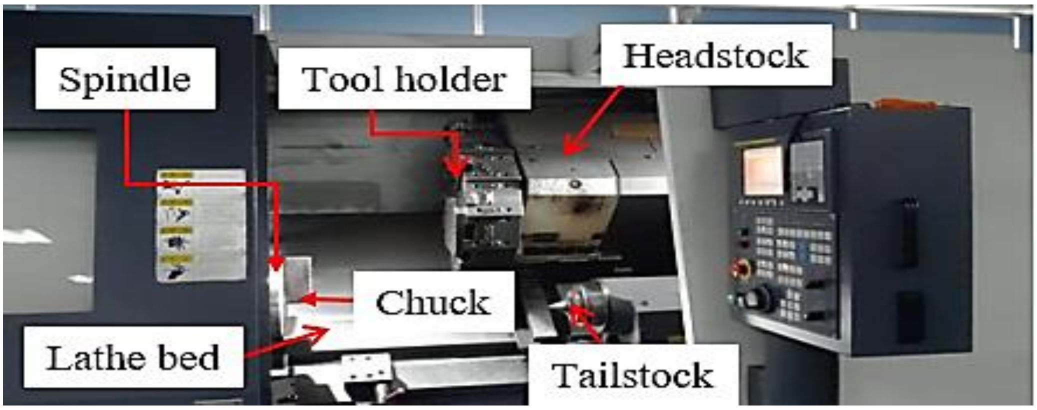

Figure 2.2: HTM-TC40 CNC Turning Center

On a lathe, the tool is tightly kept on a tool post and moves constantly along the axis of the work piece and cuts off a layer metal to form a cylindrical component as shown in Figure 2.3. The tool can be fed either linearly or perpendicularly to the workpiece axis of rotation. The workpiece has a rotary movement while the cutting tool has a linear translation. Figure 2.3 also shows the three components of the cutting force which acts on the rake side of the tool. Normal to the cutting edge is called the tangential force, P_y. This is normally the largest of all three elements and acts towards the direction of cutting velocity. The force element that acts on the tool parallel with feed direction is known as feed force, P_x. It acts normally in the direction of the main cutting forces P_y. The third element, P_z in simple turning operation is the smallest of the force components and tends to drive the tool away from the work radially.

The cutting speed (V) is the rate by which the uncut work surface passes through the tool's cutting edge, usually expressed in units of m / min. The speed at which the metal is removed by the tool from the workpiece is the cutting speed of the tool. The cutting speeds are usually between 3 and

200 m / min, [124]. The speed of cutting can be determined using the following formula (Equation (2.1)):

$$V = \frac{N\pi d}{1000} \qquad (2.1)$$

where V is the cutting speed (m/min), N is the spindle speed (rev/min) and d is the work piece diameter. Since d is constant, the speed therefore varies based on the spindle speed in which it is generally first determined prior to the actual turning operation according to G. S. Upadhyaya study [124].

The feed rate (f) is the distance that the tool travels in axial direction at each workpiece's revolution. With a very heavy cutting rate, the feed rate can reach up to 2.5 mm per revolution, and it can reach as low as 0.0125mm per revolution as stated by [124]. Equation (2.2) is normally used to calculate the feed rate;

$$Feed\ rate\ =\ feed\ \times\ N \qquad (2.2)$$

where N is the spindle speed (rev/min), feed is in mm/rev and the unit of feed rate is in mm/min. The depth of cut (w) is the thickness of the metal removed from the work piece in the radial direction. The distance from the machined surface to the uncut surface of the work piece is the perpendicular depth of the cut. A cutting depth can range from zero to over 25mm. Equation (2.3) is sometimes used to define a depth of cut;

$$depth\ of\ cut = \frac{d_1 - d_2}{2}$$

where d_1 is diameter of the work surface before cutting and d_2 is the diameter of the machined surface. The unit of a depth of cut is in mm.

The rotational speed (ω) is the number of complete rotations, turns, revolutions, cycles or rotational turns per unit time. It is a cyclic frequency, measured in radians per second or in hertz. Equation (2.4) is used to define a rotational speed;

$$\omega = \frac{v}{r}$$

where v is a tangential speed and r is a radial distance.

Figure 2.3 below shows the kinematic schematic illustration of a turning operation.

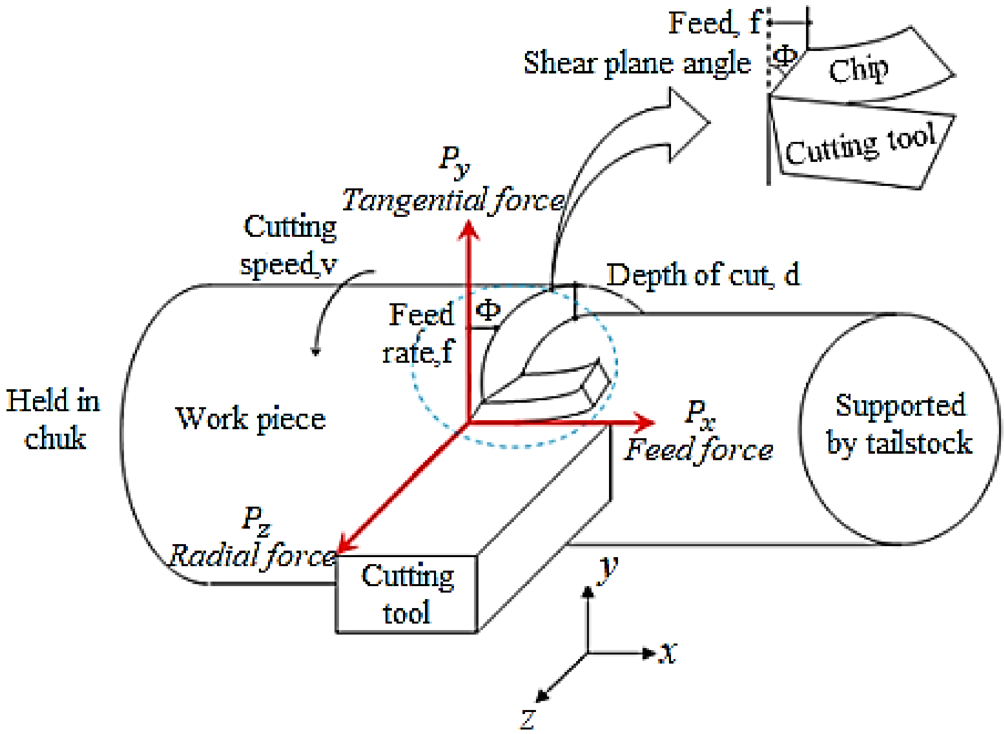

Figure 2.3: Schematic Illustration of a Turning Operation

2.4 Vibration in Machining

Machining vibrations are complex phenomena. Work pieces are cut and removed in separate sections during machining. Whenever the cutting tool takes a bite, it exerts a force on the work piece not instantly there. By deflecting or compressing molecules closer together, the work piece responds to that force and generates a mechanical stress. The mechanical stress runs through the entire work piece and the work piece works like a spring to deflect and then return into shape. This describes the phenomenon of vibration during machining process.

Vibration is characterized as any movement that repeats itself after time interval and can be categorized in various ways, [125]. During machining there are two kinds of vibrations that occur: forced and self-excited. Forced vibration is usually caused by a certain amount applied force in the machine tool, such as gear drives, imbalances of machine tool components, misalignment, motors and pumps, [126]. The simple solution to forced vibration is to isolate or eliminate the forcing component. When the force frequency of a machine tool system component is or near the natural frequency, one of the frequencies can be increased or reduced. The vibration amplitude can be reduced through increased stiffness or by a using a damping system.

The force acting on a vibrating system is generally external and movement-independent. Nonetheless, there are systems where the exciting force depends on the movement parameters of the system for example displacement, velocity or acceleration. These systems are termed as self-excited vibrating systems, since movement generates the exciting force itself [125]. The complex interaction of chip removal system dynamics and machine tool structural dynamics results in the self-excited vibration during machining. Chatter is one example of self-exciting vibrations that feeds on itself as the cutting tool passes across the work piece and creates unique loud and unwanted noise. This unwanted noise is known in machining world as chatter noise.

2.5 Chatter Noise in Turning Operation

Chatter noise in machining is complex phenomena too similar to the vibration in machining. Chatter is an abnormal tool behavior which it is one of the most critical problems in machining process and must be avoided to improve the dimensional accuracy and surface quality of the product. Chatter is a harmonic imbalance that occurs between the tool and the work piece because they are bouncing against each other. Chatter can be caused by the tool bouncing in or out of the work piece or the work piece bouncing against the tool, or both. It is not always easy to determine why chatter is happening.

Chatter needs to be taken into account during machining as it causes serious problems in machining instability. One of the most detrimental phenomena to productivity in machining is unstable cutting or chatter. To ensure stable cutting operations, cutting parameters must be chosen in such a way that they lie within the stable regions. Ideally, cutting conditions are chosen such that material removal is performed in stable manner.

However, sometimes chatter is unavoidable because of the geometry of the cutting tool and work piece. Unless avoided, chatter marks leave unacceptable vibration mark on the cut surface finish and may damage the cutting tool as can be seen in Figure 2.4 (a). A clearer picture of the chatter mark on metal work piece is illustrated in Figure 2.4 (b).

Machine tool chatter has long been studied as interesting phenomenon. Chatter is self-excited vibration that occurs in metal cutting. Meanwhile, dynamic stiffness is defined as the ratio of the amplitude of the force applied to the amplitude of the vibration [125]. A machine tool has different stiffness values at different frequencies and changing cutting parameters can affect chatter. Under such conditions the vibration starts and quickly grows. The cutting force becomes periodically variable, reaching considerable amplitudes and when the magnitude of this vibration keeps increasing, the machine tool system becomes unstable. The machined surface becomes undulated, and the chip thickness varies in the extreme so much that it becomes dissected. In general, self-excited vibrations can be controlled by increasing the dynamic stiffness of the system and damping [127].

Figure 2.4 (a) below shows a photograph of Chatter Mark on Stable and Unstable Cut, and Figure 2.4 (b) illustrates with the help of a photograph the Chatter Mark on a Work Piece.

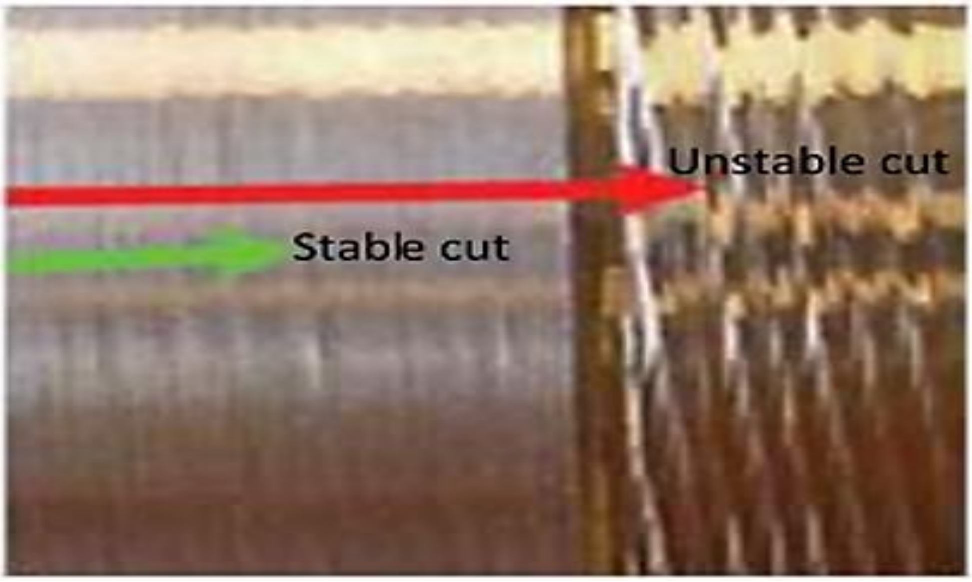

Figure 2.4 (a): Chatter Mark on Stable and Unstable Cut

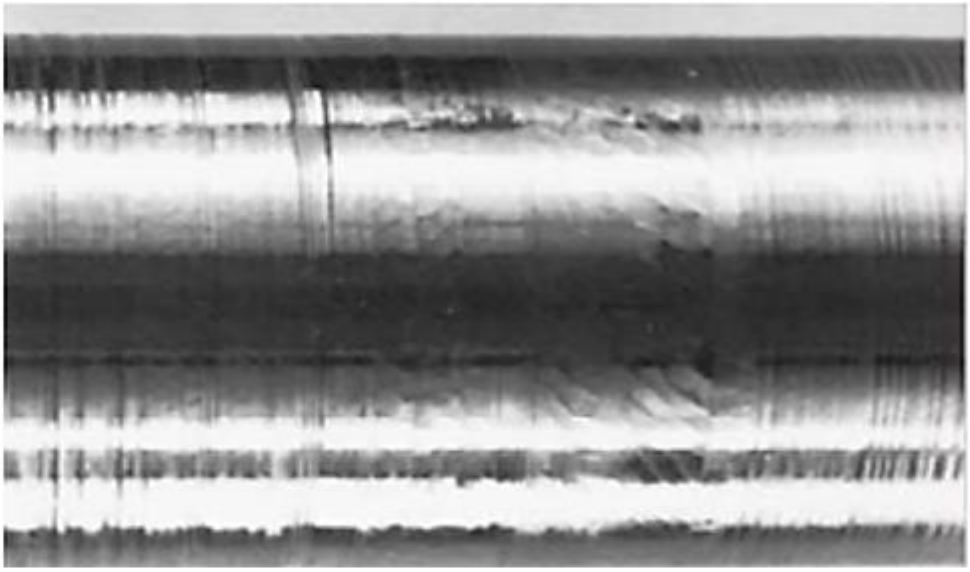
Figure 2.4 (b): Chatter Mark on Work Piece

Almost 100 years ago, Taylor [128], described machine tool chatter or chatter as the most obscure and delicate of all problems faced by the machinist. Chatter significantly affects work piece surface finish, dimensional accuracy, and cutting tool life. In an attempt to achieve high material removal rates, aggressive cutting strategy is often employed in industry. This practice may cause chatter to occur more often in a competitive production environment, and makes chatter research imperative.

Such phenomena of chatter occur during machining is due to material removal process in turning operation where both cutting tool and work piece are in contact with each other. Vibration and chatter noise are suppressed under certain conditions by this dynamic interaction between a rotating work piece and moving cutting forces from the tool. The cutting tool is subjected to a dynamic excitation due to the deformation of the work piece during cutting. The relative dynamic motion between the cutting tool and the work piece produces vibration and chatter thus affects the surface finish. Poor surface finish and dimensional accuracy of the work piece, possible damage to the cutting tool and irritating noise from excessive vibration are the results of uncontrolled vibration and chatter. Thus, vibration related problems are of great interest in turning operations. Furthermore, machine tool chatter is thought to occur for a variety of reasons. Mode coupling and regenerative chatter are two basic mechanisms that cause machine tool chatter and will be explained in the following sections. Tlusty [129], had documented much of the pioneering work in the field. In addition, Tobias and Fishwick [130], were the first to identify the mechanisms known as regeneration chatter. On the other hand, mode coupling was studied by Tlusty, [129].

Another factor that should be considered in machining is machine stiffness. Machine stiffness is recognized as one of the important parameters during machining since low machine stiffness affects the magnitude of vibration during machining (milling, turning, drilling etc.). It can have adverse effects on product surface finish where surface finish is directly affected by a dynamic displacement (vibration) between cutting tool and work piece according to M. Géradin and D. J. Rixen study [125].

2.5.1 Mode Coupling

Mode coupling is recognized as one of the causes of chatter which is often called primary chatter. Mode coupling is a mechanism of self-excitation that can only be associated with situations where the relative vibration between the tool and the work piece can exist simultaneously in at least two directions in the plane of the cut. Usually, mode coupling occurs without any interaction between the vibration of the system and undulated surface of work piece. It acts only within vibratory systems with at least two degrees of freedom, which is due to the fact that the system mass vibrates simultaneously in the directions of the degrees of freedom of the system, with different amplitudes and phase.

Mode coupling is very complex and is inherently related to the dynamics of the cutting process. It may arise from different physical causes such as the dynamical effects of the geometry of the cutting tool on the cutting process. The rotation direction of chatter vibration is an important feature to determine whether mode coupling chatter occurs or not [130].

2.5.2 Regenerative Chatter

Regenerative chatter is renowned as a secondary chatter and it is a self-excited vibration. It is caused by the regeneration of waviness of the surface of the work piece or by the oscillating cutter running over the wavy surface produced from the previous cut. It occurs whenever cuts overlap and the cut produced at time leaves small waves in the material that are regenerated with each subsequent pass of the tool on the previous cut surface [131].

The tool in the next pass encounters a wavy surface and removes a chip periodically. The chip thickness produced varies after each successive cut. This will produce vibration and depending on conditions derived further on, these vibrations may be at least as large as in the preceding pass. Thus, the cutting force, which is a function of the chip thickness, depends not only on the current position of the tool and work piece but also on the delayed value of the work piece displacement. The newly created surface is again wavy in this way the waviness is continually regenerated.

Regenerative chatter is considered to be the dominant mechanism of chatter in turning operations. If regenerative tool vibrations become large enough that the tool loses contact with the work piece, then a type of chatter known as multiple regenerative chatter occurs, [132].

The occurrence and mechanism of chatter in machining has been first investigated by Tlusty and Tobias [129] and [130]. They found that the regenerative chatter is caused by instability of the system. Meanwhile chatter prediction models have a long history that began with work by

Tlusty and Tobias [129] and [130]. These early efforts recognized that the regenerative effect was the main cause of instability, which leads to the development of chatter. Tlusty and Merrit [129] and [133] had discovered that the main sources of chatter come from stability condition of cutter, investigated conditions of stability for the cutter, structural dynamics of machines and feedback of subsequent cuts on the surface of the work piece as the main sources of chatter.

Several theories have been proposed to explain the occurrence of chatter instability for optimizing certain combination of process parameters such as feed rate, depth of cut, rotational speed, variation of chip thickness and variation of cutting force. In the work by Tobias [130], the dynamics of the cutting process were modelled and effects such as process damping were included in their stability model. Tlusty, [129] created a stability condition in which stability limits can be calculated based upon the system dynamics for orthogonal machining. Several dynamic models for regenerative chatter have been put forward, for example in the studies of Altintas and Tlusty [126] and [129]. Early stability lobe diagrams were created by Merrit, [133] based upon feedback control theory to model regenerative chatter. These early studies provided insight into the elementary chatter mechanisms.

In the past, by choosing the appropriate combination of cutting parameters for example, the feed rate, depth of cut, rotational speed, different chip thickness and variation of cutting force to prevent the occurrence of chatter during turning operation.

2.6 Regenerative Chatter Mechanism in Turning Operation

Regenerative chatter is a principal mechanism of chatter in turning operations. Tobias, [130] developed a regenerative machine tool chatter theory where the cutting force is considered to be a function of both the current and previous cuts. The theory is widely accepted as the most appropriate to describe the regenerative type chattering phenomenon, and it has become a foundation of many theoretical and experimental researches regarding cutting processes.

In this section the underlying mechanism of regenerative chatter in turning operation is explained.

Figure 2.5 can be used to illustrate one degree of freedom of regenerative chatter in turning operation.

The work piece is supported at one end by chuck and the other end by tailstock on lathe machine. The chuck is often represented with linear spring. During turning process, the work piece will rotate as it is being machined. The cutting tool movement is parallel to the longitudinal axes of the work piece and depending on the depth of cut. When the cutting tool makes contact with the work piece, it will deflect. As the cutting tool moves along its direction, there will be a variation in the magnitude and the direction of cutting forces because the previous cut leaves a wavy surface finish due to structural vibrations. The developing vibrations will lead to the increase of cutting force thus, resulting poor surface finish, [126].

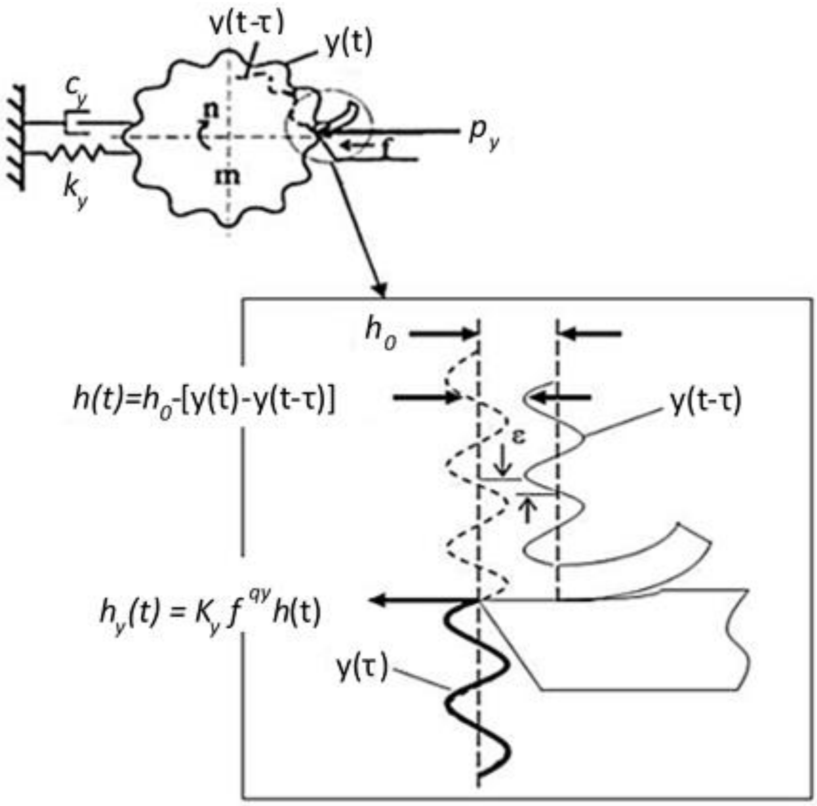

Figure 2.5: Regenerative Chatter Mechanism (Altintas, 2000)

The work piece is free to move in the feed direction and the feed cutting force, P_y applied causes the work piece to vibrate. Presume a single point cutter is fed perpendicular to the axis of cylindrical shaft. During the first revolution, the surface of the work piece is smooth which is without waves but due to the bending vibration of the work piece it will initially leave a wavy surface in the feed cutting force, P_y direction. As a second revolution takes place, the previous surface now has two waves at the inside and outside surface of the work piece. The inside surface denoted as $y(t)$ is originated from the cut made by the tool whereas the outside surface indicated by $y(t-\tau)$ is the effect of the vibrations during the previous revolution of cutting. The wavy surface leads to variable chip thickness, cutting force and vibration. This regeneration of chatter mechanism can be represented in the mathematical form below;

$$h(t) = h_0 - [y(t) - y(t-\tau)] \qquad (2.5)$$

where $h(t)$ is instantaneous chip thickness, h_0 is the intended cut, $y(t) - y(t-\tau)$ is the dynamic of chip thickness and ω is a rotation speed of the shaft (rev/s). The associated time delay is the time period τ of one revolution of the work piece.

$$\tau = \frac{2\pi}{\omega} \qquad (2.6)$$

By assuming the work piece is a one single degree of freedom in the radial direction which consists of mass and spring system, the corresponding equation of motion can be written as below;

$$m_y\ddot{y}(t) + c_y\dot{y}(t) + k_y y(t) = F_f(t) \qquad (2.7)$$

The magnitude of tangential cutting force $P_y(t)$ is proportional to the instantaneous chip thickness $h(t)$.

$$p_y(t) = K_y f^{qy} h(t) \qquad (2.8)$$

where K_y is the cutting force coefficient, f is feed rate (m/rev) and qy is the exponents determined from Han *et al.*, [134] and h is the instantaneous depth of cut. This tangential cutting force not only depends upon the present cut $y(t)$, but also on a delayed value of displacement of the previous cut of the tool $y(t-\tau)$.

2.6.1 Chatter Modelling Theory

To set up a system of dynamic equations for studying chatter onset conditions, a reliable cutting force model, a mechanistic chatter model, and an accurate work piece deformation model are required.

A large body of work has been published in chatter modelling over the last fifty years. Traditional models of the turning process consider a rigid work piece and vibration of the machine tool structure are studied by a few early researchers such as Tobias and Merrit [130] and [133]. Numerous researchers investigated single degree of freedom regenerative tool models such as Kalmar-Nagy Stepan et al. [135], and [136].

Basically, the turning cutting tools are often modelled as a lumped vibration system having one or two degrees of freedom according to Merrit and Lin [133] and [137], for describing motions of the cutting tool in the main cutting force direction or in both radial and main cutting force directions working over rigid work piece. These chatter models developed on the basis of rigid work piece assumption are generally valid for cutting tools having a long tool shank in turning operations.

Chiou and Liang, [138] established a dynamic turning model for cutting rigid work piece with a flexible cutting tool. A comprehensive expression of the equation of motion for the dynamic cutting system incorporating the effects of cutting and contact forces is established. Machining experiments were conducted on a conventional lathe with the use of a specially designed flexible tool which can only vibrate parallel to the feed and perpendicular to the cutting velocity direction. The work piece is cut so as to observe the mechanism of the cutting tool chatter stability corresponding to the continuous variation of width of cut and cutting speed. The chatter stability was observed in verification of the analytical solutions over a range of cutting velocities and width of cuts. Among these cutting conditions, flank wear has been shown to have a significant effect on the chatter stability.

The simplest model that models the tool as a one degree of freedom is underdamped linear oscillator excited by the variation in undeformed chip thickness from one revolution to another, Tobias [130]. The vast majority of these investigations employ a single degree of freedom (SDOF), representing the lumped mass behavior of the cutting tool at the cutting zone. Equation (2.9) describes the motion during cutting for a SDOF cutting tool and a rigid work piece, given as

$$m_y \ddot{y}(t) + c_y \dot{y}(t) + k_y y(t) = F_f(t) \qquad (2.9)$$

where y is the displacement, $F_f(t)$ is a time varying dynamic force due to cutting process, m_y is the mass, c_y is the damping and k_y is the stiffness of the cutting tool. Typically, the work piece is assumed to be rigid and the cutting tool to be vibrates.

Moreover, a two-degree of freedom (2DOF) is defined by a system that requires two independent coordinates to describe their motion. In chatter model, the tool and work piece are modelled as two separate single degree of freedom spring mass damper systems. They are generally in the form of coupled differential equations that is each equation involves all the coordinates. If a harmonic solution is assumed for each coordinate, the equations of motion lead to a frequency equation that gives two natural frequencies of the system. If suitable initial excitation is applied, the system vibrates at one of these natural frequencies. During free vibration at one of the natural frequencies, the amplitudes of the two degrees of freedom (coordinates) are related in a specified manner and the configuration is called a normal mode, principal mode, or natural mode of vibration. Thus, a two degree of freedom system has two normal modes of vibration corresponding to two natural frequencies, [131]. There are some investigations reported previously employing two degree of freedom model of cutting tool to represent the dynamics of chatter. Chandiramani and Pothala, [118] depicted dynamics of chatter with two degrees of freedom model of cutting tool.

Sekar et al. [139] proposed an analytical scheme for stability analysis in turning process by considering the motion of tailstock supported work piece using a compliance model of tool and work. A dynamic cutting force model based on relative motion between the cutting tool and work piece is developed to study the chatter stability. Linear stability analysis is carried out in the frequency domain and the stability charts are obtained with and without considering work piece flexibility. The research proposed a compliant two degrees of freedom dynamic cutting force model by considering the relative motion of work piece with cutting tool. Tool and work piece were modelled as two separate single degree of freedom spring-mass-damper systems. The model allows selection of different operating conditions with and without a tailstock support by accounting the fundamental natural frequency of the work piece. Effect of cutting position, work piece dimensions, cutter flexibility, and cutter damping on the dynamic stability have been presented with the proposed dynamic model.

Dassanayake, [121] investigated different stages of stability of the work piece and tool by simulating three dimensional (3D) models of work piece cutter deflections in response to a nonlinear regenerative force with a method of rotor dynamics. Tool chatter in turning process is addressed with a new perspective. Turning dynamics is investigated using a 3D model that allows for simultaneous work piece tool deflections in response to the exertion of nonlinear regenerative force. The work piece is modelled as a system of three rotors, namely, unmachined, being machined and machined, connected by a flexible shaft. Such a configuration enables the work piece motion relative to the tool and tool motion relative to the machining surface to be three dimensionally established as functions of spindle speed, instantaneous depth of cut, material removal rate and whirling. The equations of motion for the model are coupled through the nonlinear cutting force. The model is explored along with its one-dimensional (1D) counterpart, which considers only tool motions and disregards work piece vibrations. Different stages of stability for the work piece and the tool subject to the same cutting conditions are studied. Numerical simulations reveal diverse, oftentimes inconsistent, tool behaviors described by the two models. Most notably, observations made with regard to the inconsistency in describing machining stability limits raise the concern for using 1D models to obtain stability charts.

2.7 Nickel Based Superalloys

Superalloys are developed for elevated-temperature service, and are considered as one of the most important classes of engineering materials, because they could be used in a wide range of applications. The term, alloys, was first used shortly after World War II to describe a group of materials developed for uses in turbochargers, superchargers and aircraft-turbine engines which require good performance in high-temperature environment. For instances, the Nickel-based superalloys are employed in the hottest parts of machines such as the combustor and turbine [14], [101], [103], and [140] – [142].

The Nickel - based superalloys could be used both at cryogenic temperatures and temperatures approaching $1200\,°\,C\ (i.e., 2190\,°\,F)$, because the matrix of the solid solution of these alloys remains austenitic from solidification to absolute zero, [140]. In addition, these alloys provide useful corrosion resistance. Therefore, their applications appear in a wide range of industries, including Power Generation, Petrochemical, Chemical Processing, Aerospace, and Pollution Control. Superalloys are more specifically used, where high stresses such as tensile, fatigue, toughness and thermal, in combination with corrosion or oxidation resistance are required, and also in other time-dependent exposure phenomena. The reason for the growing use of the nickel-base superalloy is the higher demand of engines for aircraft and space vehicles, marine turbines, naval propulsion generator, nuclear power and chemical processor, [143].

2.7.1 Nickel-Base Super Alloy Classification

In contrast to steels and aluminium alloys, there is no systemic classification system for Ni-base alloys. That is why most Ni-base alloys are identified by their trade names or by the alloy number that the alloy manufacturer initially allocated. For example, INCONEL® alloy 600ii and HASTELLOY® alloy C - 22iii are also referred to as Alloy 600 and Alloy C - 22. Ni - base alloys are generally classified by composition, it is usually consisting of various formulations that made from elements such as nickel, cobalt, iron, and chromium as well as lesser amounts of W, Mo, Ta, Nb, Ti, and A1, which is briefly described in figure 2.6 below.

Figure 2.6 below illustrates diagrammatically the necessary Classification of Nickel - Base Alloys according to the following considerations:

1. Solid solution strengthened.
2. Precipitation strengthened.
3. Specialty alloys.

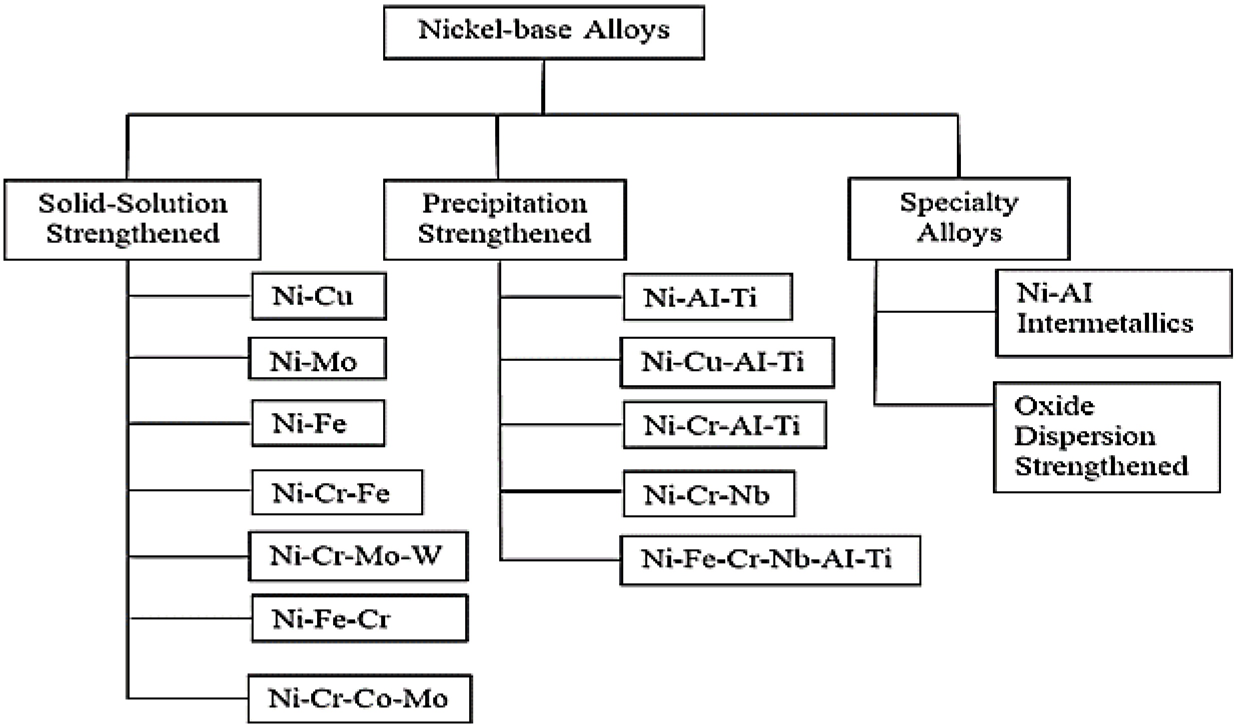

Figure 2.6: Classification of Nickel - Base Alloys

In this study, Nickel based superalloy GH4169. GH4169 superalloy have been selected (according to Chinese classification [25]). It is a Ni-Fe-Cr based superalloy used as blisks material in engines due to its excellent high-temperature properties [26]. Up to 923 K, this superalloy owns excellent mechanical performance owing to the occurrence of strengthening phases such as the γ" (Ni3Nb) phase and γ' [Ni3(Al, Ti)] phase. GH4169 alloy is a precipitation hardened, nickel-based superalloy that is extensively used in the aircraft engine industry. Rotor components, such as compressor disks, spools as well as turbine disks, compressor blades and power drive-shafts are typically fabricated from this alloy. The GH4169 alloy could provide operational conditions up to a maximum useful service temperature of about 650 ^{0}C to meet the requirements of the rotor components.

2.7.2 Properties of Nickel - Base Alloys

A large fraction of the turbine engine consists of nickel-based superalloys due to a good combination of physical and mechanical properties [26]. Typical physical properties of nickel-based superalloys are presented in Table 2.1.

Table 2.1: Typical Physical Properties of Nickel-Based Superalloys

Property	Typical Ranges
Density (g/cm^3)	7.92-9.21
Melting temperature (liquidus)	1290-1425ºC
Specific heat (j/kgK)	389-523
Electric resistivity $(n\Omega.m)$	148-1380

2.7.3 Industrial applications

Superalloys have been developed with specific properties that relate to their applications. The consumption of superalloys in the aerospace industry accounts for approximately $\sim 70\%$ with the rest utilized in chemical, structural and medical applications, see Figure 2.7 (a) [121]. Figure 2.7 (b) highlights the fact that use of composites in aero engines has increased dramatically over the past decade due to their low density and good stiffness, however nickel-based superalloys are still the most widely used material in aircraft engines, and currently accounting for $\sim 40\%$ of engine weight followed by titanium.

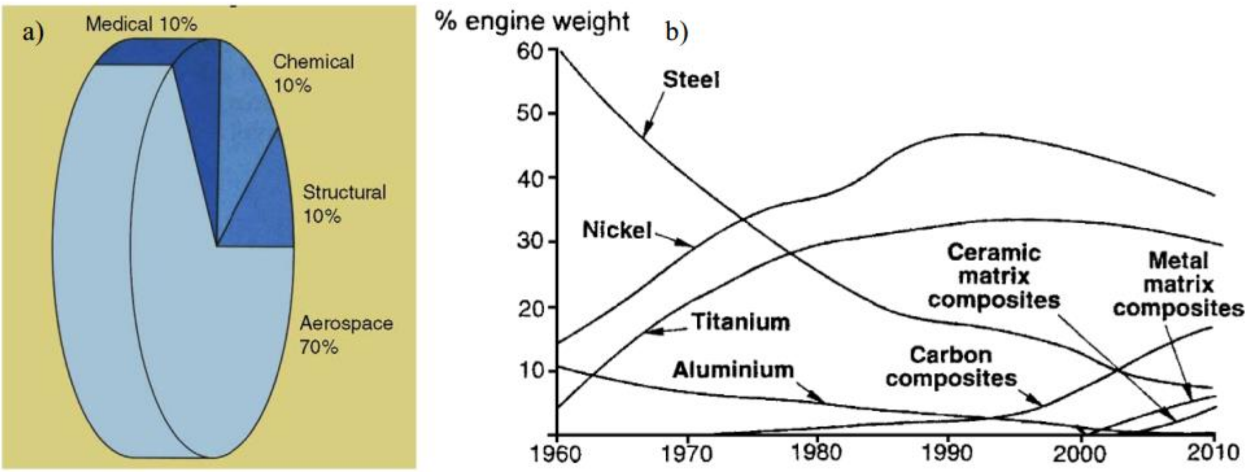

Figure 2.7: (a) Consumption of Superalloys [3] and (b) Materials Utilization in Aircraft Engines

2.8 Polycrystalline Cubic Boron Nitride

Polycrystalline cubic boron nitride (PCBN) is next to diamond on the hardness scale. It is used in the manufacturing industry as a super hard abrasive tool and as a cutting tool. As a cutting tool, PCBN is most commonly used for the machining of hardened steels, tool steels, hard cast irons, and hard facing alloys.

PCBN products can be characterised by the content of CBN and the secondary phase which can be a metal (Ni-Co alloy), carbide (TiC or WC) or ceramic (TiN, AIB2/AlN) whose proportion can vary from $\approx\ 5\ to\ 70\%$. The secondary phase may not act like a binder phase, as in a conventional cemented carbide, but serves to fill up porosity in the polycrystalline structure and in some cases provide an electrically conducting network to aid fabrication. The secondary phase can also extend the range of application of PCBN especially for finishing operations. The majority of products have a grain size between 1-3 μm.

Given below are details and characteristics of the most commonly available PCBN products according to manufacturer. N.B. There are a number of other PCBN products produced in the CIS (formerly USSR) (e.g., Yamit, Kompozit, etc.), PR China (e.g., LDP-J-CFII, FD, DLS-4, etc.) and Japan (Sunnite, QBN, JBN, Wurzin, etc.) [126], which have not been covered in this review.

2.8.1 Brief History of PCBN Development

Boron (B) and nitrogen (N) can form the boron nitride compound, which is a soft hexagonal substance like hexagonal carbon (graphite). Just as hexagonal carbon can be transformed into cubic carbon (diamond), hexagonal boron nitride (HBN) can also be transformed into cubic boron nitride (CBN). In the late 1950s, cubic boron nitride was first synthesized from hexagonal boron nitride under high-pressure and high-temperature process [144], Polycrystalline cubic boron nitride (PCBN) is produced by sintering many individual crystals of CBN together to produce a larger polycrystalline mass.

Applications of PCBN cutting tools have witnessed dramatical changes since they were first introduced in the 1970s' to meet machining requirements for a variety of work materials, especially for hardened steels, cast irons, and powder metals, [145]. Various grades of PCBN inserts were developed. Coated PCBN inserts improve tool life-time and provide excellent adhesion between the coating and the PCBN substrate interface [146].

2.8.2 The Properties of PCBN

The thermal conductivity of solid PCBN cutting tool materials has an exceptionally high value: $100\ W\ /\ m.K$, which is approximately the same as C-8 or K10 tungsten carbides and 4-5 times higher than that for ceramic cutting tool materials. For machining ferrous workpiece materials, PCBN is thermally stable. Thermal conductivity of polycrystalline diamond (PCD) cutting tool materials is nearly five times higher than that of PCBN, but is unusable for machining of ferrous workpiece materials. At moderate temperatures, PCD reacts with ferrous material and is subject to graphitization.

A selected mechanical property of PCBN, PCD, and other tool materials are summarized in Table 2.3.

Table 2.3: Properties of PCBN and Other Tool Materials

Cutting Tool Material	Knoop Hardness, GPa	Compressive Strength		Fracture Toughness	
		$ksi \times 10^6$	GPa	$Ksi - sqrt(in)$	$MPa - sqrt(m)$
Al_2O_3	16	0.580	4.00	2.12	2.33
Al_2O_3-TiC	17	0.653	4.50	3.01	3.31
Sialon	13	0.508	3.50	4.55	5.00

Tungsten carbide (K10)	13	0.653	4.50	9.83	10.80
Solid PCBN (Amborite)	28	0.551	3.80	5.73	6.30
Layered PCBN	28	0.515	3.55	3.37	3.70
Solid PCD	50	0.687	4.74	6.27	6.89
Layered PCD	50	1.102	7.60	8.01	8.80

The fracture toughness of solid PCBN tools is greater than those of ceramically made tools, as shown in Table 2.3. Solid PCBN is also better than sialon in terms of compressive strength. It means that PCBN tools can take heavier cuts than ceramic tools. The percentage of CBN particles and grain size are among the variables that influence a PCBN grade performance. The CBN content of the majority grades varies between 45% to 90%. Grain sizes vary from 8 µm (315 µ in.) for coarse-grain tools, to submicron size for fine-grain tools. A high particle concentration increases compressive strength, toughness and resistance to wear and offers greater thermal conductivity. High CBN content material tools are therefore appropriate for roughing applications. Low-content CBN tools are less thermally conductive and keep sufficient heat in the workpiece. The heat softens the workpiece at the cutting area and allows the tool to use less energy in order to separate the chip from the parent material. For finishing operations, tools with lower CBN amounts are recommended. Figure 2.9 below shows the crystal cell of CBN.

In general, due to the good physical and chemical properties of PCBN, it is suitable for processing many types of high-hardness materials, such as nickel-based superalloy.

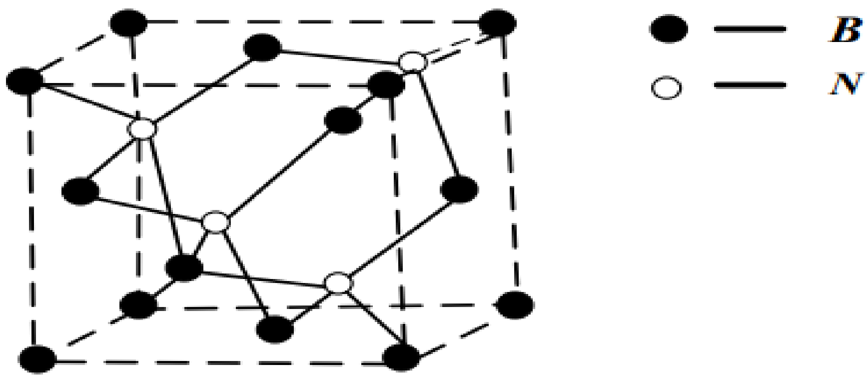

Figure 2.9: CBN Crystal Cell

2.8.3 Application of PCBN Tool

The principal applications of PCBN reflects its ability to maintain its hardness at high temperatures (Table 2.4 [118], [121], and [139]) and its relatively low solubility in iron, such that it is the most suitable tool for cutting hard ferrous alloys and some cobalt and nickel-based superalloys. George [147] asserts that while these properties afford long tool life in comparison with cemented carbide and conventional ceramic tool materials, it offers other production advantages in respect of component quality, operating costs and working conditions. In addition, when PCBN tools are used, the processing efficiency can be improved, and the processing cost can be saved by more than 50%. Higher capital cost PCBN tools can improve the stock removal rate by employing higher cutting speeds, i.e., within the range of $300 - 600\ m/min$ [103] and [142]. This significantly reduce finish machining time and provide a competitive alternative to coated carbide tools. Moreover, PCBN cutting tools can also be used for precise cutting of non-ferrous metals and sintered metals, etc., [148]. Due to all these stated benefits, the use of PCBN tools has increased in the machining of nickel alloys. A summary of PCBN application is shown in Figure 2.10.

Table 2.4: Tool Material Properties

Tool Material Property	PCBN
Typical composition*	98% CBN+2% AlB_2/AIN
Density (g/cm^3)	3.1
Hardness at RT (HV)	4000
Hardness at 1000 °C(HV)	≈ 1800
Fracture toughness (MPa $m^{1/2}$)	10
Thermal conductivity (W/m °C)	100
Young's modulus ($kNfmm^2$)	680
Coefficient of thermal expansion ($x10^{-6}$ /K)	4.9

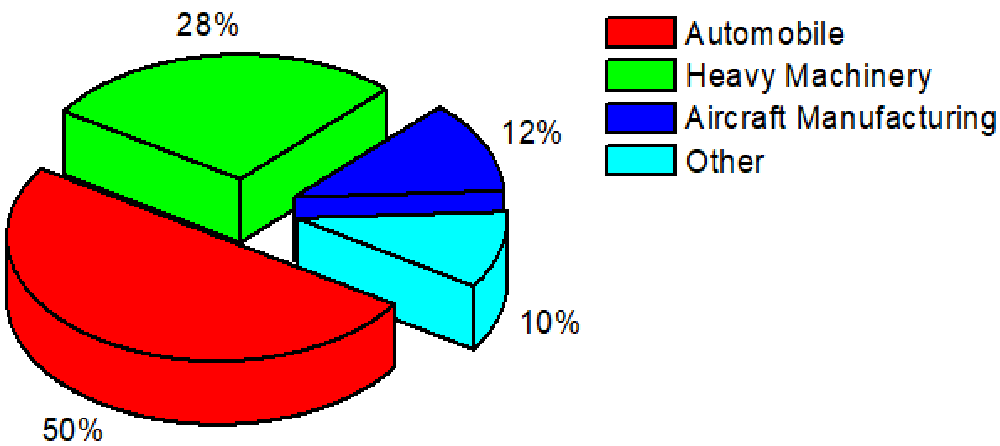

Figure 2.10: Usage of PCBN in Various Fields of Application

2.8.4 Performance of PCBN Tool

PCBN cutters are the main new type of cutters that are employed in hard-to-machine materials. The super hard cutting tools first appeared in the 1950s and 1960s. They are mainly divided into polycrystalline diamond cutting (PCD), and polycrystalline cubic boron nitride (PCBN) cutting tools. PCBN tool is the second super-hard tool material synthesized manually [148].

In recent years, new PCBN production has emerged, such as Shangao CBN100 series and CB7015 series. The CB7015 series developed by Sweden's Sandvik Company which greatly improved the processing efficiency after the combination of a new blade safety lock and high hardness materials. The good cutting performance of PCBN tool makes it suitable for different difficult-to-machine materials: hardened steel, hard cast iron, nickel-based superalloy, etc.

PCBN tools are used for high-speed machining of nickel-based alloys in order to improve the machining efficiency, also PCBN tools are conventionally used for hard turning, interrupted cutting and high-speed machining of hard cast iron, quenched steel, because of its high hardness up to HV 3000 – 5000, resistance to wear, good red hardness, thermostability and chemical inertness, low-friction coefficient and high-thermal conductivity [121] and [139]. Turning nickel-based alloys using PCBN tools was investigated frequently in recent years. Chandiramani and T. Pothala et al. [118], chose 27 types of PCBN tools for the Inconel 718 (similar to GH4169 Chinese grade) turning test, in order to study how the binders and CBN contents affected the tool life. The results showed that insert with fine grains, lower CBN content ($< 65\%$) and ceramic binder would have the longest tool life. The research conducted by Barton et al. [126] and [136], also showed that PCBN tools with low-CBN content could obtain longer tool life and better surface roughness than the binder less ones under the turning speed range of $300 - 480\ m/min$. In finish turning Inconel 718 with low-CBN content inserts, it was found that the most significant factor which affected the tool life was the cutting speed, then the feed rate and finally tool geometry. The dominant tool wear mechanisms were adhesive wear, diffusion wear, and abrasive wear [118] and [136]. In addition, the quality of the machined surface was another highly concerned problem in the high-speed machining of nickel-based superalloy with PCBN tools. B. I\cs\ik. [127], observed that surface roughness R_a below $0 \cdot 5\ \mu m$ was achieved possibly in turning Inconel 718 using PCBN inserts with modified edge at $500\ m/min$. Taylor et al. [128] also found that the honed plus chamfered cutting edge was conductive to reduce cutting forces greatly and surface damage, and then contribute to generate good surface integrity. It was noted that compressive residual stresses or low-residual tensile stresses and good surface roughness could be produced when facing of age hardened Inconel 718 using round PCBN inserts under the cutting conditions of cutting speed $150\ m/min$, small depth of cut $0 \cdot 05\ mm$, feed rate $0 \cdot 15\ mm/rev$ and sufficient cooling [129].

All the researches mentioned above are related to turning nickel-based alloys with PCBN inserts. However, the studies of turning operations using PCBN mainly concentrate on cast iron [130], cold-work tool steel [132] and titanium alloys [134] and [135]. Studies of PCBN tools in turning nickel-based superalloys were not sufficiently carried out. Thus, the present experimental work focused on the high-speed turning process of nickel-based superalloy GH4169 using PCBN tools. The aim of this research was to investigate the effect of cutting parameters (cutting speed, feed rate, and cutting depth) on cutting forces, workpiece surface roughness, and amplitude. Based on the numerical simulation results, the research also investigated the influence of cutting parameters on the vibration characteristics of cylindrical turning under the effect of regeneration chatter.

Moreover, the research focused on the influence of cutting parameters on the vibration characteristics of nickel-base superalloy with PCBN tools for high-speed turning using cylindrical turning test along with numerical simulation. In addition, this research carried out hammering modal test and orthogonal cutting test to calculate the limit stability cutting width (b_{lim}) of nickel-base superalloy and other main parts of the machine tool thereby to provide a basic system for determination of the main vibration of the system. In this research a two-degree-of-freedom dynamic model of turning regenerative chatter in the axial feed direction and radial feed direction was established to determine the stability criterion of machine tool cutting system and the cutting limit width of the machine tool cutting system was calculated, and finally a computer simulation analysis was made to investigate the factors that influence vibration characteristics of the machine tool cutting system.

Chapter 3

Mechanism Analysis and Study of Regenerative Chatter Stability

3.1 Introduction

Chatter vibrations are present almost in all cutting operations, and they represent the major obstacles in the way to achieve the desired productivity. It is well known that regenerative chatter is the most important form of vibration which deleteriously affects the machining process [149] and [150], due to its creation of excessive vibration between the tool and the workpiece. Thus, it leads to a poor surface finish, high-pitch noise, and the accelerated tool wear. All those reduce the lifetime of machine tool, and affect the safety of the machining operation. There were various techniques proposed by several researchers to predict and detect chatter, and avoid chatter occurrence in the cutting process to obtain better produced surface finishing, higher productivity, and longer lifetime for the used tool [151]. Fofana et al. [85] investigated machining stability in turning by using progressively worn tool inserts. It was demonstrated that tool wear and dynamic instability are both due to the combined effect of the contact and friction mechanisms between tool – workpiece, tool – chip and workpiece – tool – machine interactions, which lead to the occurrence chatter. The cutting force interaction between the tool and the workpiece produces vibration. When the vibration of the tool introduces a scratched line on the workpiece, the cutting process must be performed again on workpiece. The phase difference of regeneration produces two parallel lines from the cutting processes, this is an important factor that affect the machine tool cutting system. Therefore, in this chapter, we analyzed the mechanism of regenerative chatter, and discuss the factors that will influence the cutting machine system stability.

3.2 The Mechanism of Regenerative Chatter

3.2.1 Chatter Overview

The Chatter is the most obscure and delicate of all problems facing a machinist [11]. Although this statement was made by F.W. Taylor over 100 years ago, it still remains valid today. Chatter is an instability phenomenon that not only occurs in milling but also in other machining processes such as turning, drilling and grinding. Chatter results in large vibrations between the tool and the workpiece which in turn results in a nonsmoothed surface of the workpiece. This can be seen in Figure 3.1, where pictures of the resulting workpiece for a cut with and without chatter are given.

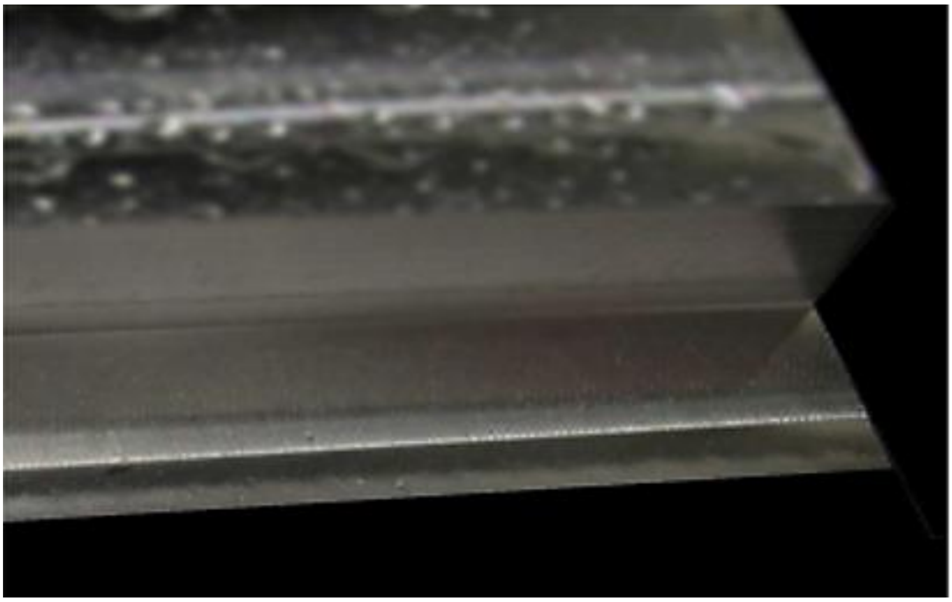

Figure 3.1(a): Detail of a Workpiece Without Chatter Marks

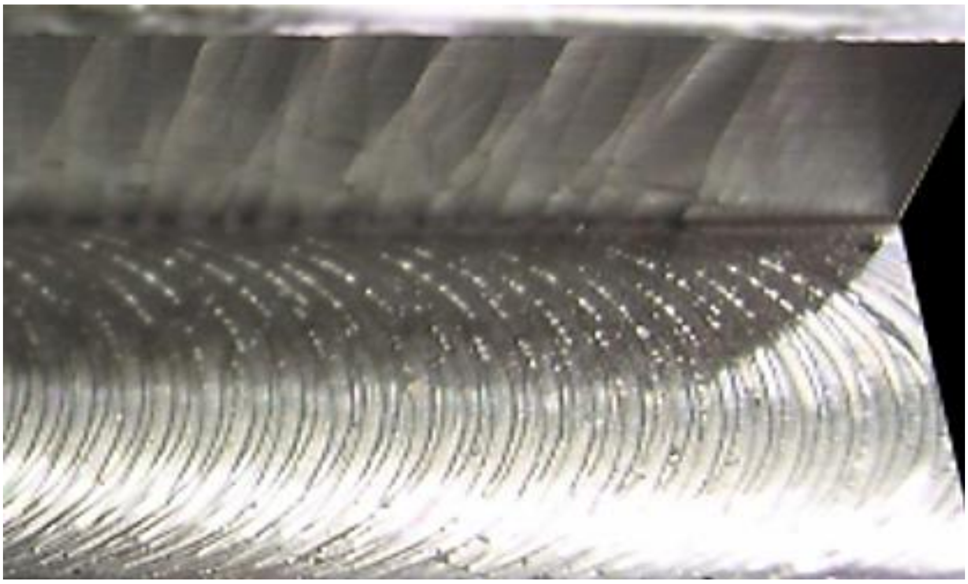

Figure 3.1(b): Detail of a Workpiece with Chatter Marks

Figure 3.1: Detail of a Workpiece Without and With Chatter Marks

Next to a nonsmoothed surface, chatter results in rapid wear of spindle and tool and the production of a significant amount of noise. In principle there are four mechanisms that describe the occurrence of chatter [152]. Firstly, chatter may occur due to variable friction between tool and workpiece [153]. Secondly, mode-coupling chatter exists when vibrations in e.g., the feed direction generate vibrations in the direction normal to the feed direction [153] and [154]. A third mechanism is due to thermo-mechanical effects on the chip formation [152]. The aforementioned methods are often defined as primary chatter. The fourth mechanism that describes the occurrence of chatter, and is often defined as secondary chatter, is regenerative chatter. Regenerative chatter occurs due to regeneration of waviness of the surface of the workpiece. Due to the fact that the spindle system is not infinitely stiff, during cutting, the cutter vibrates and leaves a wavy surface behind on the workpiece. The next tooth on the cutter encounters the waviness, left behind by the previous tooth of the cutter, and generates its own wavy surface. Consequently, a phase difference is present between the two waves which results in a rapidly varying chip thickness. As a result, the forces acting on the cutter vary. By increasing the axial depth of cut a_p, the regenerative effect becomes dominant and, in turn, chatter occurs. This results in the jumping in and out of cut of the cutter which results in a nonsmooth surface. At high spindle speeds, the primary chatter mechanisms diminish and chatter due to regeneration of the waviness of the surface is most prone to occur. Therefore, the focus in this work lies on the prevalent type of chatter, i.e., regenerative chatter.

From the limited literature available on the regenerative chatter, the study of regenerative chatter is very crucial for machining processes. Absolutely, the elimination of regenerative chatter is important to improve cutting accuracy and the productivity of the cutting.

3.2.2 Machine Cutting System

Figure 3.2 below shows a cutting system with the regenerative feedback of the cutting force which produced the displacement between the tool and the workpiece due the vibration.

Under the ideal cutting condition, a layer of workpiece is evenly cut down by a constant cutting force f_0, which will also produce a constant deformation x_0 on the machine tool structure. The constant deformation x_0 will ensure a constant cutting thickness.

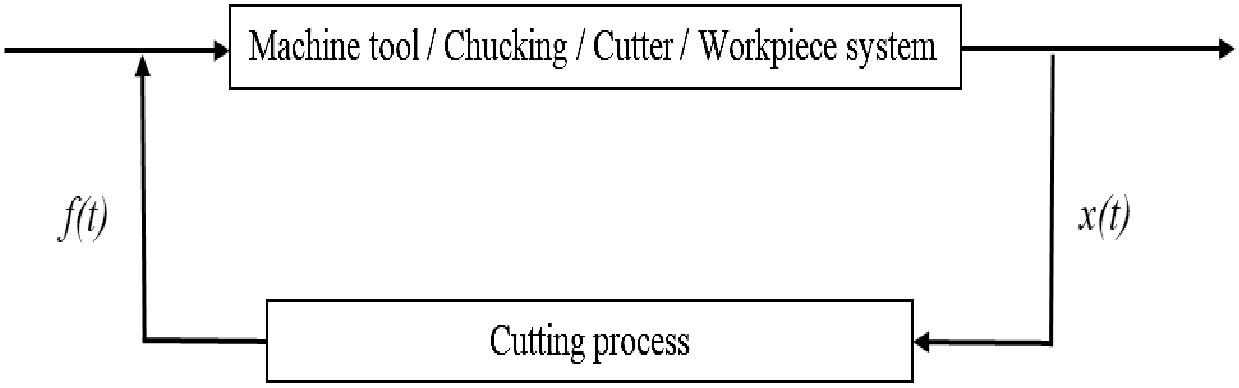

Figure 3.2: Machine Tool, Cutting Process Interaction

In the ideal cutting condition, the effect of random factors in the stability of the CNC turning operation, and a smooth cutting process is ensured. However, in practice, there are many disturbances due to various random factors resulting in a deviation from the smoothness of cutting process. As shown in Figure 3.2, the vibration displacement $x(t)$ of the machine tool cutting system is produced by the action of the cutting force $f(t)$; At the same time, the vibration displacement $x(t)$ will cause a change in the cutting thickness and counteract the cutting force $f(t)$, thus causing an input change. Hence, the cutting process can be regarded as a feedback link to adjust the interaction between the output vibration displacement $x(t)$ and the exciting input force$f(t)$. In addition, since the instantaneous cutting thickness is related to the vibration displacement of two adjacent cutting processes, there exists delayed feedback of the vibration displacement and therefore the cutting system is not affected by vibration disturbance, and the cutting operation will be stable.

3.3 Dynamic Model of Turning Regenerative Chatter

3.3.1 Turning Process

The turning process is a process of removing the excess metal layer on the surface of the workpiece by the rotation of the workpiece and the feeding motion of the tool to obtain the ideal geometric shape and produce high quality workpiece. Usually, the physical phenomena such as cutting force, cutting heat, tool wear, and chip formation which occur during cutting, have an important influence on machining efficiency, processing quality, and production cost. During the turning process, the rotation of the workpiece is the main cutting motion, and the cutting tool moves along a straight line with feed motion, as shown in Figure 3.3 below.

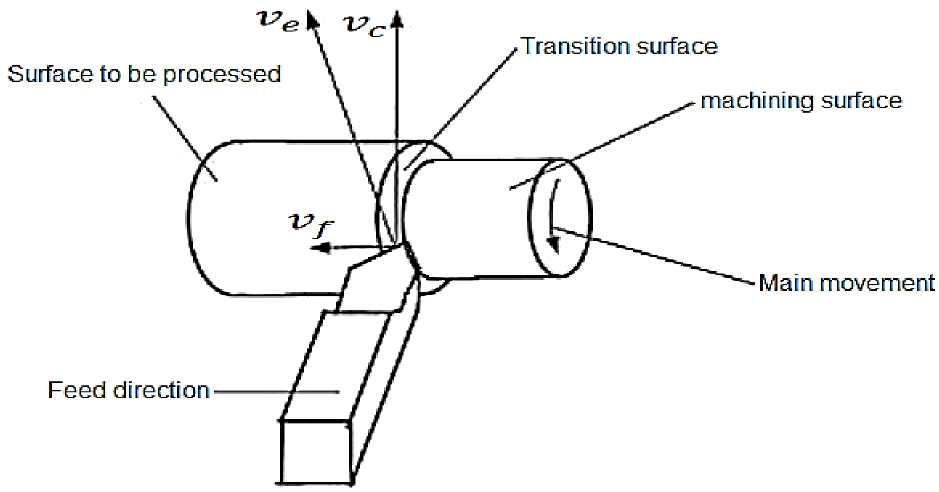

Figure 3.3: Turning Process

Turning is still one of the most widely used machining processes to produce a variety of products by mostly cutting the metals. Turning process is a process of removing the excess metal layer on the surface of the workpiece by the rotation of the workpiece and the feeding motion of the tool to obtain the ideal geometric shape and produce high quality workpiece. In turning process, regenerative chatter stability is regarded as an outcome favor in achieving reliable cutting performance. Nowadays, there is great demand in producing very high-quality parts, researchers devoted great efforts in developing theoretical and analytical means for understanding, analyzing and solving the stability of a given machining process. In general, the stability of turning process could be influenced by random variables such as machine stiffness, damping and cutting force. In addition, the physical phenomena such as cutting force, cutting heat, tool wear, and chip formation which occur during cutting, have an important influence on machining efficiency, processing quality, and production cost. During the turning process, the rotation of the workpiece is considered as the main cutting motion, and the cutting tool moves along a straight line with feed motion, as shown in Figure 3.3 above.

3.3.2 Dynamic Model of Turning Regenerative chatter

In the actual cutting process, the machine tool cutting system is usually a complex elastic structure composed of various components, and the mass and stiffness are evenly distributed. In theory, the system consists of components with infinite degrees of freedom. Usually, in the case of uniform distribution of mass and the stiffness in the system, the vibration of the elastomer system can be simplified to a system with a finite number of single degrees of freedom to obtain main characteristics and laws of lower frequency.

According to the theory of regenerative chatter and machining process, the cutting motion in the X and Y directions represent the longitudinal and radial feed directions, respectively, which are the most significant contributor to the regenerative chatter production, and the influence on the quality of the surface of the workpiece. But cutting motion in the Z direction has the least contribution to the regenerative chatter production, and the least influence on the quality of surface of the workpiece. As a result, the study of longitudinal feed in the X directions and radial feed in the Y directions are very significant. Therefore, we have established the following dynamic model of two-degree-of-freedom (2DOF) of turning regenerative chatter system.

Figure 3.3 (a) below shows Two Degrees of Freedom Cylindrical System, and Figure 3.3 (b) represents Regenerative Chatter Model in the Radial Turning.

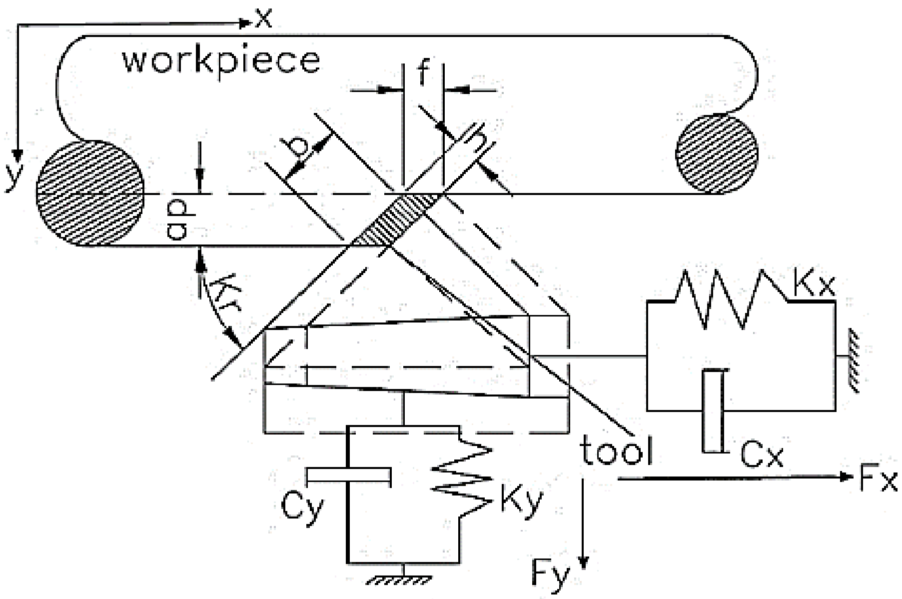

Figure 3.3 (a): Two Degrees of Freedom Cylindrical System

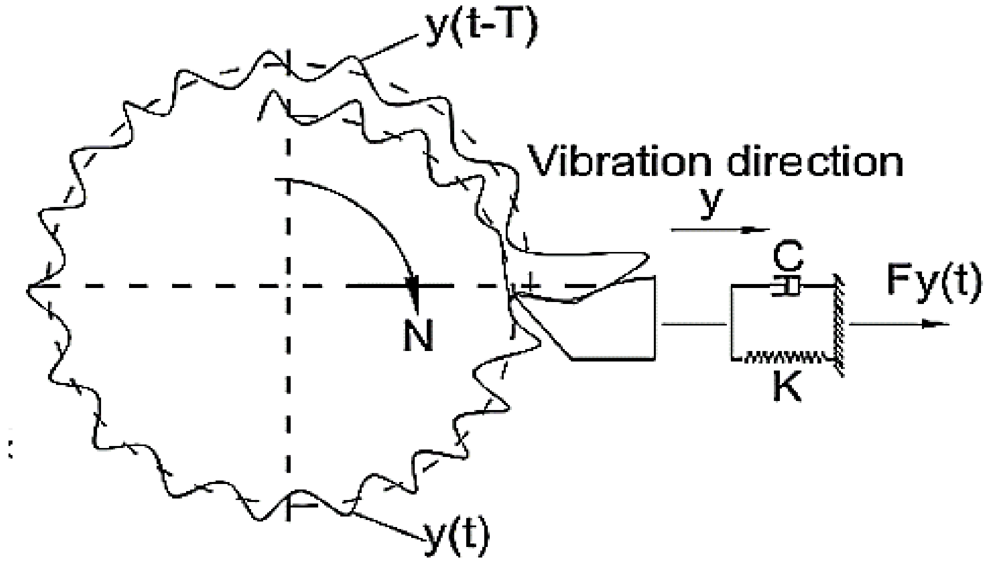

Figure 3.3 (b): Regenerative Chatter Model in the Radial Turning

For convenience of analysis, the following simplifications were applied:

1. The workpiece system is more rigid than the tool holder, and the cutting system is the main vibration system;

2. The system is vibrated linearly, and the elastic restoring force of the vibrated system is proportional to the vibration displacement;

3. The damping force of the vibrated system is proportional to the vibration velocity;

4. The dynamic change of cutting thickness is influenced by the regeneration effect;

5. The feed direction of the cutting tool has two degrees of freedom.

According to the kinetics of the model shown in Figures 3.3 (a), and 3.3 (b), the equations of motion in the X and Y directions [151] are expressed by Equations (3.1) and (3.2) respectively:

X-direction:

$$F_x(t) = m_x\ddot{x}(t) + c_x\dot{x}(t) + k_x x(t) \qquad (3.1)$$

Y-direction:

$$F_y(t) = m_y\ddot{y}(t) + c_y\dot{y}(t) + k_y y(t) \qquad (3.2)$$

Where $F_x(t)$ and $F_y(t)$ are the dynamic cutting forces of the vibrated system in the X and Y directions given in Newton, (N); m_x, m_y are the equivalent masses of the main vibrated system in the X and Y directions and given in grams (g); the equivalent masses (m_x and m_y) were calculated using the relationship between the stiffness coefficient and the frequency ($k/\omega n^2$) in the X and Y directions, respectively; c_x and c_y represent the equivalent damping coefficients of the main vibrated system in the X and Y directions and are given in $(N.s\ /mm)$; k_x and k_y are the equivalent stiffness coefficients of the main vibrated system in the X and Y directions and are given in (N/mm).

The components of the resultant dynamic cutting forces are given by Equations (3.3) and (3.4) as shown belosw:

$$F_x(t) = k_c bh(t) \qquad (3.3)$$

$$F_y(t) = k_e bh(t) \qquad (3.4)$$

Where k_c, k_e are the cutting stiffness coefficients of the main vibrated system in the X and Y directions given in $(N\ /mm^2)$; b is the cutting width (mm); $h(t)$ is the dynamic cutting thickness (mm).

The dynamic cutting thickness can be expressed as in Equation (3.5) below:

$$h(t) = fsink_r + \Delta xsink_r - \Delta ycosk_r \qquad (3.5)$$

Where f is the feed rate in (mm/rev), k_r is the side cutting edge angle of the tool, Δx and Δy are the differences between the vibration displacement in the X and Y directions and are given in (mm).

Δx and Δy can be determined by Equations (3.6) and (3.7):

$$\Delta x = \mu x(t - T) - x(t) \qquad (3.6)$$

$$\Delta y = \mu y(t - T) - y(t) \qquad (3.7)$$

Where $[x(t - T)\ -\ x(t)]$ is the dynamic chip thickness due to the tool vibration; $y(t - T)$ is the displacement of the tool during the previous pass; and $y(t)$ is the vibration displacement of the tool; μ is the overlap factor in the successive cuts; T is the time duration of one full rotation of the workpiece $(T\ =\ 60/N)$; N is the spindle speed in (rev/min).

According to Figure 3.4 below which illustrates the coincidence degree μ of external turning.

The coincidence degree μ, of the two adjacent cutting to the spindles is given in Equation (3.8) as follow:

$$\mu = \frac{CD}{AB} = \frac{DE-CE}{AB} = \frac{AB-CE}{AB} = 1 - \frac{CE}{AB} \qquad (3.8)$$

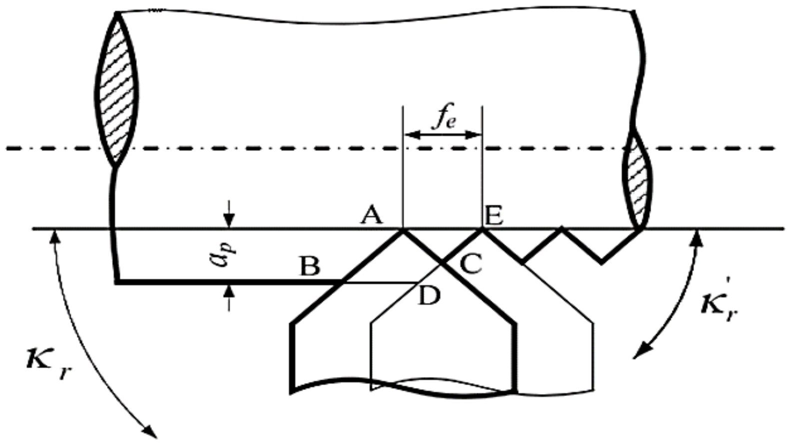

Figure 3.4: The Coincidence Degree μ of External Turning

From triangle ACE in Figure 3.4, the sine of this angle could be obtained as follows:

$$\frac{EC}{\sin k_r^{'}} = \frac{AE}{\sin(k_r + k^{'})} \qquad (3.9)$$

From Figure 3.4, $AE = f$, by plugging this in Equation (3.9) we have,

$$CE = \frac{\sin k_r^{'}}{\sin(k_r + k^{'})} \times f \qquad (3.10)$$

According to the theory of mechanical manufacturing technology:

$$AB = \frac{a_p}{\sin k_r} \qquad (3.11)$$

By substituting Equations (3.10) and (3.11) into Equation (3.8), the coincidence degree μ, which changes with the feed and depth of the cut, can be calculated using the following equation:

$$\mu = \frac{\sin k_r \sin k_r^{'}}{\sin(k_r + k_r^{'})} \times \frac{f}{a_p} \qquad (3.12)$$

k_r and k_r' are the side cutting edge and end cutting edge angles of the tool, which depend on the tested tool type (refer to Figure 3.5). According to Equation (3.12), the coincidence degree has a direct effect on regeneration chatter. Therefore, simulation of the model was performed using a variable step-size algorithm, where the program type selects the variable-step and the solver (simulation algorithm), which was ode45 (Dormand-Prince).

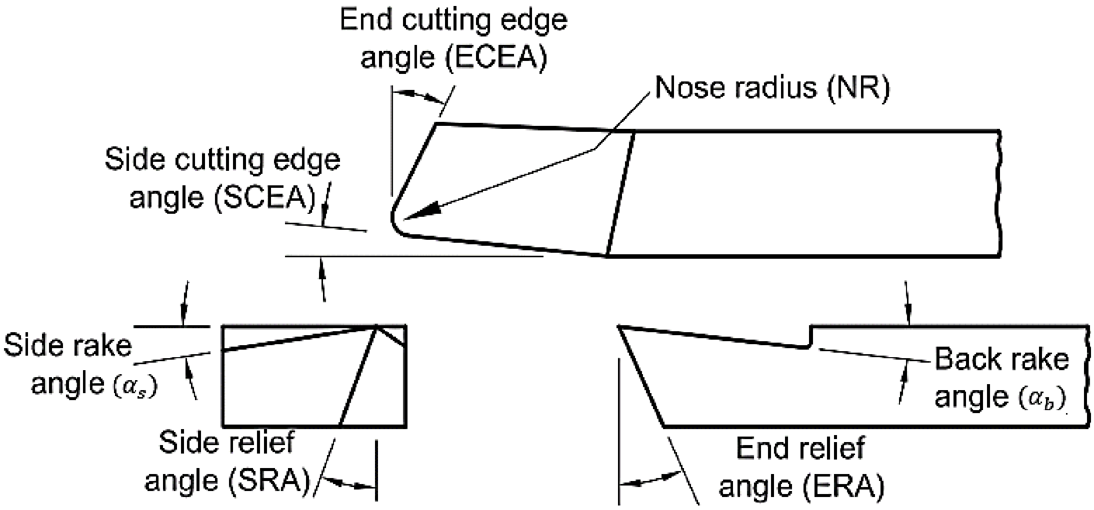

Figure 3.5: The Angles of a Single – Point Cutting Tool

Hence, the equation of motion for the dynamic model can be expressed as follows:

X-direction:

$$m_x\ddot{x}(t) + c_x\dot{x}(t) + k_x x(t) = k_{cu}[\mu x(t-T) - x(t)] \qquad (3.13)$$

Y-direction:

$$m_y\ddot{y}(t) + c_y\dot{y}(t) + k_y y(t) = k_{cv}[\mu y(t-T) - y(t)] \qquad (3.14)$$

In order to study the directions of the radial feed in the Y direction, and the axial feed in the X direction, Equation (3.14) is rewritten as follows:

$$\ddot{y}(t) + 2\omega_{ny}\zeta\dot{y}(t) + \omega_{ny}{}^2 y(t) = -\frac{\omega_{ny}{}^2 k_{cv} b[\mu y(t-T) - y(t)]}{k_y} \qquad (3.15)$$

Where: $\omega_{ny}$is the natural frequency of the machine cutting system in Y-direction (rad/s), ${\omega_{ny}}^2 = k_y/m_y$; ζ is the damping ratio in the Y-direction, $\zeta_y = c_y/2m_y\omega_{ny}$.Take $K = -{\omega_n}^2 k_{cv} b/k_y$, by substitute this value in Equation (3.15); we can obtain the following equation:

$$\ddot{y}(t) + 2\omega_{ny}\zeta_y\dot{y}(t) + {\omega_{ny}}^2 y(t) = K[\mu y(t-T) - y(t)] \qquad (3.16)$$

3.4 Study of Stability Limit for Machine Tool Cutting System

3.4.1 Calculation of Stability Limit

The displacement produced by the cutting vibration is given by:

$$y(t) = Asin(\omega t) \qquad (3.17)$$

The displacement caused by the previous cutting vibration can be written as:

$$y(t-T) = A\,sin(\,\omega t - \omega T)$$
$$= A\,sin(\,\omega t)\,cos(\,\omega T) - A\,cos(\,\omega t)\,sin(\,\omega T)$$
$$= cos(\,\omega T)y(t) - \frac{sin(\,\omega T)}{\omega}\dot{y}(y) \qquad (3.18)$$

Where: A is the amplitude in (mm), ω is the angular frequency of vibration in (rad/s). By substituting equations (3.17) and (3.18) into equation (3.16), we can obtain an expression for equation (3.19) as follows:

$$\ddot{y}(t) + \left[2\omega_{ny}\zeta - \frac{K\mu\,sin(\,\omega T)}{\omega}\right]\dot{y}(t)$$
$$+\left[{\omega_{ny}}^2 - K(1 - \mu\,cos(\,\omega T))\right]y(t) = 0 \qquad (3.19)$$

Take $y(t)$ and $\dot{y}(t)$ in the initial condition equal to zero, and by applying the Laplace / Fourier transform to Equation (3.19), we can get the following expression:

$$s^2 + \left[2\omega_{ny}\zeta - \frac{K\mu\, sin(\omega T)}{\omega}\right]s + {\omega_{ny}}^2$$
$$-K(1 - \mu\, cos(\omega T)) = 0 \qquad (3.20)$$

Take, $s = \sigma + i\omega$, according to the nature of the characteristic equation in the control theory, when $\sigma = 0$, the system is in a critical state between stability and instability. By substituting $s = i\omega$ into equation (3.20), where ω is the chatter vibration frequency, we can get the following expression:

$${\omega_{ny}}^2 - \omega^2 + 2\omega_{ny}\omega\zeta i = K(1 - \mu\, cos(\omega T))$$
$$+K\mu\, sin(\omega T)i \qquad (3.21)$$

The necessary and sufficient condition for the formula (3.21) to be established is that the real and imaginary parts at both sides of the equation are equal:

$$\begin{cases} {\omega_{ny}}^2 - \omega^2 = K(1 - \mu\, cos(\omega T) \\ 2\omega_{ny}\omega\zeta_y i = K\mu\, sin(\omega T)i \end{cases} \qquad (3.22)$$

Assuming that $\lambda = \omega/\omega_n$ and $K = -{\omega_{ny}}^2 k_{cv} b/k_y$, and substitute these values in equation (3.22), we obtain the expression,

$$\begin{cases} 1 - {\lambda_y}^2 = -\frac{k_{cv} b[1-\mu\, cos(\omega T)]}{k_y} \\ 2\zeta_y \lambda_y = -\frac{k_{cv} b\mu\, sin(\omega T)}{k_y} \end{cases} \qquad (3.23)$$

By dividing the two equations that exist in Equation (3.23), we will have the following expression:

$$\frac{1-\lambda_y{}^2}{2\zeta_y\lambda_y} = \frac{1-\mu\, cos(\omega T)}{\mu\, sin(\omega T)} \qquad (3.24)$$

By simplifying the equation above, we can get the following expression:

$$2\zeta_y\lambda_y\, cos(\,\omega T) + (1+\lambda_y{}^2)\, sin(\,\omega T) = \frac{2\zeta_y\lambda_y}{\mu} \qquad (3.25)$$

According to the angle formula auxiliary of the trigonometric function, Equation (3.25) can be transformed into the following formula:

$$\sqrt{(2\zeta_y\lambda_y)^2 + (1-\lambda_y{}^2)^2\, sin(\,\omega T+\theta)} = \frac{2\zeta_y\lambda_y}{\mu} \qquad (3.26)$$

Where:

$$\theta = tan^{-1}\frac{2\zeta_y\lambda_y}{1-\lambda_y{}^2} \qquad (3.27)$$

The formula (3.27) can be organized or rearranged as follows:

$$sin(\,\omega T+\theta) = \frac{2\zeta_y\lambda_y}{\sqrt{(2\zeta_y\lambda_y)^2+(1-\lambda_y{}^2)^2}} \qquad (3.28)$$

By solving Equation (3.28), we get the following formula:

$$\omega T = 2j\pi + sin^{-1}\frac{2\zeta_y\lambda_y}{\sqrt{(2\zeta_y\lambda_y)^2+(1-\lambda_y{}^2)^2}} - tan^{-1}\frac{2\zeta_y\lambda_y}{1-\lambda_y{}^2}$$

$$(j = 0,1,2,\ldots..) \qquad (3.29)$$

By substituting $T = 60/n$ into Equation (3.29), the corresponding spindle speed (n) can be expressed as follow:

$$n = \frac{60\omega}{2j\pi+sin^{-1}\frac{2\zeta_y\lambda_y}{\sqrt{(2\zeta_y\lambda_y)^2+(1-\lambda_y{}^2)^2}}-tan^{-1}\frac{2\zeta_y\lambda_y}{1-\lambda_y{}^2}} \quad (j = 0,1,2.\ldots.) \qquad (3.30)$$

Since the Equation (3.22) was obtained when $\sigma = 0$, Therefore, the maximum cutting width $b_{lim,y}$ in the Y direction can be obtained by substituting Equation (3.30) into equation (323) as follows:

$$b_{lim,y} = -\frac{2\zeta_y\lambda_y k_y}{k_{cv}\mu \sin\left[\sin^{-1}\frac{2\zeta_y\lambda_y}{\sqrt{(2\zeta_y\lambda_y)^2+(1-\lambda_y{}^2)^2}}-\tan^{-1}\frac{2\zeta_y\lambda_y}{1-\lambda_y{}^2}\right]} \quad (3.31)$$

In the same way, the maximum cutting width in the X direction can be obtained as follows:

$$b_{lim,x} = -\frac{2\zeta_x\lambda_x k_x}{k_{cu}\mu \sin\left[\sin^{-1}\frac{2\zeta_x\lambda_x}{\sqrt{(2\zeta_x\lambda_x)^2+(1-\lambda_x{}^2)^2}}-\tan^{-1}\frac{2\zeta_x\lambda_x}{1-\lambda_x{}^2}\right]} \quad (3.32)$$

Where $b_{lim,x}$, $b_{lim,y}$ are the directional limit cutting widths; ζ_x and ζ_y are the damping ratios of the system; λ_x and λ_y are the frequency ratios in the X and Y directions. λ_x is equal to $\omega\ /\omega_{nx}$, and λ_y is equal to $\omega\ /\omega_{ny}$ where ω is the frequency of the vibration angle and ω_{nx} and ω_{ny} are the natural frequencies of the system in the X and Y directions respectively.

3.4.2 The Stability Lobe Diagram

Pioneering work of Tlusty [42] and Tobias [43] were resulted in the first stability analysis for the orthogonal cutting process. Merritt [25] illustrated that chatter stability analysis could be characterized by a feedback loop. Thus, resulting to what called stability lobes diagram (SLD), which is an intuitive graphical tool developed with the cutting chatter development. Moreover, it is also determining the boundary range of the stable cutting area (i.e., without chatter) and an unstable cutting area (i.e., with chatter) which visualized in terms of spindle speed (n) and cutting width b_{lim}. When the dynamic parameters of the machine cutting system are known, Equations (2.30) to (2.32) can be used to find the different spindle speeds when (j = 0, 1, 2...,), the spindle speed (n) values must have to be corresponded to their specific limiting cutting width b_{lim} values. Figure 3.6 illustrates the relation between the spindle speed and the stability limit cutting width, when the spindle speed (n) increases, the limit stability cutting width b_{lim} is increased divergently and periodically. When the spindle speed (n) decreases, the limit cutting width b_{lim} value is decreased. Furthermore, it can be seen that the lobes become broader and higher as the spindle speed increases as opposed to low spindle speeds. At low spindle speeds a relatively small change in spindle speed may lead to a relatively large change in the phase difference between two consecutive teeth [117]. Due to the broader lobes at high spindle speeds, the productivity can be substantially increased when the lobes are accurately predicted by choosing a working point in a lobe (see conditionally stable area in Figure 3.6).

When the spindle speed (n) is near the trough, the corresponding limit cutting width b_{lim} value is the smallest. And when the spindle speed (n) is close to the trough, the corresponding cutting width b_{lim} value is increased with increased spindle speed, even if they are much higher than the minimum cutting width. Therefore, it is very important to select the proper spindle speed (n) for the cutting force, for a quality of the workpiece surface.

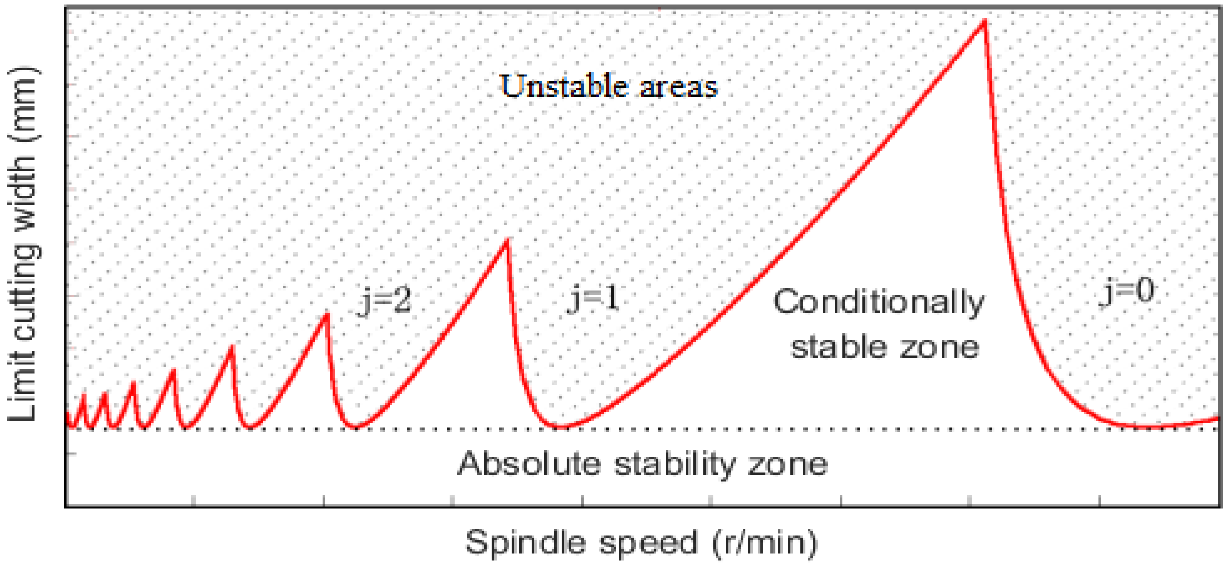

Figure 3.6: Stability Lobe Diagram

3.5 Analysis of Factors Affecting the Stability of the Machine Tool Cutting System

3.5.1 Influence of Natural Frequency on the Limit Cutting Width

Figure 3.7 below illustrates the effect of natural frequency ω_n on the limit cutting width b_{lim}.

Figure 3.7 shows the simulation results of the ultimate cutting width b_{lim} for the machine tool cutting system as it varies with the natural frequency ω_n of the vibration system while the other parameters remain unchanged.

As shown in Figure 3.7, when the other dynamic parameters remain fixed, an increase in the natural frequency ω_n of the main vibration system causes a shift on the whole lobe curve to the longitudinal coordinate.

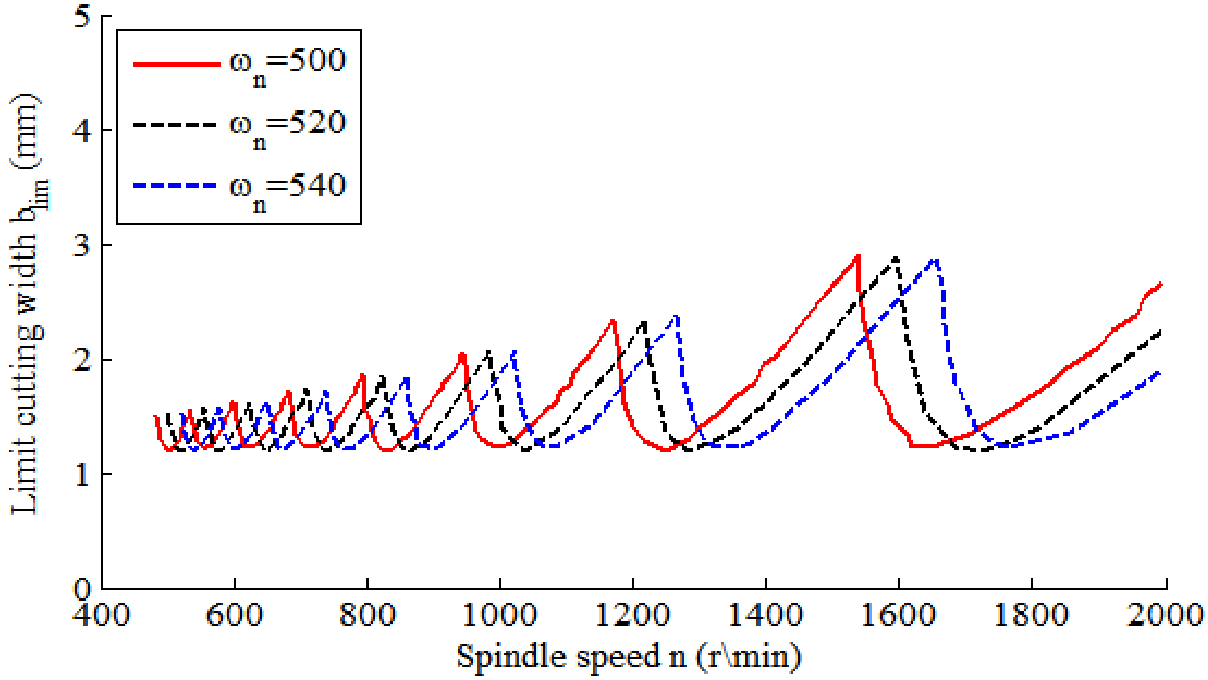

Figure 3.7 Effect of Natural Frequency ω_n on the Limit Cutting Width b_{lim}

Meanwhile, the stable cutting area formed between the lobe curves becomes wider with the increase in the natural frequency ω_n of the main vibration system. Therefore, the largest stable cutting area can be obtained, although the minimum stable cutting depth value remains unchanged.

3.5.2 The Effect of Stiffness on the Limit Cutting Width

Figure 3.8 below illustrates clearly effect of stiffness k on the limit cutting width b_{lim}.

Figure 3.8 shows the simulation results for the ultimate cutting width b_{lim} of the machine tool cutting system as it varies with the stiffness k of the vibration system while other parameters remain constant. As shown in Figure 3.8, when other dynamic parameters remain fixed, the entire lobe curve will move on the longitudinal coordinate with increasing in the stiffness k, of the main vibration system, and the horizontal position remains unchanged. Therefore, a more stable cutting area can be obtained.

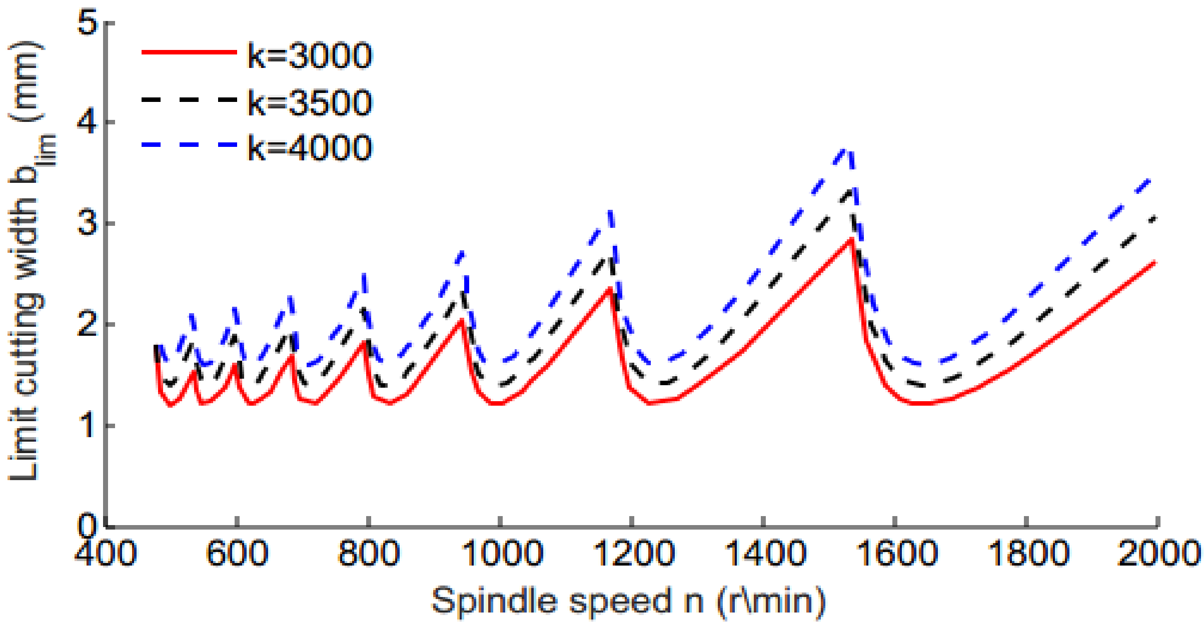

Figure 3.8: Effect of Stiffness k on the Limit Cutting Width b_{lim}

3.5.3 Influence of Unit Cutting Force Coefficient on Ultimate Cutting Width

Figure 3.9 shows the computer simulation results of the variation of the ultimate cutting width b_{lim} of the machine tool cutting system with the unit cutting force coefficient k_c of the vibration system where the other parameters remain fixed. As shown in Figure 3.9, when all the dynamic parameters are fixed except b_{lim}, the entire lobes curve will move down to the longitudinal axis with increasing unit cutting force coefficient k_c of the main vibration system, thus reducing the area of the stable cutting zone.

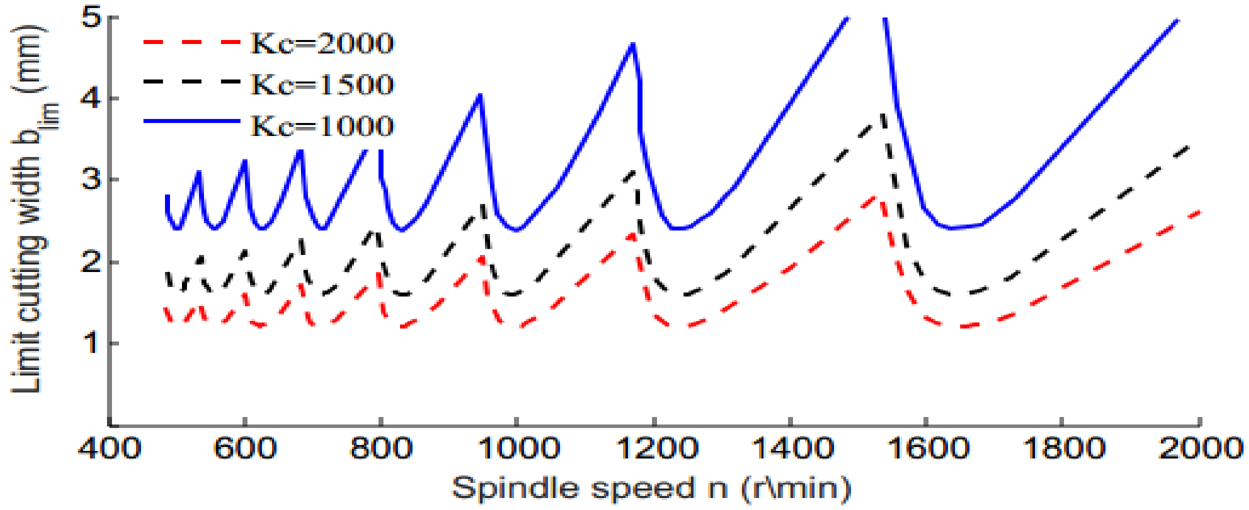

Fig. 3.9 Influence of Unit Cutting Force Coefficient k_c on the Limit Cutting Width b_{lim}

3.5.4 Influence of Damping Ratio on the Limit Cutting Width

Figure 3.10 below illustrates the influence of damping ratio ς on the limit cutting width b_{lim}.

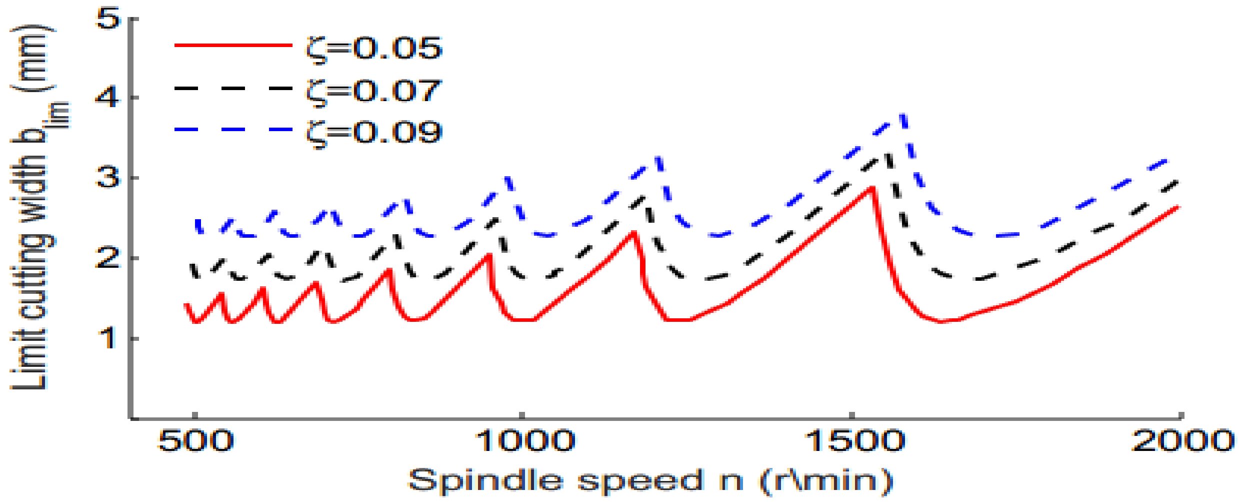

Figure 3.10: The Influence of Damping Ratio ς on the Limit Cutting Width b_{lim}

Figure 3.10 shows a computer simulation of the variation ultimate cutting width b_{lim} of the machine tool cutting system with the damping ratio ς, other parameters remain constant. As shown in the figure, when the remaining dynamic parameters are fixed, the entire lobes will move on the longitudinal coordinate with increasing damping ratio ς of the main vibration system, and the amplitude of the trough rising is larger than the peak rising. Therefore, the area of the stable cutting area will increase.

3.5.5 Effect of Coincidence Degree on the Limit Cutting Width

Figure 3.11 below shows the effect of coincidence degree μ on the limit cutting width b_{lim}.

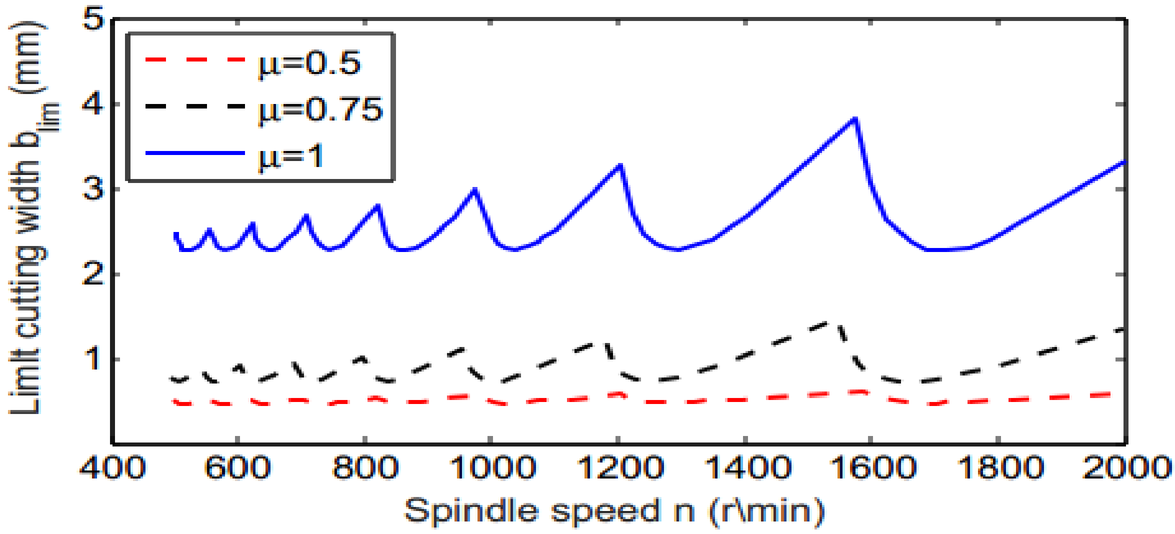

Figure 3.11: Effect of Coincidence Degree μ on the Limit Cutting Width b_{lim}

Figure 3.11 shows the computer simulation of the variation in the limit cutting width b_{lim} with the coincidence degree μ of the machine tool cutting system, with other parameters constant.

The influence of coincidence degree μ on the stability of the machine tool cutting system not only directly affect the cutting depth and feed rate, but also closely related to the main declination angle of the turning tool, which ranges from $0 \sim 1$, [155]. As shown in Figure 3.11, when the other dynamic parameters remain unchanged, the entire lobe curve will be moved into the longitudinal axis. With increasing coincidence degree μ of the main vibration system, the curve tends to be straight, and the stable area region formed between the lobe curves becomes narrow. As a result, the area of the stable cut area reduces. When the coincidence degree μ = 1, the stable cutting area of the machine tool cutting system is in the smallest measures and the regenerative chatter is the strongest.

3.6 Three Degrees of Freedom Dynamic Model

In order to simplify the analysis, it has been assumed that the turned cylindrical workpiece is a rigid body and the cutter is considered as the active body vibration. The cyclical change of the dynamic cutting force caused by the cutter – workpiece system generates chatter at axial, radial and tangential directions. According to the equivalence, simplicity and successive approximation of the kinetic model, the cutter could be seen from the perspective of three degrees of freedom elastically guided and damped system. Therefore, it can be simplified in the three axial, radial and tangential directions, as shown in Figure 3.12. Where (F_x) is the feed force, (F_y) is the back force, (F_z) is the main cutting force and (F) is the resultant force acting on the cutting tool.

For easy determination of the kinetic model of this process, the tool-workpiece system in (Figure 3.12) is replaced by the inertia element m (Figure 3.13). This describes the regenerative chatter mechanism of the process under three degrees of freedom. Where the three-dimensional model of the tool-workpiece system is represented by two plane coordinate systems. However, the mechanical model still has three degrees of freedom, where the inertia element is the mass m, the elastic elements are k_x, k_y and k_z, and the damping elements are C_x, C_y and C_z.

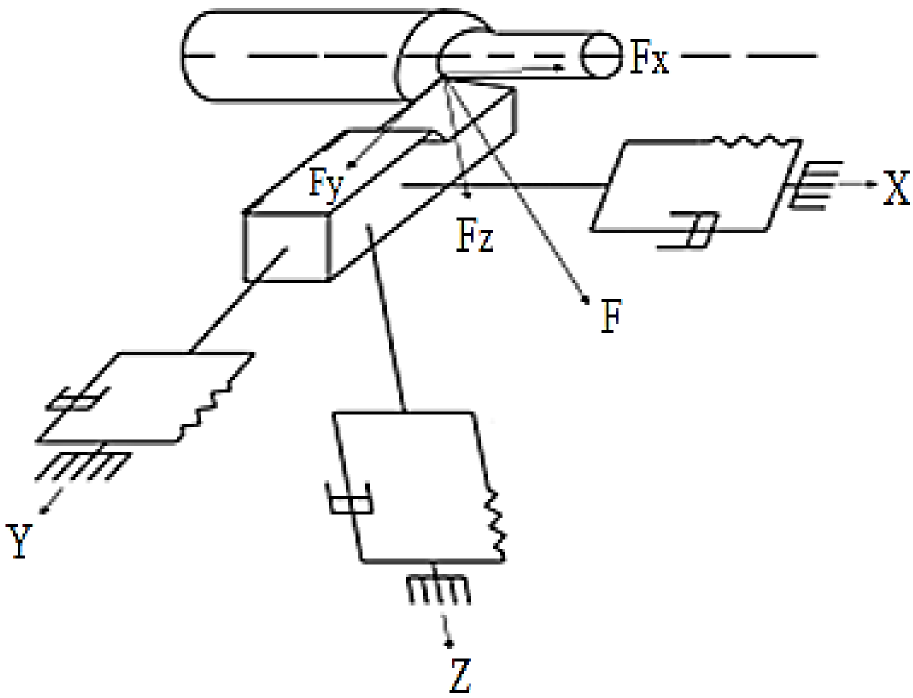

Figure 3.12: Dynamic Model of the Oblique Cylindrical Turning

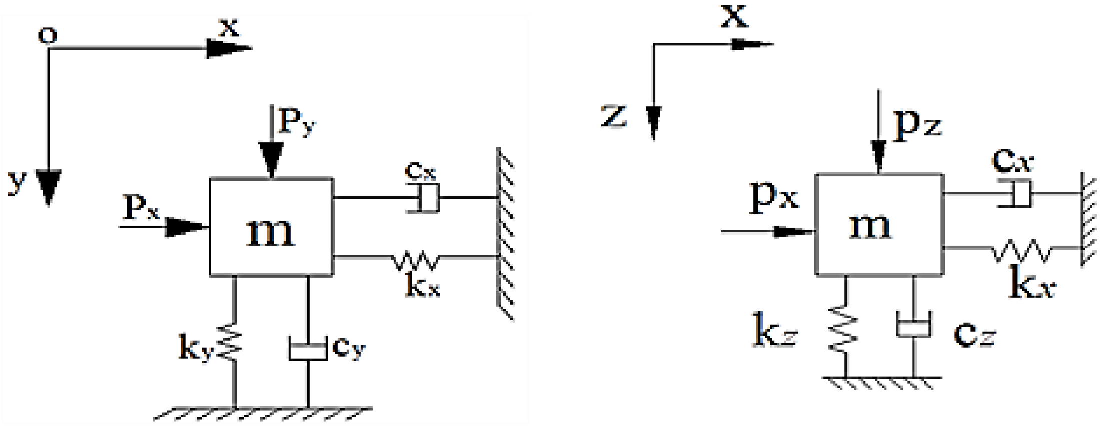

Figure 3.13: Inertia Model of the Oblique Cylindrical Turning

3.7 Results and Discussion

3.7.1 Formulation of the Dynamic Model

The actual turning process of the cylindrical workpiece is proposed to be oblique cutting as illustrated in Figure 3.14. At each revolution of the workpiece, the cutting tool moves from the position I to position II and removes layers from the workpiece in the form of chip. Where the removed layer cross-section area in the datum is called the cutting area and is denoted by the shaded region (Figure 3.14). Moreover, during cutting action, the cutting tool is subjected to a resultant cutting force (F) that has three perpendicular components. This helps in the formulation of the three-degree of freedom dynamic model that will help in the development of the required regression model for solving the problem.

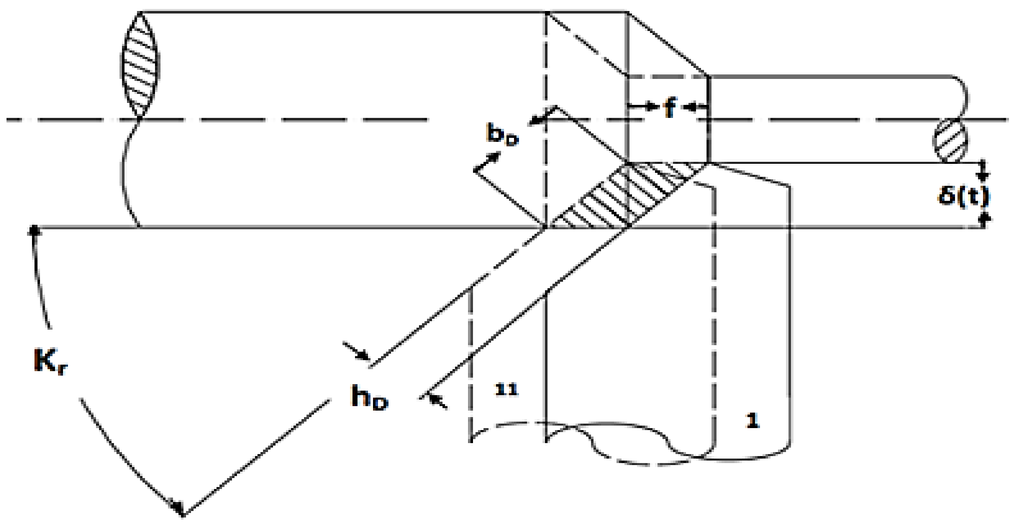

Figure 3.14: Schematic Diagram of Oblique Cylindrical Turning

Therefore, the cutting area can be calculated as follows:

$$A = h_D b_D \qquad (3.33)$$

Where: A is the cutting area, h_D uncut chip thickness, b_D uncut chip width.

$$h_D(t) = f \sin k_r + x(t) \sin k_r + y(t) \cos k_r \qquad (3.34)$$

$$b_D(l) = \frac{s(t)}{\sin k_r} \qquad (3.35)$$

Where: k_r major cutting-edge angle; $S(t)$ is the total cutting thickness of the (t) tool along the radial direction of the workpiece cutting thickness. According to the empirical formula of cutting force, resultant cutting force (F) can be expressed as follows:

$$F = k_s A \qquad (3.36)$$

Where k_s is cutting coefficient, which depends on the material and size of the workpiece, cutting tool material and geometry, chip thickness and cutting speed [114]. The selected tool geometry as recommended by the supplier is tabulated in Table 3.1 shown below.

Table 3.1: Geometric Angle of the Cutter

Major cutting-edge angle K_r / (°)	Minor cutting-edge angle $k`_r$ / (°)	Rake angle γ_0 / (°)	Angle of inclination λ_s / (°)
45	10	15	0

Combining Equation (3.33), (3.35) into Equation (3.36) to give the resultant cutting force acting on the tool. Thus, Equation (3.36) can be expressed as follows:

$$F = k_s(t)\big(f + x(t) + y(t)\big) \qquad (3.37)$$

The cutting force F is resolved into three mutually perpendicular components; axial or feed force (F_x), thurst force (F_y), and main cutting force (F_z) respectively. According to the actual machining test: k_r = 45°, y_0=15°, λ_s= 0.

The following are the approximated relationship between resultant force and its three components:

$p_x = F_f = F_x = (0.3 \sim 0.04)F_z$

$p_y = F_p = F_y = (0.4 \sim 0.5)F_z$

$p_z = F_c = F_z$
$F = (1.12 \sim 1.18)F_s$

$$\begin{cases} p_x = F_f = F_x = (0.3 \sim 0.04)F_z \\ p_y = F_p = F_y = (0.4 \sim 0.5)F_z \\ p_z = F_c = F_z, F = (1.12 \sim 1.18)\ F(s\ ) \end{cases} \quad (3.38)$$

Where: p_x, p_y and p_z are the excitation cutting forces in the z, x and y direction respectively. Hence, by substituting Equation (3.37) into Equation (3.38) the cutting force components can be expressed as follows:

$$\begin{cases} F_x = 0.30k_s s(t)\big(f + x(t) + y(t)\big) \\ F_y = 0.40k_s s(t)\big(f + x(t) + y(t)\big) \\ F_z = 0.87k_s s(t)\big(f + x(t) + y(t)\big) \end{cases} \quad (3.39)$$

3.8 Mathematical Model

The regression model development was achieved by using the kinetic model of the system (Equation (3.39)) and the principle of Newton's second law. Accordingly, the equations of motion for the vibrated system were expressed as follows:

$$\begin{cases} m\ddot{x} = +c_x\dot{x} + k_x x = F_x(t) \\ m\ddot{y} = +c_y\dot{y} + k_y y = F_y(t) \\ m\ddot{z} = +c_z\dot{z} + k_z z\ = F_z(t) \end{cases} \quad (3.40)$$

Where m_x, m_y and m_z are the masses, and c_x, c_y and $c_z$are the damping coefficients and k_x, k_y and k_z are the structure stiffness of the machine tool in the three respective directions. By making use of Equations (3.39) and (3.40), we can obtain the complete mathematical model of the three-degree of freedom vibrated system. Thus, the model is expressed by the following matrix:

$$\begin{bmatrix} m_x & 0 & 0 \\ 0 & m_y & 0 \\ 0 & 0 & m_z \end{bmatrix} \begin{pmatrix} \ddot{x} \\ \ddot{y} \\ \ddot{z} \end{pmatrix} + \begin{bmatrix} c_x & 0 & 0 \\ 0 & c_y & 0 \\ 0 & 0 & z_z \end{bmatrix} \begin{pmatrix} \dot{x} \\ \dot{y} \\ \dot{z} \end{pmatrix} +$$

$$\begin{bmatrix} k_x - 0.30k_s s(0) & -0.30k_s s(0) & 0 \\ -0.40k_s s(0) & k_y - 0.40k_s s(0) & 0 \\ -0.87k_s s(0) & -0.87k_s s(0) & k_z \end{bmatrix} \begin{pmatrix} x \\ y \\ z \end{pmatrix} =$$

$$\begin{pmatrix} 0.30k_s s(0)f \\ 0.40k_s s(0)f \\ 0.87k_s s(0)f \end{pmatrix} \qquad (3.41)$$

The value of $S\ (0)$ which is the average cutting depth can be found from the equation of motion:

$$S(t) = \mathrm{S}(0) + \mathrm{A}\sin(\omega\mathrm{t} + \varphi)\,(p - p_a) \qquad (3.42)$$

Where ω= 52 rad/s, A = 0.005m, ϕ = π/4, $S(0)$ = 0.003m.

The numerical solution for the Mathematical model can be obtained by substituting the parameters of Table 3.2 below into Equation (3.41).

Table 3.2: Input Parameters

No	Parameter	Values	unit
1.	Mass (m)	0.0235	kg
2.	Tool elastic modulus (E)	2.10×10^{11}	$N.m^{-2}$
3.	Tool-sectional area (A)	0.0001	m^2
4.	lengthening of the tool (L)	0.0900	m
5.	Total length of the tool (l)	0.0400	m
6.	cutting coefficient (k_s)	2.50×10^9	$N.m^{-2}$
7.	Depth of the cutting tool at Each time (S (0))	0.0030	m

8.	Damping ratio x direction (C_x)	0.0285	$N.s^{-1}.m^{-1}$
9.	Damping ratio y direction (C_y)	0.0157	$N.s^{-1}.m^{-1}$
10.	Damping ratio z direction (C_z)	0.0285	$N.s^{-1}.m^{-1}$
11.	Feed rate (f)	0.0003	$m.r^{-1}$

3.8.1 The Natural Frequency of Vibrated System

The next step in this analysis is to solve the system of differential equations for the vibrated motion. This enables the determination of the system frequency for un-damped n-degree of freedom vibration. In this case the general matrix equation is given as follows:

$$M\ddot{x} + Kx = 0 \qquad (3.43)$$

Where M is the mass matrix, K is the stiffness matrix, x is the generalized coordinate vector. It is assumed that the system is under harmonic vibration. Therefore, the general equation of motion can be put as follows:

$$x_i = u_i \sin(\omega_n t + \emptyset),\ i=1, 2, \ldots, n \ (3.44)$$

Where u is arbitrary constant, ω_n is the natural frequency of harmonic vibration and $\emptyset$ is the initial phase angle.

By substituting Equation (3.44) in Equation (3.43) we can get the following expression:

$$([K] - {\omega_n}^2[M])[U] = 0 \qquad (3.45)$$

In order to generate a solution for u, make its coefficient determinant equal to zero

$$\Delta(\omega_n) = det[-{\omega_n}^2 M + K] \qquad (3.46)$$

Equation (3.46), is called the natural frequency equation or characteristic equation which satisfies the conditions of the natural frequency ω_n. After the determinant $\Delta(\omega_n)$ of the characteristic equation is expanded, an (nth) order polynomial of ω_{n2} is obtained. For the positive definite system, we need to obtain the positive real roots ω_{nr} where r = 1,2, ..., n and (n) is called natural frequency of the system. In most cases, the natural frequencies are not equal and can be arranged from small to large, in ascending order; $0 \leq \omega_{n1} \leq \omega_{n2} \leq \cdots \leq \omega_{nm}$

By making use of the input parameters of Table 3.2 in equation (3.46) and the MATLAB Software, the natural frequencies of the system were calculated and listed below.

The MATLAB solution of the equation of motion is presented in Appendix 1.

ω_{n1}=2731(H_z), ω_{n2}=3233(H_z), ω_{n3}=17083(H_z)

3.8.2 The Main Modes of the Vibrated System

Information about the main modes of the vibrated system can be determined by substituting the calculated natural frequencies values into the deferential Equation (3.45). This enables the determination of the resultant modal vector u of the system which is expressed as follows:

$$u_1 = \begin{bmatrix} 5.192 \times 10^{14} \\ 6.788 \times 10^{12} \\ 1.483 \times 10^{15} \end{bmatrix},$$

$$u_2 = \begin{bmatrix} -6.25 \times 10^{12} \\ 0 \\ 1.468 \times 10^{15} \end{bmatrix},$$

$$u_3 = \begin{bmatrix} 6.632 \times 10^{12} \\ -6.522 \times 10^{14} \\ 1.895 \times 10^{13} \end{bmatrix},$$

The main modes of the matrix, $u = \begin{bmatrix} 0.3137 & 0 & 0.0830 \\ 0.0041 & 0 & -0.8162 \\ 0.8962 & 1 & 0.0237 \end{bmatrix}$

According to the above result, the main mode of the vibrated system was represented by Figure 3.15. It obvious that the chatter due to vibration for the three natural frequencies takes place at three directions (axial, radial and tangential) on the cutting tool. However, the chatter of the cutter is the large in z and x directions, while it is minimum at y-direction. The result was found to be consistent with all three natural frequencies. This is mainly due to the fact that the cutting tool is more rigid in y-direction than in x and z directions. The relative vibration of the system in the direction of the respective degrees of freedom can be obtained by the vibration pattern. The graph also shows that the vibration in the z-direction is the largest at the first-order natural frequency.

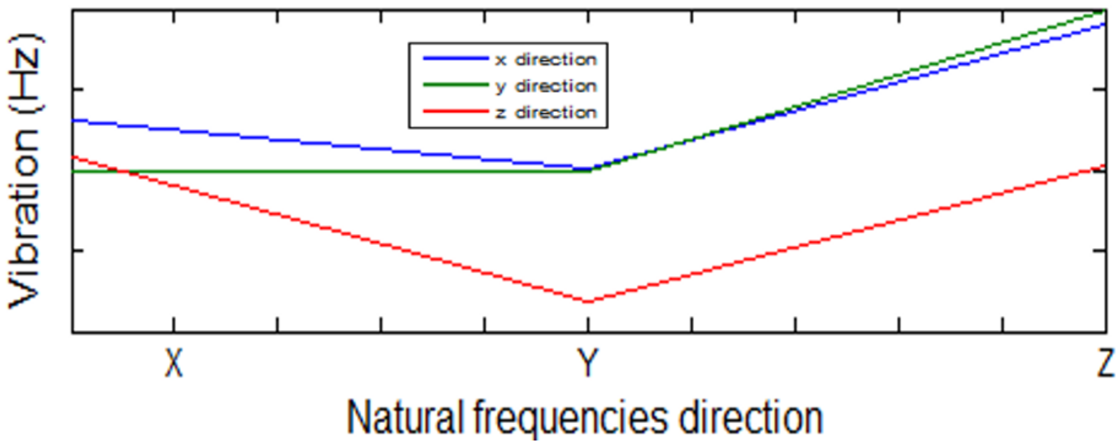

Figure 3.15: Vibration Mode of the System

3.9 Transient Response of the Cutter

According to the developed model of the three degrees of freedom cylindrical turning, it is obvious that chatter in the specified three directions is zero at the initial contact between the cutting tool and workpiece. Then it increases with the progression of the cutting action, and become stable at the transient stage. Therefore, it is desirable in this section and the following subsections to drive the mathematical expression for the chatter amplitude and speed, and the system state equation. The application of the three degrees of freedom dynamic model with the aid of MATLAB simulation can assist in the determination of transient response of the cutting tool. Based on Equation (3.41), It was assumed that at the initial contact between the cutting tool and workpiece, the amplitude and speed at all directions is zero. This is regarded as the initial condition for the Differential equation of system motion. Therefore, the differential equation of motion becomes as follows:

$$\begin{aligned}[x(0) \quad y(0) \quad z(0) \quad \dot{x(0)} \quad \dot{y(0)} \quad \dot{z(0)}]^T \\ = [0 \quad 0 \quad 0 \quad 0 \quad 0 \quad 0] \qquad (3.47)\end{aligned}$$

In general, the answer to the kinematic equation of system vibration can be solved through the differential equation of system movement. Where the numerical solution of differential equations is often transformed into a state-space equation of a standard format.

In this case, we represent the system space variables by Equation (3.48). Then the kinematic equation of the vibrated system can be transformed into a state-space equation, as shown in Equation (3.49).

$$x_1(t) = x(t)x_2(t) = \dot{x}(t)y_1(t) = y(t), \quad and \quad y_2(t) = \dot{y}(t)z_1(t) = z(t)z_2(t) = \dot{z}(t) \qquad (3.48)$$

$$\begin{bmatrix} \dot{x}_1(t) \\ \dot{x}_2(t) \\ \dot{y}_1(t) \\ \dot{y}_2(t) \\ \dot{z}_1(t) \\ \dot{z}_2(t) \end{bmatrix} = \begin{bmatrix} 0 & 1 & 0 & 0 & 0 & 0 \\ \frac{-k_1}{m} & -\frac{c_x}{m} & -\frac{k_2}{m} & 0 & 0 & 0 \\ 0 & 0 & 0 & 1 & 0 & 0 \\ -\frac{k_3}{m} & 0 & -\frac{k_4}{m} & -\frac{c_y}{m} & 0 & 0 \\ 0 & 0 & 0 & 0 & 0 & 1 \\ -\frac{k_5}{m} & 0 & -\frac{k_6}{m} & 0 & -\frac{k_7}{m} & -\frac{c_z}{m} \end{bmatrix} \begin{bmatrix} x_1(t) \\ x_2(t) \\ y_1(t) \\ y_2(t) \\ z_1(t) \\ z_2(t) \end{bmatrix} + \begin{bmatrix} 0 \\ \frac{p_1}{m} \\ 0 \\ \frac{p_2}{m} \\ 0 \\ \frac{p_3}{m} \end{bmatrix} \qquad (3.49)$$

Where: p_1= 0.30 k_sS (0)f; p_2= 0.39 k_sS (0)f; p_3= 0.87 k_sS (0)f; k_1= k_x - 0.30 k_sS (0); k_2= -0.30 k_sS (0); k_3= -0.39 k_sS (0); k_4= k_y - 0.39 k_sS (0); k_5= k_6 = -0.87 k_sS (0); k_7= k_z.

Then the initial conditions for this state of space equation can become as follows:

$$[x_1(t) \quad x_2(t) \quad y_1(t) \quad y_2(t) \quad z_1(t) \quad z_2(t)]^T = [0 \quad 0 \quad 0 \quad 0 \quad 0 \quad 0] \qquad (3.50)$$

To analyze the vibration amplitude of the vibrated system at the maximum excitation frequency, it is necessary to analyze the steady-state output value of the vibrated system at different excitation frequencies during the cutting process. Therefore, the phase angle difference is considered large, and the theoretical data is provided for the actual production situation. Using MATLAB through the complex domain frequency response faction, we can obtain the amplitude-frequency curve and the phase-frequency curve of the vibrated system as shown in Figure 3.16.

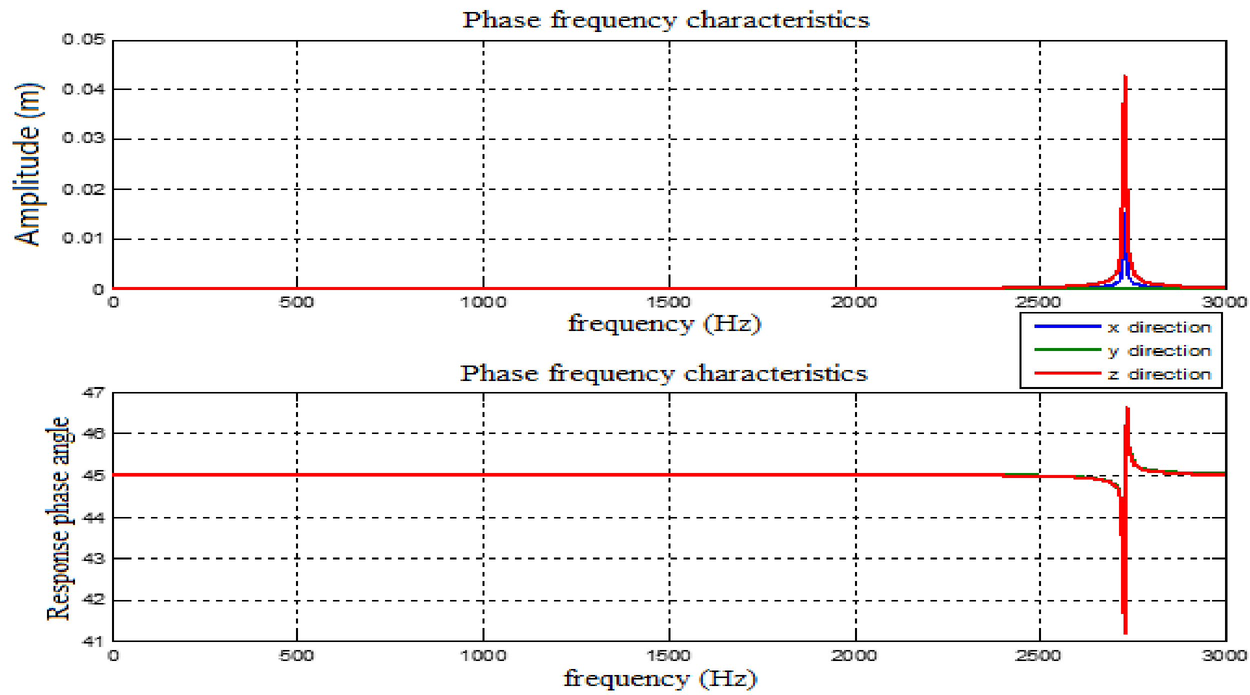

Figure 3.16: Characteristic Curves of the Vibrated System

According to the characteristic analysis of the frequency response of the regenerative chatter of the turning process, the vibration frequency of the system is found to be 2800rad /s (Figure. 3.16). The vibration amplitude and phase difference at the three vibration directions are the largest with an excitation frequency of 445.9HZ. The spindle speed is also maximum to avoid the frequency range in the workpiece, resulting in lathe regeneration flutter vibration.

3.10 MATLAB / SIMULINK Simulation

Figure 3.17 shows the block diagram for converting the state space equation of the system vibration to numerical simulation, using MATLAB / SIMULINK [116].

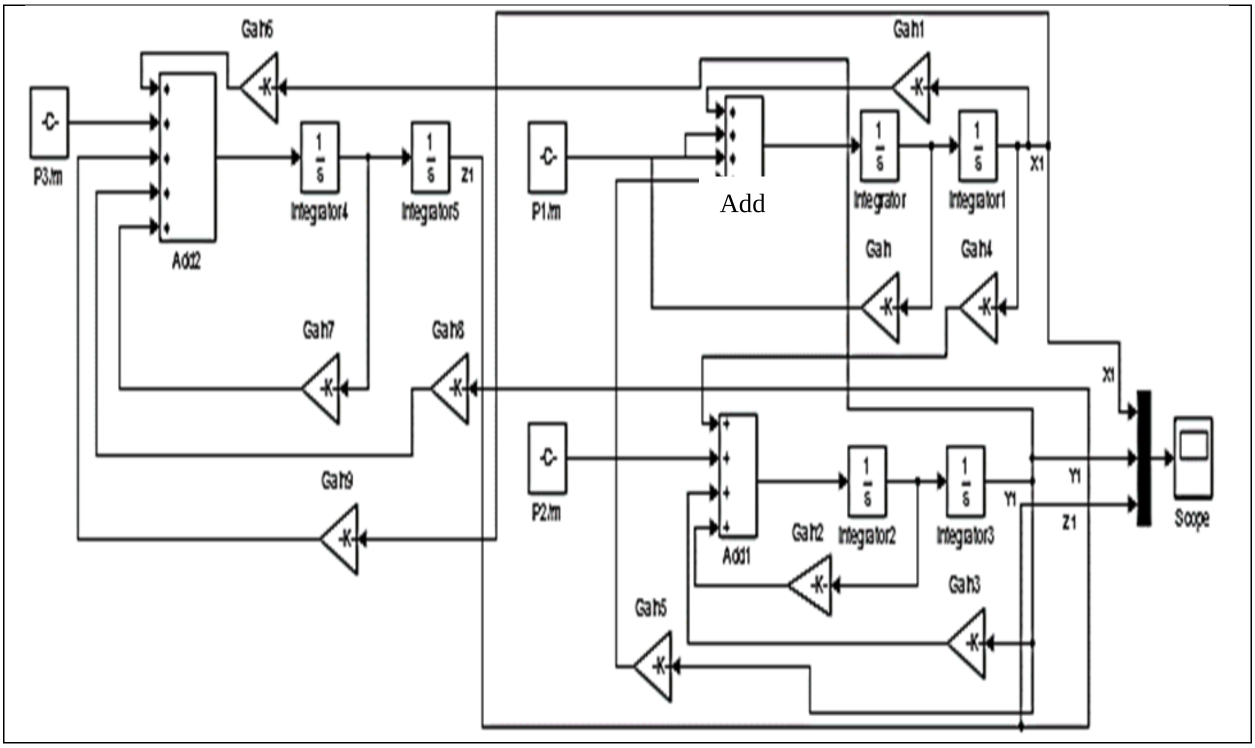

Figure 3.17: MATLAB / SIMULINK Simulation Block Diagram

By employing the MATLAB/Simulink, the turning process in question was simulated in the time from the initial contact between the cutting tool and workpiece until the cutting process becomes stable. Figure 3.18(a) shows the direction of vibration of the cutting tool. It can be seen that when the cutter touches the workpiece, the chatter at all directions is high. This attributed to the sudden change in the dynamic cutting force. As the time passes by, the chatter starts getting stable to a certain point. When the whole system gets stable, the chatter at z-direction and x directions chatter are high.

However, the chatter at y-direction is comparably small and almost negligible. This result is consistent with previous studies findings. Therefore, this proves that the kinematic model of the three degrees of freedom can adequately describes the cylindrical turning process in question. Moreover, the first natural frequency and second natural frequency of the vibration system are 2731Hz and 3233Hz, which seems to be close to each other. Therefore, the transient response of the vibration system will occur "pa" situation as shown in Figure 3.18(b).

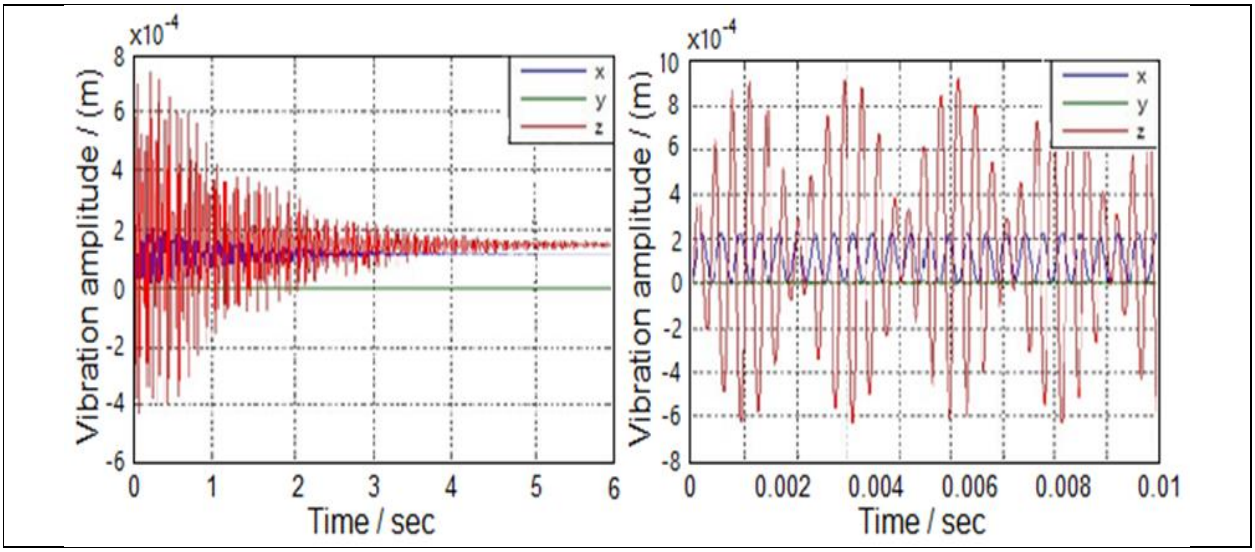

Figure 3.18: Transient Response of the Vibrated System when (a) 0<t<2 (b) 0<t<0.01

3.11 Chapter Summary

In this chapter, the chatter of cylindrical shape turning based on the regeneration effect was discussed and theoretically analyzed. The following phenomena were observed:

(1) The dynamic model of two-degree-of-freedom (2DOF) of turning regenerative chatter system was established. it is observed that the cutting motion of the axial feed in X direction, and the radial feed in the Y direction they have the greatest contribution to the regeneration effect, and has a great influence on the quality of the surface workpiece. Also, the cutting motion in the main direction (Z-direction) has a few contribution in the regeneration effect, and a little influence on the quality of the surface workpiece. This could be observed by analyzing the generating mechanism of chatter vibration in cylindrical turning machines

(2) Making use of calculation method of the limit cutting width of the machine tool cutting system was obtained, based on the principle of control theory. The stable lobe diagram of the machine tool cutting system was generated from a computer simulation, and the stability limit of the machine tool cutting system was determined. In addition, an increase in spindle speed (n) led to a periodic divergent in the stability limit cutting width b_{lim} of the system.

(3) The influence of natural frequency ω_n, stiffness k, unit cutting force coefficient k_c, damping ratio ζ and coincidence degree μ on vibration characteristics of the machine tool cutting system was analyzed using a computer simulation. It was observed that the natural frequency ω_n, stiffness k and damping ratio ζ are positively correlated with the area of the stable cutting area of the system; while the unit cutting force

coefficient k_c and coincidence degree μ are negatively correlated with the area of the stable cutting area of the system.

Chapter 4

Determination the Dynamic Parameters of the Machine Tool Cutting System

4.1 Introduction

In this chapter, the vibration characteristics of the cutting tool system in a cutting process that tested to verify the correctness of the turning regenerative chatter model based on the test conditions were discussed. Furthermore, the effect of cutting parameters on the vibration characteristics and the surface roughness of workpiece were studied through the experiment.

The process of analyzing the regenerative chatter model was utilized to determine the direction of main cutting vibration in the machine tool system, which related to with the correct establishment of the dynamic model for the regenerative chatter turning. Because, this could help to predict the stability of the machine tool's cutting system, as well it is necessary to identify the dynamic parameters accurately. Therefore, in this chapter the dynamic parameters (natural frequency ω_n, stiffness K, damping ratio ζ), and the cutting force unit coefficients (Kcu, Kcv) of the cutting process of nickel base superalloy were measured by using the hammering measurement method and the orthogonal cutting method.

4.2 Experimental Techniques

4.2.1 Introduction to Modal Analysis

The modal analysis is a method used in the identification of the vibrations in the engineering field. For a vibrating system, the vibration is quite complex and can be regarded as a combination of many kinds of motion characteristics. Each motion characteristic has a corresponding mode, and the corresponding modal parameters such as natural frequency, stiffness, damping, vibration mode, etc., which can be determined individually. Modal analysis usually composed of two parts; theoretical modal analysis and the experimental modal analysis. In the theoretical modal analysis, the modal parameters are obtained by analyzing the differential equations of the vibrating system or using the finite element calculations; in the experimental modal analysis, the modal parameters of the system obtained by analyzing the applied system external excitation and response signals, and then the inverse process of the theoretical modal analysis employed [151].

With the rapid development of electronic technology, sensor technology, and computer technology, the experimental modal analysis is becoming the favored and widely used in many industrial sectors because of its advantages, such as convenience, direct and accurate. In addition, the experimental modal analysis includes three elements as follows:

First, external excitation is applied to a point in the stationary system, and the other point of the system will produce a response signal with the time, then the input and output signals of the system collected and measured. That is, using a transfer function. To obtain the transfer function of the system, the digital signal processing technique is used such as FFT analysis method. Thereby, the system transfer function is fitted by the curve, and the modal parameters of the system are obtained.

4.2.2 Determination of Transfer Function

The machine tool system is a complex cutting system that includes n-degrees of freedom, each degree of freedom corresponds to parameters of the main vibration mode, the free vibration response in the physical coordinate system is a linear superposition of n motion for the main vibration, and the vibration differential equation which includes n degree of freedom can be expressed as follow, [156]:

$$M\ddot{x}(t) + C\dot{x}(t) + Kx(t) = f(t) \qquad (4.1)$$

Where: M, C, and K are the matrices of mass, dampers, and stiffness respectively and the representation a positive or a semi-positive symmetry matrix of the $n \times n$ degree, $x(t), x^{\cdot}(t)$, and $x^{\cdot\cdot}(t)$ are the displacement, velocity, and acceleration respectively. In the n discretized points or degrees of freedom (DOF) in the time domain, $f(t)$ is the external excitation force in the n, and the system could be stimulated by simple harmonic excitation:

$$f(t) = Fe^{j\omega t} \qquad (4.2)$$

Where: F is an amplitude matrix. The steady-state displacement response of the vibration system is:

$$x(t) = Xe^{j\omega t} \qquad (4.3)$$

Substituting Equations (4.2) and (4.3) into equations (4.1), the latter can be expressed as follow:

$$(K - \omega^2 M + j\omega C)X = F \qquad (4.4)$$

The frequency response function matrix is:

$$H = \frac{X}{F} \qquad (4.5)$$

$$H(\omega) = (K - \omega^2 M + j\omega C)^{-1} \qquad (4.6)$$

Then through a series of equations transformations, the matrix of the frequency response function can be obtained as follows:

$$H(\omega) = \sum_{i=1}^{n} \frac{\phi_i {\phi_i}^T}{k_i - \omega^2 m_i + j\omega c_i}$$

Where: $\phi_i \phi_i^T$ is the amplitude matrix for the system response.

4.2.3 Identification of Modal Parameters

After obtaining the frequency response function of the vibrating system, the modal parameters of the system are obtained by the curve measuring. Assume that there is a degree of coupling between the modes in the machine tool cutting system, and the distance between the modes is far.

Therefore, the single mode method fit used to identify the modal parameters. For this case where the natural frequencies of the modes of the vibrating system are more dispersed. It is suitable to apply the single dispersion modality method, as shown in Figure 4.1. and this could be approximated by the equation bellow when ω is close to Ωr, then:

$$H_{ij}(\omega) = \sum rH_{ij}\,(\omega) \approx_r H_{ij}(\omega) \qquad (4.7)$$

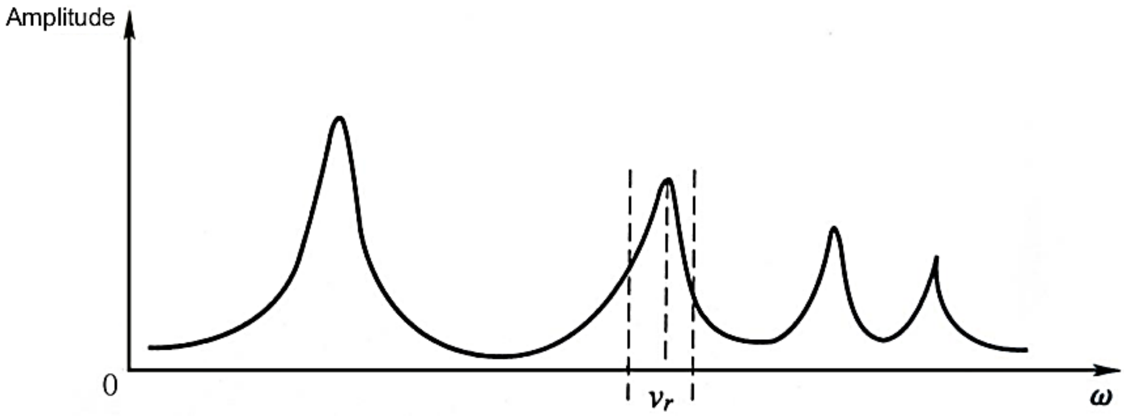

Figure 4.1: The Dispersion Modality

Where: rH is the contribution value in the frequency response function mode. Therefore, with such frequency response function one can use a system of the single degree of freedom.

$$rH_{ij}(\omega) = \frac{\phi_{ir}\phi_{jr}}{mr(\Omega_r{}^2 - \omega^2 + j2\sigma_r\omega)k_i} \qquad (4.8)$$

In the case the conditionality of the response function considered more complicated, then $rH_{ij}(\omega)$ can be expressed as follows:

$$rH_{ij}(\omega) = \frac{rR_{ij}}{2j(j\omega - s_r)} - \frac{rR_{ij}{}^{*}}{2j(j\omega - s_r{}^{*})}$$

$$= \frac{rU_{ij}+j_rV_{ij}}{2j(\sigma_r+j(\omega-v_r))} - \frac{rU_{ij}+j_rV_{ij}}{2j\big(\sigma_r+j(\omega+v_r)\big)} \qquad (4.9)$$

A real mode method can be proved as follows:

$$rR_{ij} =_r R_{ij}{}^{*} = \frac{\phi_{ir}\phi_{jr}}{m_r v_r} \qquad (4.10)$$

From Equation (4.10), the frequency response function of the system under a real mode can be obtained as follows:

$$rH_{ij}(\omega) = \frac{rR_{ij}}{2j\big(\sigma_r + j(\omega - v_r)\big)} - \frac{rR_{ij}}{2j\big(\sigma_r + j(\omega + v_r)\big)} \qquad (4.11)$$

Where: σ is the standard deviation, and rR_{ij} is called residue, which is used to identify a parameter in the process. If we want to get all the modal parameters, we need one row or one residue in the frequency response function matrix.

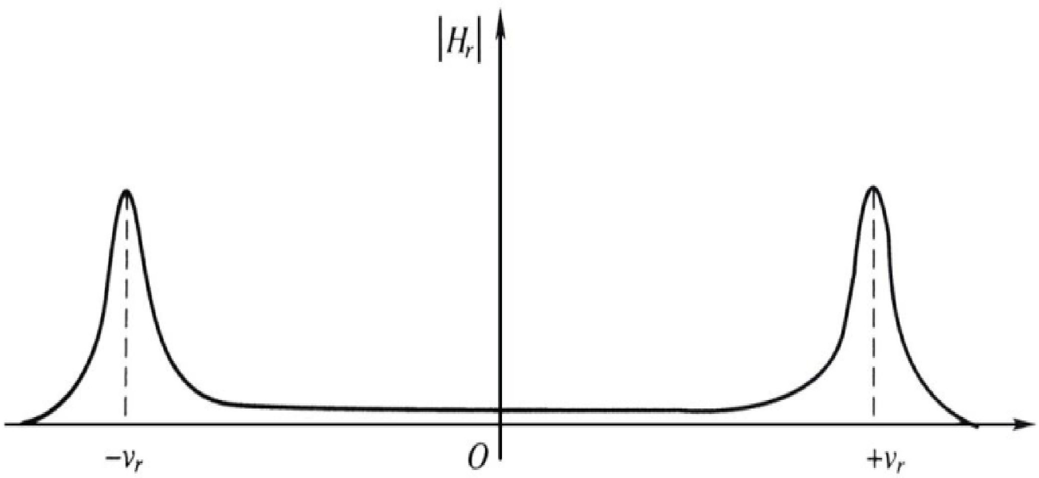

Figure 4.2: Amplitude Frequency Diagram

The amplitude frequency graph of $rH_{ij}(\omega)$ can be drawn by making use of the Equation (4.11). As shown in Figure 4.2, there is a wave peak at $-v_r$ and $+v_r$, Because the determining modal parameters usually depend on $+v_r$ in the drawn curve. Therefore, in the expression of the frequency response function only the first item was taken:

$$rH_{ij}(\omega) = \frac{rR_{ij}}{2j(\sigma_r + j(\omega - v_r))} \qquad (4.12)$$

The subscript is omitted, and the above formula can be expressed as follows:

$$rH = \frac{rR}{2} \frac{1}{\sqrt{{\sigma_r}^2 + (\omega - v_r)^2}} e^{j\alpha_r} = Re({}_r H) + j\, Im({}_r H)$$
$$= \frac{rR(v_r - \omega)}{2[{\sigma_r}^2 + (\omega - v_r)^2]} - j \frac{rR\sigma_r}{2[{\sigma_r}^2 + (\omega - v_r)^2]} \qquad (4.13)$$

Where: $\alpha_r = -\operatorname{arc} \tan^{-1}(\frac{\sigma_r}{v_r - \omega})$.

Figure 4.1 below shows the real frequency and the imaginary frequency graph.

The value of v_r and α_r are determined, according to the Equation (4.13), and then the real and imaginary parts of the frequency curve is drawn. As shown in Figure 4.3. The peak of the frequency correspond to the real part of the frequency curve is v_r.

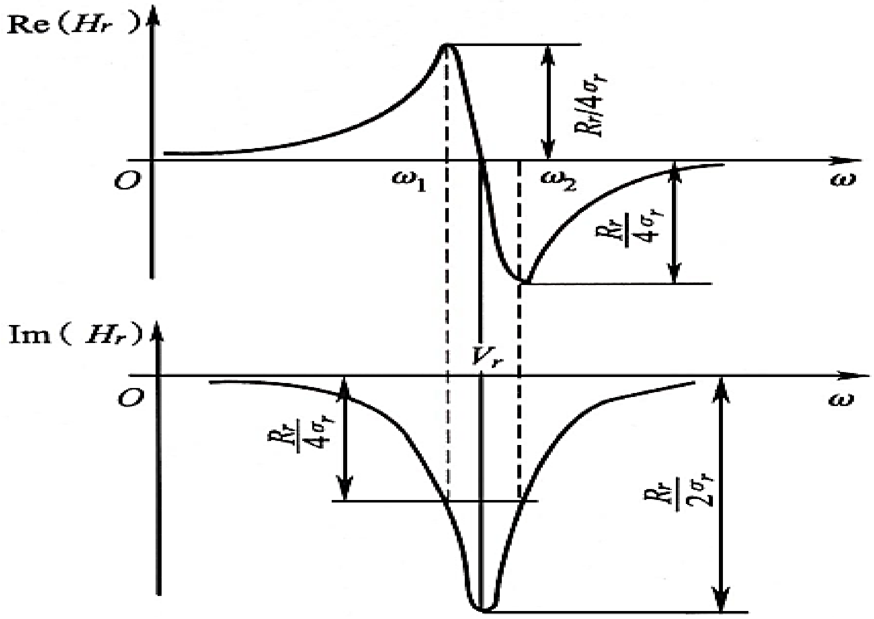

Figure 4.3: Real Frequency and Imaginary Frequency Graph

The positive and negative peak frequencies $\omega_1$and ω_2 corresponding to the real part of the frequency in curve and can be determined using the following equation:

$$\sigma_r = \frac{\omega_2 - \omega_1}{2} \qquad (4.14)$$

Under the real mode condition, when $\omega = v_r$, the real part of the frequency in curve passes through the real axis, $Re\ (r^H) = 0$, and the imaginary part of the frequency in curve corresponds to the peak value:

$$Im(_r\, H) = \frac{rR}{2\sigma_r} \qquad (4.15)$$

Therefore, the peak value of the imaginary part in the frequency in the curve can be measured, and the remained value can be calculated according to the formula above. In summary, the modal parameters can be obtained by using the real part of the frequency in the curve and the imaginary part of the frequency in the curve method.

Natural frequency:

$$\omega_n = v_r \qquad (4.16)$$

Damping ratio:

$$\zeta = \frac{\omega_2 - \omega_1}{2\omega_n} \qquad (4.17)$$

Stiffness k:

$$k = \frac{1}{2\zeta(R_a - R_b)} \qquad (4.18)$$

Where: R_a and R_b are the positive and negative peaks of the real frequency curve.

Modal mass m:

$$m = \frac{k}{{\omega_n}^2} \qquad (4.19)$$

4.3 The Measurement of the Modal Parameters of the Tool System

4.3.1 The Test Equipment

Hammer test is the most commonly used single-input and single-output modal test method. The main advantages are the equipment is simple, no support is needed, and the excitation point can be selected, and is more suitable for the test.

Figure 4.4 below illustrates Kistler 9722 A500 Type of Hammer.

Figure 4.4: Kistler 9722 A500 Type of Hammer

The hammer test usually consists of a hammer, an acceleration sensor, a charge amplifier, and a data recorder. As shown in Figure 4.4, the hammer itself is the main excitation device for the test, and it consists of a hammerhead, a piezoelectric force sensor, and a hammer handle. The hammerhead contains different materials such as steel, rubber, and polyethylene, and each material corresponds to the frequency range of response that measured. Because the sampling frequency reaches $5000\ Hz$, the steel hammer is selected.

The acceleration sensor used for the test is shown in Figure 4.5.

Figure 4.5: Kistler 8640 A50 Type of Acceleration Sensor Amplifier

The data which the accelerometer records are the force signal input by channel 1 and the acceleration signal produced by hammering along channel 2. The test equipment is shown in Table 4.1.

Table 4.1: Test Equipment

No	Name
1	Kister 9722 A500 Type of hammer
2	Kister 5134 B Type of charge amplifier
3	Kistler 8640 A50 Type of acceleration sensor
4	GL 900 high-speed isolation eight channels' data recorder

Figure 4.6 below illustrates the block diagram of the modal test system for the hammer.

The test apparatus consists of the following components:

(i) A computer device.

(ii) Multi-channel data recorder.

(iii) Charge amplifier.

(iv) Hammer supplied with force sensors.

(v) Magnetic seat.

(vi) Acceleration sensor.

(vii) Tip.

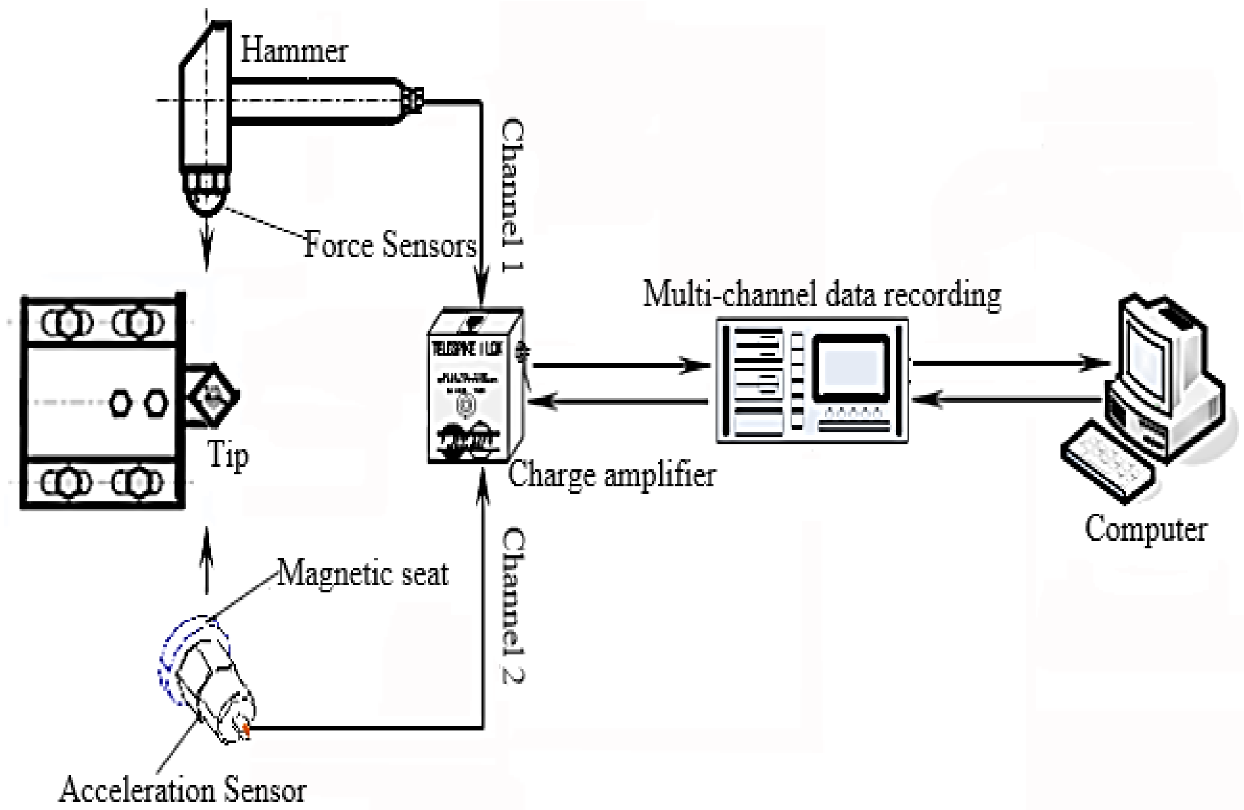

Figure 4.6: Block Diagram of the Modal Test System for Hammer

4.3.2 Test Process Experimental Procedure

The block diagram of the hammering mode testing system is shown in Figure 4.6. The frequency response characteristics of the tool system in the X and Y directions are measured by the force hammer pulse excitation method. During the test, the acceleration sensor is mounted on the tool by the magnet near the tip of the tool, and then the hammer is used to excite the acceleration sensor on the opposite side. The head of the hammer is equipped with an acceleration sensor to acquire the input pulse signal. At the same time, the response signal of the vibration is obtained by the external acceleration sensor. The modal hammer test site is shown in Figure 4.7 below.

Figure 4.7: Hammer Test Site

The hammer signal acquisition is shown in Figure 4.8 below.

Because the hammerhead area is too small, this causes difficulty in hammering. In the mode hammer test, we should pay attention to the following points:

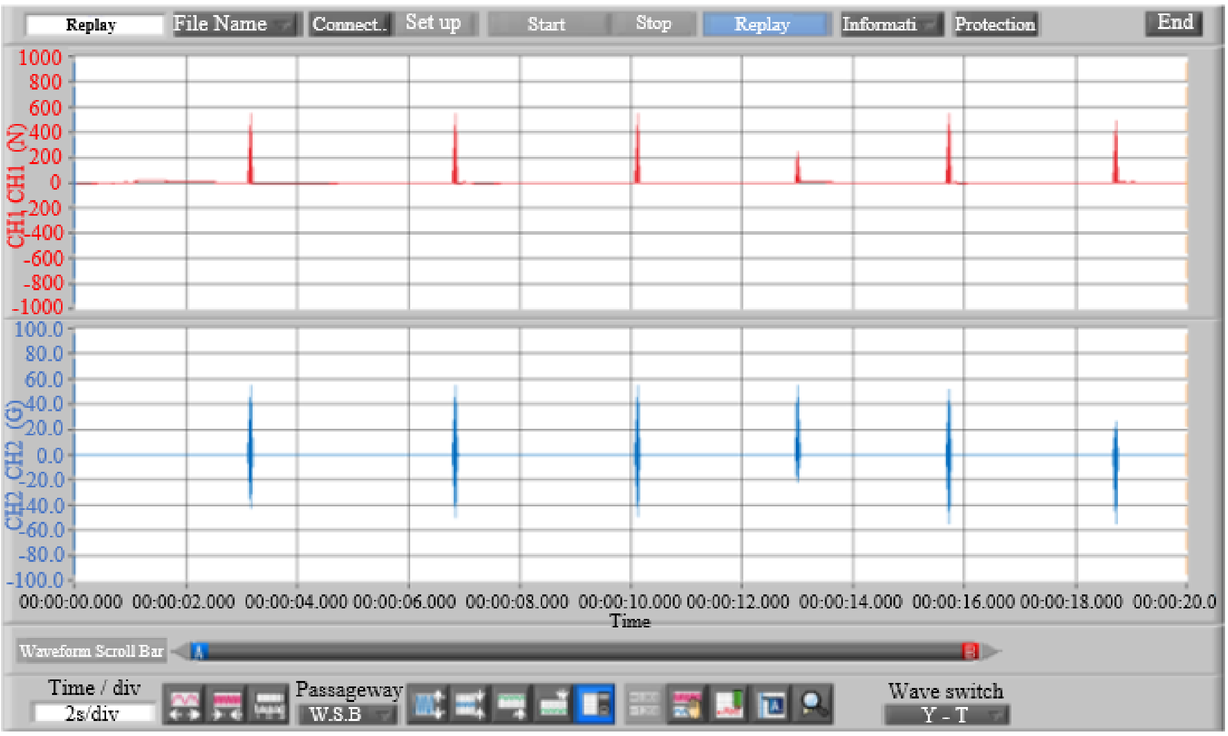

Figure 4.8: Hammer Signal Acquisition

(1) When hammering is done, the effectiveness of the hammer is judged by observing the waveform of the excitation and response in the computer. The method for determining the waveform effect of the force and acceleration signals is the same, and the waveform includes the triggering and non-triggering portions. The trigger portion contains a transient pulse signal accompanied by a short decay; the non-trigger part is a straight line and coincides with the horizontal axis, as shown in Figures 4.9 and 4.10. If the ripple is more massive, or a sharp burr, or a continuous pulse appears

in the non-trigger part, this indicates that the effect is not ideal and should be hammered again.

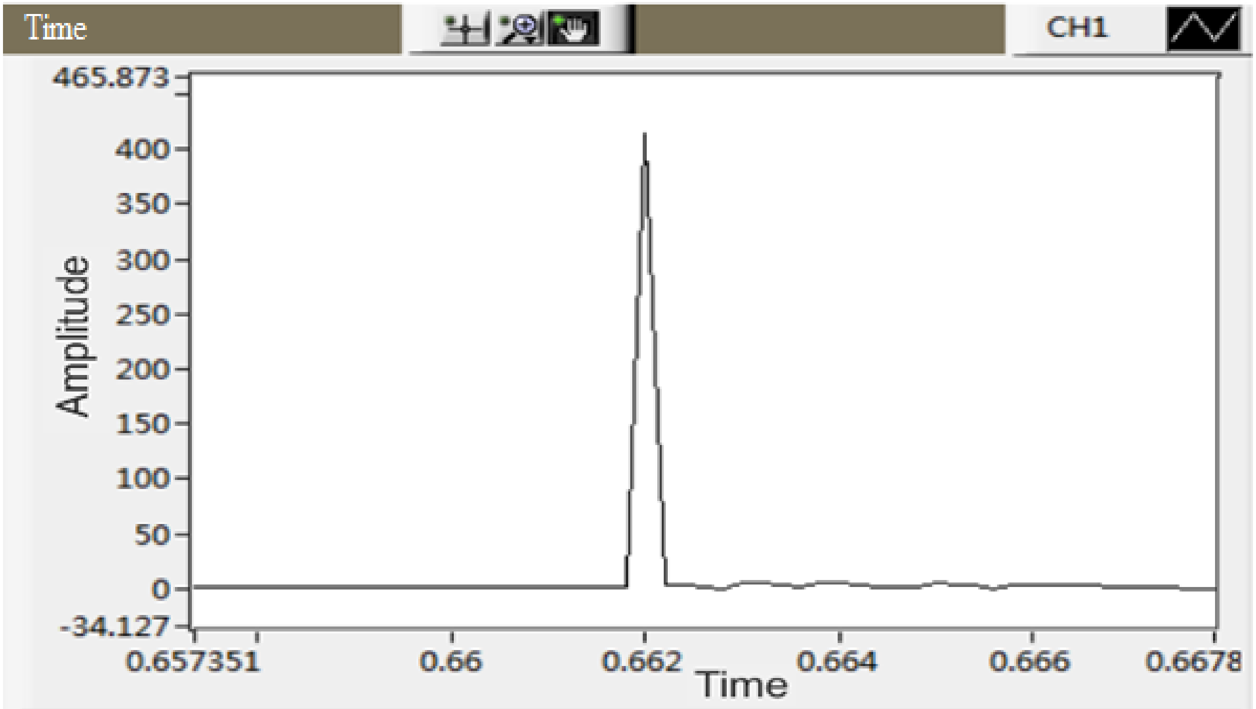

Figure 4.9: Excitation Signal: Hammer Force (N)

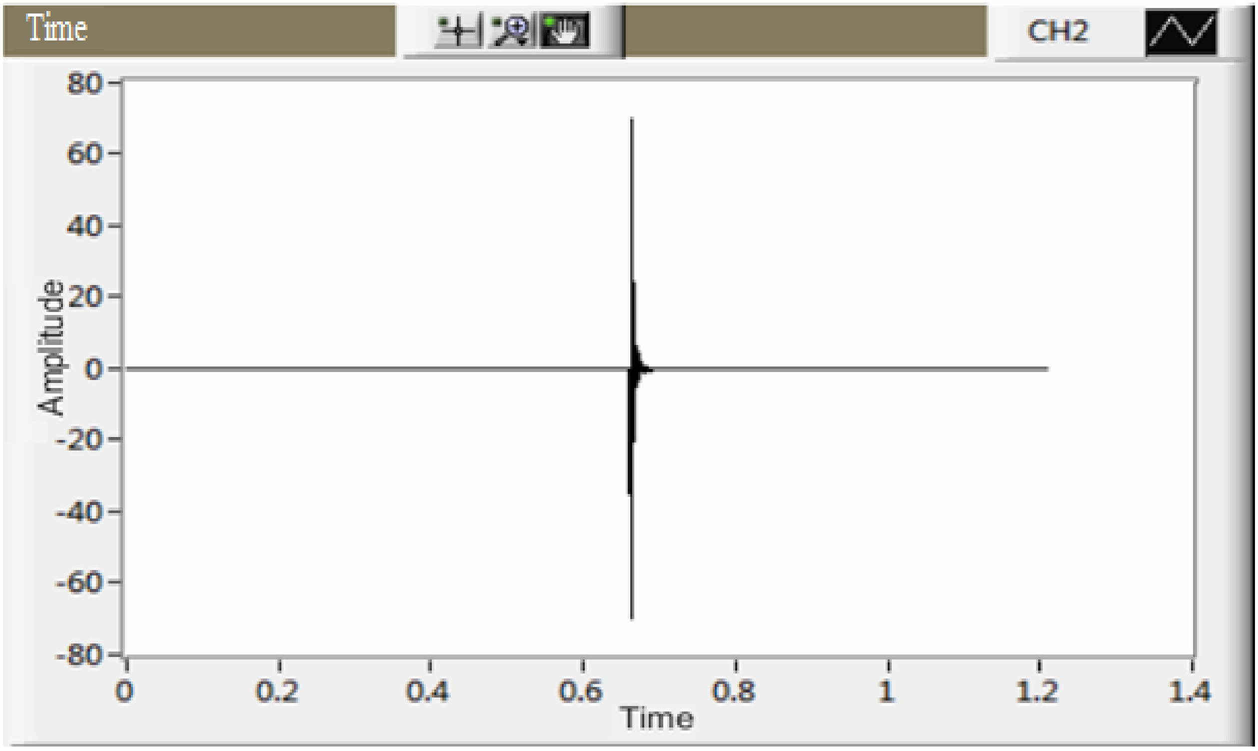

Figure 4.10: Response Signal: Acceleration (g)

(2) The location of the hammer and the installation position of the sensor should be determined according to the mode of vibration to be measured. When hammering, the node of the measured vibration type should be avoided, this because it increases the signal-to-noise ratio. Usually, the position where the maximum amplitude can be generated is the best hammering position. The acceleration sensor for the signal sampling in the X and Y directions and their installing locations are shown in Figures 4.11 and 4.12 respectively.

(3) Between any two hammering, we should make sure that the response signal is completely attenuated. Otherwise, there will be a knock phenomenon and overlap in the signals.

(4) For small damped metal structure mechanical systems, the sampling frequency setting should not be too high. Otherwise, the sampling time will be too short and the response signal will be cut off, which will lead to energy leakage.

(5) When measuring the frequency response function, the coherent function should be measured at the same time to ensure that the corresponding value of the coherence function at the apex of the amplitude-frequency curve of the transfer function is not less than 0.8. Otherwise, it is indicated that there is noise interference, and the test needs to be repeated.

Figure 4.11 below shows the Installation of the Acceleration Sensor in the X Direction, whereas, Figure 4.12 illustrates the Installation of the Acceleration Sensor in the Y Direction.

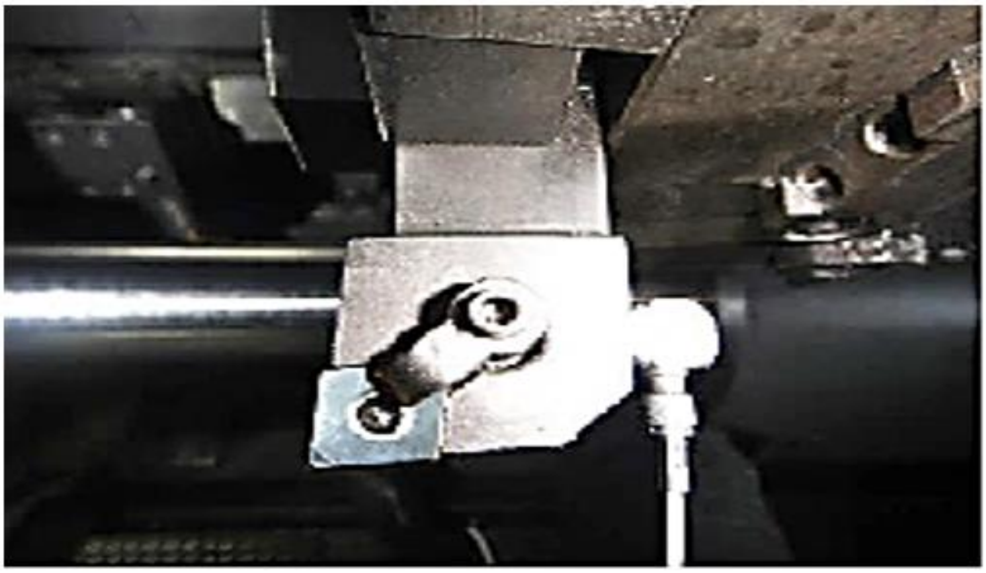

Figure 4.11: Installation of the Acceleration Sensor in the X Direction

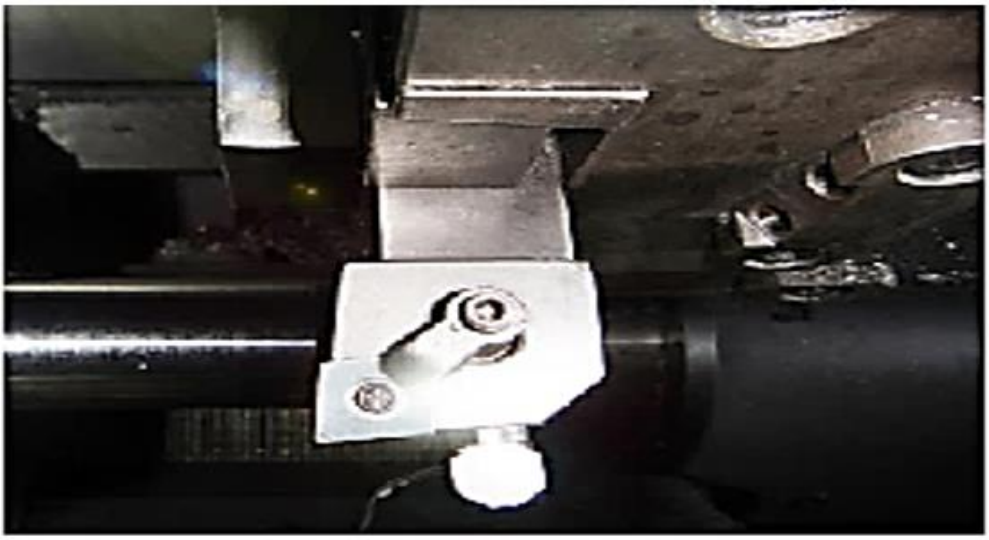

Figure 4.12: Installation of the Acceleration Sensor in the Y Direction

4.3.3 Test Results

The sample data were analyzed and the directional frequency response function (FRF) in the X and Y directions was calculated by the (HR soft (MA) V1. 9) software (Figures 4.13 and 4.14).

Figure 4.13 below illustrates graphically the frequency response function in the X direction.

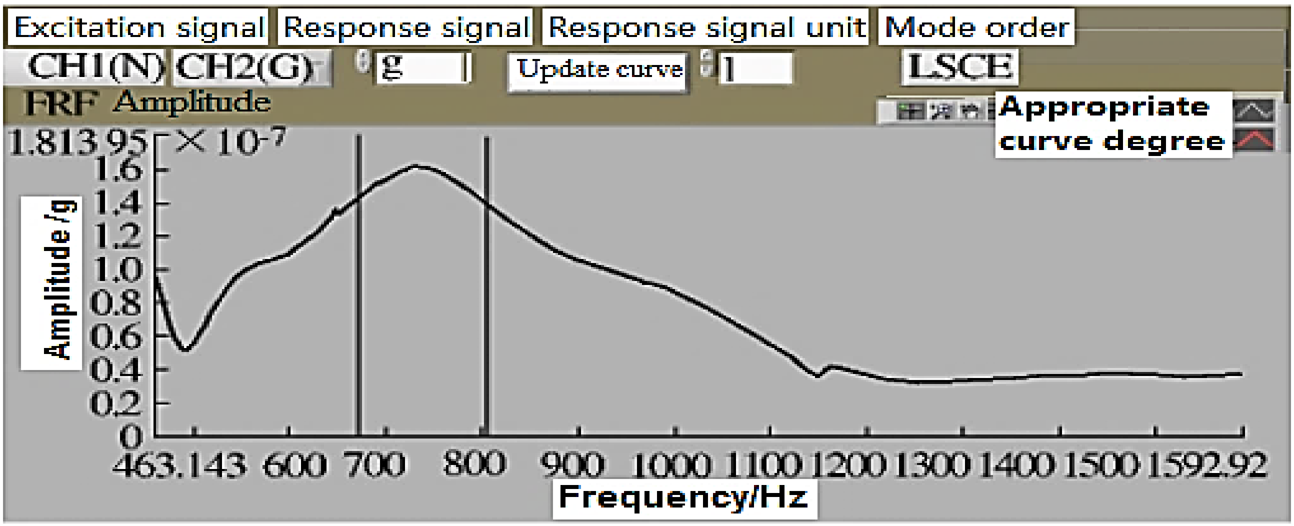

Figure 4.13: The Frequency Response Function in the X Direction

Figure 4.14 below illustrates graphically the frequency response function in the Y direction.

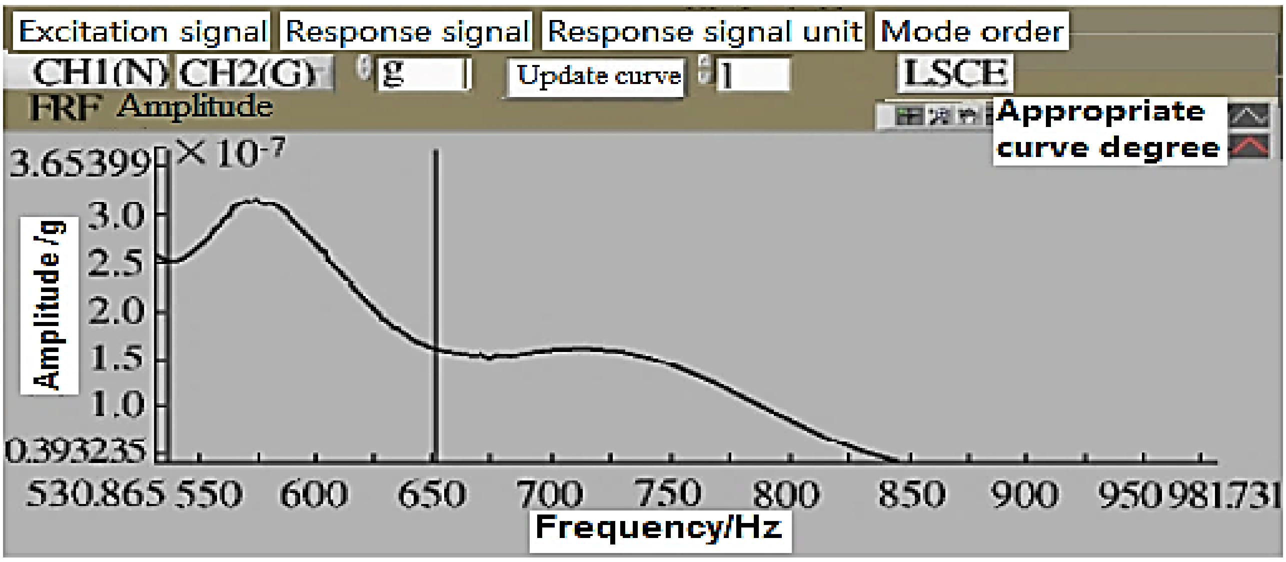

Figure 4.14: The Frequency Response Function in the Y Direction

Table 4.2 below shows the measured modal parameters (i.e., Modal frequency, Modal Damping, Modal Stiffness, and Modal Mass) in the X-direction.

Table 4.2: Measured Modal Parameters in the X-Direction

No	Modal frequency /Hz	Modal Damping /%	Modal Stiffness /N/m	Modal Mass /Kg
1	721.64	4.87	6.39×10^7	122.70
2	/	/	/	/

Table 4.3 below shows the measured modal parameters (i.e., Modal frequency, Modal Damping, Modal Stiffness, and Modal Mass in the Y-direction.

Table 4.3: Measured Modal Parameters in the Y-Direction

No	Modal frequency /Hz	Modal Damping /%	Modal Stiffness /N/m	Modal Mass /kg
1	565.96	3.12	5.23×10^7	162.94
2	708.67	3.43	9.05×10^7	180.37

Tables 4.2 and 4.3 show the measured modal parameters results in the X and Y directions. The experimental results have shown that the natural frequency values at the 1st and 2nd test in the Y direction are far apart. However, there is a convergence between natural frequency values in the X direction at 1st test which approximately equals 722 Hz and in the Y direction at 2nd test which approximately equals 709 Hz, indicating that there are modal coupling effects in the X and Y directions. According to the

natural frequency value at the main position in, the X direction 721Hz and in the Y direction 565Hz, the test results are perfectly acceptable.

4.4 The Natural Frequency of the Main Components of the Machine Tool

4.4.1 Purpose of the Experiment

In this experiment, the cutting system of the machine tool has been used as the main vibration system, and the frequency response characteristics of the other components that may have chattering were measured to determine the natural frequency of the main vibration system. In order to determine the test correctness, a test of the lathe head of machine tool that vibrate during the cutting process was conducted and the effect of the lathe head rack which cause vibration in the cutting process was studied and the test conditions were the same as in the previous section.

4.4.2 Experiment Results

Figures 4.15 and 4.16 show the frequency response curves of hammering tests for the headstock and tailstock, respectively. In order to eliminate the influence of strong noise interference on the transmission characteristics of the system, the experiment data were processed by the respective analysis.

Figures 4.15 and 4.16 illustrate clearly and respectively the Headstock Data Processing Results, and the Tailstock Data Processing Results.

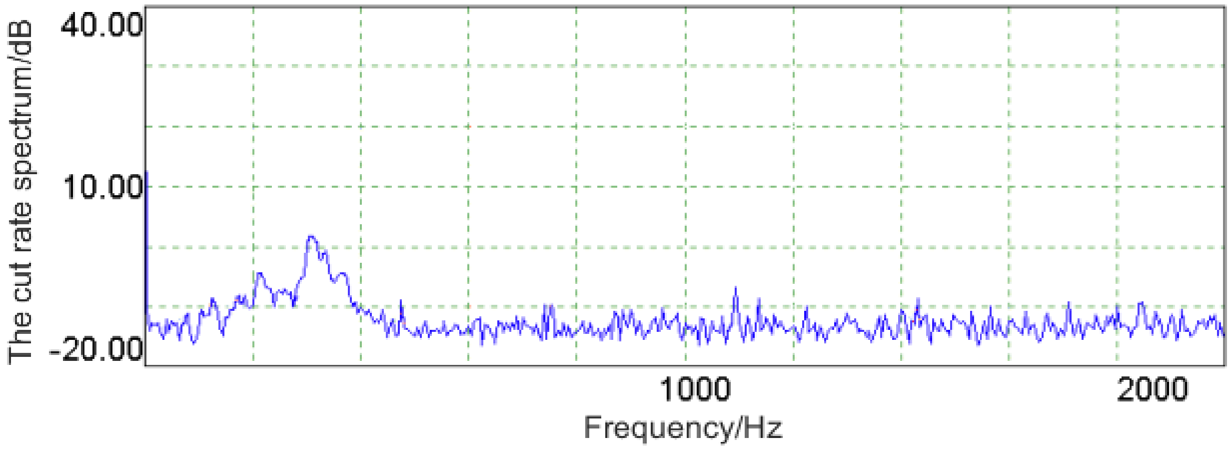

Figure 4.15: Headstock Data Processing Results

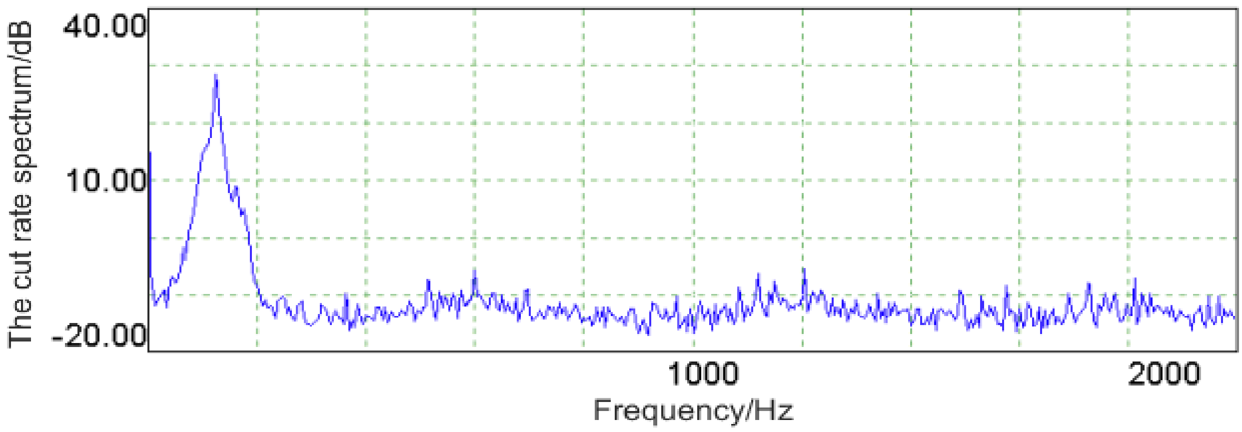

Figure 4.16: Tailstock Data Processing Results

Table 4.4 below shows the natural frequencies of the other parts (i.e., Head frame of machine tool, and Tail frame of machine tool).

Table 4.4: The Natural Frequencies of the Other Parts

Parts	1st step	2nd step
Head frame of machine tool	203	298
Tail frame of machine tool	117	/

Table 4.4 shows the modal test results of machine tool headstock and machine tool tailstock, and all observed natural frequencies was less than 300 Hz .In the machine tool cutting process, chatter usually occurs on the

weakest link of the machine tool. Besides in tool system and workpiece system, the possibility of vibration of machine tool tailstock is greater. However, the chatter frequency is impossible to occur in the low range frequency, thus excluding the possibility occurrence chatter for the headstock and tailstock of the machine tool these considered as the main body.

4.5 Calculation of the Cutting Force Coefficient Unit in X and Y Directions

4.5.1 Calculation Principle

The cutting force in the turning process is shown in Figure 4.17 below. As shown in Figure 4.17(a), F is a resultant force, and F_f, F_p, and F_z are the three force components (i.e., feed force, main force and back force), respectively.

Where: α is the angle between the resultant force F and the base force F_d, β is the angle between the feed force F_f and the base force F_d, the three force components are as follows:

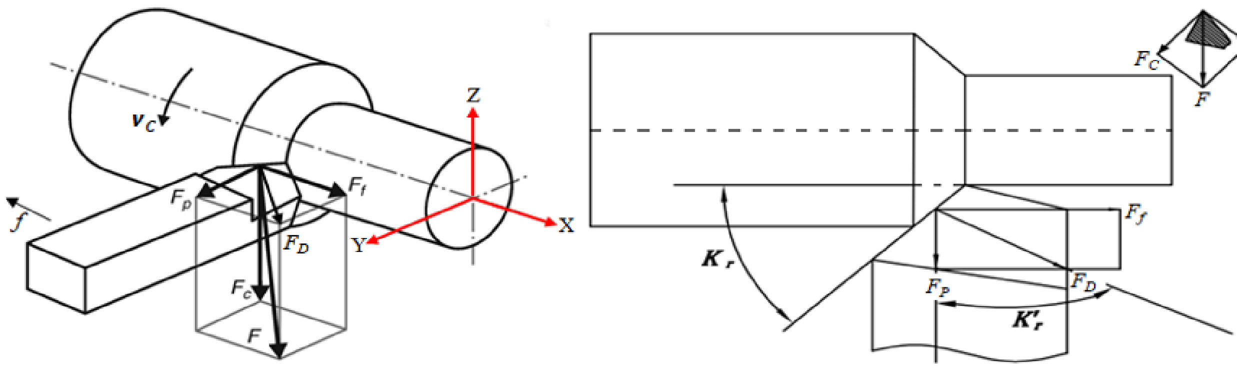

(a) (b)

Figure 4.17: Cutting Force in Turning

$$F_d = F\cos\beta \qquad (4.20)$$

$$F_f = F_d\cos\alpha \qquad (4.21)$$

$$F_p = F_d\sin\alpha \qquad (4.22)$$

Therefore,

$$F_f = F\cos\beta\cos\alpha = k_{cu}bh \qquad (4.23)$$

$$F_p = F\cos\beta\sin\alpha = k_{cv}bh \qquad (4.24)$$

Where, k_{cu} and k_{cv} are the cutting force unit coefficients in the X and Y directions, respectively, b is the cutting width, h is the cutting thickness. The resultant cutting force is calculated as follows:

$$F = k_c bh \qquad (4.25)$$

Where: k_c is cutting coefficient, which depends on the material and size of the workpiece, it can be seen from the literature that the nickel-based superalloy GH4169 after aging treatment the hardness of HB is $300 \approx 475$ 30, and the joint force per unit area of the cutting layer is $4150\ N/mm^2$ [157]. Therefore, as long as the values of α and β are determined experimentally, the cutting force unit coefficients k_{cu} and k_{cv} in both directions can be obtained.

According to the relationship between the cutting forces shown in Figure 4.17(b), we can obtain:

$$\alpha = tan^{-1}(F_p/F_f) \qquad (4.26)$$

$$\beta = tan^{-1}(F/F_d) = tan^{-1}(F/\sqrt{{F_f}^2 + {F_p}^2}) \qquad (4.27)$$

Therefore, the equations for calculating the cutting force unit coefficients k_{cu} and k_{cv} in the X and Y directions can be written as follows:

$$k_{cu} = k_c \cos\beta \cos\alpha \qquad (4.28)$$

$$k_{cv} = k_c \cos\beta \sin\alpha \qquad (4.29)$$

4.5.2 Test Method and Test Conditions

The cutting test was carried out on (Seiko HTMTC 40) CNC lathe machine; the cutting force was measured by using a Kistler 9527 B three-way dynamometer, the remaining test conditions are the same as those for subsequent cutting stability tests. The cutting force obtained by the test device and the test site are shown in Figures 4.18 and 4.19, respectively.

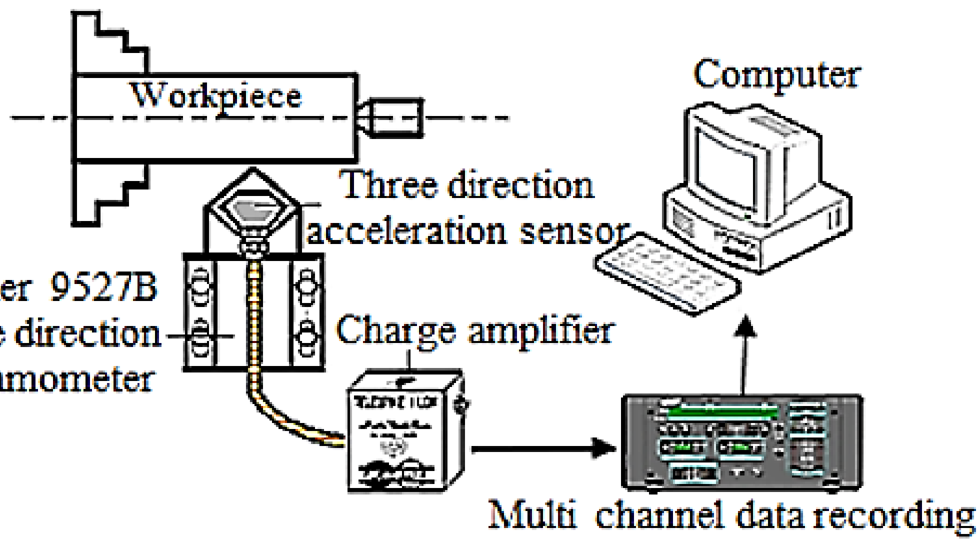

Figure 4.18: Schematic Diagram of Vibration Monitoring

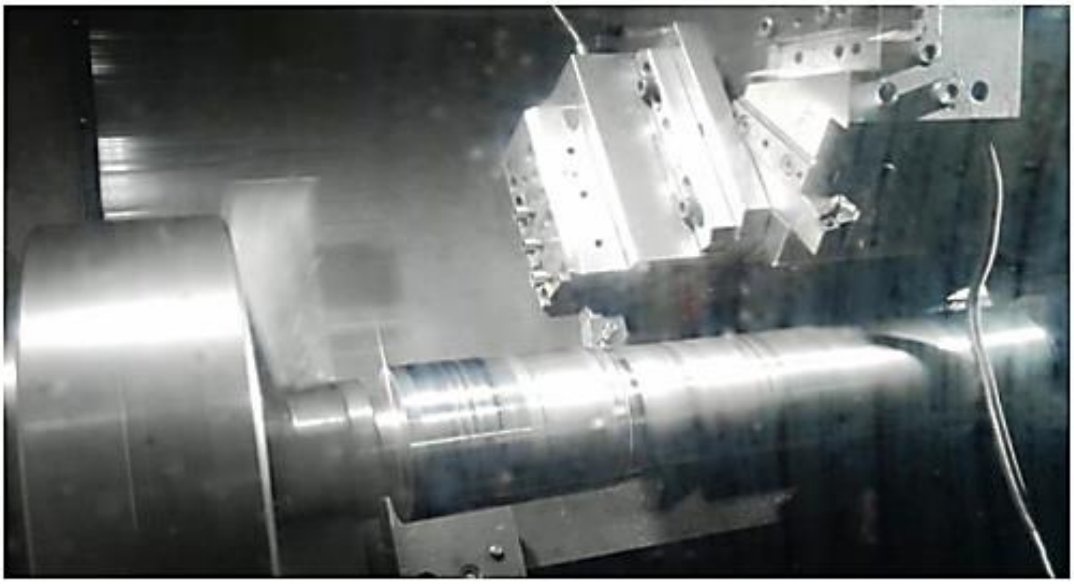

Figure 4.19 Setup of Turning Test

In this test, the cutting force values under different cutting parameters are measured separately. The more the number of test measurements, the more accurate the results obtained. However, due to the limited experimental conditions and economics, the experiment was conducted 16 times.

4.5.3 Test Results

The test results of the cutting force measurement are shown in Table 4.5.

Table 4.5: Cutting Force Measurement Test Results

Test number	Cutting speed (m/min)	Cutting depth (mm)	Feed rate (mm/r)	F_x (N)	F_y (N)	F_z (N)	F_e (N)
1	40	0.15	0.05	40.63	45.16	91.26	109.62
2	40	0.20	0.10	56.17	45.54	151.64	167.99
3	40	0.25	0.15	61.77	88.48	262.22	283.55
4	40	0.30	0.20	86.46	145.54	407.31	441.08
5	60	0.15	0.10	52.88	43.02	124.16	141.64

6	60	0.20	0.05	58.02	83.12	189.31	214.74
7	60	0.25	0.20	83.52	116.08	335.98	365.14
8	60	0.30	0.15	78.74	132.52	388.41	417.88
9	80	0.15	0.15	43.15	57.21	180.87	194.54
10	80	0.20	0.20	53.88	54.04	170.60	186.88
11	80	0.25	0.05	58.95	60.14	147.58	169.91
12	80	0.30	0.10	75.77	123.89	297.83	331.34
13	100	0.15	0.20	32.96	57.86	203.89	214.48
14	100	0.20	0.15	33.74	50.60	193.68	203.01
15	100	0.25	0.10	34.26	62.04	202.62	214.65
16	100	0.30	0.05	32.66	94.58	196.85	220.82

The α and β values obtained from the test results are shown in Table 4.6 below.

Table 4.6: The Values of α and β Obtained from the Test Results

Test number	1	2	3	4	5	6	7	8
α value	48.02°	39.03°	55.08°	59.29°	39.13°	55.08°	54.26°	59.28°
β value	56.35°	64.51°	67.63°	67.43°	61.23°	61.83°	66.94°	68.35°
Test number	9	10	11	12	13	14	15	16
α value	52.97°	45.08°	45.57°	58.55°	60.33°	56.30°	61.09°	70.95°
β value	68.38°	65.90°	60.29°	64.01°	71.91°	72.51°	70.72°	63.06°
average value	α_{average} =53.75°				β_{average} =65.69°			

Therefore, according to equations (4.20) to (4.29), the cutting force unit coefficient in the X and Y directions can be obtained separately and expressed as follows:

$$k_{cu} = k_c \cos\beta \cos\alpha = \frac{1010N}{mm^2} \qquad (4.30)$$

$$k_{cv} = k_c \cos\beta \sin\alpha = \frac{1377N}{mm^2} \qquad (4.31)$$

4.6 Prediction of Stable Limit Cutting Width

From the analysis of the theory of regenerative turning chatter in Chapter 3, it is known that the dynamic parameters of the machine cutting system are (natural frequency ω_n, stiffness k, damping ratio ζ) and the dynamic parameters of the cutting process are (cutting force unit coefficient Kc, and coincidence degree μ) are determined, the Equations (3.31) and the (3.32) can be used to obtain the b_{lim} value of the limit cutting width. Therefore, if the stable limit cutting width can be predicted before machining, the machining efficiency can be effectively provided and the machining quality can be guaranteed. From the stable lobe diagram (Lobe), it can be seen that the stable limit cutting width b_{lim} is characterized by a divergent increase and periodic cycle. Therefore, theoretical analysis shows that as long as the limit cutting width $(b_{lim})_{min}$ is predicted, the cutting system of the machine tool is kept in the stable cutting area, and no chatter will occur when machining is performed at any spindle speed. Therefore, the predicting of the limit cutting width $(b_{lim})_{min}$ has important practical significance.

According to the theory of regenerative chatter, that when the coincidence degree μ = 1, The regenerative effect reaches the maximum stage, and the vibration is the strongest at this time, and the limit cutting width of the machine tool cutting system must reach to the minimum. By compensation $\mu = 1$ in equation (3 .23) we can get the following expression:

$$\left(b_{lim,y}\right)\frac{2k_y}{k_{cv}\mu}\frac{\left(1-\lambda_y{}^2\right)^2+\left(2\zeta_y\lambda_y\right)^2}{1-\lambda_y{}^2}_{min} \qquad (4.32)$$

In equation (4.32), the minimum value is obtained when $\lambda = \sqrt{1+2\zeta}$; since the natural frequency ω_n of the system is always less than the frequency ω of the steady-state system vibration, Therefore, $\lambda = \omega / \omega_n > 1$, and therefore [158]:

$$\lambda = \sqrt{1 \pm 2\zeta} \qquad (3.33)$$

By substituting the above formula into Equation (4.32), the minimum limit cutting width can be expressed as follows:

$$\left(b_{lim,y}\right)\frac{2k_y\left(1+2\zeta_y\right)}{k_{cv}\mu}_{min} \qquad (4.34)$$

Table 4.7 below shows the kinetic parameter values obtained by experiment as follows:

Table 4.7: Test Results of the Kinetic Parameters

Direction	Dynamic parameters of main vibration system			Dynamic parameters of the cutting process
	ω_n (Hz)	K (N/m)	ζ (%)	k_c (N/mm^2)
X	721.63	6.39×10^7	3.11	1010
Y	565.95	5.22×10^7	2.49	1377

By substituting the above parameters into equation (4.34), the minimum limit cutting widths in the X and Y directions can be obtained as follows:

X-direction:

$$\left(b_{lim,x}\right)_{min} = 4.61mm \qquad (4.35)$$

Y-direction:

$$\left(b_{lim,x}\right)_{min} = 1.98\,mm \qquad (4.36)$$

From the above calculation results, we can see that the ultimate cutting depth in Y direction is less than the limit cutting width in X direction. When the cutting width reaches the limit cutting width in the Y direction, the machine cutting system will produce chatter. Therefore, the minimum limit cutting width in the Y direction is determined as the minimum limit cutting width of the machine tool cutting system. The minimum limit cutting width of the machine tool cutting system is:

$$(b_{lim})_{min} = 1.98\,mm \qquad (4.37)$$

By substituting the above kinetic parameters into equations (3.30) and (3.32), the stable lobes of the nickel-based superalloy GH4169 can be drawn, as shown in Figure 4.20.

Figure 4.2 shown below illustrates the stable turning diagram for GH4169 nickel-based superalloy.

As shown in Figure 4.20, the "gap" between adjacent two lobes are very small in the range of cutting speed suitable for turning nickel-base superalloy GH4169. Therefore, the minimum ultimate cutting depth $(b_{lim})_{min}$ can be regarded as the allowable range of maximum cutting depth in machining. In practice processing, the cutting efficiency and cutting stability should be considered comprehensively. When the cutting speed is selected, the depth of cutting away from the unstable area while ensuring maximum cutting efficiency should be selected. When the depth of cut is selected, must choose the largest cutting speed corresponding to the stable area.

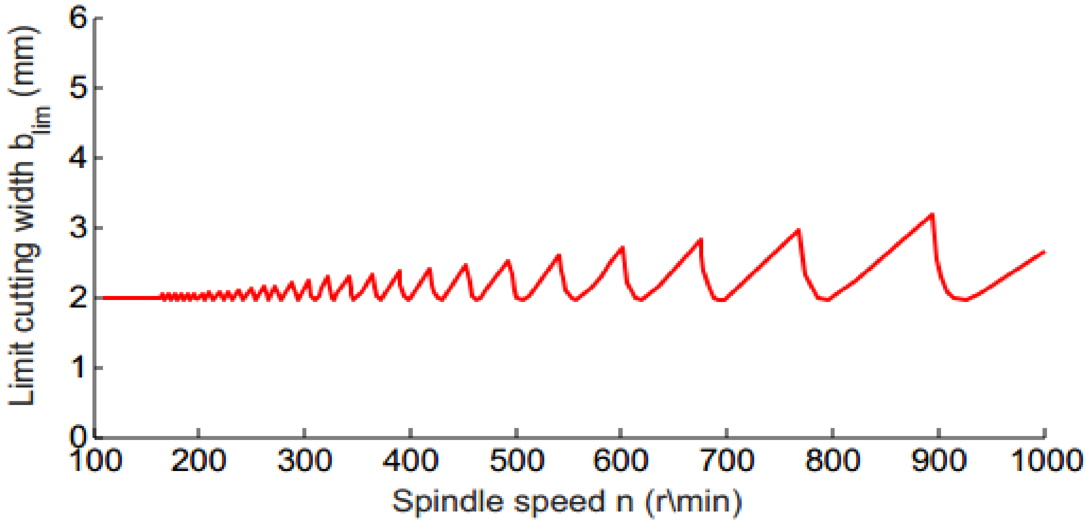

Figure 4.20: The Stable Turning Diagram for GH4169

4.7 Chapter Summary

In this chapter, the dynamic parameters of the machine tool cutting system were determined, through that the limit cutting width of the nickel-base superalloy processing was predicted, the main contents of that are as follows:

(1) In order to determine the model parameters of the tool system. The modal parameters (natural frequency ω_n, stiffness k, damping ratio ζ, model mass m) of the tool system in the X and Y directions were measured

by the model hammer test method. The experimental results showed that, the natural frequency values at the 1st and 2nd test in the Y direction are far apart, but there is a convergence between natural frequency values in the X direction at 1st test which is approximately equals 721Hz and in the Y direction at 2nd test which is approximately equals 708Hz. These results indicate that, there are coupling effects in the X and Y directions. According to the natural frequency value at the main position in the X direction (721Hz), and in the Y direction (565Hz), the test results are perfect and acceptable.

(2) In order to deselect the main vibration source of the cutting tool system. During the cutting process, chatter usually occurs at the instant the natural frequencies for the machining occur. The part where the machine tool vibrates largely, is the tailstock at the back-machine part. All tests were showed that, most values of the natural frequencies are less than 300 Hz. However, the chatter frequency is does not occur in this range of low-frequency. Thus, the possibility of vibration in the tailstock at the back-machine part was ruled out as a principal source for vibration, which leads to the chatter occurrence at the cutting process.

(3) To calculate the cutting forces unit coefficient k_{cu} and k_{cv}. According to the cutting force and the cutting motion in the turning process, the orthogonal test method is used to determine the main angles of the PCBN cutting tool of high-speed turning nickel-base superalloy, and should be

used to calculate the cutting forces unit coefficient k_{cu} and k_{cv} in X and Y directions, which they were calculated by a trigonometric function.

(4) On the basis of determining the dynamic parameters of the machine tool cutting system and of the nickel-base superalloy cutting process. It is found that, the minimum limit cutting width of the nickel-base superalloy machining is $(b_{lim})_{min} = 1.98mm$, which could be observed from the stability limit lobe diagram.

Chapter 5

The Simulation Study of Cutting Stability on Nickel-Based Super Alloy

5.1 Introduction

Rapid development of computer technology has accelerated the introduction of advanced modern engineering applications and software with practical and intuitive problem-solving features and convenient user interface. These features are quite useful to researchers in the application of the software. One of the most widely used engineering software tools is the MATLAB. In this chapter, the influence of cut parameters on vibrations, and the law of cutting chatter in the production process to improve the processing efficiency and the surface quality of workpiece using MATLAB / Simulink simulation platform to simulate regenerative chatter of the cylindrical turning are study.

5.2 MATLAB / Simulink Simulation Software

Simulink is developed by MathWorks in the late Twentieth Century, and Simulink is a software package with the capability to model, simulate, and analyze systems whose outputs change over time. Such systems are often referred to as dynamic systems. Simulink can be used to explore the behavior of a wide range of real-world dynamic systems [88]. In the environment of this software, users can directly call the existing analog modules on the screen and connect to the model structure of the system through visual modeling. After the Simulink simulation program of the object model is run, the simulation results can be obtained, and the simulation process can be intervened [13].

Simulink is applicable to linear and nonlinear systems, and also is applicable to continuous and discrete systems and continuous and discrete hybrid systems. It is applicable to both constant and variable systems. Because simulation is powerful and easy to use, it has become one of the most dynamic applications of system simulation software.

Simulink simulation provides a graphical user interface, which can directly use the mouse operation to connect the standard modules correctly. When the parameters of each module are completely set with the parameter dialog box, a dynamic system model is formed. If no parameter is set before a module is set up, the default parameter value of the module setting is the module parameter. The content of the Simulink module library is also very rich. It includes the input signal source module library (Sources), the output reception module library (Sinks), the continuous system module library (Continuous), the discrete system module library (Discrete), the mathematical operation module library (Math operations), and many of other standard modules. In addition, users can customize and create modules according to needs.

After the system model is established, then the appropriate simulation parameters and numerical algorithms are selected, and the simulation system can start the simulation program through the Simulink menu or the execution of the MATLAB command. At the time of simulation, the user can observe the simulation results through the Scope module in the Sinks module library or other display modules, and can also store the results in the MATLAB workspace for later use. The user can also adjust the system parameters to observe and analyze the changes in the simulation results, so as to get a better simulation result.

5.3 Simulation Study of Regenerative Chatter Model

5.3.1 Simulation Block Diagram

In the experimental conditions studied, the workpiece material used in this study was nickel-base superalloy GH4169. The workpiece diameter was $125\,mm$, which has a high hardness. From the above conditions, the workpiece system is more rigid than the tool holder and the cutting system is the main vibration system.

In addition to the hypothetical conditions proposed in chapter two, the proposed model has two additional hypotheses. The process damping is produced by the extrusion of the cutting tool and the machined surface, and the effect of process damping on stability is not significant in high-speed cutting, so it is not considered here. In addition, the modal hammering test in chapter three shows that there is a specific modal coupling in the X and Y directions during the actual processing, hence if the requirement of the model is high, the coupling effect of the two directions should be considered. The established model ignores the coupling in two directions because the purpose of this study is the effect of cutting parameters on regenerative chatter.

Based on the stated hypothesis above, a two-degrees of freedom simulation model of turning regeneration chatter was designed by using MATLAB/Simulink, as shown in Figure 5.1.

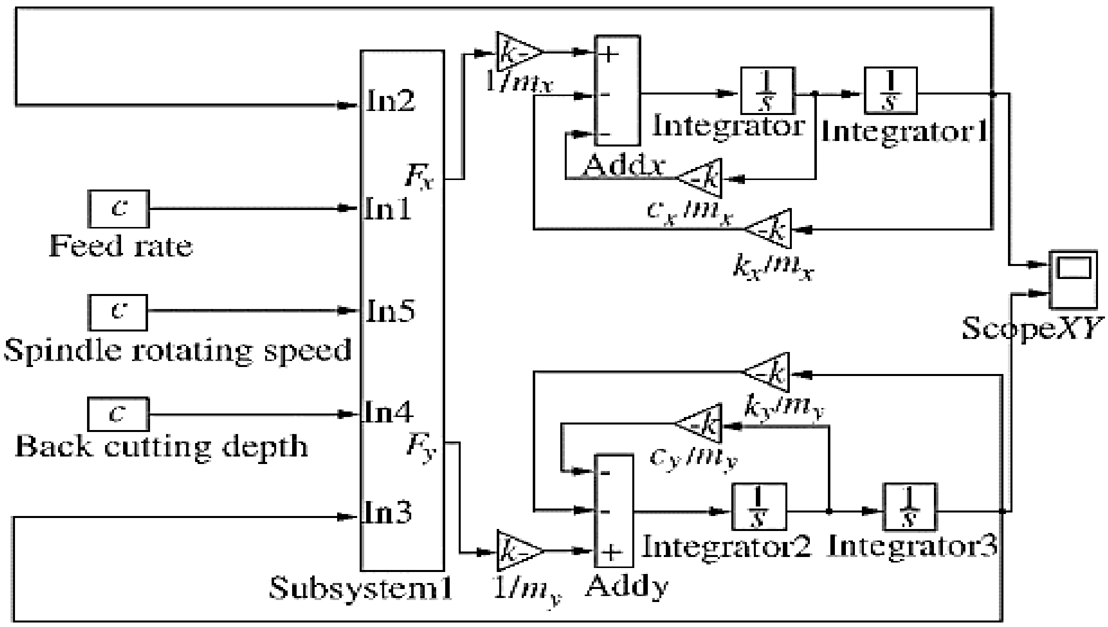

Figure 5.1: The Simulation Block Diagram of Cylindrical Turning Chatter

Using two-dimensional cylindrical turning, the chatter model with two degrees of freedom was designed using the model-measured parameters as shown in Figure 5.1. The simulation takes into consideration the X and Y directions. Two spring damping systems and an encapsulated subsystem called Subsystem1 were identified. The simulation model of the input port including feed rate, spindle speed, back cutting depth, and three manual input modules. The output port included two output modules; these were the tool point and the vibration displacement in the X and Y directions, which were varied with time.

In the block diagram of the chatter system, the oscilloscope module - "Scope XY" in the module library was utilized to model the time-dependent tool point and the vibration displacement in the direction of X and Y.

Where Subsystem1 is a packaged subsystem module and its internal structure is shown in Figure 5.2. The subsystem1 is the input ports for the subsystems In1 to In5. The (In1) is the input port for the feed rate value. The (In2) represents the input port for the vibration displacement in the X-direction. Port (In3) is assigned for inserting the input vibration displacement in the Y-direction. While ports (In4 and In5) are the input ports for back cutting depth and spindle rotating speed respectively. F_x and F_y are the output ports for the subsystem which are the dynamic cutting forces in X and Y directions. In addition, the coincidence degree μ changes when the feed rate and depth of cut are changed, and its automatically calculated according to the values of input cutting parameters.

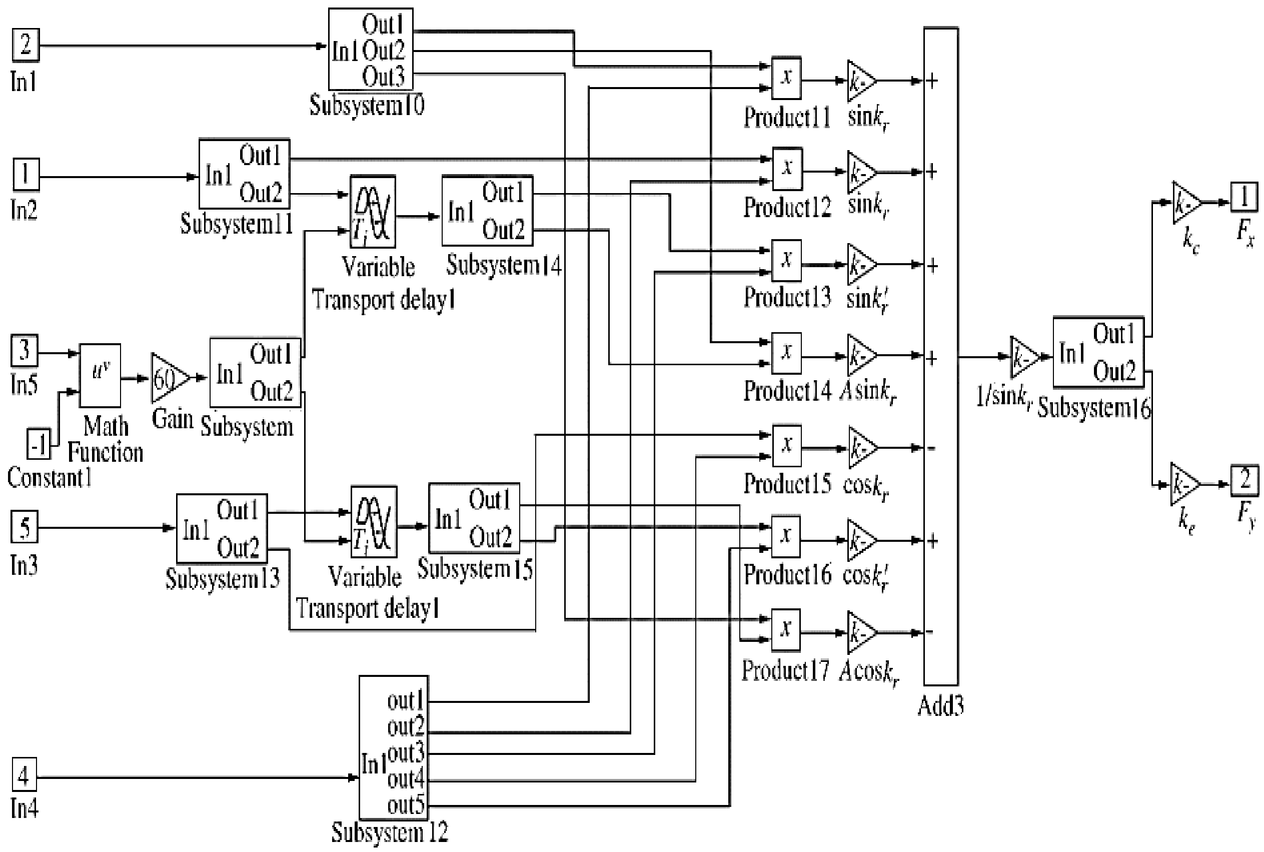

Figure 5.2: The Block Diagram of Subsystem1

Figure 5.2 shows the regeneration effect of chatter in the "Subsystem1" subsystem. "Variable Transport Delay" is the delaying of a variable time re-output module for the input signal, and this module is the combination of "Math Function" and "Gain" which constitute the rotation speed of the spindle "Spindle Speed" and has been transformed into the main link of regenerative effect.

While ($System_2$) to ($System_8$) are the inputs and multi-outputs conversion module of the signal shunting. "Product1 to Product6" are the multiplier modules, which are used for multiplying the signals. Kr and k'r are the side cutting edge and end cutting edge angles of the tool, which depend on the tested tool type (Figure 3.6). According to the definition of the coincidence degree μ (Equation 3.12), the coincidence degree has a direct effect on regeneration chatter. K_c and K_e are the proportional modules in the diagram. The average unit cutting force coefficients were assigned to X and Y directions respectively.

5.3.2 Simulation Parameters Setting

In this section, the variable step size algorithm is used for the simulation algorithm. In the variable step size algorithm, the size of the step is proportional to the signal speed change. The calculation accuracy of the step size was controlled by the admissible error limit, and the system automatically adjusts the step size when the error exceeds the admissible error. (To set the iteration of i) In each iteration step, the program subtracts the calculated value from the expected value and it gets an error $e(i)$, if $e(i)$ satisfies the condition: $e(i) \leq max$ (relative admissible error limit, absolute tolerance limit), then the iteration is positive. Otherwise, the program will automatically reduce the step length and repeat the above process until the above condition was achieved. The simulation parameters are determined as follows:

Start time options: 0s;

Stop time options: 10s;

The program type selects the variable-step and the solver (simulation algorithm), which was ode45 (Dormand-Prince) method, the step size is set to $10^{-5}\, sec$. Dormand-Prince method is based on the expressions Rung-Kutla (4,5) and Dormand-prince combination algorithm, for most simulation models, Dormand-prince method is always the best choice. Therefore, ode45 is usually used as a default algorithm; and the maximum step size option is: $1/60$;

The relatively tolerance default value is: '1e-3', and this default value means that the computed state is accurate to within 0.1%; the relative tolerance to auto is actually the default value of 1e-3.

In addition, all the initial values of the integrator module were set to zero. The measured modal parameters were the main input values. The other parameter used in this simulation were shown in Tables 4.3 and 4.4, respectively.

5.4 Numerical Simulation and Analysis

5.4.1 Simulation Verification of Stability Limit

To study the influence of cutting depth on the stability of the system, the cutting parameters employed during this simulation were: cutting speed $v\ = 80\, m\ /min$, and the feed rate $f\ \ = 0.15mm\ /r$ are, and they were fixational during the simulation. The vibration time-domain diagram and frequency domain diagram of the cutting tool in the X and Y directions, corresponding of the different cutting depths were depicted as follows:

Figure 5.3(a) below illustrates graphically the Time and Frequency Domain Signals in the X Direction.

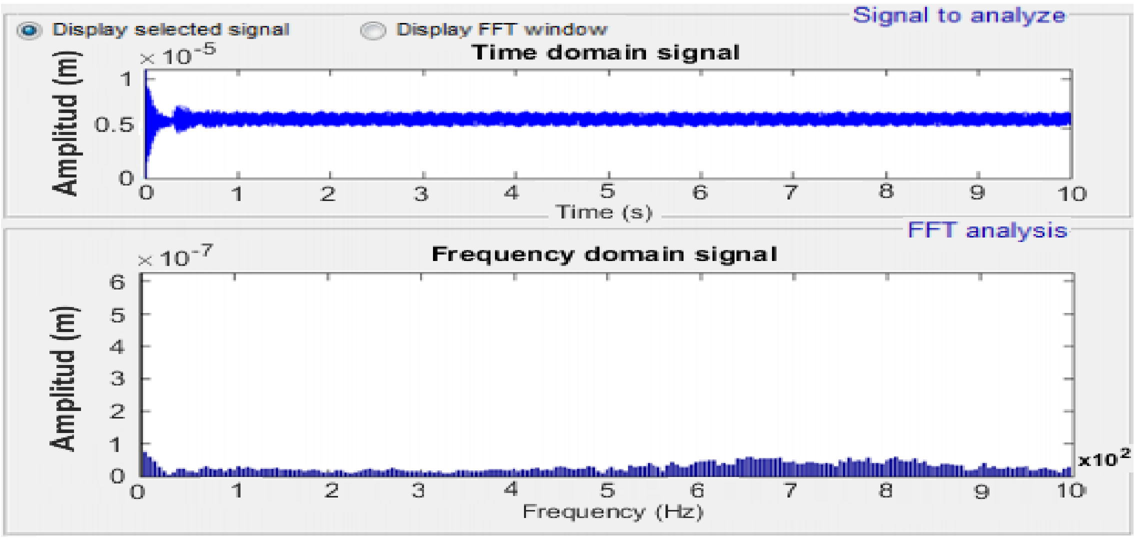

Figure 5.3(a): Time and Frequency Domain Signals in the X Direction

Figure 5.3(b) below illustrates graphically the Time and Frequency Domain Signals in the Y Direction.

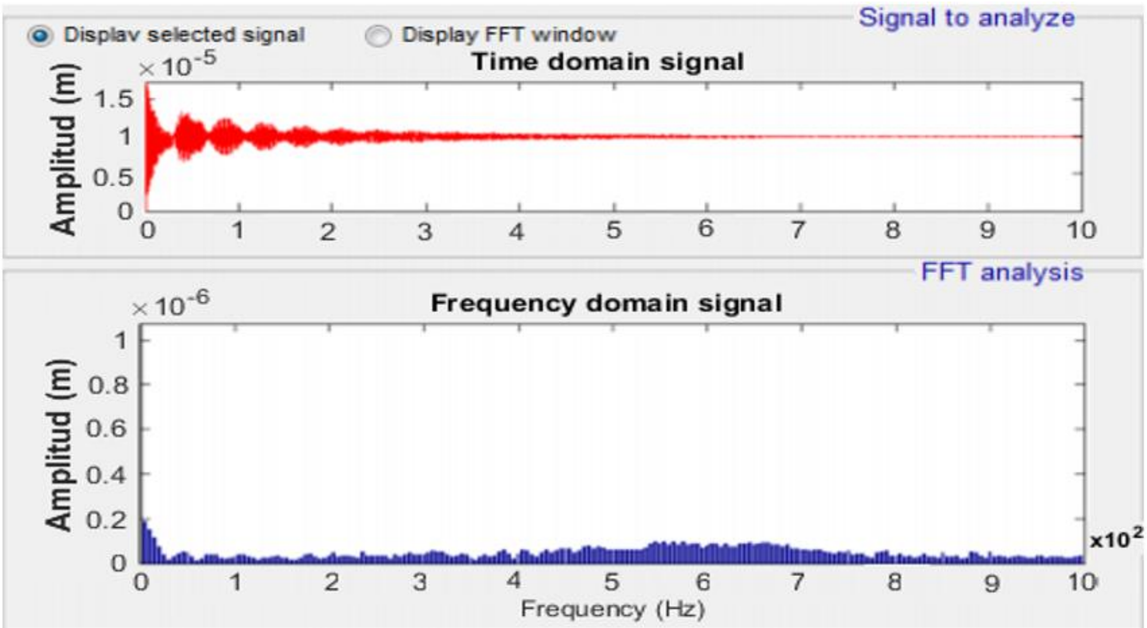

Figure 5.3(b): Time and Frequency Domain Signals in the Y Direction

Figure 5.3 above shows the time-domain and vibration frequency domain signals in X and Y directions at simulation parameters: $v = \frac{80m}{min}, f = \frac{0.15mm}{rev}, a_p = 1.5mm.$

Figure 5.3 above shows the tool vibration in the X and Y directions at a cutting speed that equals to $\left(80\frac{m}{min}\right), feed\ rate\ which\ equals\ to\ (0.15\ mm/rev),\ \ and\ cutting\ depth\ which\ equals\ to\ \ (1.5\ mm).$

In this case, the time domain amplitude in the X direction remains stationary but slowly attenuates while the amplitude in the Y direction decreases rapidly after experiencing severe fluctuations. And, it is observed that the frequency distribution of the system vibration is uniform in the X and Y directions, and the system is in a stable cutting state in the X and Y directions.

Figure 5.1 below shows the time-domain and vibration frequency domain signals in X and Y directions at simulation parameters: $v = \frac{80m}{min}, f = \frac{0.15mm}{rev}, a_p = 1.98mm.$

Figure 5.4 below shows the tool vibration in the X and Y directions at a cutting speed which equals to $(80\ m/min), feed\ (0.15\ mm/rev), and\ cutting\ depth\ (1.98\ mm)$. In this case, the cutting depth in the Y direction was predicted, and the ultimate cutting depth was stable.

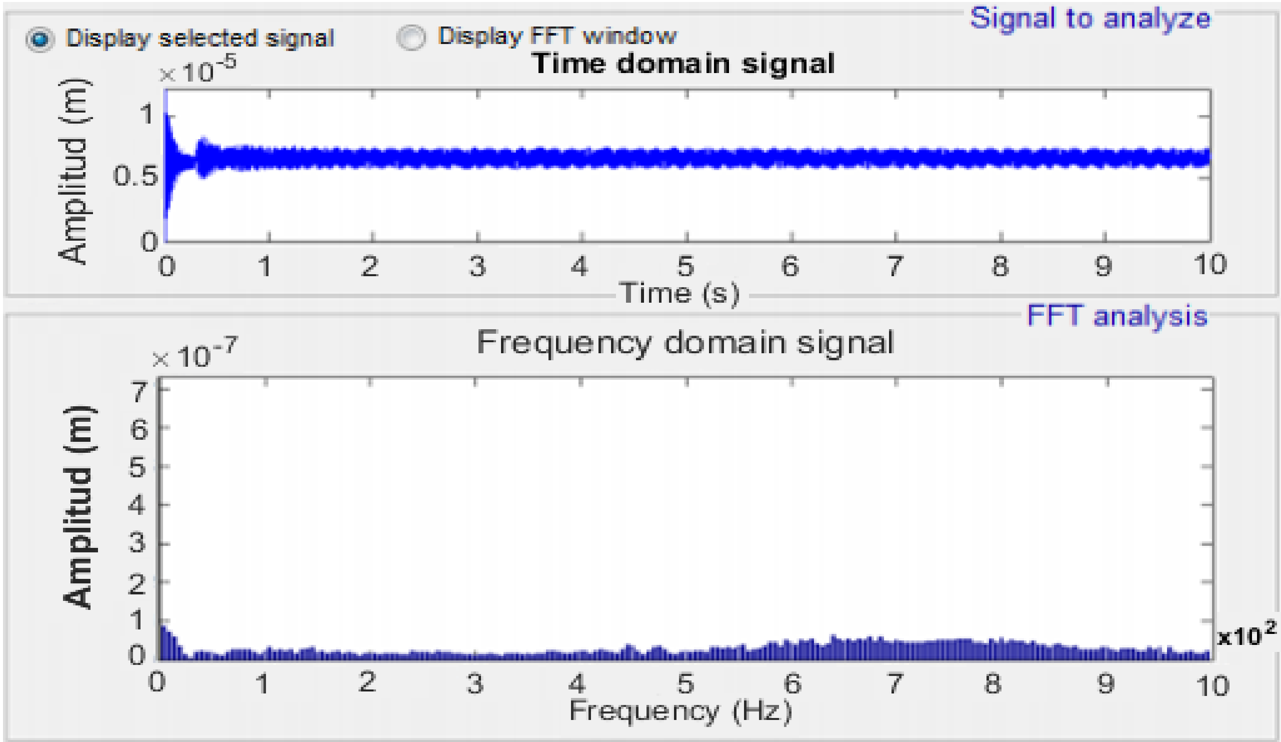

Figure 5.4(a): Time and Frequency Domain Signals in the X Direction

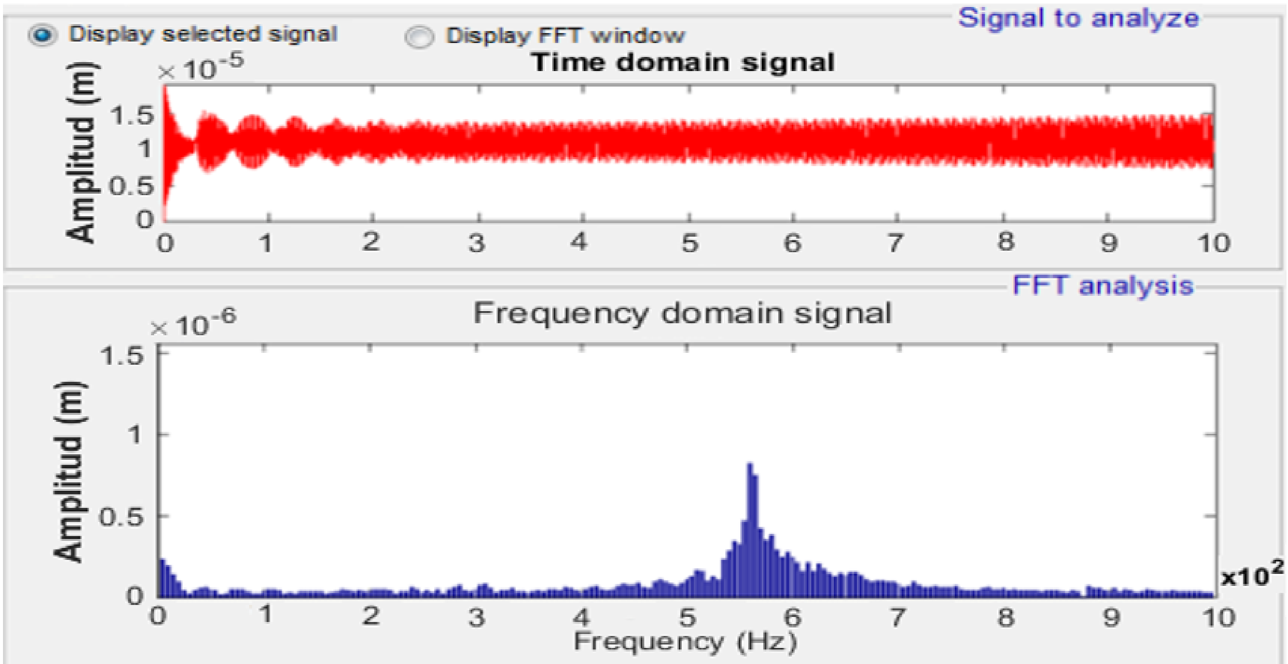

Figure 5.4(b): Time and Frequency Domain Signals in the Y Direction

Through observing the time domain waveform, we can see that the time domain amplitude in X direction remains stationary and slowly decaying, while the amplitude of the vibration in the Y direction is around to be diverge. During observing the spectrum, the frequency distribution of the system is regular in the X direction, and the frequency distribution of system vibration is around 560 Hz in the Y direction, with a peak in vibration. Therefore, the system is in a stable cutting state in the X direction, while it is in a critical state in the Y direction.

Figure 5.5 below illustrates the time-domain and vibration frequency domain signals in X and Y directions at simulation parameters: $v = 80m/min, f = 0.15mm/rev, ap = 3mm$

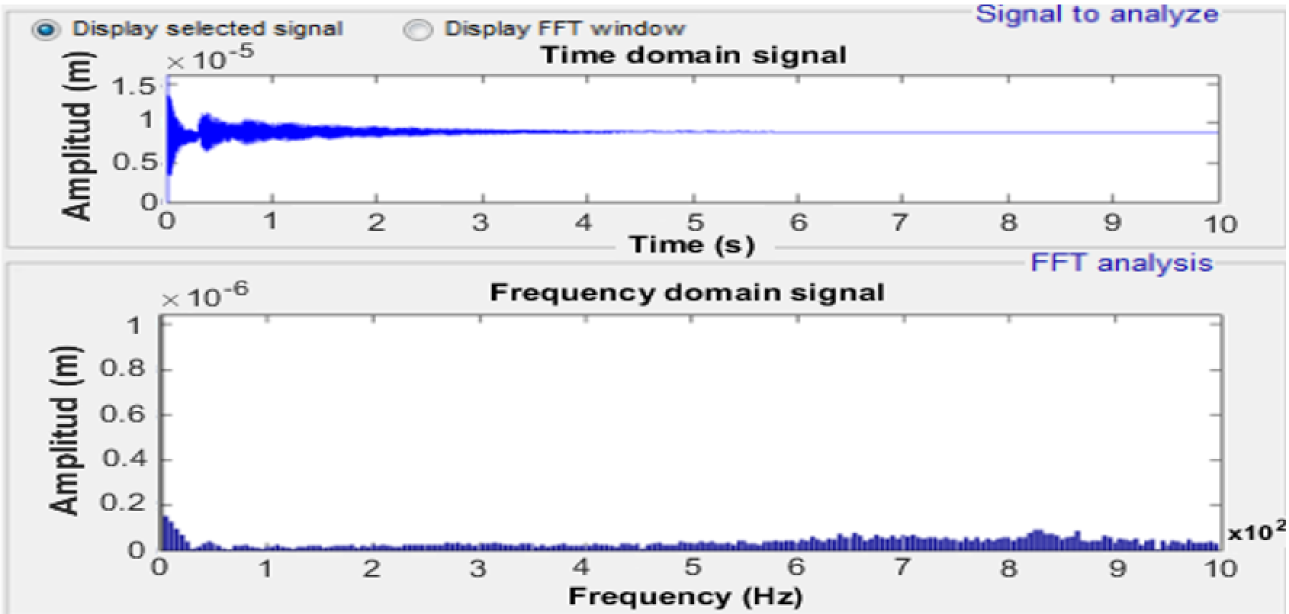

Figure 5.5(a): Time and Frequency Domain Signals in the X Direction

Figure 5.5 illustrates that, the tool vibration in the X and Y directions at a cutting speed equals to $\left(80\frac{m}{min}\right), feed\ rate\ equals\ to\ (0.15\, mm/rev), and\ cutting\ depth\ equals\ (3\ mm)$.

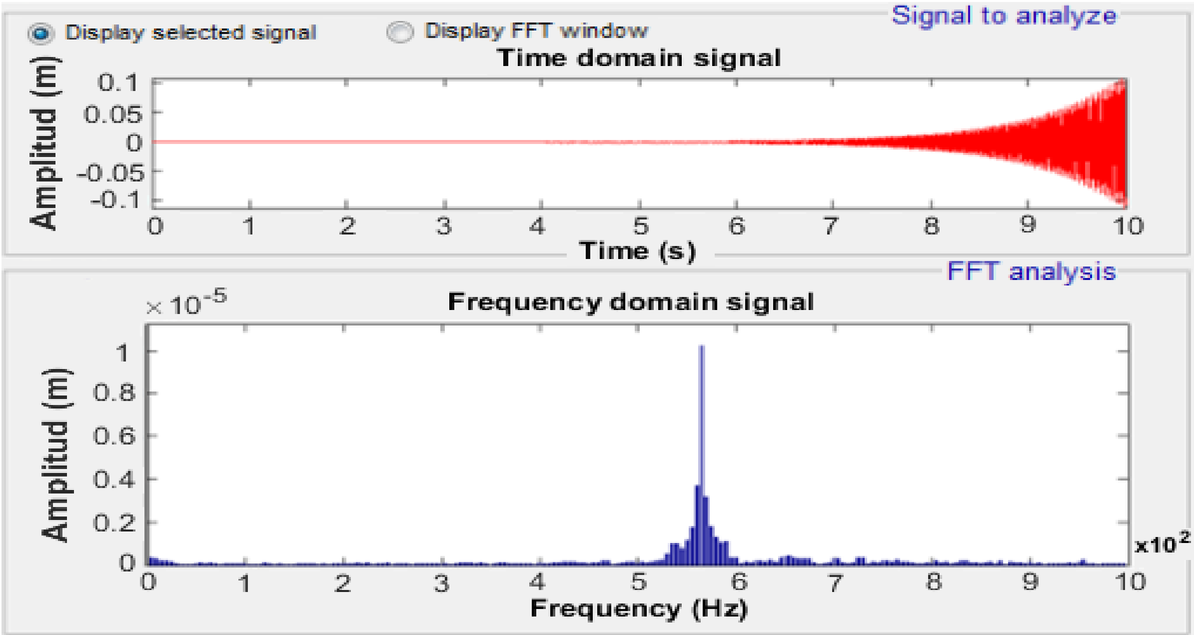

Figure 5.5(b): Time and Frequency Domain Signals in the Y Direction

In this case, the amplitude of the tool in the X direction is increased faster, while it is increased slowly in the Y direction and thus, the vibration is enhanced. It is observed that, the energy of the system vibration was found concentrated near 560 Hz. During this case, the system is still in a steady state in the X direction and unstable state in the Y direction.

Figure 5.2 below illustrates the time-domain and vibration frequency domain signals in X and Y directions at simulation parameters: $v = 80m/min, f = 0.15mm/rev, a_p = 4.56mm$.

Figure 5.6 which is shown below, illustrates the tool vibration in the X and Y directions at a cutting speed equals to $(80\ m/min), feed\ (0.15\ mm/rev), and\ cutting\ depth\ (4.56\ mm)$. In this case, the cutting depth is the stable limit cutting depth that we could be predicted in the X direction.

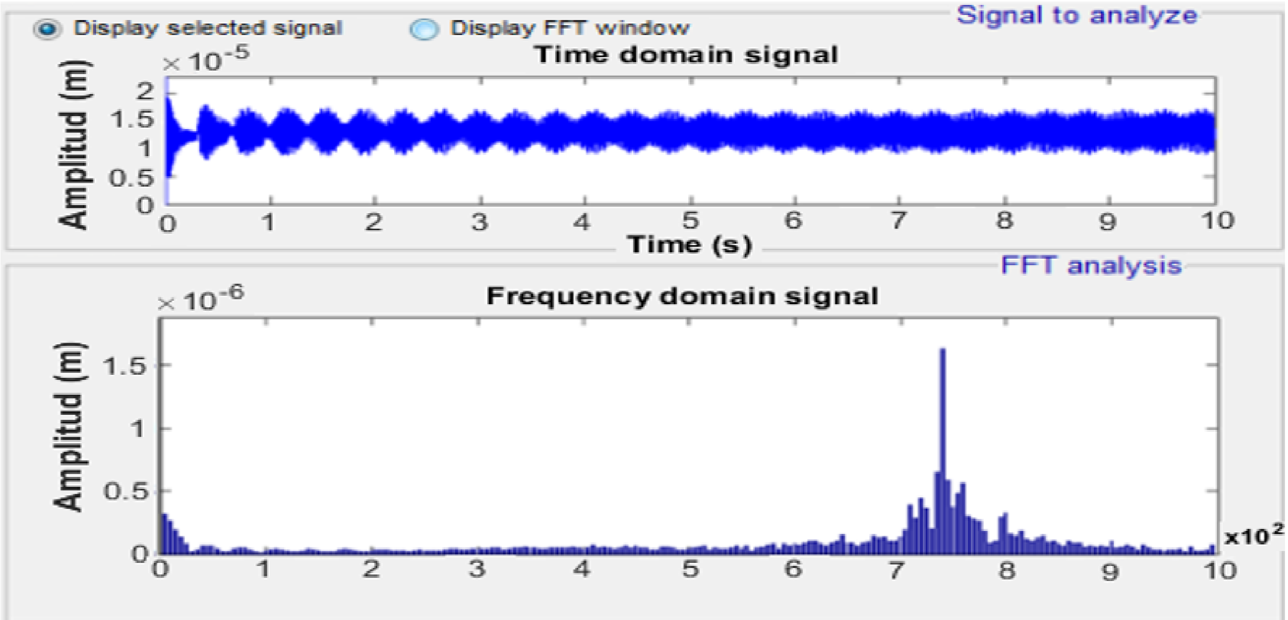

Figure 5.6(a): Time and Frequency Domain Signals in the X Direction

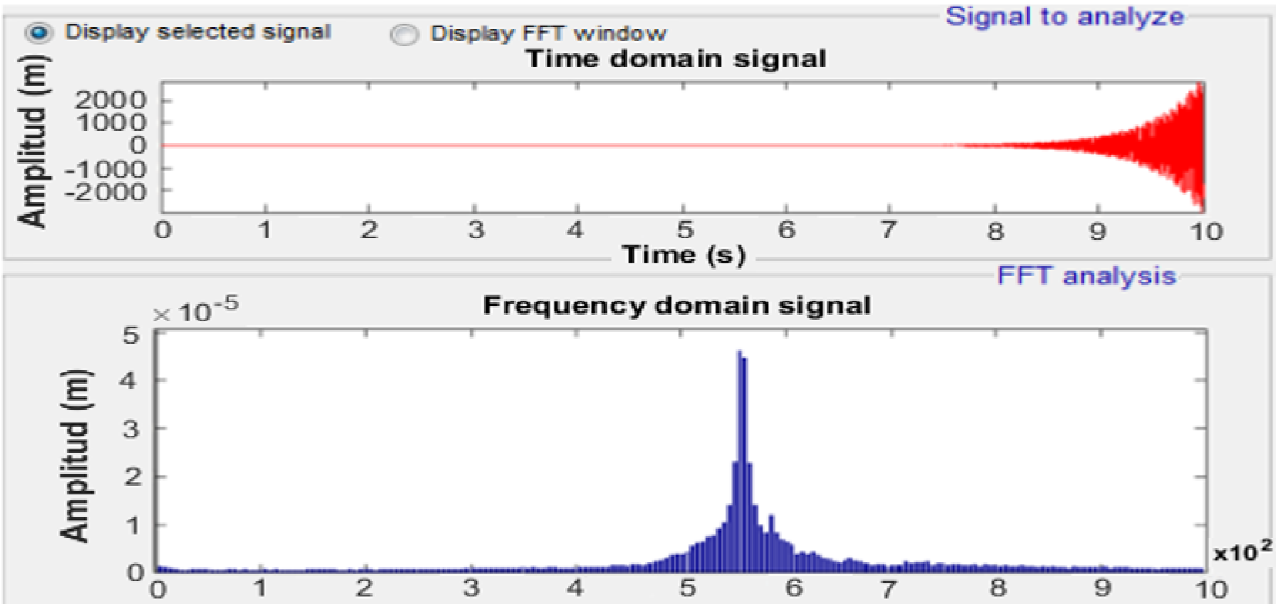

Figure 5.6(b): Time and Frequency Domain Signals in the Y Direction

Through the time-domain, it can be seen that the amplitudes in the X and Y directions increases significantly with the depth of cut continues to increase. Moreover, it was observed that, the degree of vibration frequency in the X direction increases gradually with the convergence in amplitude, while the amplitude in the Y direction decreases gradually. It can be seen from the observation of the spectrum that, the system vibration frequency distribution is near 720 Hz in the X direction, and it concentrates near 560 Hz in the Y direction. At this point, the system is in a critical state in the X direction, but still unstable in the Y direction.

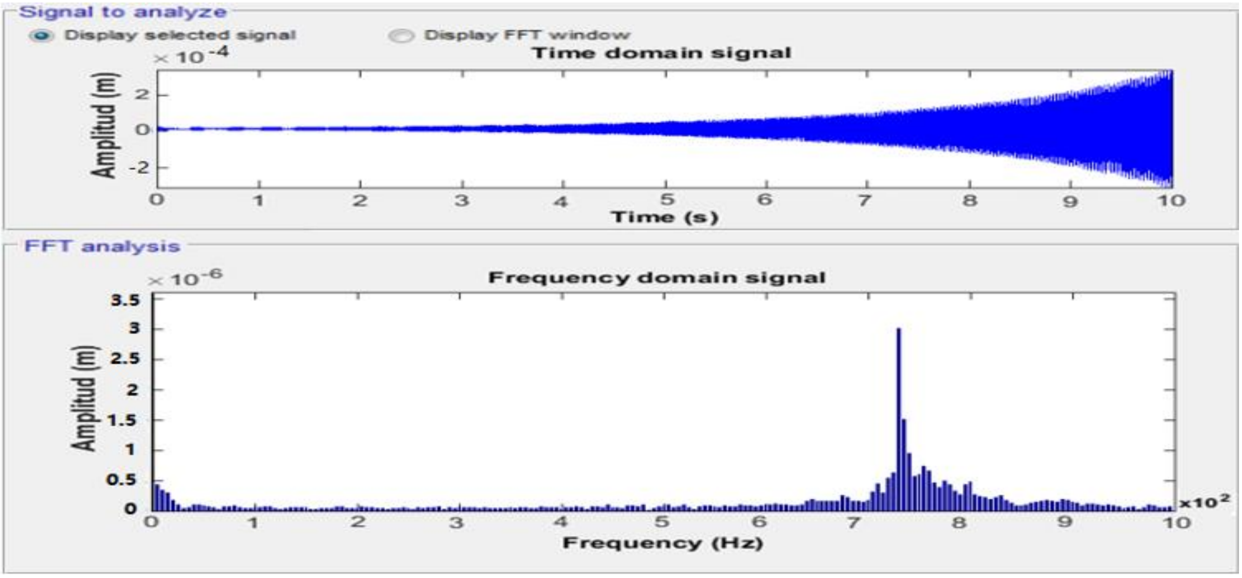

Figure 5.7(a) Time and Frequency Domain Signals in the X Direction

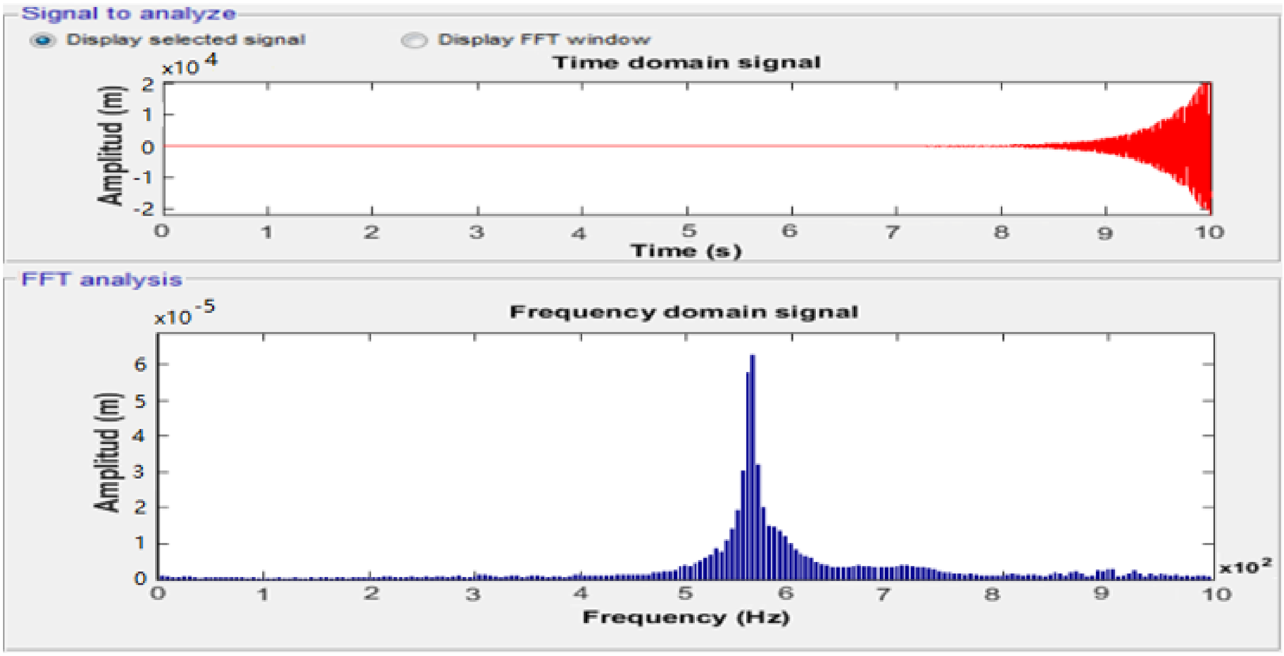

Figure 5.7(b) Time and Frequency Domain Signals in the Y Direction

Figure 5.3 above shows the time-domain and vibration frequency domain signals in X and Y directions at simulation parameters: $v = 80m/min, f = 0.15mm/rev, a_p = 5mm$

Figure 5.7 which is shown above, illustrates the tool vibration in the X and Y directions at a cutting speed $v = 80m/min, feed\ rate\ f = 0.15mm/r, and\ cutting\ depth\ a_p = 5mm$. In this case, Through the time-domain wave, it can be seen that, with the increase in cutting depth the amplitudes in the X and Y directions are different. The vibration frequency of the system showed that the value of the vibration frequency in the X direction approaches 720 Hz. Whereas, it approaches 560 Hz in the Y direction. At this stage, the system is in unstable state in the X and Y directions.

In summary, at the one direction when the cutting depth is equal to the stable limit cutting depth, the amplitude in that direction is almost constant. Otherwise, when the depth of cut is less than the stable limit cutting depth of the system, the system vibration decreases rapidly in this direction. When the cutting depth is greater than the limit cutting depth in the specific direction, the amplitude of the system is gradually increasing, and the vibration strengthens.

From the above simulation, it can be seen that the system first reaches a chattering state in the Y direction, and as the cutting depth continues to increase, the system then reaches a chattering state in the X direction. In the actual cutting process, the first cutting depth that causes unstable cutting in the system should be considered as the stable limit cutting depth of the system.

In addition, according to the analysis of energy supplement, when the cutting depth does not achieve the stability limit to the system, the negative work produced by the positive damping during the cutting process is greater than the positive work produced by the negative damping, and the vibrations will consume energy of the system quickly. When the cutting depth achieve the stability limit to the system, the positive work produced by the negative damping is equal to the negative work produced by the positive damping. It was observed in one of the cycles that the supplemental energy of the system is balanced with the energy dissipated, and the system is in a stable vibration state. When the cutting depth exceeds the stability limit of the system, the negative work produced by the positive damping is less than the positive work produced by the negative damping, and the vibrations consuming the energy of the system continuously, which leads to the instability of the system.

5.4.2 The Effect of Cutting Speed on Chatter Characteristics

Since the simulation tests are carried out in the stable cutting area, the system is in a stable vibration state, so the average effective values of vibration signal were studied. the time-domain signals at different cutting speeds were recorded, and the average values of the whole cutting process were calculated as shown in Table 5.1.

Table 5.1: The Vibration Parameters at Different Cutting Speeds

Direction	Cutting speed (m/min)	40	60	80	100	120
X	Mean amplitude (μm)	0.560	0.576	0.586	0.593	0.573
Y	Mean amplitude (μm)	0.993	1.014	0.982	1.041	1.014

Figure 5.8 shows the fluctuations of the system amplitude in X and Y directions. It was observed that, the effect of cutting speed on the system vibration characteristics is not obvious. It was observed that, the amplitude in the x-direction tends to fluctuate with the increase of cutting speed, and it resorts to increase and decrease with the increase of the cutting speed in the y-direction. When the system is in a stable cutting state, the system vibration characteristics fluctuate while the cutting speed changes, but the fluctuation in overall directions is semi-stable and accompanied by little changes. In addition, when the system is in the unstable cutting state, the system vibration characteristics are greatly influenced by the cutting speed; this can be seen from the stability limit lobe diagram.

Figure 5.8 below illustrates graphically the effect of cutting speed on chatter action.

In the process of regenerative chatter, cutting speed is closely related to the chatter characteristics caused by the cutting process. According to the theory of self-excited vibration, it is known that when the phase difference between two adjacent cuts of the workpiece is $0 \leq \phi \leq 180°$, the system will absorb energy from the cutting process and stores it.

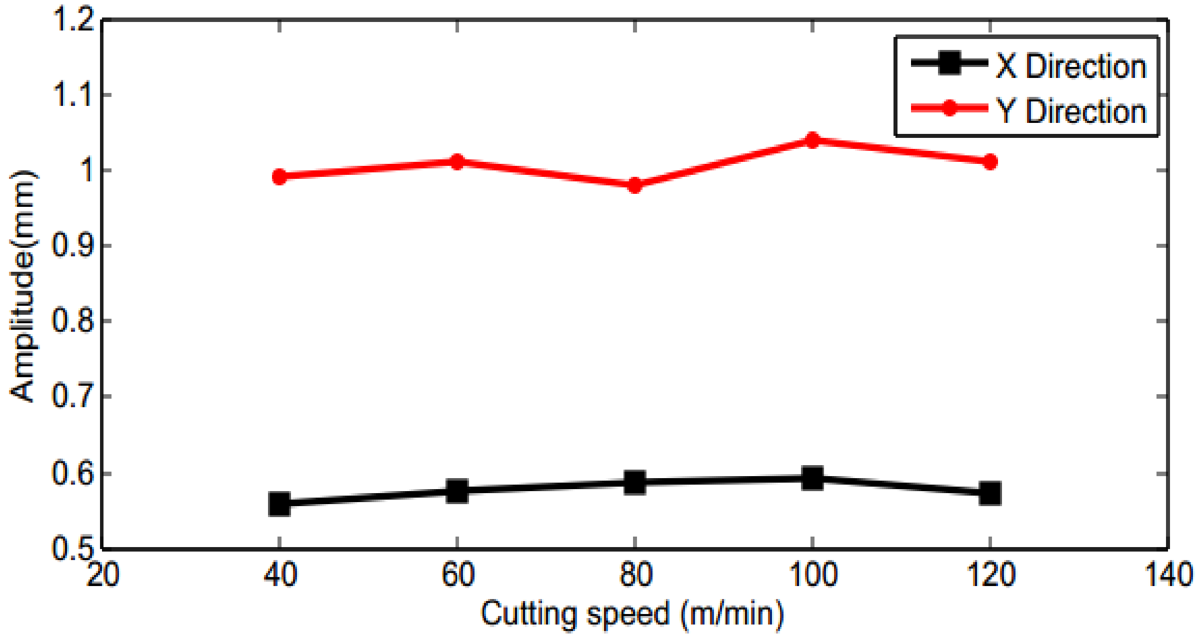

Figure 5.8: The Effect of Cutting Speed on Chatter

In this stage the amplitude of the system increases gradually and it reaches the maximum value at $\phi = 90°$. At this time, the system is in the most unstable state cutting. When the phase difference between two adjacent cuts of the workpiece is $180° \leq \phi \leq 360°$, the system works to release energy stored from the cutting process and the amplitude is reduced, and it reaches to the minimum value at $\phi = 270°$. At this time, the system is in the most stable state, this evidences from Equations (3.18) and (3.19) in chapter 3.

The phase difference between the two adjacent cutting is as follows:

$$\phi = \omega T \qquad (5.1)$$

Take $T = 60/n$, where n is the spindle speed of machine tool in (rev/min), and substitute this value in Equation (5.1), thus equation (5.1) becomes as follows:

$$\phi = 60\omega/n \qquad (5.2)$$

When the vibration frequency approaches the natural frequency of the system the chatter state is reached, and the vibration of the system is most intense, then Equation (5.2) is rewritten as follows:

$$\phi = 60\omega_n/n \qquad (5.3)$$

The cutting speed is replaced by the upper formula and the value of ϕ is obtained, the vibration characteristics of the system can be judged by observing the relative position in the coordinate system.

Figure 5.9 below shows the Vibration Characteristics in X-direction during the Chatter Action.

As shown in Figure 5.9, when the system reaches the chatter state in the X direction, the system vibration characteristics are in the order from strong to weak as follows: V4＞V3＞V2＞V5＞V1.

As shown in Figure 5.10, when the system reaches chatter state in the Y direction, the system vibration characteristics are in the order from strong to weak as follows: V4＞V5＝V2＞V1＞V3.

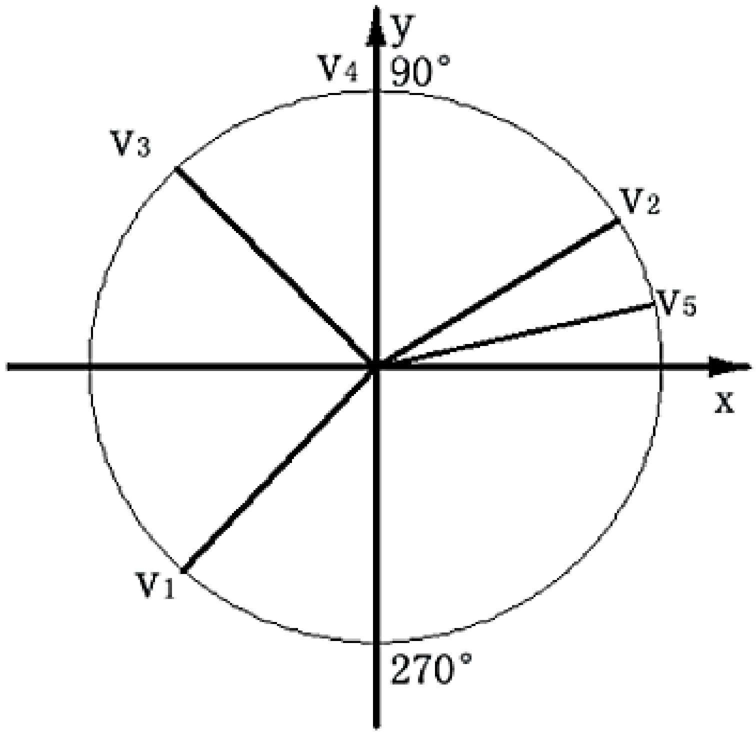

Figure 5.9: Vibration Characteristics in X-Direction during Chatter

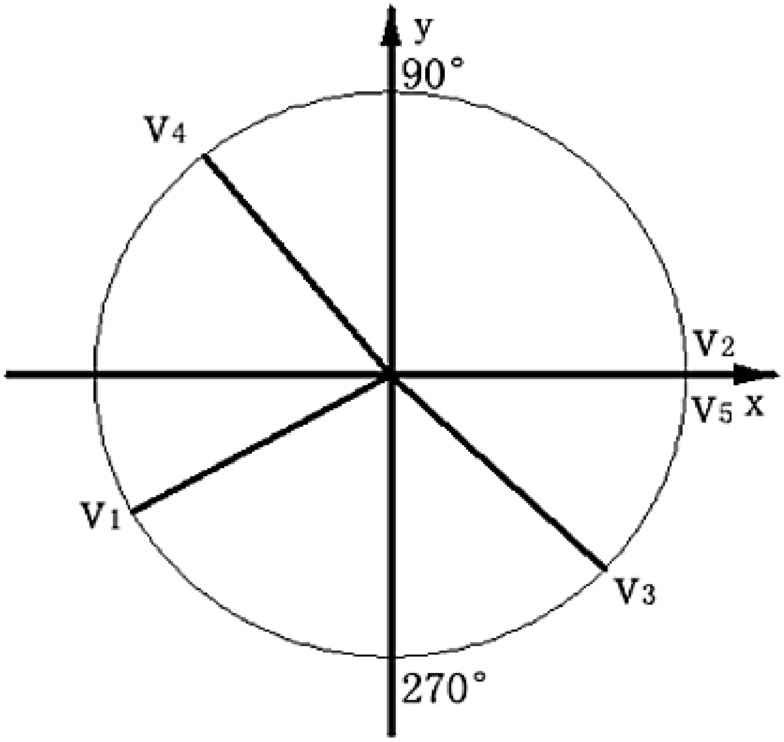

Figure 5.10: Vibration Characteristics in Y-Direction during Chatter

In summary, by selecting the appropriate cutting speed to control the phase difference between the two adjacent cuts of the workpiece, the occurrence of chatter vibration can be avoided reasonably and effectively.

5.4.3 Influence of Feed Rate on Chatter Characteristics

The recording of the time domain signals at different feed rates and calculations for the average value of the whole cutting process are shown in Table 5.2. As shown in Figure 5.11, with the increase feed rate, the vibration characteristics in the X and Y directions have the same change trend both showing a linear decreasing trend, and the system is in a stable cutting state within this range. When the feed rate reaches the minimum value $\mathrm{f} = 0.25\mathrm{mm/rev}$, then the system will be at its weakest state. In simulation, the self-excited vibration caused by the regeneration effect dominates the system vibration characteristics. Therefore, from the definition of coincidence degree μ, with the increase feed rate, the coincidence degree μ of the system will gradually decrease, resulting in a weak regeneration effect, which in turn weakens the system vibration.

Table 5.2: The Vibration Parameters under Different Feed Rates

Direction	Feed rate (mm/rev)	0.05	0.10	0.15	0.20	0.25
X	Mean amplitude (μm)	0.977	0.801	0.586	0.401	0.195
Y	Mean amplitude (μm)	1.634	1.285	0.982	0.693	0.328

Figure 5.11 below shows the effect of feed rate on chatter action.

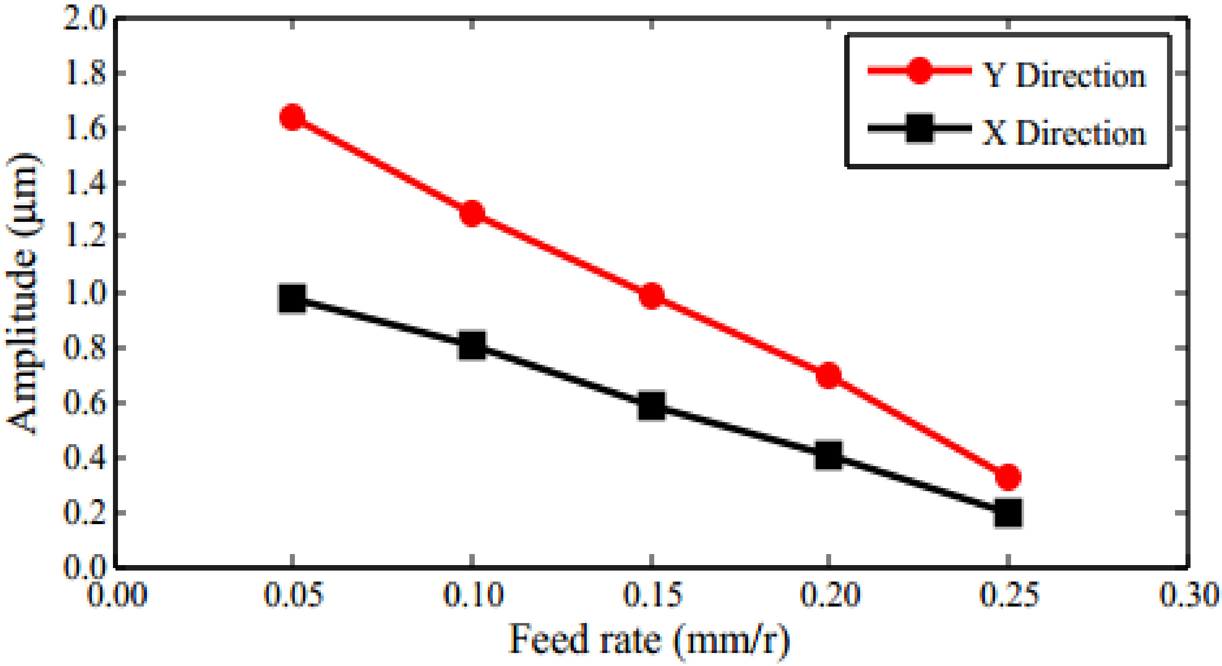

Figure 5.11: The Effect of Feed Rate on Chatter

5.4.4 Influence of Cutting Depth on Chatter Characteristics

The recording of the time-domain signals at different feed rates and the calculation of the average value of the whole cutting process are shown in Table 5.3.

Table 5.3: The Vibration Parameters under Different Cutting Depths

Direction	Cutting depth (mm)	0.15	0.20	0.25	0.30	0.40
X	Mean amplitude (μm)	0.352	0.453	0.587	0.704	0.822
Y	Mean amplitude (μm)	0.593	0.786	0.982	1.181	1.382

Figure 5.12 below shows The Effect of Cutting Depth on Chatter Action.

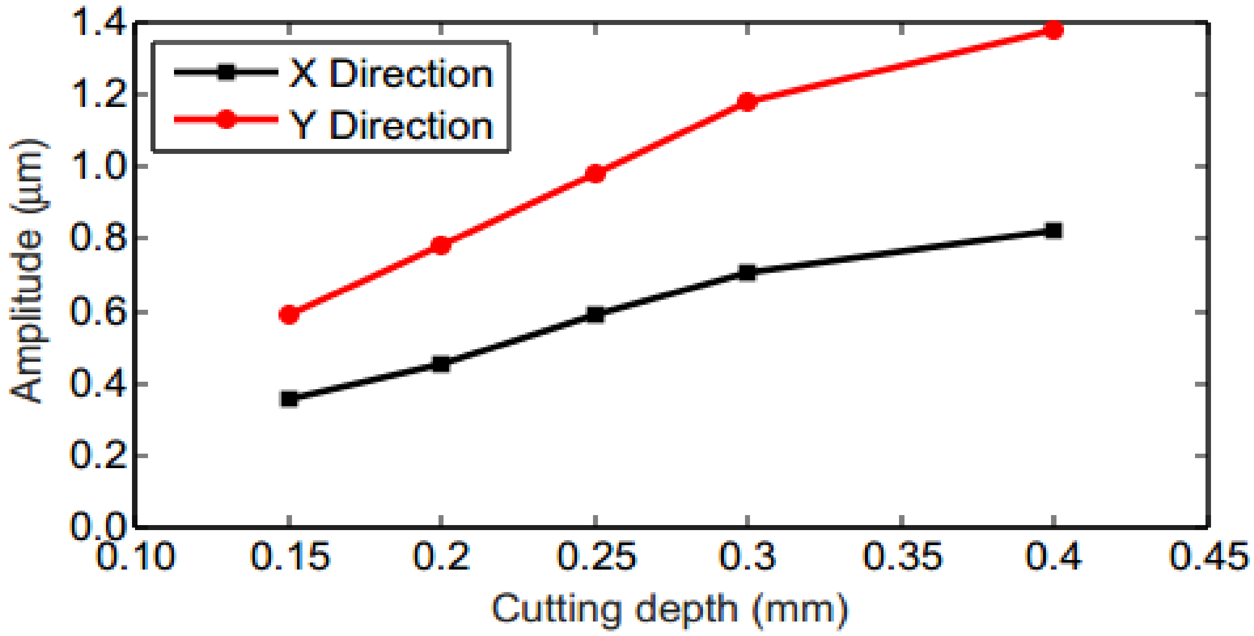

Figure 5.12: The Effect of Cutting Depth on Chatter

Figure 5.12 shows that with increase in the cutting depth, the variation trend of the vibration characteristics in the X and Y directions are the same, and the amplitude trend is linearly increasing, and when the cutting depth value reaches $a_p = 0.4mm$, the system vibration is the strongest at this time. Within this range, the system is in the stable cutting state. Similarly, the self-excited vibration caused by the regenerative effect dominates the system vibration characteristics, so the theory of regenerative chatter in machine tool cutting system shows that the dynamic cutting force that will cause the system to maintain self-excited vibration will increase gradually. This can be seen from the stability limit lobe diagram. When the cutting width approaches the limit cutting width of the system, the regeneration effect increases gradually, resulting in the intense vibration of the system.

5.5 Chapter Summary

This chapter discusses the simulation study of turning chatter model using MATLAB/Simulink tool. The major contribution was summarized as follows:

1. A two degree of freedom regenerative chatter model for cylindrical turning was designed by using MATLAB/Simulink software. Based on the cutting parameters such as cutting speed, feed rate, and cutting depth a fast-effective method to determining the stable state of the cutting system was established.
2. Numerical simulation was carried out to verify the influence of the limit cutting width stability in the machine tool cutting system, as predicted in Chapter three. The simulations results show that the system first reaches the chatter state in the Y direction, and with the increase of cutting depth, the system reaches the chatter state in the X direction. In the actual cutting process, the first cutting depth that causes unstable cutting of the system should be regarded as the stable ultimate cutting depth of the system. It is found that, the main direction of the cutting chatter is Y direction.
3. Based on the results of numerical simulation, the influence of cutting parameters such as cutting speed, feed rate and cutting depth on the vibration characteristics of cylindrical turning under regeneration effect was studied. In the stable cutting state, the system fluctuates with the change of cutting speed, but the overall trend was stable and

the influence is negligible. In the unstable cutting state, the cutting speed has a great influence on the vibration characteristics of the system. With increase in the feed rate, the coincidence degree of the system will decrease gradually, resulting in the weakening of regeneration effect, so the vibration of the system will also be weakened. As the cutting depth increases, the dynamic cutting force needed to maintain the self-excited vibration of the system will gradually increase, resulting in the regeneration effect gradually strengthened, eventually leading to intensified vibration of the system.

Chapter 6

Experimental Study of the Cutting Stability and Machined Surface Quality on Nickel-Base Super-Alloy

6.1 Introduction

In this chapter, the vibration characteristics of tool system in cutting process, and the turning chatter were studied, based on the experimental conditions. In addition, the effects of cutting parameters on the vibration characteristics for cylindrical turning were studied. The influence of vibration characteristics on the surface roughness of workpiece was studied in details.

6.2 Experimental Design

6.2.1 The Experimental Setup

(1) The accuracy of the limit cutting width obtained by the simulating is verified by the variable cutting depth test method.

(2) Through the turning experiment, the influence of cutting parameters such as cutting speed, feed rate and cutting depth on the vibration characteristics of GH4169 alloy is analyzed, and the correctness of the simulation model is verified.

(3) Based on the influence of cutting parameters on vibration characteristics, the influence of cutting speed, feed rate and cutting depth on the surface roughness of GH4169 alloy is analyzed.

6.2.2 The Test Equipment

(1) Figure 6.1 below shows Haitian Seiko HTM-TC40 CNC lathe. TC series of CNC turning machine/mill – turning center are produced in Haitian Precision Machinery Co. Ltd. Which has adopted the advanced technology from DAINICHI. Under the feature of logical structure, high rigidity, steady performance, reliable quality, those lathes are widely applied to the field of automobile, gas engine, aviation, electric setting, all-purpose machine and so on.

Figure 6.1: Haitian Seiko HTM-TC40 CNC Lathe

The main technical parameters of the machine are as follows:

Main motor power is $37\ (kw)$; maximum machining length is $2750\ mm$; maximum turning machine diameter is $660mm$; maximum speed spindle is $2000\ rpm$; maximum clamping weight is $500\ kg$.

(2) Figure 6.2 below shows the 5134B type adjustable channel settings for constant current level, time constant, low pass filter cutoff, gain and overload levels.

Figure 6.2: The Kistler 5134B Type Charge Amplifier

The 5134B can be configured to read the TEDS sensitivity or accept a user specified sensitivity and automatically scale the channel range and gain to utilize the Full-Scale Output (FSO). Alternately, the 5134B can be configured for similar operation as the predecessor 5134A, as a basic amplifier without automatic scaling based on channel sensitivity. The 5134B permits system level selection for FSO (±10 V or ±5 V), Sensitivity (TEDS or User) and Scaling (Automatic or Basic Amplifier). This amplifier is mainly used for measuring mechanical quantities such as pressure, force, and acceleration. In addition, the setting parameters are adjusted within ± 999,000 PC, so that the data that was recorded is not lost in case of power failure.

(3) Figure 6.3 below shows a self-contained, compact, lightweight, multi-channel data logger with 8 analog measurement channels, each with input-to-output and channel-to-channel isolation.

Figure 6.3: High-Speed Data Recorder Entirely Isolated Contains 8 Channels (GL900)

Measurements per channel of 20 mV to 500 V FS across 14 programmable ranges allow the GL900 to adapt to a wide range of signal types. The GL900 allows data to be recorded to internal high-speed volatile RAM memory (64 MB) at rates as fast as 100,000 Hz. The GL900 features built-in USB and Ethernet ports to facilitate data transfer to a connected PC either in real time or from its memory for analysis and archiving. Measurement protocols may also be uploaded from the PC to the instrument. An optional battery pack allows power- independent operation and failsafe measurement continuity during a power failure.

(4) Figure 6.4 below shows the Kistler 8765A250M5 triaxial accelerometer sensor, is a miniature, 6-gram center hole triaxial accelerometer with a ± 250 g measurement range and 20 mV/g sensitivity. The triaxial design permits simultaneous shock and vibration measurements in three perpendicular axes: X, Y and Z.

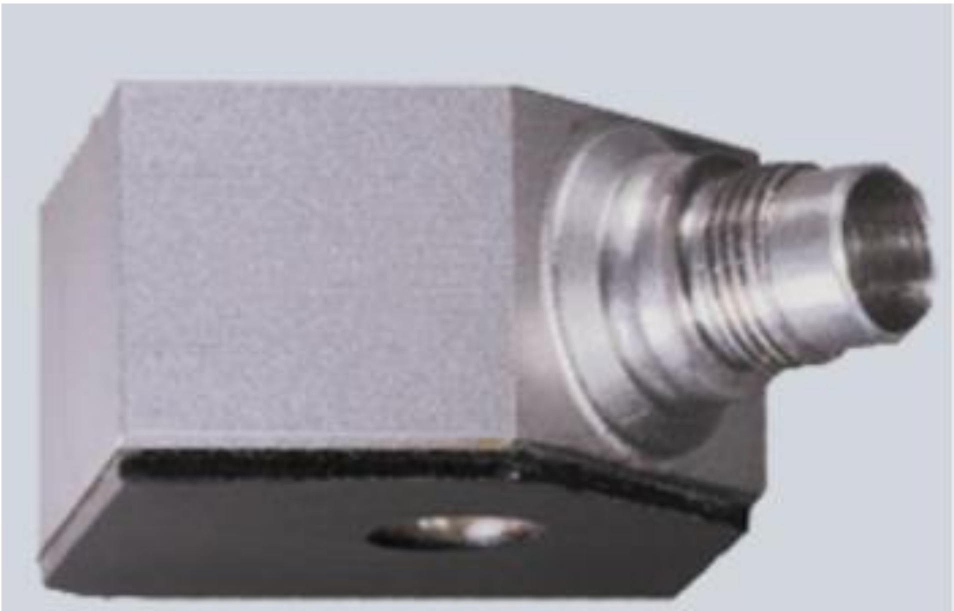

Figure 6.4: Kistler 8765A250M5 Type Sensor

The extremely low weight of Type 8765A250M5 accelerometer is highly attractive where mass loading of test structure is a major concern. Applications include subsystem vibration testing for aerospace applications. The accelerometer is ground isolated and optional Kistler shielded cables are known for offering high measured signal integrity for the intended applications. In addition, the center-hole mounting permits flexibility for 360 ° orientation of the cable allowing for a wide selection of locations for mounting. Type 8765A250M5 also offers high sensitivity over a wide frequency range, resolving a wide range of vibration measurements.

(5) Figure 6.5 shown the TR 200 surface roughness meter device. Surface Roughness Tester (TR 200) is a cost-effective roughness measuring equipment which supports a dozen of parameters, it operates through the handheld menu with 13 roughness parameters. According to the processing adopted and control using DSP (digital signal processor), which has the advantages of fast measurement, low power consumption, and ease of use. Well suited for on-site roughness testing.

Figure 6.5: TR 200 Surface Roughness Meter

During the measuring procedure the sensor moves linearly along the measured length. The probe moves accordingly to the profile on the surface. These movements are converted into electric signals which are amplified, filtered and converted into digital signals by an A/D converter. These signals are then refined in the main processor as Ra and Rz values (or Rq and Rt metrics) and displayed on the screen.

6.2.3 Experimental Material

(1) Workpiece Material

In this experiment, the material of workpiece is a nickel base super-alloy GH4169, the workpiece size is $\Phi 125 \times 600mm$, the brand is Inconel 718, the amount of nickel ranges from $50\%{\sim}55\%$.

The heat treatment method is as follows:

Heating for 1 hour up to a temperature of $980\ ℃$, then after 8 hours the heat decreases to $720\ ℃$, then the heat decreases to $620℃$ at a rate of $50℃/h$, and the air is cooled to room temperature. The mechanical properties and chemical composition of the workpiece were given in Tables 6.1 and 6.2, respectively shown below.

Table 6.1 below illustrates the mechanical properties of GH4169 alloy such as tensile strength $\sigma_b in\ MPa$, yield strength $\sigma_{p0.2}\ in\ MPa$, elongation $\sigma_5\ in\ \%$and Brinell hardness HB.

Table 6.1: The Mechanical Properties of GH4169 Alloy

Tensile strength σb/MPa	Yield strength σp0.2 / MPa	Elongation σ5 / %	Brinell hardness HB
965	550	30	≥ 363

Table 6.2 below constitutes the chemical composition as (wt.-%) of GH4169 alloy.

Table 6.2: Chemical Composition (wt.-%) of GH4169 Alloy

C	Mn	Si	P	Cr	Ni
0.80	0.35	0.35	0.15	17.0-21.0	50.0-55.0
Nb	Cu	Mo	Al	Ti	Fe
4.75-5.50	0.30	2.80-3.30	0.30-0.70	0.75-1.15	Bal

(2) Tool Material

PCBN tool is the suitable for the high-speed cutting, because it has high hardness and good machinability at high temperature (1000 ℃). It has been found to be the best choice for processing nickel-base super-alloy. Therefore, in this experiment the cutting tool designation used in this test was a CNGA120408 type 2, PCBN blade on an MCLNL type tool holder from Zhuzhou Diamond Cutting Tool Co., Ltd. The cutting trails were excircle dry turning.

6.2.4 Experiment Method

(1) Device Connection

A cutting test on samples of a nickel alloy rod GH4169 with a diameter of 125 mm was carried out on (Seiko HTMTC40) CNC lathe machine as shown in Figure 4.19. The test was performed with a varied depth of cut to assess the vibration of the cutting tool system as shown in Figure 4.18. The cutting trails were excircle dry turning. The vibration signals from the cutter are collected by using (Kistler three - direction acceleration sensor) with a sampling frequency of 5000 Hz, and then they are sent to the computer for analysis and calculation by the GL 900-APS Ver.2.01 software. The vibration signal acquisition interface is shown in Figure 6.6.

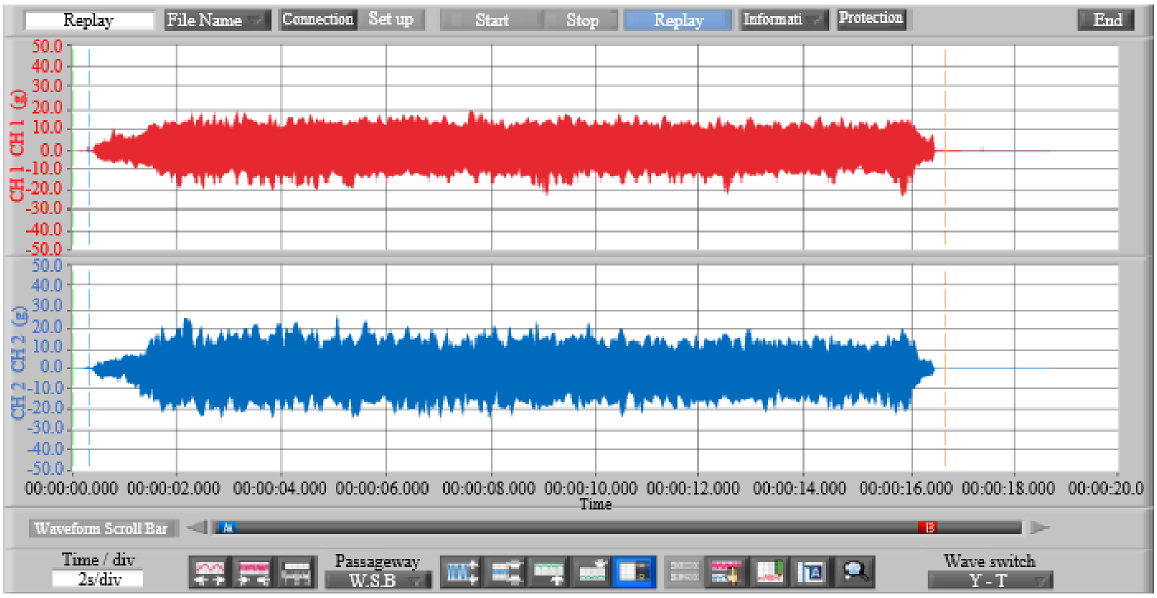

Figure 6.6: The Vibration Signal Acquisition Interface

(2) Selection of Cutting Parameters

Cutting speed usually has the greatest effect on tool wear and should not be too high or too low. For the typical nickel-based super-alloys cutting process, the cutting speed employed during this test ranges from 40 ~ 120 m/min.

In order to avoid the effects of the work hardening caused by the nickel-base super-alloys processing, a larger cutting depth is usually used during processing. Thus, the tool is prevented from cutting the hard layer. However, the PCBN tools are usually used for finishing, and the nickel-based super-alloys require the higher precision machining. In addition, due to the hardness power of the machine, the cutting depth should not be too large, in processing stage, the cutting depth is usually less than 2mm, and the feed rate is less than 0.4mm/rev. Therefore, during this experiment, the cutting depth is in the range of 0.15 ~ 0.4 mm, and the feed rate is in the range 0.05 ~ 0.25 mm / rev. The parameters of this study are shown in Tables (6.3 – 6.5).

Table 6.3: Test Parameters of Variable Cutting Speed

The cutting depth a_p (mm)	0.25	Feed rate f (mm/rev)	0.15
Cutting speed V (m/min)	40, 60, 80, 100, 120		

Table 6.4: Test Parameters of Variable Feed Rate

Cutting speed V (m/min)	80	The cutting depth ap (mm)	0.25
Feed rate f (mm/rev)	0.05, 0.10, 0.15, 0.20, 0.25		

Table 6.5: Test Parameters of Variable Cutting Depth

Cutting speed V (m/min)	80	Feed rate f (mm/r)	0.15
The cutting depth ap (mm)	0.15, 0.20, 0.25, 0.30, 0.40		

6.3 Identification of Chatter and Verification of Stability Limits

6.3.1 Identification of Chatter

The main feature of the identification of chatter in the test is the machined surface which has a clearly visible vibration pattern, accompanied by sharp noises at the same time. When time domain signals are analyzed during the occurrence of the chatter, the amplitude of the vibration signal is obviously larger than the amplitude at the normal cutting state. By analyzing the frequency domain signal in chattering state the vibration energy is concentrated in a very narrow frequency range, thus amplitude is higher than the amplitude in other frequencies, and the frequency structure tends to be single [148].

6.3.2 Testing Method

In order to verify the limit cutting depth predicted by the simulation, the variable cutting depth in this experiment is as shown in Figure 6.9. The workpiece is turned into a cone with a cone angle $20°$ at varied cutting depths, while the cutting speed and the insertion speed were maintained at invariant quantities. With the axial feed of the lathe tool, the cutting depth increases. When the cutting depth reached the limit cutting depth, the system vibration suddenly increased, leaving a tool mark on the workpiece surface, and at this stage the cutting process was stopped. Since PCBN tools are only used for finished conditions, the cutting depth is usually less than 1mm, because when the cutting depth is too large, it leads to a serious wear in the tool. Therefore, in the verification test, a cemented carbide blade YD15 was used. This blade is usually used in rough machining conditions, and the allowable depth of cut is $2{\sim}6\ mm$ to realize the test conditions. The cutting parameters employed during this test were: $cutting\ speed\ v\ =\ 80\ m/min$, $initial\ cutting\ depth\ a_{p0}\ =\ 0.1\ mm$. The feed was selected to be as small as 0.15 mm/rev in order to increase the effect of regenerative vibration due to the increase of cutting depth. At the end of the experiment, the distance from the feed rate to the vibrating mark was measured by L_{lim}, and the side cutting edge angle of the tool in the experiment $kr = 0°$, and $b_{lim} \approx a_{plim}$ were used.

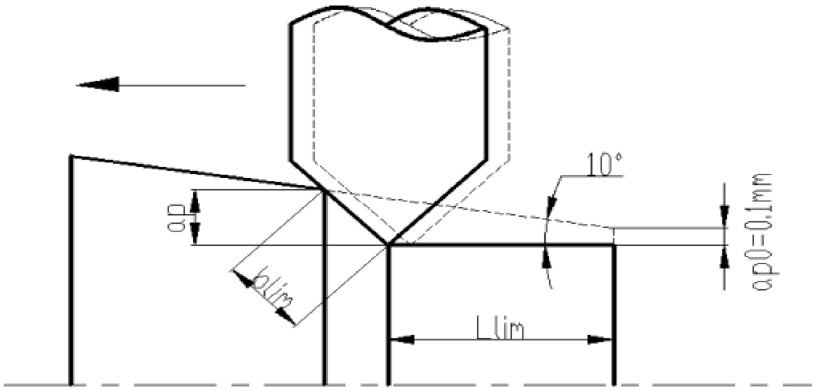

Figure 6.7: Sketch of Variable Cutting Depth Test

According to Figure 6.7, the equation for calculating the limit cutting depth is:

$$a_{plim} = \tan 10^o + 0.1 \qquad (6.1)$$

6.3.3 Experiment Results

Figure 6.8 shows the vibration time-domain diagram in the X and Y directions. It can be observed that at the beginning of the cutting action, the amplitude increases steadily with the increase of the cutting depth. When the cutting action is continued to $25s$ the amplitudes of X and Y suddenly increase, and the vibration in the Y direction was remarkably stronger than that that in the X direction. This vibration is accompanied by the tool scratched lines on the machined surface of the workpiece as shown in Figure 6.9.

Figure 6.8 below illustrates graphically the Time-Domain Waveform of X Direction and Y Direction. Whereas, Figure 6.11 illustrates the Chatter Marks on the workpiece.

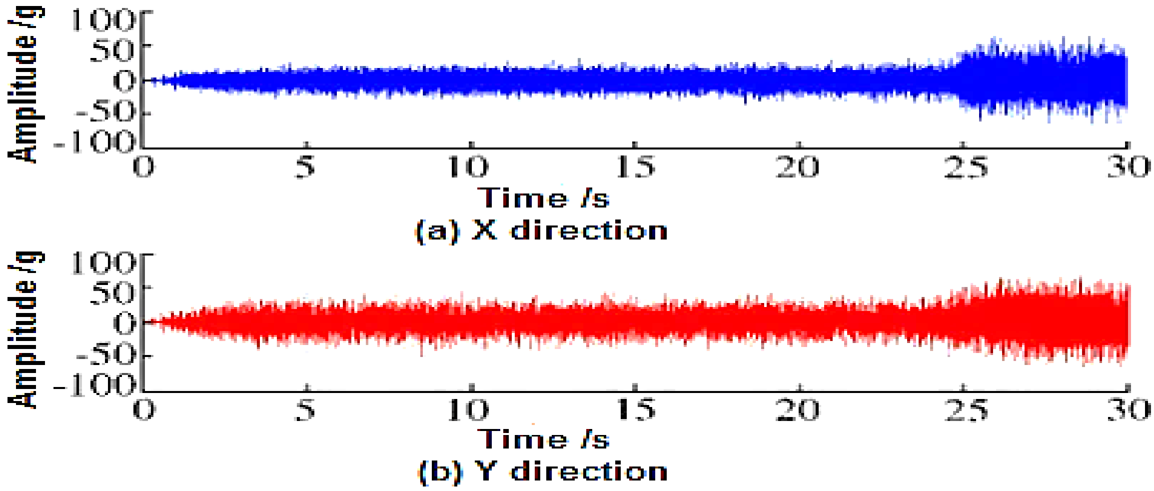

Figure 6.8: Time-Domain Waveform of X Direction and Y Direction

Figure 6.9: Chatter Marks

Therefore, in order to study the change of the vibration amplitude and the frequency during the cutting process, data were processed at 5 s, 15 s, and

25 s, and the sampling time was 1.2s. These values were selected to view the samples at three different cutting durations. The time-vibration frequency plots of 5 s and 15 s in the X and Y directions are shown in Figures 6.10 and 6.11, respectively.

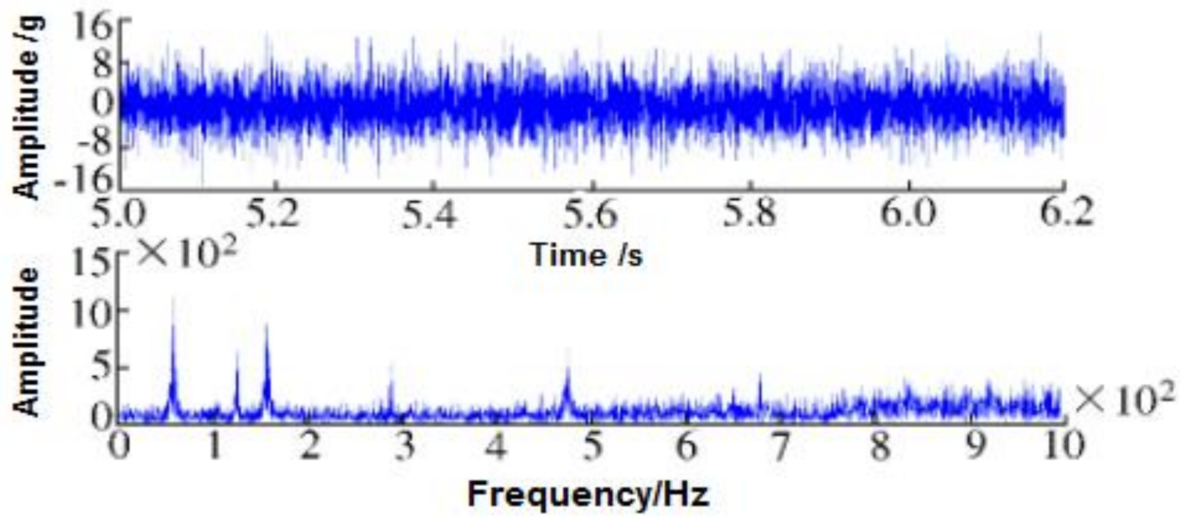

Figure 6.10(a): Amplitude vs Frequency in the X-Direction at 5 s

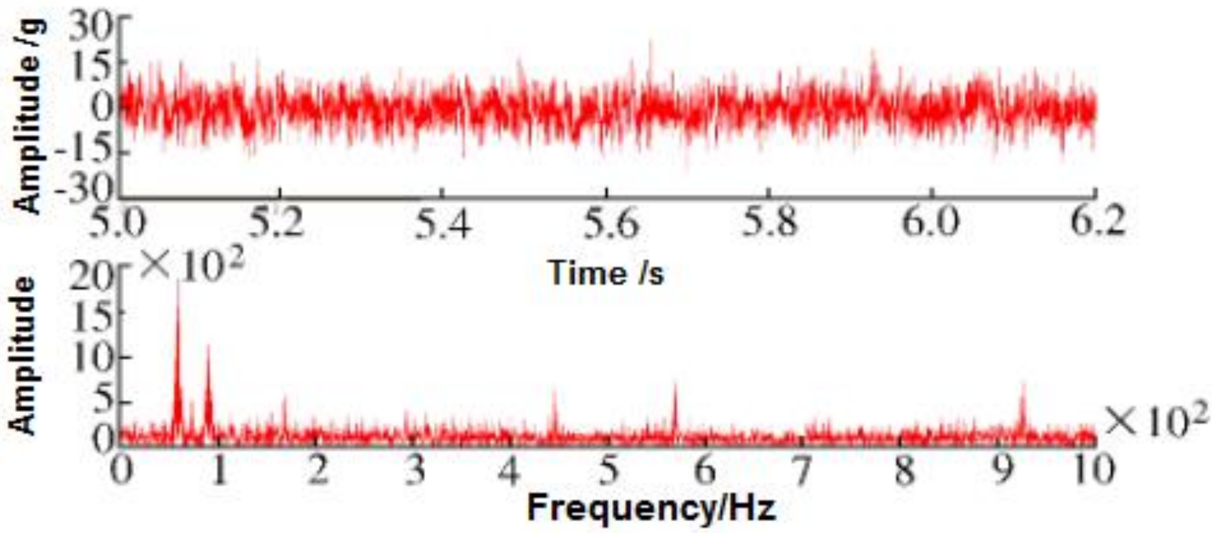

Figure 6.10(b): Amplitude vs Frequency in the Y-direction at 5 s

Figure 6.10 Time-Frequency Diagram of Vibration in the X and Y Directions at 5 s.

Figure 6.10 shows the acceleration signal and a spectrum in the X and Y directions respectively, at 5s. From calculations, the peak signal value in the X direction was 26.04 g, the effective value is 4.01 g, and the peak signal value in the Y direction was 37.66 g, and the effective value is 4.95 g. The experimental results show that the amplitude of X and Y increased gradually with the increase of cutting depth before 25 s. It was observed that the vibration degree in the Y direction was larger than that in the X direction. During this period, although there were peaks that appeared in the frequency domain, they were concentrated in the low-frequency range, i.e., below 100 Hz (Figure 6.12). In addition, it was observed that the overall frequency distribution was more uniform, which indicates that the forced vibration prevailing system was in a stable cutting state. Thus, the amplitude of the vibration signals in the X and Y directions obviously increased and the degree of dispersion was higher.

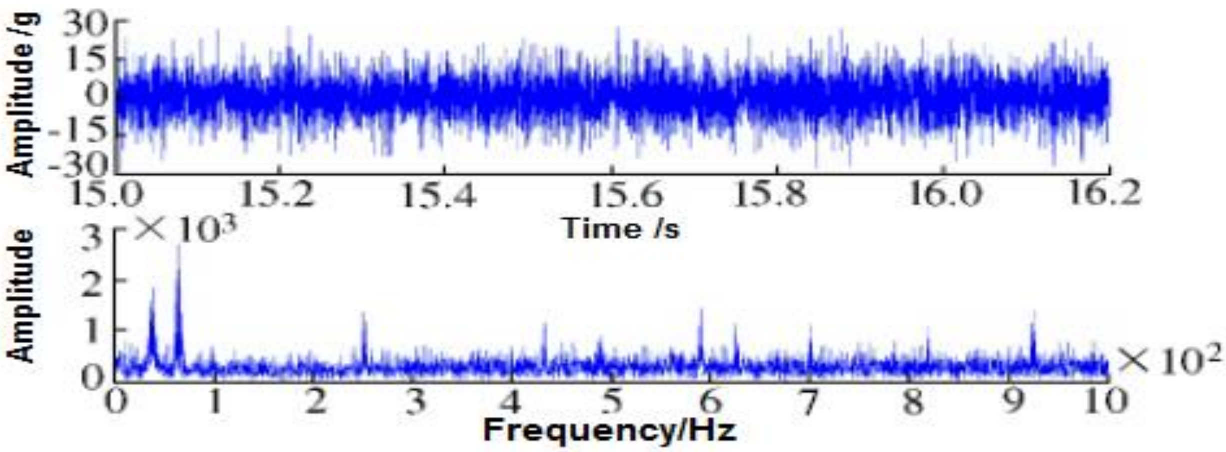

Figure 6.11(a): Amplitude vs Frequency in the X-Direction at 15 s

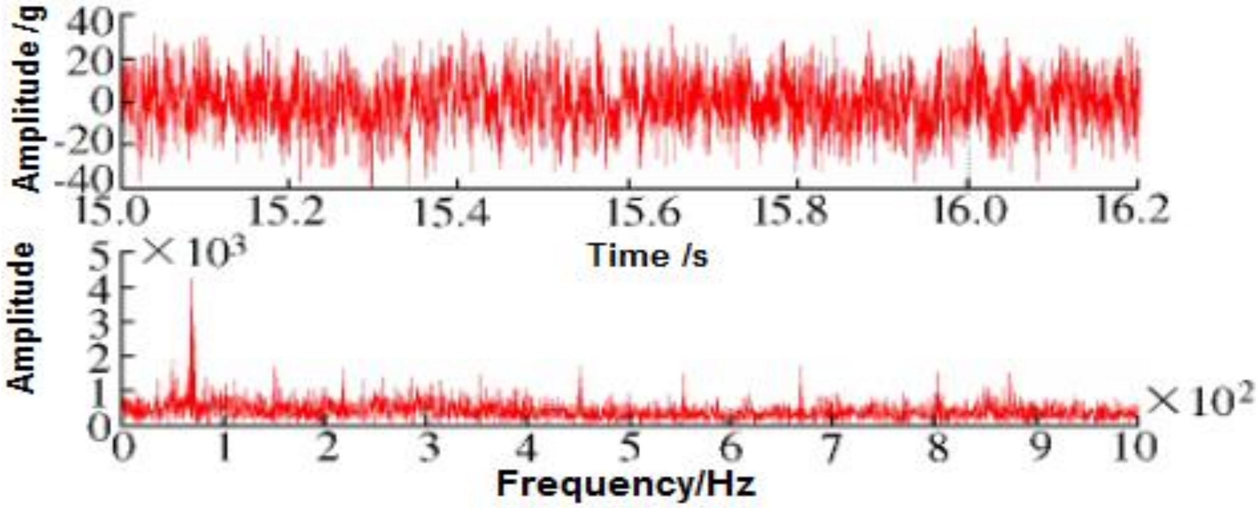

Figure 6.11(b): Amplitude vs Frequency in the Y-Direction at 15 s

Figure 6.11 Time-Frequency Diagram of Vibration in the X and Y Directions at 15 s

Figure 6.11 shows the acceleration signal and a spectrum in the X and Y directions at 15 s respectively. From calculations, the peak signal value in the X direction was 58.30 g, the effective value is 7.65 g. Similarly, the peak signal value in the Y direction was 74.08 g, and the effective value is 11.28 g. In addition, it was observed that the system vibration amplitude at the first 5 seconds increases, which indicates that the forced vibration prevailing system was in a stable cutting state.

Figure 6.12 shows the acceleration signal and a spectrum in the X and Y directions at 25 seconds respectively. From calculations, the peak signal value in the X direction was 77.52 g, the effective value is 11.16 g. The peak signal value in the Y direction is 107.94 g, and the effective value is 15.85 g. The experimental results show that when cutting action continues to 25 s, the amplitudes in the X and Y directions continue to increase and the degree of dispersion increases significantly.

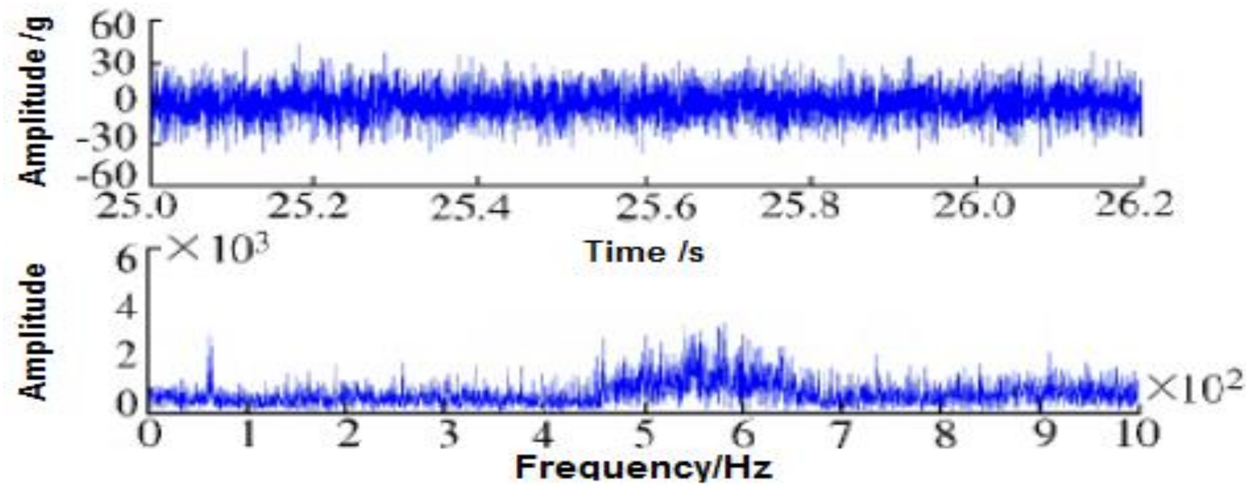

Figure 6.12(a): Amplitude vs Frequency in the X-Direction at 25 s Direction

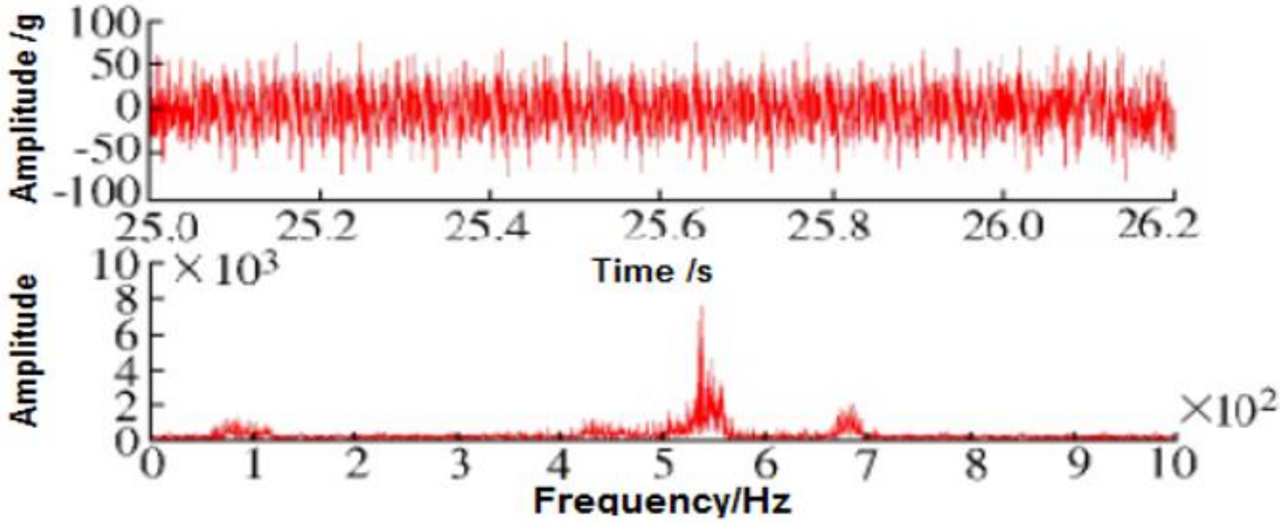

Figure 6.12(b): Amplitude vs Frequency in the Y-Direction at 25 s

Although the degree of vibration in the X direction is exacerbated, there is no energy concentration in the frequency domain. However, the energy in the Y direction is mainly concentrated at a frequency range of about 538 Hz. In this case, the frequency structure tended to be noticeable, so the vibration mode of the system had changed from forced vibration to transition and from forced vibration to intensive self-excited vibration, achieving an unstable cutting state.

In summary, the measured values of L_{lim} and a_{plim} were found to be $12.88\,mm$ and $2.37\,mm$ respectively. Comparing with the results obtained from the simulation, the error rate of the limit cutting depth was:

$$\frac{2.37 - 1.98}{2.37} = 16.45\%$$

6.4 Effect of Cutting Parameters on Vibration Characteristics

6.4.1 Effect of Cutting Speed

Figures 6.13 and 6.14 below illustrates graphically the Vibrational Frequency Diagram at $V = 40\,m/min$ and $V = 60\,m/min$ in the X and Y directions respectively.

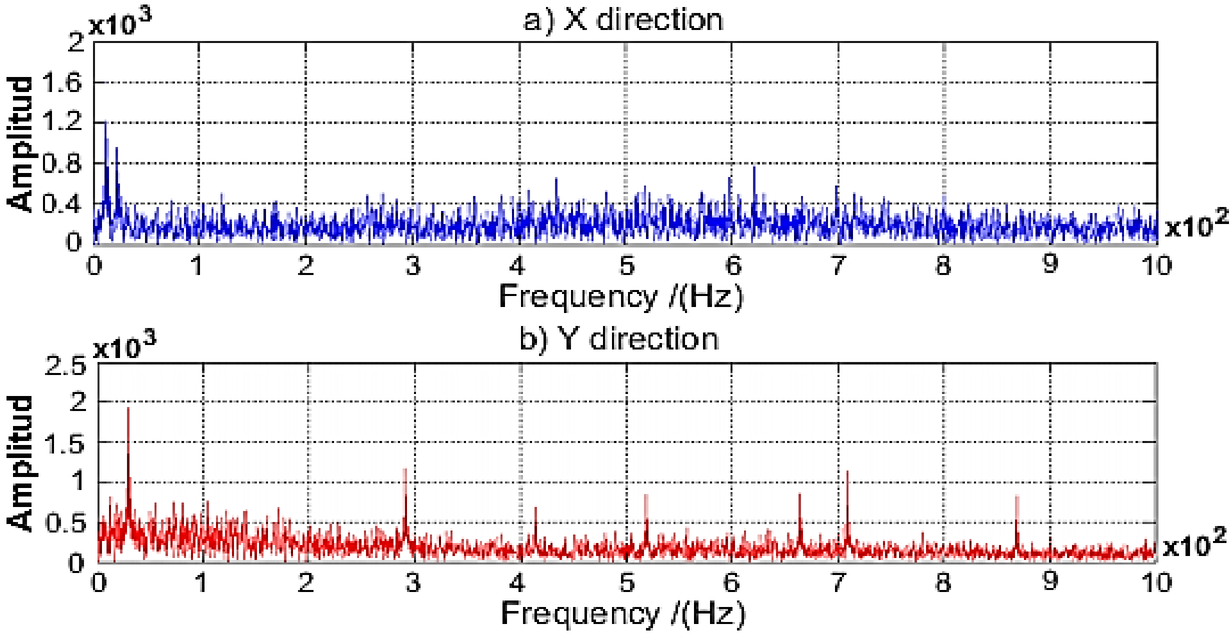

Figure 6.13: Vibrational Frequency Diagram at $V = 40\,m/min$

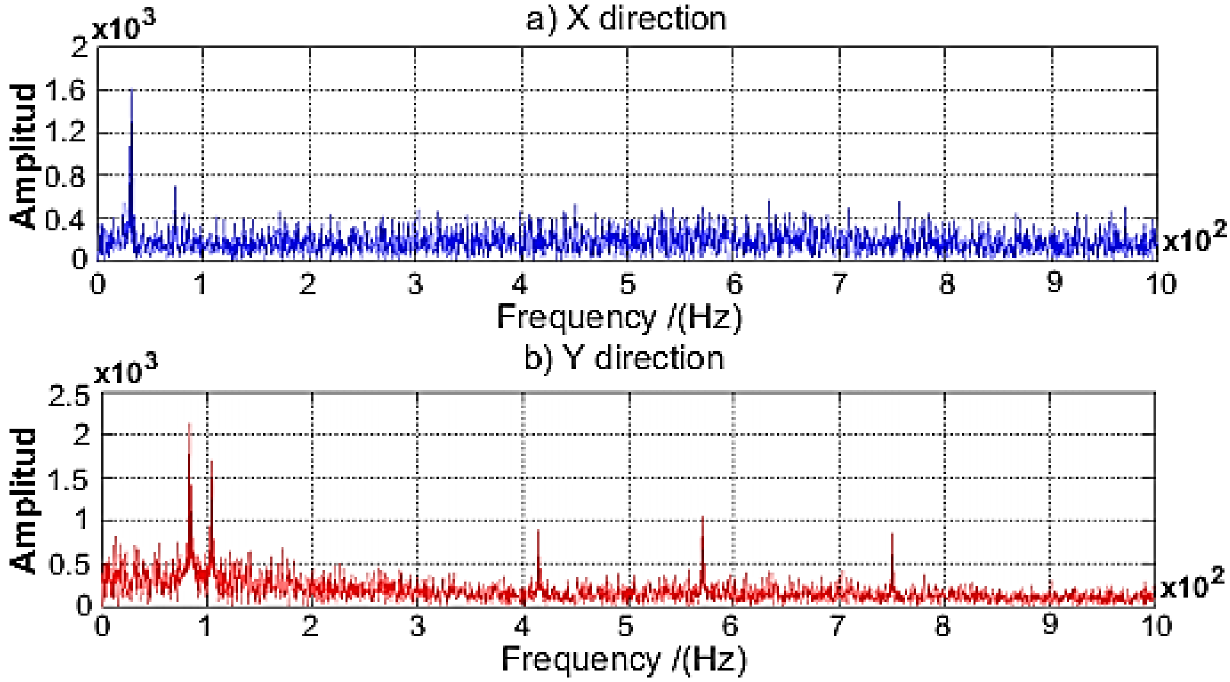

Figure 6.14: Vibrational Frequency Diagram at $V = 60\ m/min$

The vibration acceleration signals at different cutting speeds were sampled, where the sampling frequency is 5000 Hz, and the sampling time is 1 second.

Figures 6.13 and 6.14 below show the vibration spectra in the X and Y directions when the cutting speed is $v = 40m / min,\ and\ 60m / min$. It was found that at the low cutting speed, the system is subjected to forced vibration under the effect of cutting force. Thus, it can be seen in the Figures 6.13 and 6.14 that the peak frequency appears in the low-frequency range which is less than 100 HZ.

The measurement of the acceleration peaks of the time domain at different cutting speeds and the calculation of the effective values of the whole cutting process are shown in Table 6.6.

Table 6.6 below illustrates the vibration parameters at different cutting speeds in the X and Y directions which include peak acceleration and the Effective value.

Table 6.6: The Vibration Parameters at Different Cutting Speeds in the X and Y Directions

direction	Cutting speed (m/min)	40	60	80	100	120
X	Peak acceleration (g)	8.80	9.68	10.99	10.25	8.79
	Effective value (g)	1.46	1.61	2.82	1.77	1.21
Y	Peak acceleration (g)	11.94	13.32	15.07	14.15	12.01
	Effective value (g)	1.81	2.36	3.95	2.42	1.26

In the measured parameters, the acceleration peak represents the maximum value of the acceleration during the whole cutting process, which affects the cutting condition for a brief moment during the machining process. The magnitude of the acceleration in the whole cutting process is expressed by the effective value, which reflects the smoothness of the whole process. Figure 6.15 shows that when the cutting speed increases, the acceleration peaks and the effective values in X and Y directions are increased, and the vibration intensity is larger in Y direction than in X direction. In this case, the system is in stable cutting state. At first, it was also observed that the increase in the cutting speed also leads to increase in vibration. This vibration reaches the maximum value when the cutting speed reaches $80\ m\ /\ min$, and then gradually decreases with the increase in cutting speed. The peak frequency appears in the low-frequency range of less than 100 HZ (Figure 6.14). As a result of low cutting speed, the cutting force is reduced.

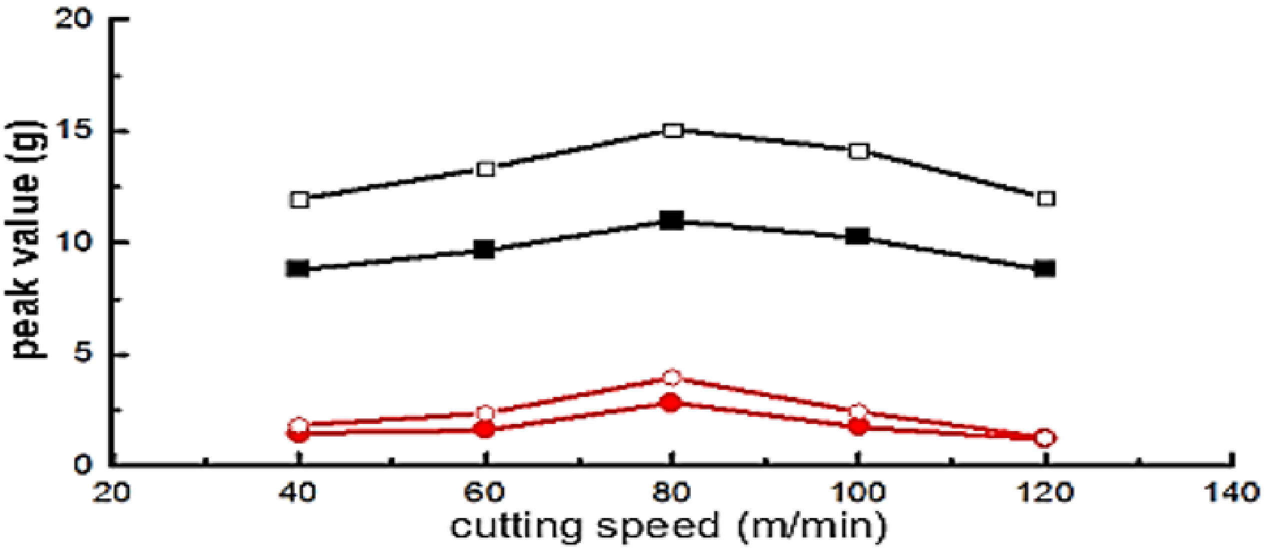

Figure 6.15: The Effect of Cutting Speed on the Peak Value

When the cutting speed reaches $80m/min$, and due to the low-thermal conductivity of nickel-based super-alloy, the heat generated during cutting process is accumulated in the cutting area, which leads to softening of the cutting area, resulting in reduced strength of the workpiece material. Therefore, the required cutting force is gradually reduced. Thus, the effect of the cutting force on the forced vibration of the system was reduced. In addition, for high-speed cutting, the cutting thickness of the deformed region is reduced due to the increase in the shear angle, so the cutting force is reduced, resulting in a decrease in vibration. From the above analysis, we can see that with changes in the cutting speed, the main factors that dominate the system is the forced vibration caused by the cutting force. During this process, the effect of cutting chatter is not obvious.

6.4.2 Effect of Feed Rate

Figures 6.16 and 6.17 show the vibrational spectrum in the X and Y directions for the feed rates $f = 0.20mm/rev \; and \; f = 0.25mm/rev$, respectively. As the feed rate increases, the system will be gradually weakened by the self-excited vibration, and the forced vibration will gradually increase. Therefore, we can see from the figures that the peak frequency is gradually shifted from the high frequency band to the low frequency range which is less than 100 Hz.

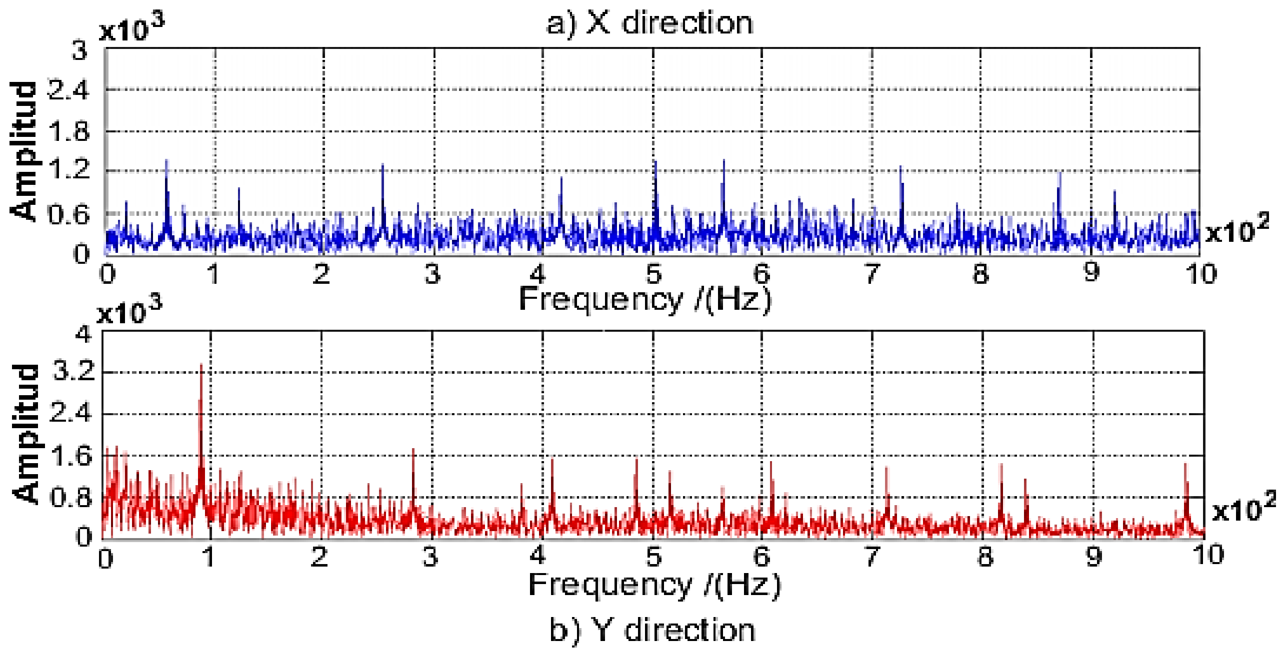

Figure 6.16: The Vibrational Spectrum in the X and Y Directions at $f = 0.20mm/rev$

The measurement of the peak acceleration of the time domain at different feed rates and the calculation of the effective values of the whole cutting process are shown in Table 6.7.

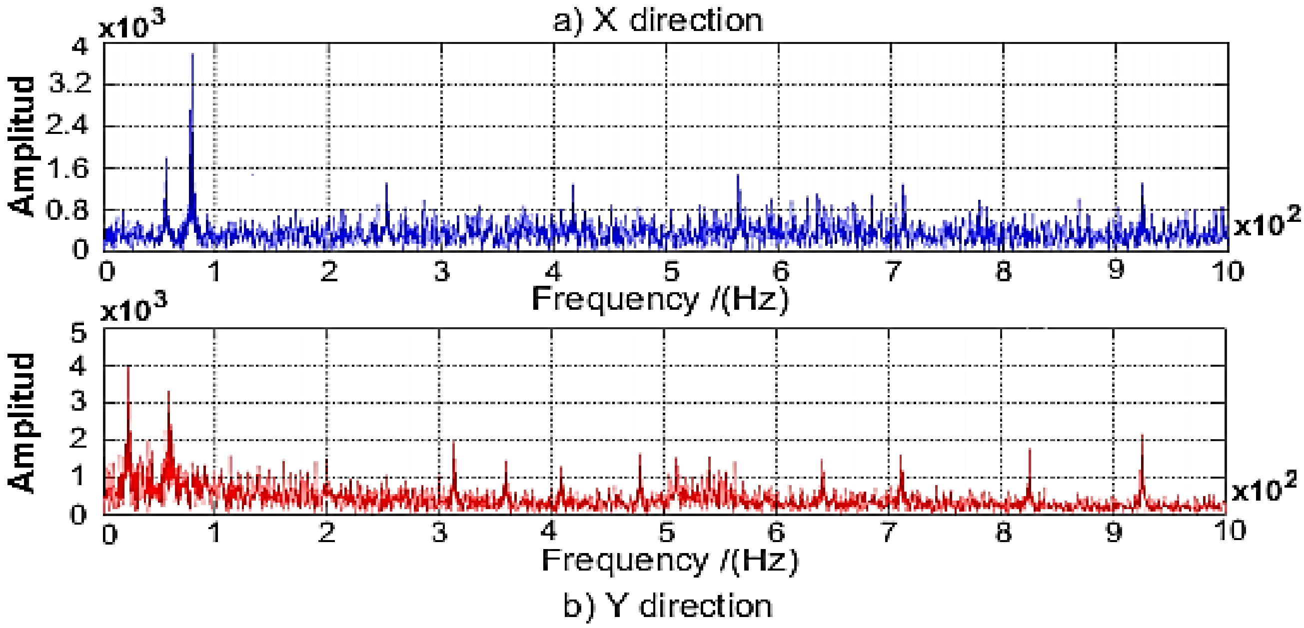

Figure 6.17: The Vibrational Spectrum in the X and Y Directions at $f = 0.25mm/rev$

Table 6.7 The vibration parameters at different Feed rates

direction	Feed rate (mm/rev)	0.05	0.10	0.15	0.20	0.25
X	Peak acceleration (g)	15.75	12.76	10.99	11.26	12.29
	Effective value (g)	4.67	3.39	2.82	3.19	3.61
Y	Peak acceleration (g)	23.89	21.01	15.07	15.54	17.72
	Effective value (g)	5.63	5.36	3.95	4.24	5.28

Figure 6.18 shows that with the increase in feed rate, the acceleration peak, and the effective value in the X and Y directions firstly decrease and

then increase. During this period, the system is in a stable cutting state. At first, the system vibration decreases with the increase of feed rate. This vibration reaches a minimum value at $f = 0.15 mm/rev$. At this point, the tool vibration is the weakest. When the feed rate increases, the vibration decreases rapidly in all directions. When the feed rate reaches $0.15\ mm/rev$, the vibration in all directions increases smoothly. According to the definition of coincidence degree μ in the machine tool cutting system, when the feed rate value is small, the system coincidence degree μ is large, the regeneration effect is strong, the cutting thickness is smaller, the resulting cutting force is low, and the forced vibration of the workpiece is weakened. Therefore, the dominant vibrations on the system are the self-excited vibrations caused by the regenerative effect. However, with the increased feed rate, the system coincidence degree μ gradually decreases, thus leads to a decrease of regenerative chatter effect. But, with the increases feed rate to $0.15\ mm\ /\ rev$, and with the feed rate continues to increase, the cutting thickness and the cutting area gradually increase, resulting in the increase of energy amount required during the cutting process. As a result, the system was obliged by the cutting force to enhance the vibration.

From the above analysis, it is observed that, when $f\ <\ 0.15 mm/rev$, the effect of system by the self-excited vibration caused by the regenerative effect is greater than the effect of the system by the forced vibration caused by the cutting force. The regeneration effect is the main factor of the system vibration, which leads to weakening the system vibration. When $f > 0.15mm/r$ev, the forced vibration effect on the system caused by the cutting force is greater than the system effect by the self-excited vibration caused by the regenerative effect. Thus, resulting in the enhancement of the system vibration.

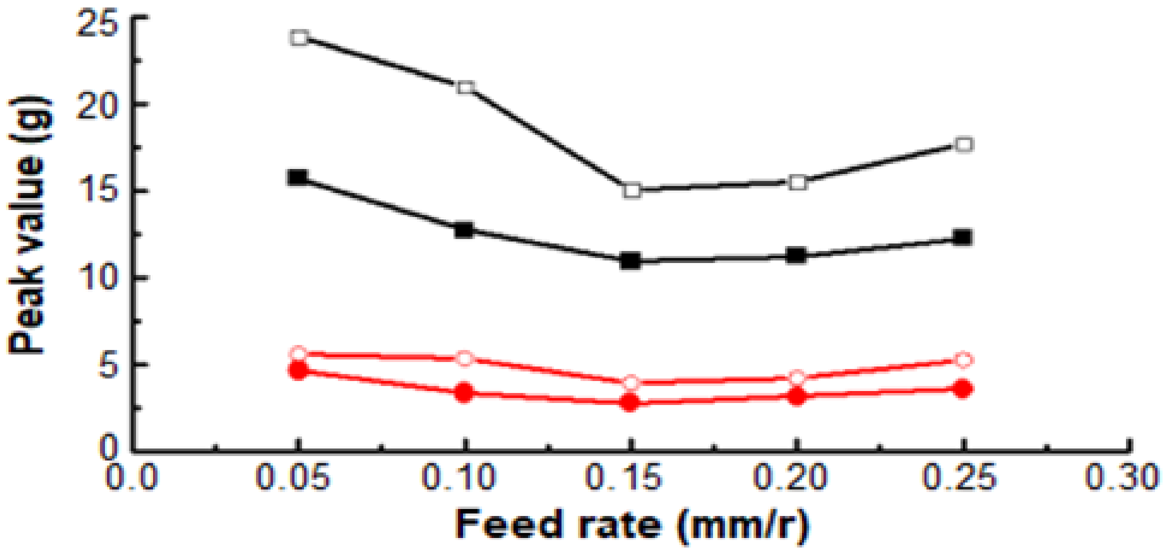

Figure 6.18: Influence of Feed Rate on Vibration

6.4.3 Effect of Cutting Depth

Figures 6.19 and 6.20 show the vibration spectrum in the X and Y directions at the cutting depth $a_p = 0.30mm\ and\ a_p = 0.40mm$, respectively. With increasing cutting depth, the forced vibration and self-excited vibration of the system will gradually increase. It can be seen from the figures that the peak value in the whole frequency domain increases with the increase of the cutting depth, especially in the low-frequency range of less than 100

Hz, and the peak value increases more significantly, indicating that the system is mainly affected by forced vibration.

Figure 6.19 below illustrates graphically Vibrational Frequency Diagram at $a_p = 0.3mm$.

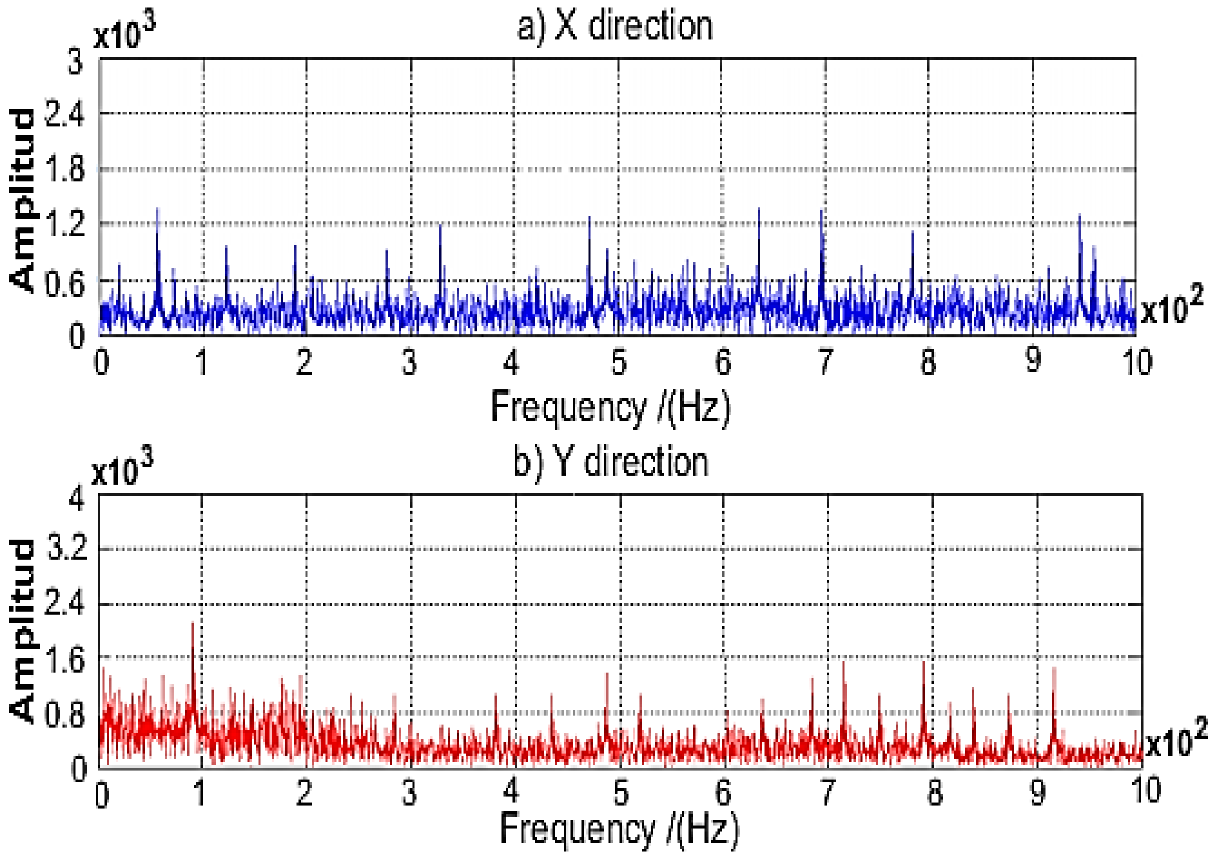

Figure 6.19: Vibrational Frequency Diagram at $a_p = 0.3mm$

Figure 6.20 below illustrates graphically Vibrational Frequency Diagram at $a_p = 0.4mm$.

The corresponding calculations of peak acceleration for the time domain at different feed rates and the effective values of the cutting process in the X and Y directions are shown in Table 6.8 below.

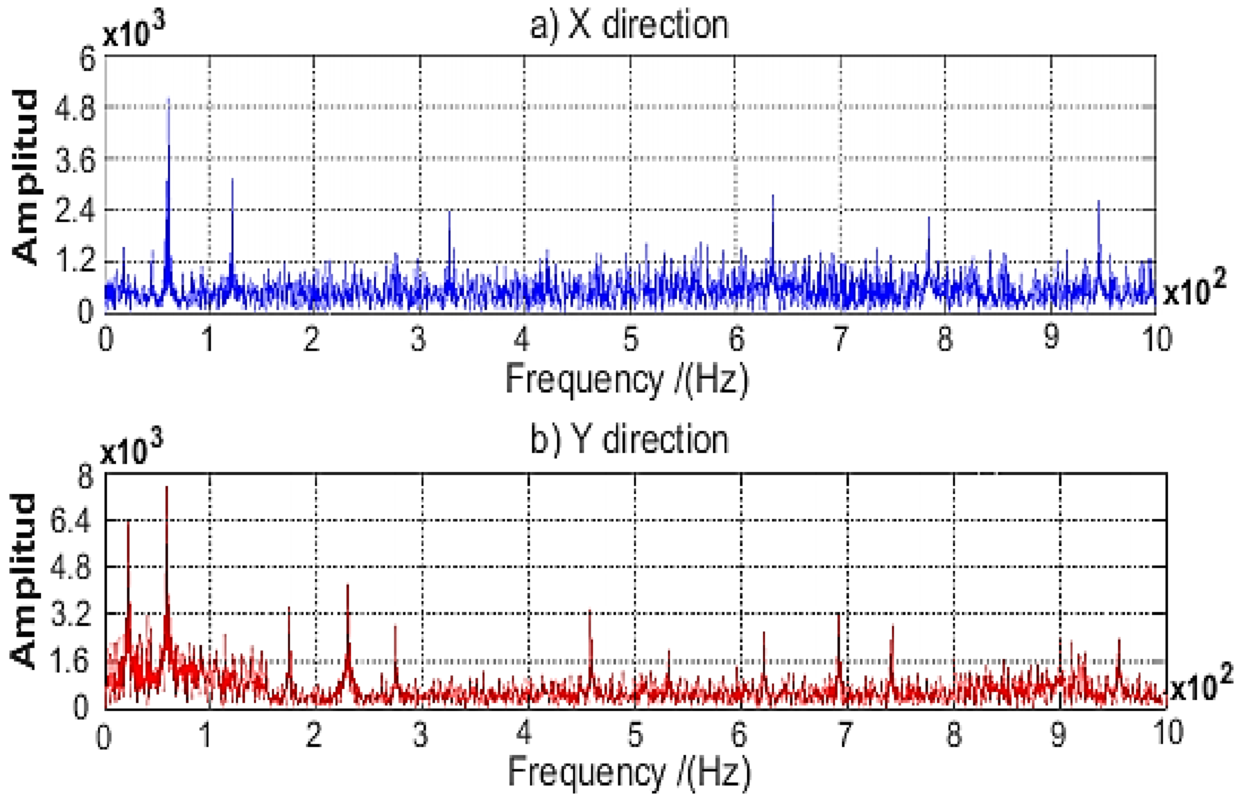

Figure 6.20: Vibrational Frequency Diagram at $a_p = 0.4mm$

Table 6.8: The Vibration Parameters at Different Cutting Depth

direction	Cutting depth (mm)	0.15	0.50	0.25	0.30	0.4
X	Peak acceleration (g)	7.26	8.70	10.99	12.29	17.58
	Effective value (g)	1.27	2.23	2.82	3.75	6.75
Y	Peak acceleration (g)	9.69	11.21	15.07	17.96	26.88
	Effective value (g)	2.09	3.44	3.95	5.31	9.02

Figure 6.21 below illustrates graphically the effect of cutting depth on Vibration.

Figure 6.21 shows that, with the increase cutting depth, the peak acceleration and the effective value in the X and Y directions increases linearly. When the cutting depth reaches $a_p = 0.4mm$. At this point, the system vibration is the strongest. In the cutting process, the energy amount required to overcome the deformation force and friction force of the material increases with the increasing cutting force in the cutting area.

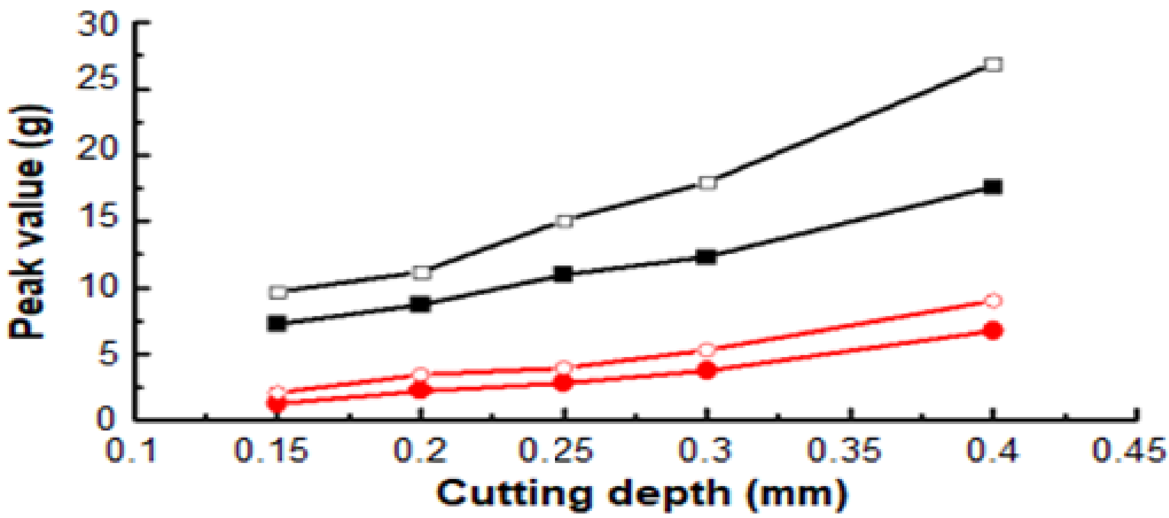

Figure 6.21: Effect of Cutting Depth on Vibration

Consequently, the system is obliged through the force produced by the cutting process to enhance vibration. As the cutting depth increases the cutting width increases. The cutting width has a little effect on the deformation and friction coefficient. Therefore, the cutting force increases proportionally with the increasing depth of cut, and that is reflected in the vibration characteristics. On the other hand, the theory of regenerative chatter of machine tool cutting system shows that with the increase of cutting depth, the dynamic cutting force required to maintain the self-excited vibration of the system gradually increases. It can be noticed that, from the stability lobe diagram of the system, when the cutting width gradually approaches the limit cutting width of the system, the regeneration effect is gradually increased, which makes the system vibration gradually becomes stronger. From the above analysis, it can be concluded that, with the increase of cutting depth, the system is subjected to the forced vibration caused by the cutting force and the self-excited vibration caused by the regenerative effect, which leads to the system vibration.

6.5 Effect of Cutting Parameters on Workpiece Surface Roughness

Surface roughness R_a is defined as an important parameter used to indicate the level of surface roughness. In theory, without considering the other factors, the surface roughness is affected by the feed rate and tool radius, but in the actual processing, the surface roughness is affected by the (cutting parameters, tool parameters, workpiece material, and the cutting vibration and other factors). Many studies have shown that the surface roughness of the workpiece is occurring by the high-frequency vibration of the tool [151]. Therefore, in this chapter, based on the experiments, the vibration influence of the cutting parameters and tool on the surface roughness of workpiece were studied.

6.5.1 Effect of Cutting Speed

Figure 6.22 below shows the influence of cutting speed on the surface roughness in high-speed turning of nickel-base super-alloy GH4169. When the cutting width is used within the limits of system stability, the cutting width is less than the limit cutting width.

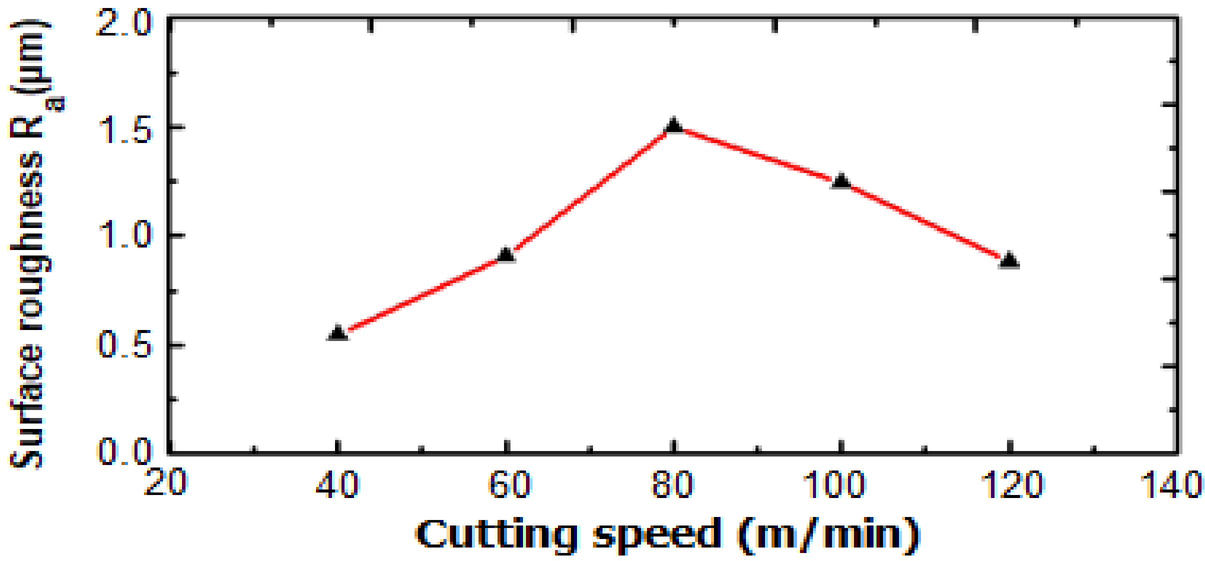

Figure 6.22: Effect of Cutting Speed on Surface Roughness

Therefore, the system vibration occurs in the stable cutting area. At low cutting speeds, the system is subjected to the forced vibration produced by the cutting force. As a result, the system vibration and the roughness of the workpiece surface increases gradually, and as the cutting speed increase to $80m/min$, the system vibration is weakened by the forced vibrations produced by the cutting force. The resulting phenomenon is that the surface roughness of the workpiece is decreased gradually whenever the cutting speed continues to increase.

From the above analysis, it can be seen that, the residual height of the workpiece surface is unchanged in theory because the feed rate is unchanged. Therefore, in this experiment, the cutting speed and tool vibration are the common factors that affect the surface roughness.

6.5.2 Effect of Feed Rate

Figure 6.23 below shows the influence of feed rate on surface roughness in high-speed turning of nickel-based super-alloy GH4169. When the cutting width was used within the limits of system stability, the cutting width is less than the limit. Therefore, the system vibration occurs in the stable cutting area. In the experiment, with the increase feed rate, the surface roughness of the workpiece increased gradually. As seen in Figure 6.22, when the feed rate $f < 0.15\, mm$ / $r$ev, the surface roughness of the workpiece slowly increases. At first, the residual height for the workpiece surface is smaller.

At this point the thickness of the workpiece is small, so the system is exposed to the forced vibration caused by the cutting force, and the system is more affected by the self-excited vibration caused by the regeneration effect. With the increased feed rate, the residual height of the workpiece surface increases gradually, the system is affected by the forced caused by the cutting force, and the influence of the self-excited vibration caused by the regeneration effect on the system is decreasing, and the interaction between the residual height on the workpiece surface and the system vibration leads to a slow increase in the surface roughness of workpiece. When the feed rate reaches $0.15\ mm\ /\ rev$, the effect of the self-excited vibration caused by regenerative effect on the system decreases gradually. Whenever, the feed rate continues to increase, the system is forced to vibrate by the cutting force and gradually becomes the main vibration for the system. Based on the increase of the residual height of the surface workpiece and its interaction with system vibration, this leads to the workpiece surface roughness which increases obviously.

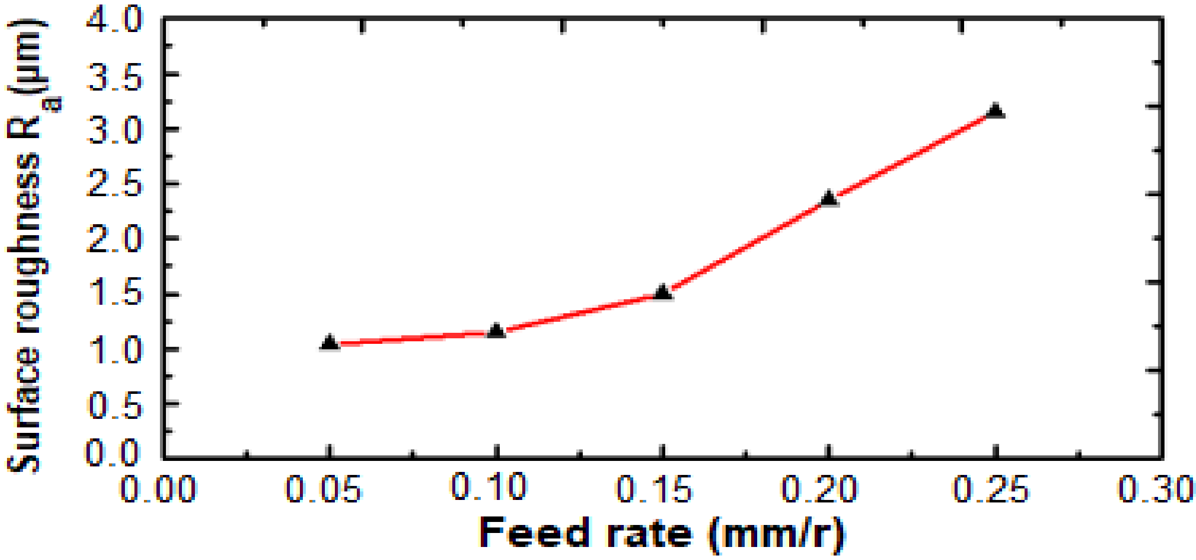

Figure 6.23 Influence of Feed Rate on Surface Roughness

From the above analysis, it can be seen that, in the stable cutting area, with the increased feed rate, the surface roughness of the workpiece increases gradually. Although the system is exposed to combined factors of forced vibration and self-excited vibration, but the feeding rate is still the main factor that affects the surface roughness of the workpiece.

6.5.3 Effect of Cutting Depth

Figure 6.24 below shows the influence of cutting depth on surface roughness in the high-speed turning of nickel-based superalloy GH4169. As shown, the change trend of the surface roughness with cutting depth is similar to the direction of the cutting vibration with the cutting depth. When the cutting width was used within the limits system stability, the cutting width is less than the limit cutting width. Therefore, the system vibration occurs in the stable cutting area. In the experiment, with the increase in cutting depth, the surface roughness of workpiece is increased gradually, but the direction of increase is more moderate, which indicates that the cutting is in the stable cutting area, and the influence of the cutting depth on the surface roughness is a small. On the other hand, the dynamic cutting force required for the system to maintain self-excited vibration increases gradually due to the cutting depth increase. As a result, the system exposed to forced vibration and self-excited vibration. This leads to the increase of the surface roughness. In addition, in the depth test, when the cutting depth reaches the stable limit cutting depth, the system produces a strong self-excited vibration which indicates that the chatter state is reached. This vibration is accompanied by the tool scratched lines on the machined surface of the workpiece.

From the above analysis, it can be seen that, in the stable cutting area, with the increase feed rate, the surface roughness of the workpiece increases gradually. Although the system is exposed to combined factors of forced vibration and self-excited vibration, but the feeding rate is still the main factor affects the surface roughness of the workpiece.

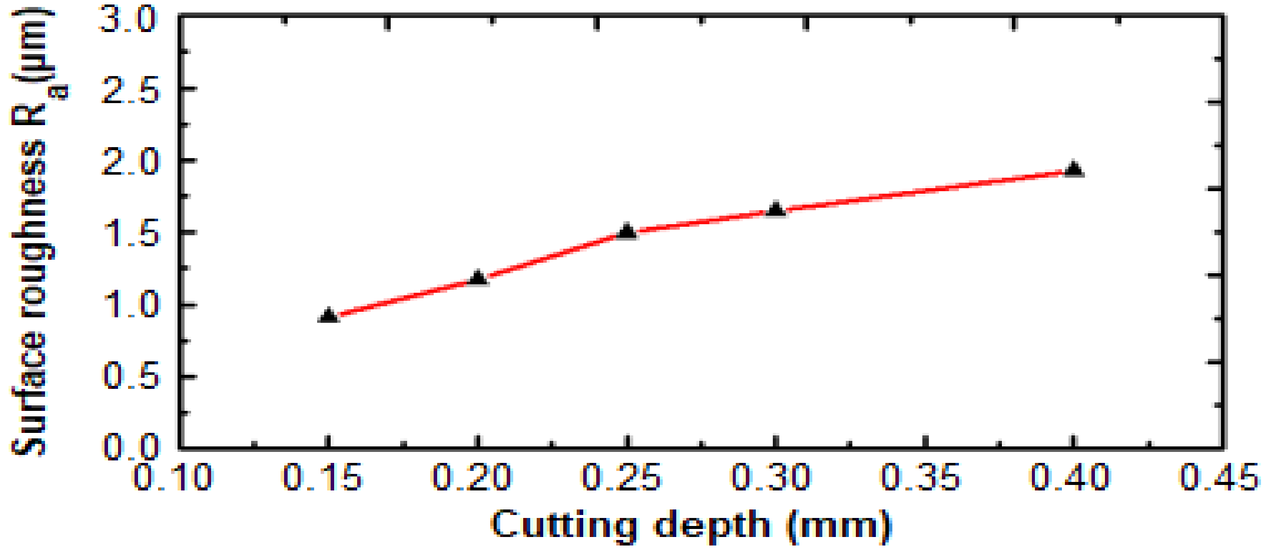

Figure 6.24 Effect of Cutting Depth on Surface Roughness

6.6 Chapter Summary

In this chapter, the cutting stability and the surface quality of nickel base super-alloy are studied. The main conclusions are:

(1) To validate the main vibration system, the limit cutting width predicted from nickel-base super-alloy turning was verified by the variable depth of cut. The frequency of the cutting chatter was 538 Hz, which is close to the natural frequency of 565 Hz of the cutting tool system in the Y direction. This indicates that when the stiffness and quality of the workpiece system are much higher than those of the cutting tool system, the system vibration of the tool is reasonable. Both the simulation and the cutting experiments

showed that with increasing cutting depth, the tool system first achieves an unstable cutting state in the Y direction. Therefore, the Y direction is the main vibration direction of the cutting chatter.

(2) The influence of cutting parameters (cutting speed, spindle speed, feed rate and cutting depth) on the vibration characteristics of nickel-based super-alloy with PCBN Cutting Tools in high-speed turning was studied by comparing the cylindrical turning test results with the numerical simulation results. The results show that when the cutting speed is varied, the forced action is the main cause of vibration. When the cutting speed $v\ is\ < 80\ m/min$ the system vibration increases gradually and when $v > 80m/min$, the system vibration decreases gradually. When the feed rate is $f\ <\ 0.15mm/r$ev, the system is exposed to the self-excited vibration instead of forced vibration. In this case, the system is dominated by self-excited vibration, that leads to the weakness of the vibration system and when the feed rate is $f\ >\ 0.15mm/r$ev, the system is exposed to forced vibration, which is stronger than self-excited vibration.

(3) With the increase of the cutting depth, the system was affected by the forced vibration produced by the cutting force and the self-excited vibration caused by the regenerative chatter effect which results in vibration enhancement. The influence of cutting parameters on the surface roughness was analyzed by using a single factor cylindrical turning test considering machining vibration. Theoretically, when the feed rate is

constant, the residual surface height of the workpiece is constant. Therefore, the vibration of the cutting tools caused by the change of cutting speed and cutting depth is the main factor affecting the surface roughness. When the feed rate changes, although the system is still affected by the forced vibration and self-excited vibration, the feed rate is still the main factor affecting the surface roughness.

Chapter 7

Results and Discussion

7.1 Simulation

The simulation was carried out at constant cutting speed $(80m/min)$ and feed $(0.15mm/rev)$ while the depth of cut was set to be varied at four levels $(1.5mm, 1.98mm, 2.5mm, and\ 4.56mm)$.

Figure 7.1 below illustrates with the aid of neat graphs the Vibration Time Diagram of X and Y under Different Cutting Parameters (a) $V = 80\ m/min, f = 0.15mm/r$, $a_p = 1.5\ mm\ (b)\ V = 80\ m/min, f = 0.15mm/r, a_p = 1.98mm.$

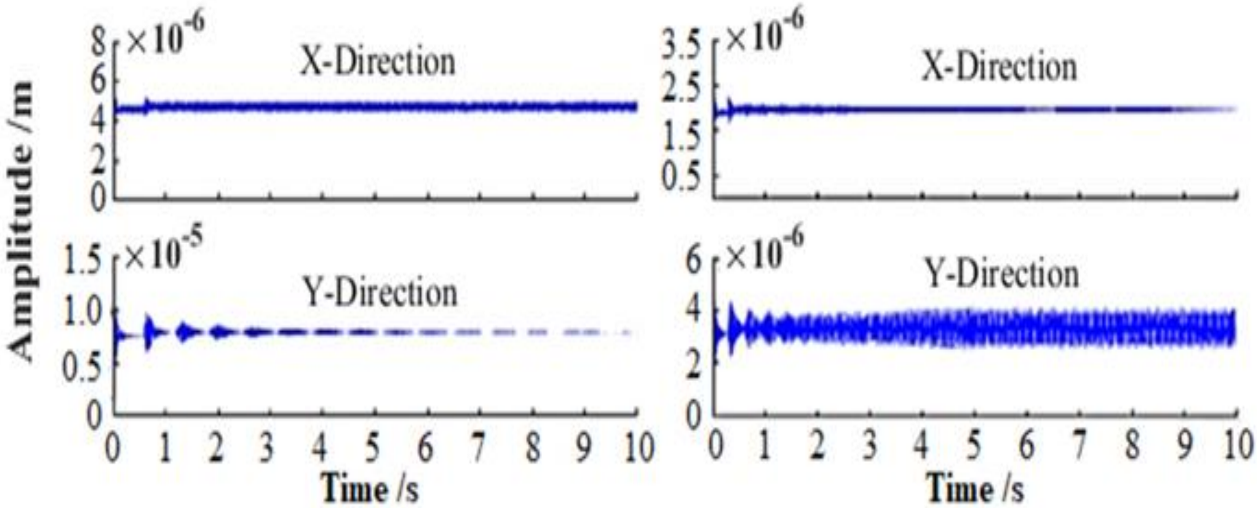

Figure 7.1 Vibration Time Diagram of X and Y under Different Cutting Parameters (a) $V = 80\ m/min, f = 0.15mm/r, a_p = 1.5\ mm\ (b)\ V = 80\ m/min, f = 0.15mm/r, a_p = 1.98mm$

Figure 7.1 below illustrates with the aid of neat graphs Vibration Time Diagram of X and Y under Different Cutting Parameters (c) $V =$

$80\ m/min, f = 0.15mm/rev$, $a_p = 2.5\ mm$ (d) $V = 80\ m/min, f = 0.15mm/rev, a_p = 4.56\ mm$

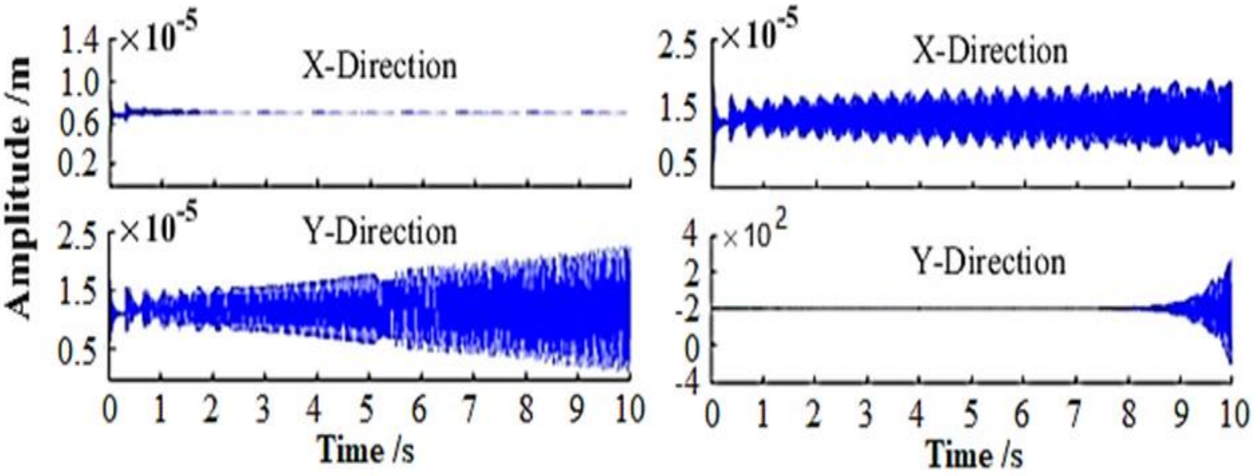

Figure 7.1 Vibration Time Diagram of X and Y under Different Cutting Parameters (c) $\boldsymbol{V = 80\ m/min, f = 0.15mm/rev, a_p = 2.5\ mm}$ $\boldsymbol{(d)\ V = 80\ m/min, f = 0.15mm/rev, a_p = 4.56\ mm}$

At cutting depth 1.5 mm, the tool vibration in the X and Y directions is shown in Figure 7.1(a). In this case, the system is in a stable cutting state. However, when the cutting depth reaches 1.98 mm, the tool vibration in the X direction is attenuated. While the amplitude in the Y direction is almost constant and is in a critical divergent state (Figure 7.1(b)). Therefore, this value of the depth of cut (1.98 mm) is taken as the limit cutting depth in the Y direction. When the cutting depth continues to increase to 2.5 mm, the amplitude of the tool in the X and Y directions increases, and thus the vibration is enhanced (Figure 7.1(c)). Hence, the tool vibration in the X direction is in a convergent state while in Y direction it tends to diverge the unstable cutting state. When the cutting depth continues to increase to 4.56 mm, the vibration in the X direction tends to diverge up unstable cutting conditions (Figure 7.1(d)). It is concluded that, the tool system first reaches the unstable state in the Y direction and then with increasing depth of cut it reaches the unstable state in the X direction.

7.2 Turning Test

The cutting test on the samples of nickel alloy rod GH4169 having a diameter of $125\,mm$ was carried out on (Seiko HTMTC40) CNC lathe machine (Figure 7.3). The test was performed at a varied depth of cut to assess the vibration of the cutting tool system (Figure 7.4).

Figure 7.3 shown below illustrates the setup of turning test, while Figure 7.4 shown below illustrates schematic diagram of vibration monitoring.

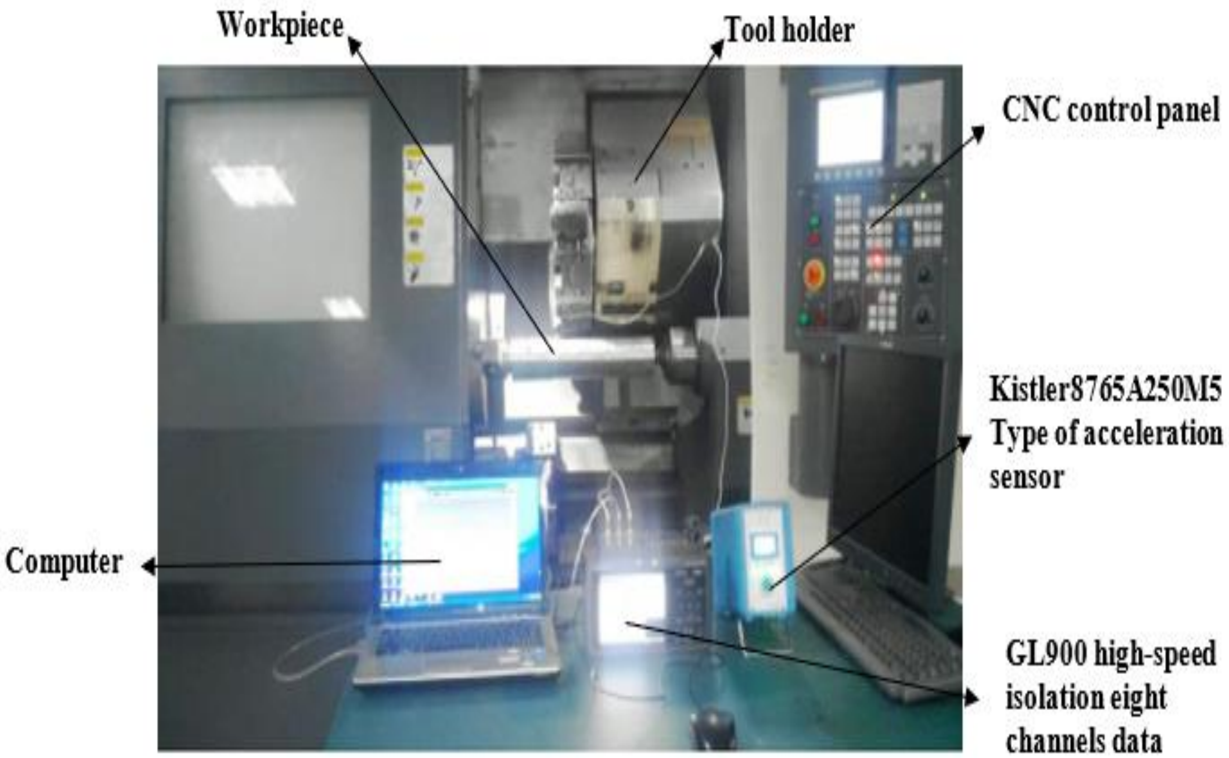

Figure 7.3: Setup of Turning Test

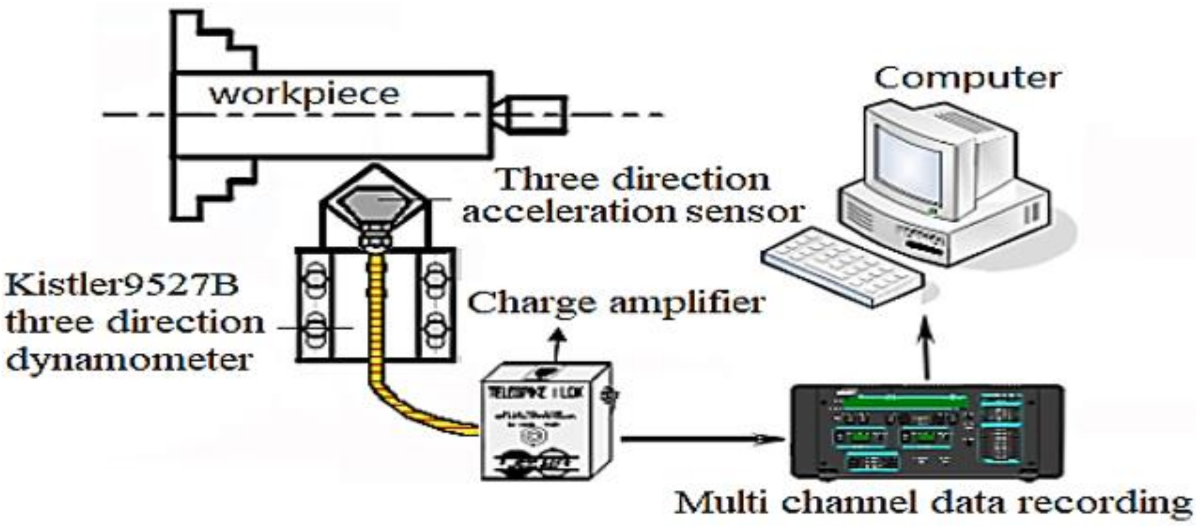

Figure 7.4 Schematic Diagram of Vibration Monitoring

The cutting tool designation used in this test is CNGA120408 - type 2, PCBN blade on an MCLNL type tool holder. The cutting trails were excircle dry turning. The vibration signals from the cutter are collected by using (Kistler 8765A250M5) three acceleration sensors with a sampling frequency of 5000 Hz. The workpiece is turned into a cone with a cone angle of 20° at varied cutting depth. While the cutting speed and the insertion speed are maintained at invariant quantities. When the cutting depth reaches the limit cutting depth, the system vibration suddenly increases leaving a tool mark on the workpiece surface, and at this stage, the cutting process was stopped. The cutting parameters employed during this test are cutting speed $v = 80\ m/min$, the initial cutting depth $a_{p0} = 0.1\ mm$. The feed was selected to be as small as $0.15\ mm/rev$ in order to increase the effect of regenerative vibration due to the increase of cutting depth. At the end of the experiment, the distance from the feed rate to the vibrating mark is measured by L_{lim}, and the side cutting edge angle of the tool in the experiment $kr = 0°$, and $b_{lim} \approx a_{plim}$ are used.

Figure 7.5 below illustrates the Schematic Diagram of the Cutting Depth Method.

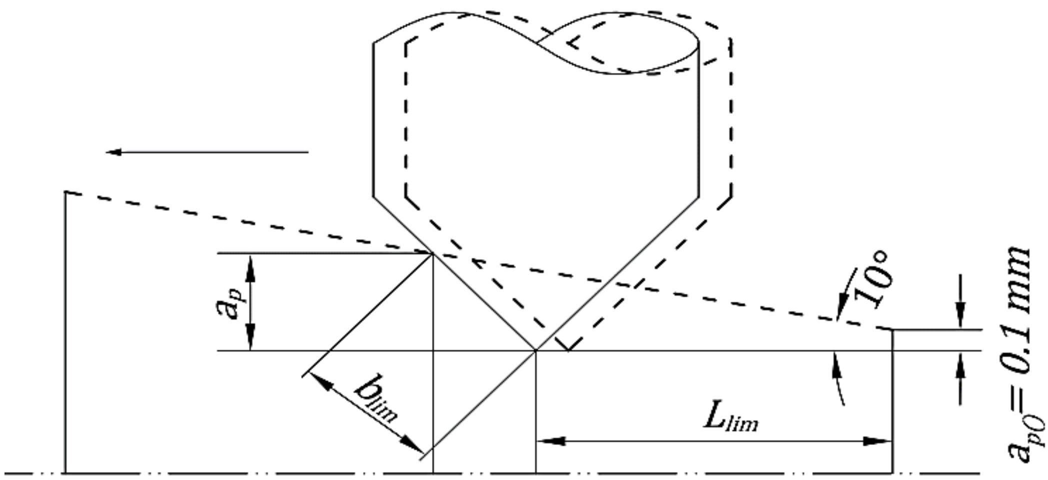

Figure 7.5: Schematic Diagram of the Cutting Depth Method

According to Figure 7.5, the equation for calculating the limit cutting depth can be obtained by using (Equation (6.1))

$$a_{plim} = \tan 10^{o} + 0.1 \qquad (6.1)$$

Figure 7.6 below shows the vibration time-domain diagram in X and Y directions. It can be realized that at the beginning of cutting action, the amplitude increases steadily with the increase of cutting depth. When cutting action continued to 25s, the amplitudes of X and Y suddenly increase, and the vibration in the Y direction is remarkably stronger than that in the X direction. This vibration was accompanied by the tool scratched lines on the machined surface of the workpiece as shown in Figure 7.7.

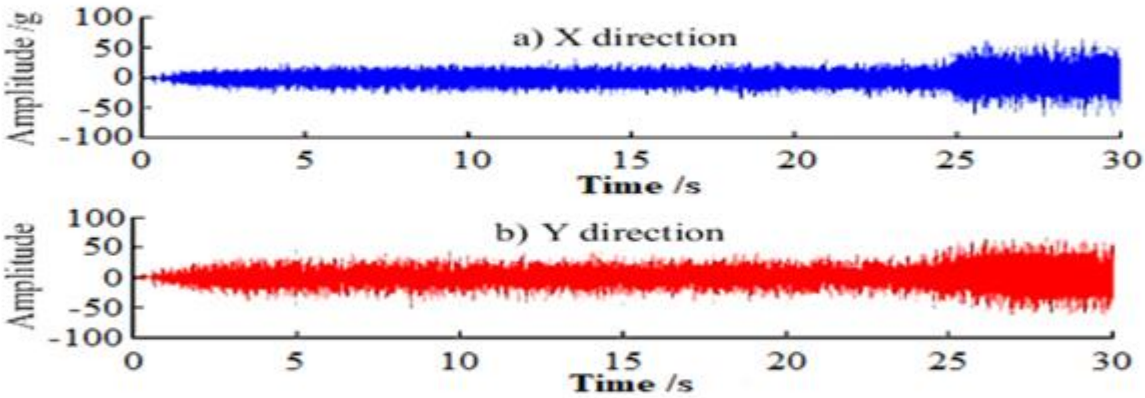

Figure 7.6 The Time-Domain Waveform of the X and Y Directions

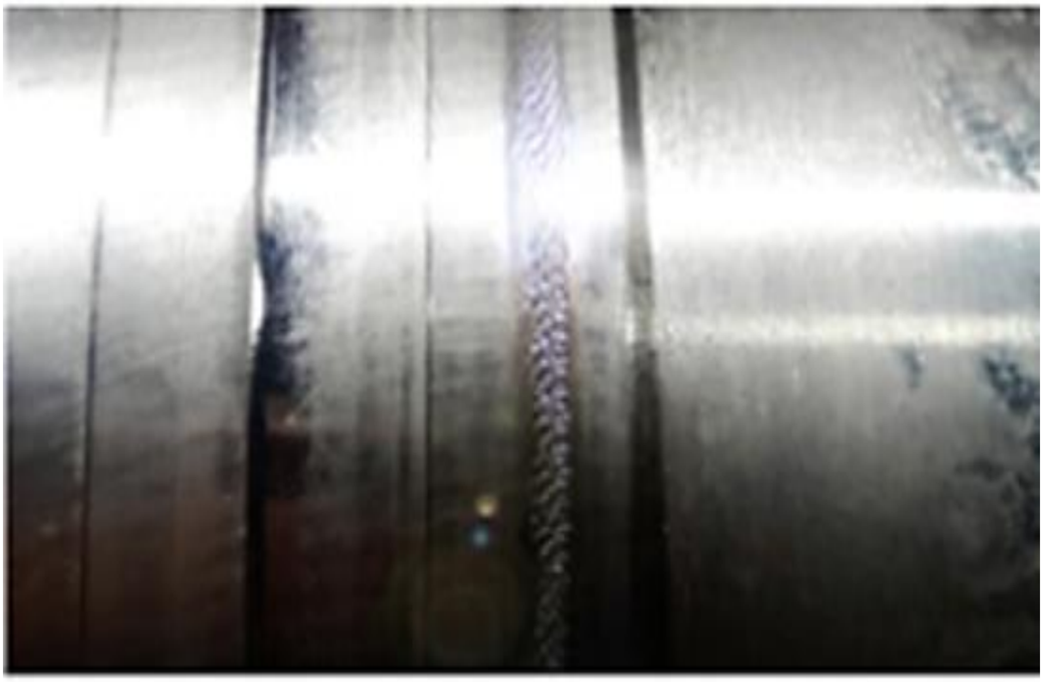

Figure 7.7 Chatter Marks

Therefore, in order to study the change of the vibration amplitude and the frequency during the cutting process, data were processed at 5s, 15s, and 25s. These values were selected to view the samples at three different cutting durations. The time-vibration frequency plots of 5s and 15s in the direction of X and Y are shown in Figure 7.8 and Figure 7.9 respectively.

Figure 7.8(a) shows the Time-Frequency Diagram of Vibration in the Direction of X At 5s.

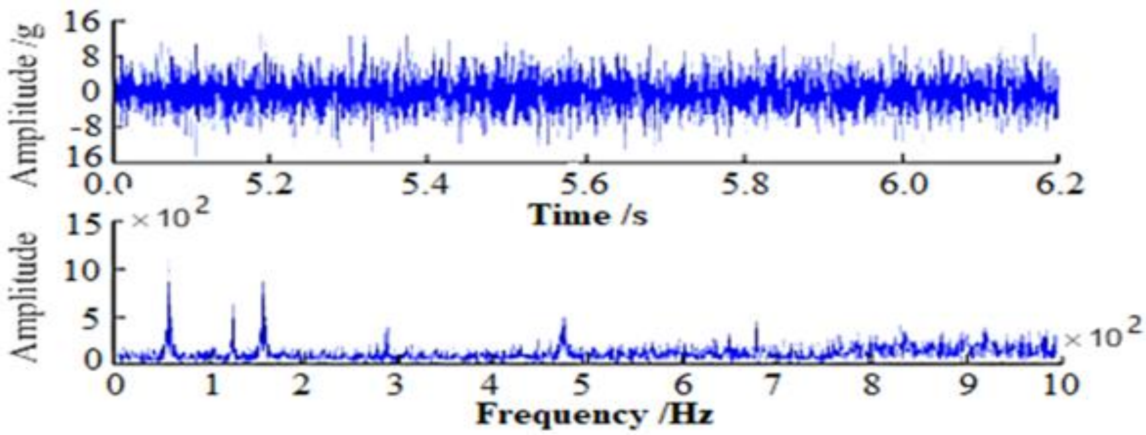

Figure 7.8(a) Time-Frequency Diagram of Vibration in the Direction of X At 5s

Figure 7.8(b) shows the Time-Frequency Diagram of Vibration in the Direction of Y At 5s.

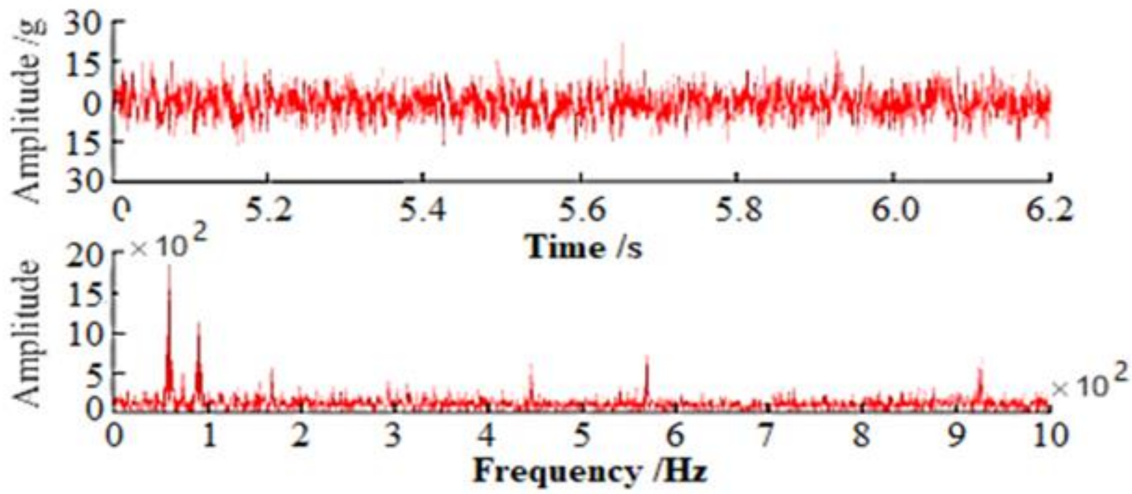

Figure 7.8(b) Time-Frequency Diagram of Vibration in the Direction of Y At 5s

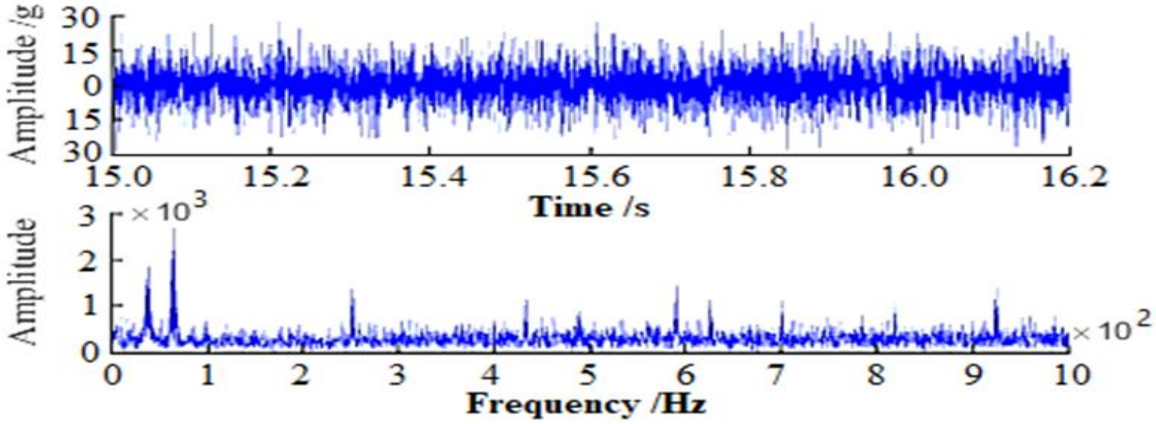

Figure 7.9(a) Time-Frequency Diagram of Vibration in the Direction of X At 15s

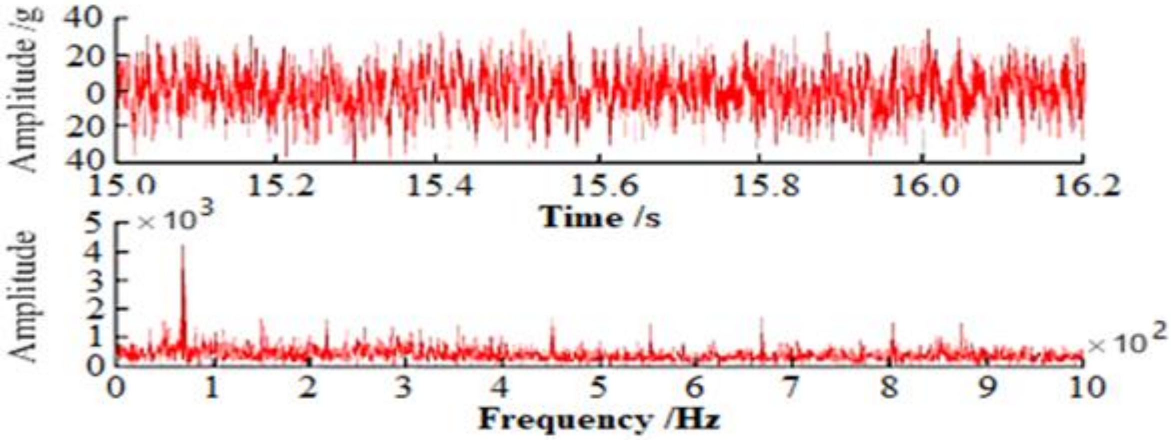

Figure 7.9(b) Time-Frequency Diagram of Vibration in the Direction of Y At 15s

The experimental results show that the amplitude of vibration of X and Y increases gradually with the increase of cutting depth before 25 s. It is noticed that, the vibration degree in the Y direction is larger than that in the X direction. During this period. Although there are peaks which appear in the frequency domain, however, they are concentrated in the low-frequency range of less than 100 Hz (refer to Figure 7.10). In addition, it can be noticed that, the overall frequency distribution is more uniform, which indicates that the forced vibration prevailing system is in a stable cutting state. Thus, the amplitude of the vibration signals in X, and Y directions are obviously increased, and the degree of dispersion is higher.

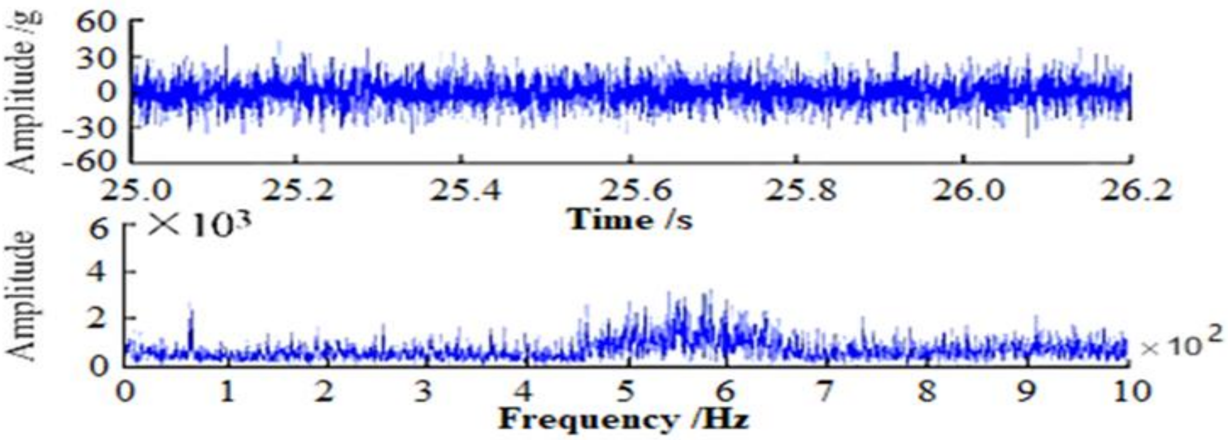

Figure 7.10(a): Time-Frequency Diagram of Vibration in the Direction of X At 25s

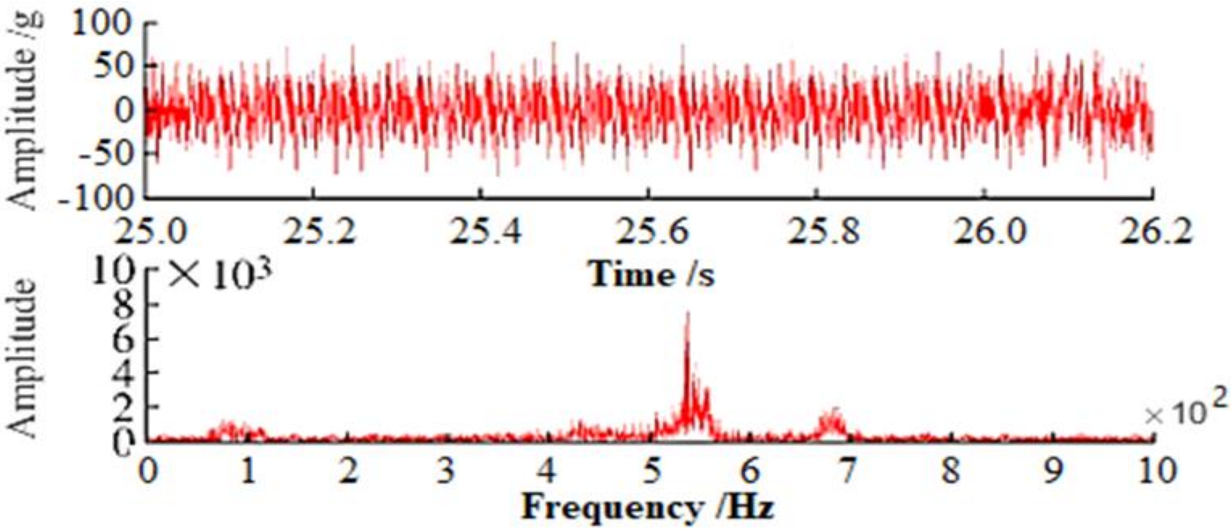

Figure 7.10(b): Time-Frequency Diagram of Vibration in the Direction of Y At 25s

It can be concluded that when cutting action continues to 25 s, the amplitude in the X and Y directions continues to increase, and the degree of dispersion increases significantly. Although the degree of vibration in the X direction is exacerbated, there is no energy concentration in the frequency domain. However, the energy in the Y direction is mainly concentrated at a frequency range of about 538 Hz. In this case, the frequency structure tends to be noticeable, so the system has changed vibration mode from forced vibration to transition, and from forced vibration to intensive self-excited vibration in order to achieve an unstable cutting state. In summary, the measured values L_{lim} and a_{plim} were found to be equal to 12.88 mm and 2.37 mm respectively. In comparing with the results obtained from the simulation, the error rate of the limit cutting depth is:

$$\frac{2.37 - 1.98}{2.37} = 16.45\%$$

7.3 Chapter Summary

In this chapter, the dynamic parameters of the machine tool cutting system were determined, through that the limit cutting width of the nickel-base superalloy processing was predicted. The main contents of that are as follows:

(1) In order to determine the model parameters of the tool system: The modal parameters (natural frequency ω_n, stiffness k, damping ratio ζ, model mass m) of the tool system in the X and Y directions were measured by the model hammer test method. The experimental results showed that, the natural frequency values at the 1st and 2nd test in the Y direction are far apart, but there is a convergence between natural frequency values in the X direction at 1st test which is 721Hz and in the Y direction at 2nd test

which is 708 Hz (refer to Tables 4.2 and 4.3). This indicates that, there are coupling effects in the X and Y directions. According to the natural frequency value at the main position in the X direction (721Hz), and in the Y direction (565Hz) (refer to Figures 4.13 and 4.14), the test results are perfect and acceptable.

(2) In order to deselect the main vibration source of the cutting tool system: During the cutting process, chatter usually occurs at the instant of occurrence of the natural frequencies for the machining. The part where the machine tool is most to be vibrate, is the tailstock at the back of the machine body. All tests were showed that, most values of the natural frequencies are less than 300 Hz. However, the chatter frequency does not occur in this range of low-frequency. Thus, the possibility of vibration in the tailstock was ruled out as a principal source of vibration that leads to the chatter occurrence at the cutting process.

(3) Calculation of the cutting forces unit coefficient kcu and kcv : According to the cutting force and the cutting motion in the turning process, the orthogonal test method is used to determine the main angles of the PCBN cutting tool of high-speed turning nickel-base superalloy. The cutting forces unit coefficient kcu and kcv in X and Y directions should be calculated. A trigonometric function is used in their calculations.

(4) On the basis of determining the dynamic parameters of the machine tool cutting system and of the nickel-base superalloy cutting process, it is

found that, the minimum limit of the cutting width of the nickel-base superalloy machining is $(b_{lim})_{min} = 1.98\ mm$, and it can be seen from the stability limit lobe diagram (refer to Figure 4.20).

In summary, the measured values of $L_{lim}\ and\ a_{plim}$ were found to be $12.88\ mm\ and\ 2.37\ mm$ respectively. Compared with the measured limit cutting depth from the experimental test, the error was found to be 16.45%. Therefore, the simulation result of the regenerative chatter model is reasonable in accuracy and effectiveness.

Chapter 8

Conclusions and Recommendations for Future Works

8.1 Conclusions

In this research, the mechanism of cutting chatter, cutting performance of nickel-based superalloy, and the research review of cutting tool materials were studied. The study is based on the theories and methods of metal cutting principle, cutting chatter, cutting experimental tests, and MATLAB software.

The chatter stability of high-speed turning of nickel-based superalloy with PCBN cutting tool was explored, and the effect of cutting parameters on chatter stability, and surface quality of workpiece was studied.

The main innovations and contributions to science are highlighted below:

1) A two-degree-of-freedom regenerative chatter model for cylindrical turning was established (refer to Figure 3.4(a)). Based on the generating mechanism of vibration and chatter in cylindrical turning, the dynamic model of two-degree-of-freedom regenerative turning chatter in axial and radial feeding directions was established (refer to Figure 3.4(b)), the stability criterion of machine tool cutting system was determined, and the calculation method of the ultimate cutting width of machine tool cutting system was obtained, the influence of various factors on vibration

characteristics of machine tool cutting system was analyzed by computer simulation.

2) The dynamic parameters of machine tool cutting system were determined. Based on the correct establishment of the mechanical model of chatter vibration in regenerative turning, the dynamic parameters of the cutting system (natural frequency, stiffness k, damping ratio ζ, (refer to Table 4.7)), and the dynamic parameters of nickel-based superalloy (cutting stiffness coefficient K_{cu}, K_{cv} (refer to Equations 4.30 and 4.31)) of the cutting process, were determined by the hammering modal test, and orthogonal cutting test. The predicted limit cutting depth of the two-degrees of freedom turning regenerative chatter is determined as 1.98 mm. Modal tests were carried out on other main parts of machine tools, and the possibility of using them as main vibration system of machine tools was excluded.

3) According to the two-dimensional cylindrical turning, the chatter model was designed using the model-measured parameters as shown in Figure 5.1. Then MATLAB / Simulink software was used to simulate the model, and an effective method to determine the stable state of cutting was established based on the number of cuts. The stability limit cutting depth of nickel-based superalloy was predicted by simulation model, and the main vibration direction of chatter during cutting was determined. According to the results of numerical simulation, the effects of cutting

parameters such as cutting speed, feed rate and cutting depth on the vibration characteristics of circular turning under regeneration effect were obtained.

4) The correctness or validity of the selection of the main vibration system was verified by cutting depth test, and the predicted ultimate cutting width of turning nickel-base superalloy was verified, the error was found to be 16.45%. Based on the single factor cylindrical turning test and numerical simulation results, the influence of spindle speed, feed rate and cutting depth on the vibration characteristics of high-speed turning nickel-base superalloy GH4169 with PCBN cutting tool was obtained, and the variation of surface roughness with cutting parameters was obtained under the effect of machining vibration.

8.2 Recommendations for Future Works

Based on the results from the present research, the following areas have been identified which warrant further investigation.

1) The external turning regenerative chatter model established in this thesis is based on the fact that the workpiece quality and stiffness are much larger than the tool system. Therefore, it is reasonable to use the tool system as the main vibration system. However, in the processing of nickel-based superalloy workpieces, it is necessary to consider the vibration of

the tool and the workpiece, so it is necessary to establish a dynamic model of the "workpiece-tool" system.

2) In the future work, by studying the impact of vibration in the X and Y directions on the surface topography, together with the remaining height of the workpiece surface and the cutting vibration, a simulation model of the workpiece's surface roughness must be established so as to achieve the expected surface roughness value, and to select the cutting parameters.

References

[1] Dr. Osama Mohammed Elmardi Suleiman Khayal, 2019. Mechanical Vibrations Book in Arabic Language, Noor Publishing, Germany, ISBN: 978-613-9-43200-4.

[2] Dr. Osama Mohammed Elmardi Suleiman Khayal, 2020. Mechanical Machinery Maintenance Book in Arabic Language, Noor Publishing, Germany, ISBN: 978-620-0-78138-3.

[3] Dr. Osama Mohammed Elmardi Suleiman Khayal, 2021. Manufacturing Processes Book in Arabic Language, Noor Publishing, Germany, ISBN: 978-620-0-77960-1.

[4] Dr. Osama Mohammed Elmardi Suleiman Khayal, 2020. Heat Exchangers Book in Arabic Language, Noor Publishing, Germany, ISBN: 978-620-0-77806-2.

[5] Dr. Osama Mohammed Elmardi Suleiman Khayal, 2020. Strength of Engineering Materials in Arabic Language, Noor Publishing, Germany, ISBN: 978-620-0-78134-5.

[6] H. Schulz and T. Moriwaki, “High-speed machining,” CIRP Ann. Technol., vol. 41, no. 2, pp. 637 – 643, 1992.

[7] I. Dul, “Application and processing of nickel alloys in the aviation industry,” Weld. Int., vol. 27, no. 1, pp. 48 – 56, 2013.

[8] R. Zhu, Y. He, and H. Qi, “High Temperature Corrosion and High Temperature Corrosion Resistant Materials,” Shanghai Sci. Tech. Press. Shanghai, pp. 339 – 350, 1995.

[9] I. A. Choudhury and M. A. El-Baradie, “Machinability of nickel-base super alloys: a general review,” J. Mater. Process. Technol., vol. 77, no. 1, pp. 278 – 284, 1998.

[10] M. Siddhpura and R. Paurobally, “A review of chatter vibration research in turning,” Int. J. Mach. tools Manuf., vol. 61, pp. 27 – 47, 2012.

[11] F. W. Taylor, On the Art of Cutting Metals..., vol. 23. American society of mechanical engineers, 1906.

[12] Q. Huang, G. B. Zhang, X. Y. Zhang, and D. CAO, “Experimental analysis on regenerative chatter model,” J. Vib. Eng., vol. 21, no. 6, pp. 547 – 552, 2008.

[13] R. Q. Guo, S. Wu, and Z. Li, “Modeling and Analysis on regenerative fluttering for cylindrical turning,” Chinese J. Constr. Mach., vol. 13, pp. 252 – 257, 2015.

[14] E. O. Ezugwu, J. Bonney, and Y. Yamane, “An overview of the machinability of aeroengine alloys,” J. Mater. Process. Technol., vol. 134, no. 2, pp. 233 – 253, 2003.

[15] J. Gradišek et al., “On stability prediction for milling,” Int. J. Mach. Tools Manuf., vol. 45, no. 7, pp. 769 – 781, 2005.

[16] J. Tlusty and F. Ismail, “Basic non-linearity in machining chatter,” CIRP Ann., vol. 30, no. 1, pp. 299 – 304, 1981.

[17] A. Gasparetto, “A system theory approach to mode coupling chatter in machining,” J. Dyn. Syst. Meas. Control, vol. 120, no. 4, pp. 545 – 547, 1998.

[18] K. F. Y. Junyi, “FUZZY STABILITY ANALYSIS OF MODE COUPLING CHATTER ON CUTTING PROCESS,” Chinese J. Mech. Eng., vol. 11, no. 2, pp. 109 – 114, 1998.

[19] B. C. Gegg, C. S. Suh, and A. C. J. Luo, “Machine Tool Vibrations and Cutting Dynamics.” Springer Science+ Business Media, LLC, 2011.

[20] M. Wiercigroch and A. M. Krivtsov, “Frictional chatter in orthogonal metal cutting,” Philos. Trans. R. Soc. London. Ser. A Math. Phys. Eng. Sci., vol. 359, no. 1781, pp. 713 – 738, 2001.

[21] C. H. Dai Depai, “The Nonlinear Theoretic Research about Cutting Chatter of Machine tool [J],” J. Vib. Eng., vol. 5, no. 4, pp. 335 – 342, 1992.

[22] P. Stelter, “Nonlinear vibrations of structures induced by dry friction,” Nonlinear Dyn., vol. 3, no. 5, pp. 329 – 345, 1992.

[23] R. S. Hahn, "On the theory of regenerative chatter in precision-grinding operations," Trans. ASME, pp. 593 – 597, 1954.

[24] S. A. Tobias and W. Fishwick, "Theory of regenerative machine tool chatter," Eng., vol. 205, no. 7, pp. 199 – 203, 1958.

[25] H. E. Merritt, "Theory of self-excited machine-tool chatter: contribution to machine-tool chatter research," J. Eng. Ind., vol. 87, no. 4, pp. 447 – 454, 1965.

[26] N. H. Hanna and S. A. Tobias, "A theory of nonlinear regenerative chatter," ASME J. Eng. Ind., vol. 96, no. 1, pp. 247 – 255, 1974.

[27] S. Hanmin, "Effects of some non-linear factors on machine tool chattering and their mathematical models," J. Huazhong Univ. Sci. Technol., vol. 6, p. 19, 1984.

[28] W. Ya, "Chatter and Control of Machine Tool Cutting System." Science Publishing Company: New York, NY, USA, 1993.

[29] L. Shen, X. Ding, T. Li, X. Kong, and X. Dong, "Structural dynamic design optimization and experimental verification of a machine tool," Int. J. Adv. Manuf. Technol., pp. 1 – 14, 2019.

[30] I. Chowdhury, M. M. Sadek, and S. A. Tobias, "Determination of the dynamic characteristics of machine tool structures," Proc. Inst. Mech. Eng., vol. 184, no. 1, pp. 943 – 960, 1969.

[31] R. S. Hahn, “Design of Lanchester damper for elimination of metal cutting chatter,” Trans. ASME, vol. 73, pp. 331 – 336, 1951.

[32] S. Ema, “Suppression of chatter vibration of boring tools using impact dampers,” vol. 40, pp. 1141 – 1156, 2000.

[33] S. E. Semercigil and L. A. Chen, “Preliminary computations for chatter control in end milling,” J. Sound Vib., vol. 249, no. 3, pp. 622 – 633, 2002.

[34] A. Rashid and C. M. Nicolescu, “Design and implementation of tuned viscoelastic dampers for vibration control in milling,” Int. J. Mach. Tools Manuf., vol. 48, no. 9, pp. 1036 – 1053, 2008.

[35] M. Wang, T. Zan, Y. Yang, and R. Fei, “Design and implementation of nonlinear TMD for chatter suppression: An application in turning processes,” Int. J. Mach. Tools Manuf., vol. 50, no. 5, pp. 474 – 479, 2010.

[36] Y. Yang, J. Munoa, and Y. Altintas, “Optimization of multiple tuned mass dampers to suppress machine tool chatter,” Int. J. Mach. Tools Manuf., vol. 50, no. 9, pp. 834 – 842, 2010.

[37] E. C. Lee, C. Y. Nian, and Y. S. Tarng, “Design of a dynamic vibration absorber against vibrations in turning operations,” J. Mater. Process. Technol., vol. 108, no. 3, pp. 278 –2 85, 2001.

[38] K. J. Liu and K. E. Rouch, “Optimal passive vibration control of cutting process stability in milling,” J. Mater. Process. Technol., vol. 28, no. 1–2, pp. 285 – 294, 1991.

[39] J. Saffury and E. Altus, “Optimized chatter resistance of viscoelastic turning bars,” J. Sound Vib., vol. 324, no. 1–2, pp. 26 – 39, 2009.

[40] N. D. Sims, “Vibration absorbers for chatter suppression: a new analytical tuning methodology,” J. Sound Vib., vol. 301, no. 3–5, pp. 592 – 607, 2007.

[41] Y. S. Tarng, J. Y. Kao, and E. C. Lee, “Chatter suppression in turning operations with a tuned vibration absorber,” J. Mater. Process. Technol., vol. 105, no. 1–2, pp. 55 – 60, 2000.

[42] J. Tlusty, “The stability of the machine tool against self-excited vibration in machining,” Proc. Int. Res. Prod. Eng. Pittsburgh, ASME, vol. 465, pp. 465 – 474, 1963.

[43] S. A. Tobias and W. Fishwick, “The chatter of lathe tools under orthogonal cutting conditions,” Trans. ASME, vol. 80, no. 2, pp. 1079 – 1088, 1958.

[44] N. H. Kim, D. Won, and J. C. Ziegert, “Numerical analysis and parameter study of a mechanical damper for use in long slender endmills,” Int. J. Mach. Tools Manuf., vol. 46, no. 5, pp. 500 – 507, 2006.

[45] J. C. Ziegert, C. Stanislaus, T. L. Schmitz, and R. Sterling, “Enhanced damping in long slender end mills,” J. Manuf. Process., vol. 8, no. 1, pp. 39 – 46, 2006.

[46] Y. Chen, X. G. Wang, C. Sun, F. Devine, and C. W. De Silva, “Active vibration control with state feedback in woodcutting,” Modal Anal., vol. 9, no. 6, pp. 645 – 664, 2003.

[47] J. L. Dohner, T. D. Hinnerichs, J. P. Lauffer, C.-M. Kwan, M. E. Regelbrugge, and N. Shankar, “Active chatter control in a milling machine,” in Smart Structures and Materials’ 97, 1997, pp. 281 – 294.

[48] J. L. Dohner et al., “Mitigation of chatter instabilities in milling by active structural control,” J. Sound Vib., vol. 269, no. 1, pp. 197 – 211, 2004.

[49] K. Nagaya, J. Kobayasi, and K. Imai, “Vibration control of milling machine by using auto-tuning magnetic damper and auto-tuning vibration absorber,” Int. J. Appl. Electromagn. Mech., vol. 16, no. 1–2, pp. 111 – 123, 2002.

[50] M. Shiraishi, K. Yamanaka, and H. Fujita, “Optimal control of chatter in turning,” Int. J. Mach. tools Manuf., vol. 31, no. 1, pp. 31 – 43, 1991.

[51] S. G. Tewani, K. E. Rouch, and B. L. Walcott, “A study of cutting process stability of a boring bar with active dynamic absorber,” Int. J. Mach. Tools Manuf., vol. 35, no. 1, pp. 91 – 108, 1995.

[52] C. M. Kwan et al., “H/sub/spl infin//control of chatter in octahedral hexapod machine,” in Proceedings of the 1997 American Control Conference (Cat. No. 97CH36041), 1997, vol. 2, pp. 1015 – 1016.

[53] M. A. Marra, B. L. Walcott, K. E. Rouch, and S. G. Tewani, “Vibration control for machining using H/sub/spl infin//techniques,” in Proceedings IEEE Southeastcon’95. Visualize the Future, 1995, pp. 436 – 442.

[54] M. A. Marra, B. L. Walcott, K. E. Rouch, and S. G. Tewani, “H/sub/spl infin//-vibration control for machining using active dynamic absorber technology,” in Proceedings of 1995 American Control Conference-ACC’95, 1995, vol. 1, pp. 739 – 743.

[55] M. Chen and C. R. Knospe, “Control approaches to the suppression of machining chatter using active magnetic bearings,” IEEE Trans. Control Syst. Technol., vol. 15, no. 2, pp. 220 – 232, 2007.

[56] S. Kern, C. Ehmann, R. Nordmann, M. Roth, A. Schiffler, and E. Abele, “Active damping of chatter vibrations with an active magnetic bearing in a motor spindle using l-synthesis and an adaptive filter,” in Proceedings of 8th International Conference Motion Vibration Control, 2006.

[57] S. Kern, A. Schwung, and R. Nordmann, “Gain-scheduling approaches for active damping of a milling spindle with speed-dependent dynamics,” in Proceedings of the 9th International Conference on Motion and Vibration Control, München (Deutschland), 2008.

[58] C. R. Knospe, “Active magnetic bearings for machining applications,” Control Eng. Pract., vol. 15, no. 3, pp. 307 – 313, 2007.

[59] A. Preumont, Vibration control of active structures: an introduction, vol. 246. Springer, 2018.

[60] Y. Zhang and N. D. Sims, “Milling workpiece chatter avoidance using piezoelectric active damping: a feasibility study,” Smart Mater. Struct., vol. 14, no. 6, p. N65, 2005.

[61] J. R. Pratt and A. H. Nayfeh, “Design and modeling for chatter control,” Nonlinear Dyn., vol. 19, no. 1, pp. 49 – 69, 1999.

[62] J. R. Pratt and A. H. Nayfeh, “Chatter control and stability analysis of a cantilever boring bar under regenerative cutting conditions,” Philos. Trans. R. Soc. London A Math. Phys. Eng. Sci., vol. 359, no. 1781, pp. 759 – 792, 2001.

[63] B. Chung, S. Smith, and J. Tlusty, “Active damping of structural modes in high-speed machine tools,” J. Vib. Control, vol. 3, no. 3, pp. 279 – 295, 1997.

[64] A. Ganguli, A. Deraemaeker, M. Horodinca, and A. Preumont, “Active damping of chatter in machine tools-demonstration with a ‘Hardware-in-the-Loop’simulator,” Proc. Inst. Mech. Eng. Part I J. Syst. Control Eng., vol. 219, no. 5, pp. 359 – 369, 2005.

[65] A. Ganguli, A. Deraemaeker, I. Romanescu, M. Horodinca, and A. Preumont, “Simulation and active control of chatter in milling via a mechatronic simulator,” J. Vib. Control, vol. 12, no. 8, pp. 817 – 848, 2006.

[66] J.-H. Kyung and C.-W. Lee, “Controller design for a magnetically suspended milling spindle based on chatter stability analysis,” JSME Int. J. Ser. C Mech. Syst. Mach. Elem. Manuf., vol. 46, no. 2, pp. 416 – 422, 2003.

[67] J. Pan and C.-Y. Su, “Chatter suppression with adaptive control in turning metal via application of piezo actuator,” in Proceedings of the 40th IEEE Conference on Decision and Control (Cat. No. 01CH37228), 2001, vol. 3, pp. 2436 – 2441.

[68] M. Ries, S. Pankoke, and K. Gebert, “Increase of material removal rate with an active HSC milling spindle,” in Conference proceedings of the adaptronic congress, 2006.

[69] A. H. El-Sinawi and R. Kashani, “Improving surface roughness in turning using optimal control of tool’s radial position,” J. Mater. Process. Technol., vol. 167, no. 1, pp. 54 – 61, 2005.

[70] G. Pan, H. Xu, C. M. Kwan, C. Liang, L. Haynes, and Z. Geng, “Modeling and intelligent chatter control strategies for a lathe machine,” Control Eng. Pract., vol. 4, no. 12, pp. 1647 – 1658, 1996.

[71] D. J. Segalman and J. M. Redmond, “Method and apparatus for suppressing regenerative instability and related chatter in machine tools.” Google Patents, 2001.

[72] M. Wang and R. Fei, “Chatter suppression based on nonlinear vibration characteristic of electrorheological fluids,” Int. J. Mach. Tools Manuf., vol. 39, no. 12, pp. 1925 – 1934, 1999.

[73] M. Wang and R. Fei, “On-line chatter detection and control in boring based on an electrorheological fluid,” Mechatronics, vol. 11, no. 7, pp. 779 – 792, 2001.

[74] G. Park, M. T. Bement, D. A. Hartman, R. E. Smith, and C. R. Farrar, “The use of active materials for machining processes: A review,” Int. J. Mach. Tools Manuf., vol. 47, no. 15, pp. 2189 – 2206, 2007.

[75] M. Shiraishi, E. Kume, and T. Hoshi, “Suppression of machine-tool chatter by state feedback control,” CIRP Ann., vol. 37, no. 1, pp. 369 – 372, 1988.

[76] Y. Fulun and Y. Junyi, “Present Situation of Research on Prediction and Control of Cutting Chatter,” J. Jilin Univ. Technol. (Natural Sci. Ed., no. 1, p. 21, 1992.

[77] T.-C. Tsao, M. W. McCarthy, and S. G. Kapoor, “A new approach to stability analysis of variable speed machining systems,” Int. J. Mach. Tools Manuf., vol. 33, no. 6, pp. 791 – 808, 1993.

[78] Y. F. W. H. B. Shanfei and Q. Simao, "A STUDY ON STABILITY OF TIME-VARYING FEED RATE MACHINING SYSTEM," Trans. CHINESE Soc. Agric. Mach., vol. 4, 1995.

[79] F. Yang, B. Zhang, and J. Yu, "Chatter suppression via an oscillating cutter," J. Manuf. Sci. Eng., vol. 121, no. 1, pp. 54 – 60, 1999.

[80] G. Quintana and J. Ciurana, "Chatter in machining processes: A review," Int. J. Mach. Tools Manuf., vol. 51, no. 5, pp. 363 – 376, 2011.

[81] M. Weck, E. Verhaag, and M. Gather, "Adaptive control for face-milling operations with strategies for avoiding chatter vibrations and for automatic cut distribution," Ann. CIRP, vol. 24, no. 1, pp. 405 – 409, 1975.

[82] T. Sata and T. Inamura, "Development of method to predict and prevent chattering in metal cutting," Ann CIRP, vol. 24, pp. 309 – 314, 1975.

[83] B. E. Clancy and Y. C. Shin, "A comprehensive chatter prediction model for face turning operation including tool wear effect," Int. J. Mach. Tools Manuf., vol. 42, no. 9, pp. 1035 – 1044, 2002.

[84] M. A. Davies, J. R. Pratt, B. S. Dutterer, and T. J. Burns, "The stability of low radial immersion milling," CIRP Ann., vol. 49, no. 1, pp. 37 – 40, 2000.

[85] M. S. Fofana, K. C. Ee, and I. S. Jawahir, "Machining stability in turning operation when cutting with a progressively worn tool insert," Wear, vol. 255, no. 7–12, pp. 1395 – 1403, 2003.

[86] H. W. Zhao, X. J. Wang, and J. Y. Yu, “Prediction of stability limits for regenerative machining chatter system,” Grinder Grind., vol. 1, pp. 62 – 64, 2003.

[87] J. LI, H. XIE, Z. SHENG, and Y. LIU, “Modeling and Simulation of Regenerative Chatter Stability in CNC Lathing Process [J],” J. Northeast. Univ. (Natural Sci., vol. 1, p. 29, 2013.

[88] Y. ZHANG, Y. HE, and X. CHEN, “Simulation Analysis on the Cylindrical Turning Based on MATLAB/Simulink [J],” Mech. Res. Appl., vol. 2, p. 11, 2013.

[89] C. J. Salomon, “Process for machining metals of similar acting materials when being worked by cutting tools,” Ger. Pat., vol. 523594, 1931.

[90] H. A. Youssef, Machining of stainless steels and super alloys: traditional and nontraditional techniques. John Wiley & Sons, 2015.

[91] A. Altin, M. Nalbant, and A. Taskesen, “The effects of cutting speed on tool wear and tool life when machining Inconel 718 with ceramic tools,” Mater. Des., vol. 28, no. 9, pp. 2518 – 2522, 2007.

[92] T. Kitagawa, A. Kubo, and K. Maekawa, “Temperature and wear of cutting tools in high-speed machining of Inconel 718 and Ti-6Al-6V-2Sn,” Wear, vol. 202, no. 2, pp. 142 – 148, 1997.

[93] D. Jianxin, C. Tongkun, and L. Lili, “Self-lubricating behaviors of Al2O3/TiB2 ceramic tools in dry high-speed machining of hardened steel,” J. Eur. Ceram. Soc., vol. 25, no. 7, pp. 1073 – 1079, 2005.

[94] L. Settineri, M. G. Faga, and B. Lerga, “Properties and performances of innovative coated tools for turning Inconel,” Int. J. Mach. Tools Manuf., vol. 48, no. 7–8, pp. 815 – 823, 2008.

[95] C. Ducros, V. Benevent, and F. Sanchette, “Deposition, characterization and machining performance of multilayer PVD coatings on cemented carbide cutting tools,” Surf. coatings Technol., vol. 163, pp. 681 – 688, 2003.

[96] R. Arunachalam and M. A. Mannan, “Machinability of nickel-based high temperature alloys,” Mach. Sci. Technol., vol. 4, no. 1, pp. 127 – 168, 2000.

[97] T. Harada et al., “Development of a coated PCBN tool,” SEI Tech. Rev. Ed., pp. 81 – 86, 2001.

[98] G. Poulachon, A. Moisan, and I. S. Jawahir, “Tool-wear mechanisms in hard turning with polycrystalline cubic boron nitride tools,” Wear, vol. 250, no. 1–12, pp. 576 – 586, 2001.

[99] A. E. Diniz, J. R. Ferreira, and others, “Influence of refrigeration/lubrication condition on SAE 52100 hardened steel turning at

several cutting speeds," Int. J. Mach. Tools Manuf., vol. 43, no. 3, pp. 317 – 326, 2003.

[100] G. de Siqueira Galoppi, M. Stipkovic Filho, and G. F. Batalha, "Hard turning of tempered DIN 100Cr6 steel with coated and no coated CBN inserts," J. Mater. Process. Technol., vol. 179, no. 1–3, pp. 146 – 153, 2006.

[101] J.-P. Costes, Y. Guillet, G. Poulachon, and M. Dessoly, "Tool-life and wear mechanisms of CBN tools in machining of Inconel 718," Int. J. Mach. Tools Manuf., vol. 47, no. 7, pp. 1081 – 1087, 2007.

[102] W. F. Sales, L. A. Costa, S. C. Santos, A. E. Diniz, J. Bonney, and E. O. Ezugwu, "Performance of coated, cemented carbide, mixed-ceramic and PCBN-H tools when turning W320 steel," Int. J. Adv. Manuf. Technol., vol. 41, no. 7–8, pp. 660 – 669, 2009.

[103] W. Grzesik, Advanced machining processes of metallic materials: theory, modelling and applications. Elsevier, 2008.

[104] M. H. Xiao, N. He, L. Li, and H. B. Liu, "Experimental studies on notch wear for high-speed machining of nickel-based superalloy with ceramic tools," China Mech. Eng., vol. 19, no. 10, pp. 1188 – 1192, 2008.

[105] R. Peng, M. Liao, Y. Tan, and X. Liu, "Experimental study on prestressed cutting of nickel-based superalloys," Jixie Gongcheng Xuebao (Chinese J. Mech. Eng., vol. 48, no. 19, pp. 186 – 191, 2012.

[106] J. Barry and G. Byrne, “The mechanisms of chip formation in machining hardened steels,” J. Manuf. Sci. Eng., vol. 124, no. 3, pp. 528 – 535, 2002.

[107] M. Tiffe, J. Saelzer, and A. Zabel, “Analysis of mechanisms for chip formation simulation of hardened steel,” Procedia CIRP, vol. 82, pp. 71 – 76, 2019.

[108] A. A. Cardi, H. A. Firpi, M. T. Bement, and S. Y. Liang, “Workpiece dynamic analysis and prediction during chatter of turning process,” Mech. Syst. Signal Process., vol. 22, no. 6, pp. 1481 – 1494, 2008.

[109] A. A. Cardi, On the development of a dynamic cutting force model with application to regenerative chatter in turning. Georgia Institute of Technology, 2009.

[110] X. Han, H. Ouyang, M. Wang, N. Hassan, and Y. Mao, “Self-excited vibration of workpieces in a turning process,” Proc. Inst. Mech. Eng. Part C J. Mech. Eng. Sci., vol. 226, no. 8, pp. 1958 – 1970, 2012.

[111] J. Tlusty, “Dynamics of high-speed milling,” J. Eng. Ind., vol. 108, no. 2, pp. 59 – 67, 1986.

[112] M. K. Das and S. A. Tobias, “The relation between the static and the dynamic cutting of metals,” Int. J. Mach. Tool Des. Res., vol. 7, no. 2, pp. 63 – 89, 1967.

[113] J. Tlusty, “Analysis of the state of research in cutting dynamics,” CIRP Ann, vol. 27, no. 2, pp. 583 – 589, 1978.

[114] M. A. M. Fadulalmula, H. Zhu, H. A. Wahab, and H. A. Elkariem, “Modeling and analysis of three-degree of freedom regenerative chatter in the cylindrical lathe turning,” Int. J. Emerg. Technol. Adv. Eng., vol. 5, no. 1, pp. 43 – 49, 2015.

[115] S. A. Tobias, “Machine tool vibration research,” Int. J. Mach. Tool Des. Res., vol. 1, no. 1–2, pp. 1 – 14, 1961.

[116] J. Tlusty, “Manufacturing Processes and Equipment. (Prentice Hall, NJ).,” 2000.

[117] Y. Altintas and M. Weck, “Chatter stability of metal cutting and grinding,” CIRP Ann. Technol., vol. 53, no. 2, pp. 619 – 642, 2004.

[118] N. K. Chandiramani and T. Pothala, “Dynamics of 2-dof regenerative chatter during turning,” J. Sound Vib., vol. 290, no. 1–2, pp. 448 – 464, 2006.

[119] E. Budak and E. Ozlu, “Analytical modeling of chatter stability in turning and boring operations: a multi-dimensional approach,” CIRP Ann., vol. 56, no. 1, pp. 401 – 404, 2007.

[120] E. Ozlu and E. Budak, “Comparison of one-dimensional and multi-dimensional models in stability analysis of turning operations,” Int. J. Mach. Tools Manuf., vol. 47, no. 12–13, pp. 1875 – 1883, 2007.

[121] A. V Dassanayake and C. S. Suh, “On nonlinear cutting response and tool chatter in turning operation,” Commun. Nonlinear Sci. Numer. Simul., vol. 13, no. 5, pp. 979 – 1001, 2008.

[122] N. Suzuki, K. Nishimura, E. Shamoto, and K. Yoshino, “Effect of cross transfer function on chatter stability in plunge cutting,” J. Adv. Mech. Des. Syst. Manuf., vol. 4, no. 5, pp. 883 – 891, 2010.

[123] Z. Dombovari, D. A. W. Barton, R. E. Wilson, and G. Stepan, “On the global dynamics of chatter in the orthogonal cutting model,” Int. J. Non. Linear. Mech., vol. 46, no. 1, pp. 330 – 338, 2011.

[124] G. S. Upadhyaya, “Trent E.M., Wright P.K.: Metal cutting (4th edition), ‘Butterworth-Heinemann’, Boston, 2000,” Sci. Sinter., vol. 36, no. 1, pp. 54 – 54, 2004.

[125] M. Géradin and D. J. Rixen, Mechanical vibrations: theory and application to structural dynamics. John Wiley & Sons, 2014.

[126] Y. Altintas and A. A. Ber, “Manufacturing automation: metal cutting mechanics, machine tool vibrations, and CNC design,” Appl. Mech. Rev., vol. 54, no. 5, 2001.

[127] B. I\cs\ik, “Experimental investigations of surface roughness in orthogonal turning of unidirectional glass-fiber reinforced plastic composites,” Int. J. Adv. Manuf. Technol., vol. 37, no. 1–2, pp. 42 – 48, 2008.

[128] F. W. Taylor, “On the art of cutting metals/Frederick Winslow Taylor,” New York Publ. by Am. Soc. Mech. Eng., p. 744, 1907.

[129] J. Tlusty, “The stability of the machine tool against self-excited vibration in machining,” Proc. Int. Res. Prod. Eng. Pittsburgh, ASME, vol. 465, 2000.

[130] S. Tobias, “The chatter of lathe tools under orthogonal cutting conditions,” Trans ASME, vol. 80, pp. 1079 – 1085, 1999.

[131] K. R. Kashyzadeh and M. J. Ostad-Ahmad-Ghorabi, “Study of Chatter Analysis in turning tool and control methods--A Review,” Int. J. Emerg. Technol. Adv. Eng., vol. 2, no. 4, pp. 1 – 5, 2012.

[132] H. M. Shi and S. A. Tobias, “Theory of finite amplitude machine tool instability,” Int. J. Mach. Tool Des. Res., vol. 24, no. 1, pp. 45 – 69, 2004.

[133] H. E. Merrit, “Theory of self-excited-tool chatter: Research 1,” ASME J. Eng. Ind., vol. 87, pp. 447 – 454, 1965.

[134] X. Han, H. Ouyang, M. Wang, N. Hassan, and Y. Mao, “Self-excited vibration of workpieces in a turning process,” Proc. Inst. Mech. Eng. Part C J. Mech. Eng. Sci., vol. 226, no. 8, pp. 1958 – 1970, 2012.

[135] T. Kalmár-Nagy, G. Stépán, and F. C. Moon, “Subcritical Hopf bifurcation in the delay equation model for machine tool vibrations,” Nonlinear Dyn., vol. 26, no. 2, pp. 121 – 142, 2001.

[136] T. Insperger, D. A. W. Barton, and G. Stépán, “Criticality of Hopf bifurcation in state-dependent delay model of turning processes,” Int. J. Non. Linear. Mech., vol. 43, no. 2, pp. 140 – 149, 2008.

[137] S. C. Lin, R. E. DeVor, and S. G. Kapoor, “The effects of variable speed cutting on vibration control in face milling,” J. Eng. Ind., vol. 112, pp. 1 – 11, 1990.

[138] R. Y. Chiou and S. Y. Liang, “Chatter stability of a slender cutting tool in turning with tool wear effect,” Int. J. Mach. Tools Manuf., vol. 38, no. 4, pp. 315 – 327, 1998.

[139] M. Sekar, J. Srinivas, K. R. Kotaiah, and S.-H. Yang, “Stability analysis of turning process with tailstock-supported workpiece,” Int. J. Adv. Manuf. Technol., vol. 43, no. 9–10, pp. 862 – 871, 2009.

[140] E. O. Ezugwu, “Key improvements in the machining of difficult-to-cut aerospace superalloys,” Int. J. Mach. Tools Manuf., vol. 45, no. 12 – 13, pp. 1353 – 1367, 2005.

[141] R. M’Saoubi, J. C. Outeiro, H. Chandrasekaran, O. W. Dillon Jr, and I. S. Jawahir, “A review of surface integrity in machining and its impact on functional performance and life of machined products,” Int. J. Sustain. Manuf., vol. 1, no. 1 – 2, pp. 203 – 236, 2008.

[142] L. Garimella, P. K. Liaw, and D. L. Klarstrom, “Fatigue behavior in nickel-based superalloys: A literature review,” JOM J. Miner. Met. Mater. Soc., vol. 49, no. 7, pp. 67 – 71, 1997.

[143] N. Rene, “Nickel-Based Superalloys,” no. September 2015, Elsevier, pp. 1 – 7.

[144] B. Kennedy, “Making the Grade,” Appl. PCBN Grades Enhanc. Met. Oper., vol. 54, 2002.

[145] T. J. Broskea, “Analyzing PCBN tool wear,” Mod. Mach. Shop (USA), vol. 73, no. 8, pp. 86 – 93, 2001.

[146] D. Huddle and S. Carboloy, “Knowledge is power with PCBN,” Cut. Technol, pp. 40–42, 2003.

[147] S. George, “Cutting Tools Application,” p. 153, 2002.

[148] W. Ji, X. L. Liu, H. Y. Li, H. Y. You, and M. C. Fan, “Research of PCBN Tool Wear Mechanism in Turning Ni-based Superalloy,” in Advanced Materials Research, 2013, vol. 820, pp. 185 – 189.

[149] T. L. Schmitz and K. S. Smith, "Frequency Response to Improved Productivity. Machining Dynamics." Springer, New York, 2008.

[150] F. Lianyu, Y. Junyi, and B. Ming, "Study on the phase characteristics of cutting chatter," J. Vib. Eng., vol. 13, no. 4, pp. 510 – 515, 2000.

[151] X. J. Wang, "Study on the prediction of stability limits in turning," Doctoral dissertation, Shandong University of Technology, Shandong, Zibo, Zhangdian, 2005, 20 – 39, 2005.

[152] M. Wiercigroch and E. Budak, "Sources of nonlinearities, chatter generation and suppression in metal cutting," Philos. Trans. R. Soc. London. Ser. A Math. Phys. Eng. Sci., vol. 359, no. 1781, pp. 663 – 693, 2001.

[153] N. H. Cook, "Self-excited vibrations in metal cutting," J. Eng. Ind., vol. 81, no. 2, pp. 183–186, 1959.

[154] G. Radons and R. Neugebauer, Nonlinear dynamics of production systems. Wiley Online Library, 2004.

[155] W. Xiankui, "Modern manufacturing technology and its development [J]," Mod. Manuf. Eng., vol. 1, no. 1, pp. 1 – 8, 2008.

[156] F. Zhifang and H. Hongxing, "Theory and application of modal analysis." Shanghai: Shanghai Jiao Tong university press, 2000.

[157] Y. S. Zhai, S. Qiao, X. L. Liu, and Q. Hu, “The Simulation Analysis and Experimental Research on the Process of PCBN Cutting Super-alloy,” in Key Engineering Materials, 2014, vol. 589, pp. 88–93.

[158] S. Hu, F. Liu, Y. He, and T. Hu, “An on-line approach for energy efficiency monitoring of machine tools,” J. Clean. Prod., vol. 27, pp. 133–140, 2012.

Student Autobiography

Personal Data:

Name Mubarak Ahmed Mohammed Fadulalmula

Nationality Sudanese

Religion Muslim

Date of Birth Kosti - White Nile state -01/01/1974

Marital Status Married

Telephone 008618846130971

E-mail mubarak651@hotmail.com

Academic Qualifications:

1- Bachelor in Mechanical Engineering – Mechanical Engineering Department – College of Engineering and Technical Studies – Elimam Elmahdi University- Sudan – on 22 July 2002.

2- Master in Mechanical Manufactures and their Automation – Mechanical Engineering Department – Tianjin University of Technology and Education–China - on 25 May 2013.

Work Experience:

1- Teaching assistant – Department of Mechanical Engineering – Faculty of Engineering & Technical Studies – University of Elimam Elmahdi – Kosti – Sudan – 01/08/2006.

2- Lecturer – Department of Mechanical Engineering – Faculty of Engineering & Technical Studies – University of Elimam Elmahdi – Kosti – Sudan – 26/08/2013.

3- Head of Technical Diploma Department – Faculty of Engineering and Technical Studies - University of Elimam Elmahdi – Kosti – Sudan – 01/05/2020 – 28/03/2021.

4- Examinations Committee Member – Faculty of Engineering & Technical Studies– University of Elimam Elmahdi – Kosti – Sudan – for One Year.

5- Head of Academic office – Faculty of Engineering and Technical Studies - University of Elimam Elmahdi – Kosti – Sudan – 31/01/2013.

6- Mechanical engineer in Kenana Sugar Company Factory, section Mills & Cane Yard, in the Post of Shift Mills Engineer from 2006 to 2010.

Short Courses:

1. Basic Concepts of AutoCAD and MATLAB – College of Computer Science & Information Technology – Elimam Elmahdi University-

Sudan – on 03 July 2014.

2. Professional Development of University Professors – Department of quality and self-evaluation – Elimam Elmahdi University- Sudan – on 06 Feb 2015.

Workshops & Training Courses:

1- Certificate of diploma for computer sciences and programming from National Union UNESCO Clubs in 2004.

2- Optimize Your Manager in 24-28 August 2008.

3- Rolling Bearing Technology in 08-11 September 2008.

4- Certificate in professional project management from university of sciences & technology in 2009.

Skills:

1- Writing and speaking in languages (Arabic, English and Chinese).

2- Computer Microsoft office programs (Word, PowerPoint, and Excels).

Publications:

1- Regenerative Chatter Evaluation when Turning Nickel based Superalloy GH4169 Using PCBN Cutting Tool.'' Journal of Engineering and Technological Sciences. Vol.51, No.4,2019,556–572. (EI accession number: 20194207552171).

2- Modeling and analysis of three-degree of freedom regenerative chatter in the cylindrical lathe turning.'' Journal of Vibroengineering Procedure. Vol.12, p38-43. (EI accession number: 20173304048288).

3- Reliability of chatter stability in CNC turning process by Monte Carlo simulation method.'' Journal of Vibroengineering Procedure, v12, p29-37. (EI accession number: 20173304048289).

4- Damping effect on chatter stability of turning and milling processes.'' Journal of Vibroengineering Procedia, v13, p7-14. (EI accession number: 20175004517871).

PERSONAL QUALITIES:

- Excellent time Management Skills.
- Ability to Adapt under Pressure situation.
- Spirit of collegiality and collaboration.
- Ability to deal with multicultural and the ethnic groups.

Supervisor Autobiography

Dr. Osama Mohammed Elmardi Suleiman Khayal was born in Atbara City, Sudan in 1966. He received his diploma degree in mechanical engineering from Mechanical Engineering College, Atbara, Sudan in 1990. He also received a bachelor degree in mechanical engineering from Sudan University of science and technology – College of engineering, Khartoum, Sudan in 1998, and a master degree in solid mechanics from Nile valley university (Atbara, Sudan) in 2003, and a PhD in mechanics of materials (structural engineering in composite materials) in 2017. He contributed in teaching some subjects in other universities such as Red Sea University (Port Sudan, Sudan), Kordofan University (Obayed, Sudan), Sudan University of Science and Technology (Khartoum, Sudan), Blue Nile University (Damazin, Sudan) , Kassala University (Kassala, Sudan), Elsheikh Abdallah Elbadri (Berber, Sudan) and Merowe Technical College (Merowe, Sudan). In addition, he supervised more than three hundred under graduate studies in diploma and B.Sc. levels and about fifteen master degree theses and six doctoral degree dissertations. The author wrote about hundred engineering books written in Arabic language, and seventy books written in English language and more than hundred research article papers in fluid mechanics, thermodynamics, internal combustion engines, heat and mass transfer, mechanical instrumentation and control systems, mechanical vibration, industrial and manufacturing engineering, engineering economics, operational research, design of engineering projects, mechanical and production engineering maintenance, human resources and personnel management, advanced mechanics of materials and analysis of composite structures. He authored more than three hundred lectures notes in the fields of mechanical, production and civil engineering. He is currently an associate professor in the Department of Mechanical Engineering, Faculty of Engineering and Technology, Nile Valley University Atbara, Sudan and now he is the faculty dean. His research interest and favorite subjects include structural mechanics, applied mechanics, control engineering and instrumentation, computer aided design, design of mechanical elements, fluid mechanics and dynamics, heat and mass transfer and hydraulic machinery. The author also works as a technical manager and superintendent of Al – Kamali mechanical and production workshops group which specializes in small, medium and large automotive overhaul maintenance and which situated in Atbara city in the north part of Sudan, River Nile State.